UNIVERSITY OF SOUTHAMPTON

Measurement and Simulation of Partial Discharges within a Spherical Cavity in a Solid Dielectric Material

by

Hazlee Azil Illias

A thesis submitted for the degree of
Doctor of Philosophy

in the
Faculty of Physical and Applied Science
School of Electronics and Computer Science

May 2011

UNIVERSITY OF SOUTHAMPTON

ABSTRACT

FACULTY OF PHYSICAL AND APPLIED SCIENCE
SCHOOL OF ELECTRONICS AND COMPUTER SCIENCE

Doctor of Philosophy

MEASUREMENT AND SIMULATION OF PARTIAL DISCHARGES WITHIN A SPHERICAL CAVITY IN A SOLID DIELECTRIC MATERIAL

by Hazlee Azil Illias

For high voltage components, the measurement of partial discharge (PD) is used in the performance assessment of an insulation system. Through modelling the PD process, a better understanding of the phenomenon may be attained. In this work, a model for a spherical cavity within a homogeneous dielectric material has been developed using Finite Element Analysis (FEA) software in parallel with MATLAB programming code. The model has been used to study the effect of various applied stresses and cavity conditions on PD activity and also the electric field and temperature distributions within the cavity.

The experimental measurement of PD activity within a spherical cavity has also been undertaken. The measurements were performed for different amplitudes and frequencies of the applied voltage, a range of spherical cavity sizes and temperature variation of the material. The obtained results show that PD is strongly influenced by various conditions of the cavity and applied stress. The cycle to cycle behaviour of PD events, discharge phase and magnitude distributions, numbers of PDs per cycle, total charge magnitude per cycle, mean charge magnitude and maximum charge magnitude for each experiment have been obtained and analysed.

The simulation results from the PD model have been compared with the measurement results. It is found that certain model parameters are dependent on the applied stress and cavity conditions. Parameters that clearly affect PD activity can be readily identified. These parameters include; the effective charge decay time constant, the cavity surface conductivity, the initial electron generation rate, the inception field, the extinction field and the temperature decay time constant in the cavity. The influences of surface charge decay through conduction along the cavity wall and temperature and pressure change in the cavity on PD activity have also been studied.

Contents

List of Figures

List of Tables

Nomenclature

c	Cavity capacitance (F)
c_e	Electron thermal velocity (ms^{-1})
d	Cavity diameter (mm)
e	Electric charge of the electron (C)
f	Frequency of the applied voltage (Hz)
f_c	Field enhancement factor in the cavity
h_{mat}	Thickness of the material (mm)
h_{small}	thickness of the small epoxy block (mm)
k_{cav}	Thermal conductivity of the cavity ($WK^{-1}m^{-1}$)
k_{mat}	Thermal conductivity of the material ($WK^{-1}m^{-1}$)
m_e	Electron mass (kg)
n_e	Number of electrons in the streamer channel
p_0	Initial pressure in the cavity (kPa)
r	Cavity radius (mm)
q_{max}	Maximum charge magnitude (pC)
q_{min}	Minimum charge magnitude (pC)
q_{PD}	PD charge magnitude (pC)
$q_{PDtotal}$	Total PD charge magnitude (pC)
t	Time (s)
t_{PD}	Time of PD occurrence (s)
C_{cav}	Specific heat capacity of the cavity ($Jkg^{-1}K^{-1}$)
C_{mat}	Specific heat capacity of the cavity ($Jkg^{-1}K^{-1}$)
C_{a1}	Bulk material capacitance in cavity-free region (F)
C_{a2}	Bulk material capacitance in cavity-free region (F)
C_a	Equivalent bulk material capacitance in cavity-free region (F)
C_{b1}	Bulk material capacitance in series with the cavity (F)
C_{b2}	Bulk material capacitance in series with the cavity (F)
C_b	Equivalent bulk material capacitance in series with the cavity (F)
C_c	Equivalent cavity capacitance (F)
D_f	Electric displacement field (Cm^{-2})
E_{cav}	Field in the cavity centre ($kV{\cdot}mm^{-1}$)

E_{cav0}	Field in the cavity centre in the absence of surface charge ($kV \cdot mm^{-1}$)
E_{ext}	Cavity extinction field ($kV \cdot mm^{-1}$)
E_{ext0}	Initial cavity extinction field ($kV \cdot mm^{-1}$)
E_{inc}	Cavity inception field ($kV \cdot mm^{-1}$)
E_{inc0}	Initial cavity inception field ($kV \cdot mm^{-1}$)
E_{ons}	Field on the cavity surface ($kV \cdot mm^{-1}$)
E_s	Field due surface charge ($kV \cdot mm^{-1}$)
$E_{sfreePD}$	Field due to free surface charge immediately after a PD event ($kV \cdot mm^{-1}$)
$E_{strapPD}$	Field due to trapped charge immediately after a PD event ($kV \cdot mm^{-1}$)
E_{sPD}	Field due to surface charge immediately after a PD event ($kV \cdot mm^{-1}$)
E_{PD1}	Cavity field of the previous PD occurrence ($kV \cdot mm^{-1}$)
E_{PD2}	Cavity field of the current PD occurrence ($kV \cdot mm^{-1}$)
E_0	Applied field ($kV \cdot mm^{-1}$)
I_{cav}	Current through the cavity (A)
J_{cav}	Current density in the cavity (Am^{-2})
J_f	Free current density (Am^{-2})
L	Likelihood of a PD occurrence
N_e	Electron density (Cm^{-3})
N_{es}	Electron generation rate due to surface emission (s^{-1})
N_{es0}	Initial electron generation rate due to surface emission (s^{-1})
N_{es0H}	Higher initial electron generation rate due to surface emission (s^{-1})
N_{es0L}	Lower initial electron generation rate due to surface emission (s^{-1})
N_{et}	Total electron generation rate (s^{-1})
N_{ev}	Electron generation rate due to volume ionization (s^{-1})
N_{PD}	Number of free electron generated due to previous PD per unit time (s^{-1})
Q_{cav}	Heat source density in the cavity (Wm^{-3})
Q_{mat}	Heat source density in the material (Wm^{-3})
R	Random number
T_{amb}	Ambient temperature (K)
T_{cav}	Temperature in the cavity (K)
T_{mat}	Temperature of the material (K)
T_{ons}	Temperature on the cavity surface (K)
T_0	Initial temperature in the cavity (K)
U_{app}	Applied voltage amplitude (V)
U_{ext}	Cavity extinction voltage (V)
U_{inc}	Cavity inception voltage (V)
U_{incapp}	Measured cavity inception voltage (V)
V	Potential (V)
V_c	Voltage across the cavity capacitance (V)
V_0	Potential at time zero (V)
α	Stress coefficient for the cavity surface conductivity ($mm \cdot kV^{-1}$)

α_e	Coefficient related to electron energy distribution and mean free path
β	Thermal coefficient for the cavity surface conductivity (K)
ε_{rcav}	Permittivity of the cavity
ε_{rs}	Permittivity of the cavity surface
ε_{rmat}	Permittivity of the material
κ	Constant for inception field equation ($\mathrm{kV{\cdot}mm^{-1}}$)
λ_e	Electron mean free path (m)
ρ_{cav}	Density of the cavity ($\mathrm{kgm^{-3}}$)
ρ_f	Free charge density ($\mathrm{Cm^{-3}}$)
ρ_{mat}	Density of the material ($\mathrm{kgm^{-3}}$)
σ_{cav}	Cavity conductivity ($\mathrm{Sm^{-1}}$)
σ_{cavmax}	Maximum cavity conductivity ($\mathrm{Sm^{-1}}$)
σ_{cav0}	Initial cavity conductivity ($\mathrm{Sm^{-1}}$)
σ_e	Electron conductivity in the plasma ($\mathrm{Sm^{-1}}$)
σ_{mat}	Material conductivity ($\mathrm{Sm^{-1}}$)
σ_s	Cavity surface conductivity ($\mathrm{Sm^{-1}}$)
σ_{smax}	Maximum cavity surface conductivity ($\mathrm{Sm^{-1}}$)
σ_{s0}	Initial cavity surface conductivity ($\mathrm{Sm^{-1}}$)
τ_s	Cavity surface time constant (s)
τ_{mat}	Material time constant (s)
τ_{dec}	Effective charge decay time constant (s)
τ_{stat}	Statistical time lag (s)
τ_{Tdecay}	Temperature decay time constant (s)
χ	Constant for inception field equation ($\mathrm{kV{\cdot}mm^{-1}K^{-1}}$)
Δt_0	Time step during no PD event (s)
Δt_1	Time step during PD event (s)
Ω	Cavity volume ($\mathrm{m^3}$)

AC	Alternating current
DAC	Damped alternating current
DC	Direct current
DSO	Digital signal oscilloscope
EGR	Electron generation rate
FEA	Finite Element Analysis
FDM	Finite Difference Method
GUI	Graphical user interface
LDPE	Low density polyethylene
MSE	Mean square error

PC	Personal computer
PD	Partial discharge
PDE	Partial differential equation
PE	Polyethylene
PRPDA	Phase resolved partial discharge analysis
PSA	Pulse sequential analysis
RMS	Root mean square
UV	Ultraviolet
VFPRPDA	Variable frequency phase resolved partial discharge analysis
VLF	Very low frequency

Acknowledgements

My upmost gratitude goes to God, the most gracious, most merciful, for all the blessings, which helped me to cope throughout this project.

I would like to give my deepest appreciation to my supervisors, Dr George Chen and Professor Paul Lewin for their continuous supports, time and valuable discussions in this research. They gave endless efforts, guidance, ideas and suggestions in assisting me to solve the problems encountered.

I would like to thank the University of Malaya, Malaysia for offering me the opportunity to do further studies abroad and Malaysian Ministry of Higher Education for providing me the scholarship.

Thanks to the Tony Davies High Voltage Laboratory for funding me during my remaining six month's stay with the Electrical Power Engineering (EPE) group.

I am grateful to Dr Liwei Hao, my colleague from the EPE group for assisting me with the experiment setup and sharing relevant knowledge and information.

Special thanks to Mr Neil Palmer and the lab technicians for supporting the entire lab works needed on time.

I thank to my friends for their care, support and faithful friendship. They kept my moral and spirit high throughout my studies.

Last but not least, thanks to my families in Malaysia for all their endless prayers, thought and supports, which have provided me strength and courage to complete this research.

To my dearest family...

Chapter 1

Introduction

1.1 Background

The diagnosis and performance assessment of an insulation system within a high voltage component are very important. Defects that exist within an insulation system can lead to insulation degradation, which may lead to breakdown of the insulation and consequently result in failure of the whole high voltage component. Examples of high voltage components which are prone to breakdown are power transmission lines, power cables, power generators and power transformers. One of the important phenomena to be considered in insulation diagnostics and performance assessment is partial discharge (PD) measurement. Insulation degradation due to defects present within it is nearly always linked to PD.

PD is a discharge event that does not bridge the electrodes of an electrical insulation system under high voltage stress. PD normally happens at defect sites, such as voids, cavities, cracks, joints and delaminations. Since PD only occurs within the defect in the insulation, it does not cause direct breakdown of the insulation immediately because the surrounding insulation is strong enough to avoid a complete breakdown of the material. Although PD does not cause immediate breakdown, it indicates the presence of a defect within the insulation which can affect its performance in a long term. For example, PD at a defect site within a high voltage application might cause energy loss and gradually degrade the insulation system [1]. The degradation of insulation due to repetition of PD may lead to system breakdown under certain conditions, depending on the type and location of the defect and the quality of the insulation design [2].

Failures in high voltage components due to insulation breakdown can result in costly and time consuming maintenance as the whole component may need to be replaced. Therefore, it is important to avoid such failure in insulation of high voltage applications before breakdown happens. This can be achieved through performing consistent maintenance on the related component by analysis and measurement of its insulation

properties. Thus the cost of maintenance can be reduced and the quality and reliability of the insulation system can be improved.

1.2 Motivation

PD measurement of insulation is an important diagnostic tool for insulation systems, as obtained results can be used to assess the condition of high voltage plant. One defect that generally exists within solid dielectric insulation is the presence of a void or cavity. Typically they are gas-filled and may be formed during the insulation manufacturing process. These defects might not be detectable during the factory testing but their effect might become obvious when under service stress. Since occluded gaseous voids within the insulation are potential sources of PD, they can lead to continuous deterioration of the insulation and consequently cause breakdown. Therefore, as PD monitoring has become an essential tool in assessing the performance of insulation materials, the modelling of PD is important in assisting the better understanding of PD phenomenon.

A lot of research has been reported on modelling of PD in cavities within dielectric insulation materials. The benefit of modelling PD activities is that the parameters affecting PD activity under different conditions can be readily assessed. The well-known PD models are the three capacitance model or so called 'abc' model [3–6], Pedersen's model [7–12], Niemeyer's model [13, 14] and Forssen's models, which uses the Finite Element Analysis (FEA) method [15–19]. A review of these models is detailed in Chapter 2.

There are various methods and techniques of measuring PD activity within insulation system in the past and present. Those measurement methods are used to evaluate and monitor the condition of the insulation. The PD measurement methods that are widely been used in insulation diagnosis are Pulse Sequence Analysis (PSA) technique [20] and Variable Frequency Phase Resolved Partial Discharge Analysis (VF-PRPDA) [21, 22]. Some traditional methods for PD activity measurement include Phase Resolved Partial Discharge Analysis (PRPDA) [5, 23, 24], the very low frequency (VLF) method and the damped ac voltage (DAC) method, [25–29]. These methods are also discussed in detail in Chapter 2.

1.3 Thesis objectives and aims

In this work, the measurement and simulation of PD activity within a spherical cavity have been performed for different amplitudes and frequencies of the applied voltage, cavity diameters and temperatures of the material. A spherical cavity is chosen as the shape of the cavity because in reality the most common types of cavity that exist within

insulation are spherical or ellipsoidal. Measurement and simulation of PD activity in a spherical cavity bounded by a solid dielectric insulation material under the changing sequence of the applied voltage amplitudes, applied frequencies and the material temperatures has not been widely reported. Therefore, comparisons between measurement and simulation results under different conditions have been performed. The model proposed in this work includes the effect of surface charge decay through surface conduction and temperature change in the cavity due to PD event.

The main objectives of this thesis are:

1. to develop a model describing PD activity within a spherical cavity in a homogeneous dielectric material in two-dimensional geometry using FEA method
2. to increase the understanding of PD phenomenon in a spherical cavity for different conditions of the cavity and stresses through PD model
3. to investigate the influence of spherical cavity sizes, applied voltage amplitudes, frequencies of the applied voltage and temperatures of the material on PD activity through PD measurements
4. to identify critical parameters from the model affecting PD through comparison between simulation and measurement results; these parameters are the statistical time lag, charge decay time constant, cavity surface conductivity, initial electron generation rate, inception field, extinction field and temperature decay time constant
5. to investigate the surface charge decay through conduction along the cavity wall after a PD occurrence for different applied stresses and cavity conditions
6. to study the effect of temperature change in the cavity after each PD on the next sequence of following PD
7. to compare the measurement and simulation of cycle to cycle behaviour of PD sequences

1.4 Contribution of the thesis

In this work, the modelling of PD activity in a spherical cavity within solid dielectric material has been further developed using the Finite Element Analysis (FEA) method. The advantage of using FEA in PD modelling is PD activity within a spherical cavity having a non-uniform electric field distribution also the temperature distribution in the cavity can be modelled precisely. This is an added advantage of using FEA model compared to an analytical approach. The modelling of two-dimensional electric field and

temperature distributions gives an insight into pre-disdischarge events that are occurring in the cavity.

In the FEA model that has been developed in this work, the role of cavity surface conductivity on the sequence of PD events has been included. This allows the effect of surface charge conduction along the cavity wall on the sequence of PD event can be studied for different sequences of amplitudes and frequencies of the applied voltage and temperatures of the material and for different cavity sizes. This has been achieved through comparison between measurement and simulation results. The charge conduction along the cavity wall has been associated with charge movement along the cavity wall, which depends on the magnitude and direction of the electric field in the cavity and on the cavity surface. The model simulation results have been improved by using the effect of charge conduction along the cavity wall on cavity surface conductivity, which depends on the electric field and cavity surface temperature.

A model using non-direct parameters for determination of electron generation rate has been found to effectively reproduce the measurement results, yet provides qualitative analysis on PD behaviour under different conditions of the applied stress and the cavity conditions. Thus, the model that has been developed is more flexible than previous approaches and adaptable to the conditions of the applied stress and the cavity conditions. The model has also been found to be consistent with the literature even though non-direct parameters have been determined using sensitivity anaylsis. This approach yields the lowest mean square error in comparison of simulation results with a range of measurement data.

The PD model has been extended to include the effect of temperature and pressure change in the cavity due to a PD event. The pressure change in the cavity is set as dependent on the temperature distribution, which in turn affects the cavity inception field level and the occurrence of PD events. Although many assumptions were used to model the temperature change in the cavity due to PD events, the obtained simulation results show that the sequence of PD events are affected differently for different conditions of the stress and cavity.

There are few reported works on the measurement of PD activity within cavities of different spherical cavity size but much reported research on different cylindrical cavity sizes. Manufacturing of a spherical cavity in a dielectric material is quite difficult because the gas bubble needs to be injected into the material at the right time during the curing process. Moreover, it is difficult to ensure that the initial conditions of the spherical cavity, such as the initial cavity pressure are the same.

A new method of manufacturing a single spherical cavity in a dielectric material has been introduced. The cavity is prepared by injecting a specific amount of air into a small amount of material during curing process. Then the material containing the cavity is cast into a larger amount of the material and left for curing process. Using

this technique, the material that is wasted due to unacceptable cavity shape after air injection can be minimised.

1.5 Thesis outline

This report is divided into 9 chapters. Chapter 1 contains the motivation of this work, the objective of the overall work and contributions in this work. Chapter 2 explains the background and literature review related to this work. This includes the introduction of PD, the PD event within a cavity, the generation of initial free electrons and the factors affecting PD in a cavity such as the statistical time lag, time constants, surface charge decay and pressure and temperature change in the cavity. In Chapter 3, the model and simulation program that have been developed are described. The development of the PD model using FEA software in parallel with MATLAB is detailed. This chapter includes the calculation of the inception field, initial electron generation rate equations, discharge model process, surface charge decay mechanism and temperature change in the cavity. The flowcharts of the MATLAB code are included. Chapter 4 details the preparation of the test samples and the measurement of PD activity for different conditions of the cavity and applied stresses that have been performed. The descriptions of the experiment, the process of sample preparation, the measurement methods and the data representation are explained. Chapter 5 presents the results obtained from the experiment and Chapter 6 presents the results from the simulation. Chapter 7 compares the measurement and simulation results that have been obtained for different amplitudes and frequencies of the applied voltage while Chapter 8 compares the measurement and simulation results for different cavity sizes and the temperatures of the material and the cycle to cycle behaviour of PD events that have been obtained. Finally, Chapter 9 details the discussion, conclusions and further work of this project.

Chapter 2

Partial Discharge Measurement and Simulation

This chapter concentrates on introducing concept of partial discharge (PD), PD mechanism in a cavity, measurement techniques that are used in PD measurement for insulation diagnosis, PD modelling which has increased the understanding of PD phenomenon and parameters associated with PD activity that been identified from PD models. The measurement techniques that are discussed which are used for PD measurement are Variable Frequency Phase Resolved Partial Discharge Analysis (VFPRPDA), Pulse Sequential Analysis (PSA), Phase Resolved Partial Discharge Analysis (PRPDA), Very Low Frequency (VLF) and Damped AC (DAC) methods. PD models which have enhanced the understanding of PD phenomenon are detailed; namely, three capacitance model, Pedersen's model, Niemeyer's model and Finite Element Analysis (FEA) model. Parameters from the models which have been identified to affect PD activity, such as time constants, statistical time lag and inception field are also detailed.

2.1 Partial discharge within a cavity in a solid dielectric

Partial discharge (PD) is a discharge event that does not bridge the electrodes within an electrical insulation system under high field stress. When PD happens, discharge starts from one end of the cavity surface, bridging through the gas-filled cavity and reaches the other end of the cavity surface. Thus, PD only bridges the cavity and does not bridge the whole insulation between electrodes. PD normally happens in the presence of defect within an insulation under a high electric field. Examples of defects that may exist in polymeric insulation are voids, cracks, cavities or delaminations.

Partial discharge in a solid dielectric material usually occurs in gas-filled cavities within the material. Since the permittivity of the gas is less than the permittivity of the

surrounding material, the electric field in the cavity is higher than the material. When the electric field in the cavity is sufficiently high and the breakdown strength of the gas in the cavity is exceeded, PD can occur [30, 31]. During the PD event, the gas changes property from a non-conducting to a conducting condition, resulting in the electric field within the cavity dropping from a higher to a lower value in a very short period of time [32]. Figure 2.1 shows a basic diagram of PD within a cavity in a dielectric material which is stressed under a high electric field.

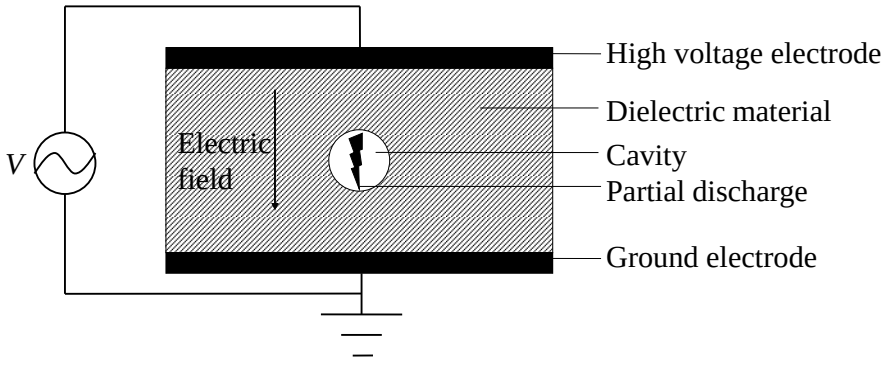

FIGURE 2.1: Basic diagram of PD within a cavity in a dielectric material.

The effect of PD within a cavity in high voltage insulation can be very serious because it can ultimately lead to complete failure of the whole system. Repetition of PD causes progressive chemical deterioration of the material. The chemical transformation on the cavity surface may increase the conductivity of the cavity surface. It may also cause the pressure in the cavity to change due to creation of gaseous by-products, depending on the type of the gas content in the cavity and the material surrounding the cavity [33]. It is theoretically proposed that cumulative effect of PD in a cavity is the formation of numerous, branching partially conducting discharge channels in the material, called electrical treeing [2, 34]. Electrical treeing is a significant degradation mechanism that can lead to insulation breakdown and consequently leading to breakdown of the insulation system when the tree channels form a conducting path between the electrodes [34–36].

There are several types of discharge other than partial discharge, including surface discharge and corona discharge. Surface discharge is a discharge event that occurs on an insulation surface where the tangential field across the surface is high. This discharge can bridge the potential difference between the high voltage source and the ground electrode through cracks or contaminated paths on the insulation surface. Examples of surface discharge in the field are on the insulation surface of a high voltage cables or at the end-windings of stator windings of large generators [21]. Corona discharge is discharge in gas due to a locally enhanced field from a sharp point of an electrode which ionizes the surrounding gas molecules [37].

2.2 Partial discharge mechanism

The study of PD can be subdivided into three main categories, namely PD models, ageing and degradation models and breakdown models. However, the main focus of this work is modeling of PD activity within a cavity in a solid dielectric material prior to the development of degradation. In example, the model in this work does not consider degradation of the cavity surface charges due to chemical and physical modifications as a result of PD repetitions. For this purpose, all PD measurements are limited to a short duration of the applied stress, i.e. only up to maximum 10 hours of the applied stress. An understanding of the PD mechanism is required before developing a PD model. A cavity is a gas-filled void within a dielectric material which may be created during manufacturing process, installation or operation of a high voltage system [38,39]. To ensure PD activity occurs in a cavity, the electric field in the cavity must exceed the breakdown strength of the gas and there must also be free electrons available to initiate an electron avalanche [25,40]. The electric field at which the breakdown strength of the gas in the cavity is exceeded is defined as the cavity inception field, E_{inc}.

Since the breakdown strength of the gas is lower than the dielectric material, discharge occurs at an electric field lower than the breakdown strength of the solid material. When the electric field in the cavity is higher than the breakdown strength of the gas and there is an electron available, the electron will be accelerated by the applied electric field in the cavity. When the electron accelerates across the cavity, it will interact with neutral gas molecules. If the energy of the accelerated electron is high enough, it will ionize any gas molecule it collides with, resulting in the release of a new electron, positive ion, heat and other byproducts in the cavity. This process is called ionization. The recently generated free electron collides with other gas molecules in the cavity and this process repeats. More free electrons are generated, resulting in an increase in the number of electrons. The repetition of gas ionization is called as electron avalanche.

The electron avalanche may grow significantly in size until it forms channels in the cavity. The pattern of channels formed determines the type of the discharge. A streamer discharge type is considered in this work because PD pulses produced from streamer discharge are large enough to be detected by PD measurement equipment [13], where its duration is usually between 1 to 100 ns [41] and its magnitude is larger than 10 pC. The streamer is an ionized channel with branches of electron avalanches which consist of moving free electrons under the influence of the applied field. During the avalanche process, the temperature in the cavity increases due to heat energy released from ionization. This causes the pressure in the cavity to increase. The conductivity of the streamer also increases due to the movement of free electrons in the streamer. Thus, the current in the channel increases and this results in further increment of the cavity conductivity.

As streamer develops, the electric field in the cavity decreases [37]. Figure 2.2 illustrates

this event. Referring to Figure 2.2(a), before a discharge occurs, the electric field in the cavity, E_{cav} is equal to f_cE_0 where f_c is the modification factor of the applied field in the cavity, depending on the cavity geometry and the material permittivity and E_0 is the applied field. The field f_cE_0 is called the Laplacian field. Referring to Figure 2.2(b) and Figure 2.2(c), when a discharge occurs, as opposite charges reach the other end of the cavity surface, an electric field that is opposite of f_cE_0 develops. This opposing field, E_s which is due to charge accumulation on the cavity surface after a PD, is called the Poisonnian field [14]. The electric field in the cavity, E_{cav} is defined as

$$E_{cav} = f_cE_0 + E_s \tag{2.1}$$

Thus, the electric field in the cavity is reduced after a PD. Since the discharge happens very rapidly, typically over a few nanoseconds, the field in the cavity drops sharply over a short duration [13]. When the electric field in the cavity decreases, free electrons lose their energy and the current and conductivity in the streamer channel decrease. When the field in the cavity drops to less than the extinction field, E_{ext} the streamer channel collapses and discharge stops.

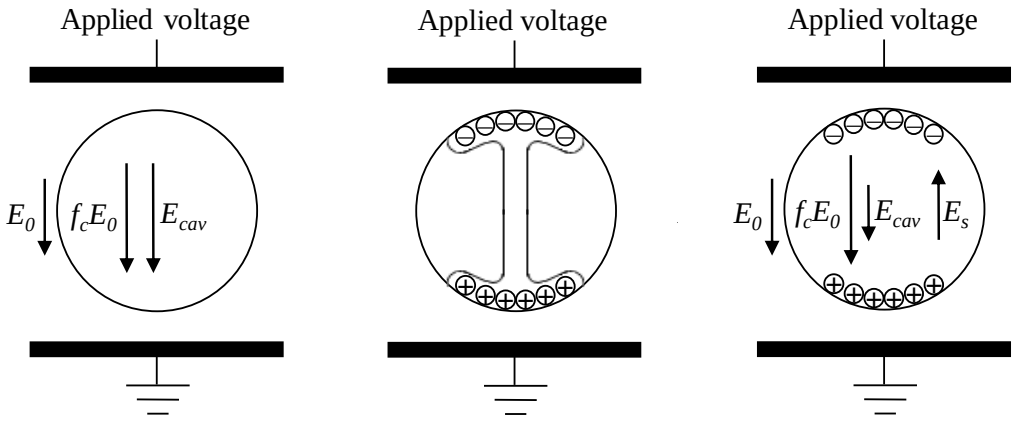

(a) Before PD (b) During PD (c) After PD

FIGURE 2.2: Schematic diagram of PD event.

2.3 Partial discharge measurement techniques

2.3.1 Pulse Sequential analysis (PSA)

Pulse sequential analysis (PSA) has been used to monitor the degradation of an electrical equipment by analysing the sequence of each PD event, which is evaluated through the voltage or time difference between two consecutive discharge distributions [20, 40]. This method is different from classical methods because it does not ignore the individual

discharge sequence and it is not based on distributions of the magnitude and phase of PD. However, in reality, PD occurrence is determined by the local electric field within the cavity but not the phase of the applied voltage. Thus, through analysing the sequence of discharges, local defects can be characterized more precisely and single or multiple discharge sites can be clearly distinguished. The PSA method also manages to reveal the effect of surface charge accumulation after each discharge, where each discharge changes the local conditions for the generation of the next PD and the phase of discharges are shifted because of surface charge accumulation [42].

2.3.2 Variable Frequency Phase Resolved Partial Discharge Analysis (VFPRPDA)

A technique that is widely used in PD monitoring and measurement system is known as Variable Frequency Phase Resolved Partial Discharge Analysis (VFPRPDA) [21,22]. VFPRPDA can measure PD as a function of frequency of the applied voltage and this is its advantage because more information about the conditions of a material can be obtained. VFPRPDA provides a pattern of the numbers of PD occur with a specific charge magnitude and at phase of the applied voltage. This method has been used to study the PD frequency dependent behaviour within a cylindrical cavity in a dielectric material for frequency 10 mHz 100 Hz [22]. The influence of cavity size and cavity location within the material on PD frequency dependent nature and the effect of variable applied frequency on PD activities on in-service aged machine insulation have also been studied using VF-PRPDA [43,44]. The measurement results show that the PD pattern is strongly dependent on the frequency of the applied voltage.

2.3.3 Previous PD Measurement methods

Prior to the VF-PRPDA technique, there are many traditional ways of measuring PD activity in insulation diagnostics. One of the techniques is Phase Resolved Partial Discharge Analysis (PRPDA), where PDs are measured at the power frequency of the applied voltage [23]. PRPDA is one of the established tools for insulation system diagnosis. The PRPD patterns have been used widely in characterizing the stage of insulation aging through changes in PRPD patterns [5,24]. The PRPDA method has been used to detect and locate PD activity in high voltage components, such as in cable insulation and cable joints [21]. PRPD patterns can be represented by phase and discharge magnitude distributions, which has been used to classify the types and locations of discharge sources with the aid of statistical tools [45,46]. Other traditional PD measurement methods include the very low frequency (VLF) method, which measures the phase and magnitude of PD at frequency 0.1 Hz of the applied voltage and the damped ac voltage (DAC) method, which measures PD activity at damped ac voltages in the range

of frequency 20-1000 Hz with different settling time [25–29]. The VLF method is only good for cables or plant that are predominantly capacitive, i.e. they can retain surface charges accumulated at the defect site for a longer period of time. Under a very low frequency stress, surface charges that have accumulated since previous PD occurrence may have decayed completely when the next PD is likely to occur. This may result in the obtained PD patterns to be very different than at power frequency. Thus, insulation must be able to retain surface charge accumulated at the defect site for a longer period of time when VLF method is used in PD measurement.

2.4 Partial discharge modelling

2.4.1 Three capacitance models

A previous PD model using a three-capacitor circuit model or 'abc' model representing an isolated cavity within a dielectric material has been developed [45]. Discharge is represented by an instantaneous change in the charging of a capacitance in the test object. A similar model has been used to study PD behaviour [3–6]. The statistical behaviour of this three-capacitance circuit is very complex even though the circuit is simple and deterministic [6]. However, this model is not realistic in describing cavity properties because in a real cavity, there is surface charge accumulation on the cavity surface after a discharge occurs and the cavity surface is not an equipotential surface [47]. There is an improved 'abc'-model which has considered charge accumulation on the cavity surface after a discharge [48]. The discharge is simulated as a time and voltage dependent resistance, which represents the discharge event as a change in the cavity from being insulating to conducting.

Figure 2.3 shows typical the three-capacitance equivalent circuit or 'abc' model of a cavity within a dielectric material. C_{a1} and C_{a2} represent the capacitance in the material which is cavity-free, C_{b1} and C_{b2} represent the capacitance in the material in series with the cavity, C_c represents the cavity capacitance and V is the applied voltage. The simplified equivalent circuit can be derived from the geometry, as shown in Figure 2.3(b), where C_a is the equivalent parallel capacitance of C_{a1} and C_{a2}, C_b is the equivalent series capacitance of C_{b1} and C_{b2} and V_c is the voltage across the cavity.

Discharge is assumed to occur when the voltage across the cavity capacitance, V_c is higher than the inception voltage, U_{inc} and stops when it is less than the extinction voltage, U_{ext}. When a discharge occurs, C_c is short circuited, causing a fast transient current to flow in the circuit due to voltage difference between the voltage source and across C_b. A fast transient voltage signal is created due to sudden voltage drop due to impedance of the external circuit.

Although this model is simple, it can represent the transient related to a discharge

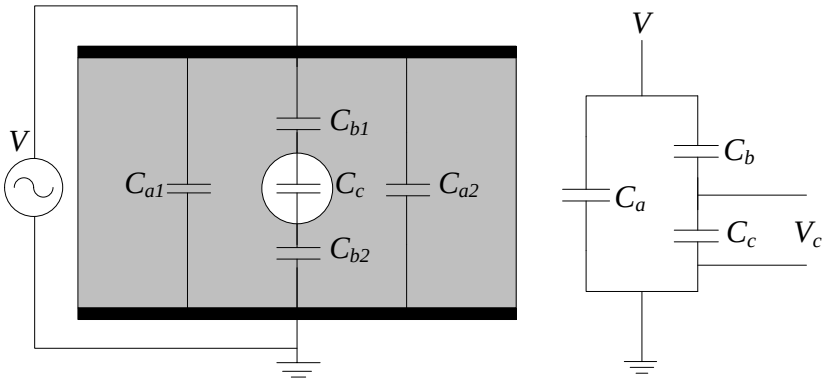

(a) Overall model (b) Simplified model

FIGURE 2.3: The three-capacitance equivalent circuit representing PD in a cavity.

event, such as the PD current pulse and apparent charge magnitude as a function of time, which is resulted from a voltage across the cavity due to a discharge. However, the disadvantages of the capacitance models are the cavity surface is not an equipotential surface, there is surface charge accumulation along the cavity wall and the transient cannot be related to changes in capacitance as has been suggested by the induced charge concept model.

2.4.2 Pedersen's model

Pedersen introduced the induced charge concept which is associated with partial discharge in a cavity [7–12]. The induced charge is expressed as the difference between the charge on the electrode before and after a discharge occurrence in the cavity. Charge deployment on the cavity surface during the PD occurrence increases the surface charge density, reducing the electric field in the cavity and discharge stops once the field becomes less than a certain value. The induced positive and negative charges on both cavity surfaces build dipole orientation, as a result of field due to these charges. This will induce charge on the electrode as well. The induced charge on the electrode due to charge distribution on the cavity surface, q has been defined as

$$q = -\vec{\mu} \bullet \vec{\nabla}\lambda = -\left(\int_s \vec{r}\sigma dS\right) \bullet \vec{\nabla}\lambda \tag{2.2}$$

where $\vec{\mu}$ is the dipole moment induced due to charge deposition on the cavity surface, S, $\vec{r}$ is the radius vector along the surface S, σ is the charge density deposited on the cavity surface and λ is a dimensionless scalar function which depends on the position of dS, which is obtained from Laplace's equation.

If the cavity geometry is considered either as a spherical or ellipsoidal cavity, the induced charge on the electrode or the apparent charge magnitude from Equation 2.2 can be

expressed as

$$q = -K\Omega\varepsilon(E_{inc} - E_{ext})\vec{\nabla}\lambda_0 \tag{2.3}$$

where K is a dimensional constant which depends on the cavity size and geometry, Ω is the cavity volume, ε is the material permittivity, and E_{inc} is the inception field, the field when a PD occurs, and E_{ext} is the extinction field, the field when PD stops and λ_0 is the solution to Laplace's equation at the location of the cavity for the cavity free material [11]. The boundary condition to solve the Laplace equation is $\lambda_0 = 1$ at the measuring electrode and $\lambda_0 = 0$ at another electrode.

The transient related to induced charge has been observed, by looking at the potential and charge on the electrode before and after a PD occurs [11]. Before a PD occurs, the potential and charge on the electrode is V and Q. After a PD occurs, the potential on the electrode drops by ΔV but the charge on the electrode increases by ΔQ, which is the charge supplied from the external system to the electrode. Thus, the induced charge on the electrode can be written as

$$q = C\Delta V + \Delta Q \approx C\Delta V \tag{2.4}$$

where C is the capacitance of the system. If the impedance of the circuit is large for the current due to the discharge, the term ΔQ in Equation 2.4 can be neglected.

2.4.3 Niemeyer's model

A PD model that simulates a discharge of streamer type has been developed previously [13]. The model includes, in detail, the mathematical model of initial electron generation equations, model of streamer process and the estimation of PD charge magnitude. The electric field in the cavity is obtained by solving Poisson's equation and the field enhancement in the cavity is averaged to obtain a field enhancement factor. This factor is used to estimate the field enhancement due to the applied field and due to the surface charge in a cavity. The model is then used to simulate PD activity in a spherical void and the results are compared with experimental data. Poisson's equation is solved because there is the effect of field due to surface charge on the net electric field in the cavity. The initial free electron generation for a PD to occur has been categorized into surface emission and volume ionization, where associated equations relating to physical parameters of the material have been derived.

The PD real charge magnitude was calculated by using $c\Delta U_{PD}$, where ΔU_{PD} is the voltage drop across the cavity due to PD and c is the cavity capacitance which depends on the cavity geometry [13]. The apparent charge due to a PD is measured as the charge

induced on the measurement electrode, which depends on the cavity location within the material, the cavity shape, the gas pressure and the cavity orientation against the applied field [9, 11, 49].

The simulation agrees with experimental data qualitatively and quantitatively although there is a slight disagreement in the phase and magnitude distributions of PD. Another PD model also uses the similar field enhancement estimation method to simulate PD mechanism at high temperature within a spherical cavity in an epoxy resin [50]. A stochastic discharge model has been developed and used to simulate a streamer type PD in spherical cavity within an epoxy resin and the model has been used to characterize PD in voids and the change in behaviour due to aging [14]. Although these models provide good descriptions of PD activity, the comparison between experiment and simulation results is only undertaken for a single value of applied stress.

2.4.4 Finite Element Analysis model

A field-based PD model has been developed using a Finite Element Analysis (FEA) software by Cecilia Forssen from KTH Royal Institute of Technology in Stockholm, Sweden [15, 17, 19]. The model has been used to simulate PD frequency dependent behaviour within a cylindrical cavity in a dielectric material at variable frequency of the applied voltage. The model geometry consists of two spherical electrodes, a dielectric material and a cylindrical cavity. The model is simulated dynamically and is interfaced with a MATLAB code. The discharge process is modelled as an increase of the conductivity in the cavity and the electric field in the model is calculated numerically using FEA method. The apparent charge magnitude is calculated by time integration of current through the ground electrode during a PD event. The charge conduction along the cavity wall has been modelled by using different cavity surface conductivity value, which depends on the amount of free surface charge along the cavity wall. The simulation results have been compared with the measurement data. The results are in general agreement but with a slightly difference, which might be due to the over-simplified initial electron generation rate equation in the model. A similar PD model has also been developed in the University of Southampton using COMSOL and MATLAB software to compare the simulation results with the previous model [51, 52].

2.5 Initial Electron Generation

One of the conditions for a PD to occur within a cavity in a dielectric material is that there must be an initial free electron available to start an electron avalanche [30]. From the past PD models, the main source of an initial free initial electron can be subdivided into two category, surface emission and volume ionization [13, 25].

2.5.1 Surface emission

Surface emission is an electron generation process where free electrons are emitted from the cavity surface under the influence of an electric field and temperature. Sources of surface emission are detrapping of electrons from shallow traps on or near the cavity surface, electron injection from the electrode, free electrons that still remain on the surface due to a previous discharge and electrons released due to impact ionization processes. Surface emission from the cavity wall is the main source of free electrons in a cavity with ongoing PD activity [13,53]. Surface emission is enhanced by the detrapping of electrons from the shallow traps in the cavity surface due to previous PD as charges in shallow traps are easier to detrap than in deeper traps. This process can be further enhanced by increasing the electric field or cavity temperature [54]. Initial electron generation is highly dependent on the applied voltage amplitude, material conductivity and permittivity, as well as the size, shape and location of the cavity within the material.

Electron avalanche can develop along the cavity surface that is parallel with the applied field. When an electron from the cavity surface is released by photo ionization, electron ionizations can happen along the cavity wall. The resulting electron avalanche along the cavity wall causes electrons accumulation at one end of the cavity surface but the same amount of positive charges are trapped in the material region where the electrons have accumulated. This case normally happens in a very narrow cavity which is parallel with the applied electric field.

2.5.2 Volume ionization

Sources of volume ionization of initial electron generation are radiative gas ionization by energetic photon and field detachment of electrons from negative ions [55]. Volume conduction depends on the gas pressure, gas volume exposed to the ionization and the gas contents in the cavity. Radiation ionization is a process where an electron is released from a neutral gas molecule by highly-energetic particles. It is the main source of initial free electron in cavities that have never experienced PD yet because the detrapping work function of the cavity surface is normally higher than an active cavity [13]. A free electron can also be generated by photo ionization, where the gas molecule absorbs light of sufficient energy and causes an electron to leave the gas molecule.

2.6 Parameters affecting PD activity

PD within a cavity in a solid dielectric material is known to be influenced by the applied stresses and the cavity conditions. The stress conditions that affect PD within a cavity are the amplitude, frequency and waveform shape of the applied voltage and the ambient

temperature of the material [21, 25, 44, 56–58] [15, 59]. The cavity conditions that influence PD activity are the size and shape of the cavity, the location of the cavity within the dielectric and the humidity level and initial pressure in the cavity [22, 43, 60–62]. From previous PD models, parameters that are affecting PD activity are time constants related to charge transport and the PD charge decay rate, the statistical time lag, temporal pressure change in the cavity and the inception field.

2.6.1 Time constants

The charges due to PD that are accumulated on the cavity surface may decay with time [13, 14, 50]. Surface charge can decay through charge recombination in the cavity, conduction along the cavity wall, charge movement into the deeper traps in the cavity surface and charge neutralization by gas ions from natural background radiation in the cavity. The PD charge decay has been considered in several PD models [13, 14, 63, 64].

There are three time constants related to charge transport and the PD charge decay rate associated with electric field distributions on the cavity surface [13, 15, 25]. They are the cavity surface time constant, τ_s, the effective charge decay time constant, τ_{dec} and the material time constant, τ_{mat}. These time constants determine the variation of PD phase and charge magnitude distributions.

After a PD occurs in a cavity, there are charges accumulated on the cavity surface, which may be able to move freely along the cavity wall through cavity surface conduction. When opposite sign charges meet each other on the cavity wall, charge recombination occurs, resulting in the amount of free surface charge to decay. This decay rate is determined by the cavity surface time constant, τ_s. It depends on the value of cavity surface conductivity, σ_s [13, 14, 22, 63–65]. If σ_s is higher, the cavity surface charge decay rate is faster, reducing the initial electron generation rate between two consecutive discharges [25]. If the period of the applied voltage is larger than τ_s, the charge decay rate through surface conduction is significant. The relationship between τ_s and σ_s has been developed by using the RC cavity model, which has found that τ_s is shorter when σ_s is higher [13, 25]. An increase in the cavity surface conductivity is believed to be due to chemical deterioration of the cavity surface altered by repeated discharges and the aging state of the cavity [64, 66]. Aged cavity surfaces, which have been exposed to PD activity experience physical and chemical modifications that are responsible for an increase in cavity surface conductivity [66, 67].

Some charges due to PD a event in a cavity will be trapped in shallow traps within a dielectric material when they reach the cavity surface. After certain period of time, these charges may have moved into deeper traps of the material near the cavity surface. The rate of charge movement from shallow traps into deeper traps is determined by the charge decay time constant, τ_{dec} [13, 14, 50]. A smaller time constant means a faster rate

of charge decay through charge movement into deeper traps. If the period of the applied voltage is larger than τ_{dec}, the charge decay rate is significant. This causes the electron generation rate to decrease but the local electric field remains unaffected because charges in deeper traps still contribute to the field of the cavity surface. However, electrons in deeper traps are less likely to contribute to the initiation of a PD than those in shallow traps.

Surface charges that have accumulated along the cavity wall after a PD occurs may also move into the bulk material through material volume conduction. This results in the amount of surface charges along the cavity wall to decrease with time. The decay rate of surface charge through this mechanism is controlled by the material time constant, τ_{mat} [22]. It depends on the material conductivity [22]. A smaller τ_{mat} causes faster surface charge decay rate, reducing the field of cavity surface charge and the number of electrons available for the next PD becomes lower. However, the surface charge decay rate through volume conduction in the material is generally slow compared to the frequency of the applied voltage used in the experiment due to a very low value of material volume conductivity. This type of surface charge decay is not significant, therefore, it is neglected in the developed model for this thesis.

2.6.2 Statistical time lag

When the inception field in the cavity, E_{inc} has been exceeded, a free electron may not be present to start an electron avalanche. Hence, there may be a delay before PD occurrence. This delay can be represented as a statistical time lag, τ_{stat}, which indicates the time difference between the field in the cavity exceeds E_{inc} and the PD event [13, 15, 17]. Due to τ_{stat}, discharge often occurs at field higher than E_{inc}.

Because of the variation of the electron generation rate with stress conditions, the statistical time lag will be dependent on the amplitude and frequency of the applied voltage. At higher frequencies, the time interval between consecutive PD occurrences is reduced and more charges from previous PD are available for the next PD. Thus, the electron generation rate is higher; reducing the statistical time lag and the next discharge might start immediately after the inception field is exceeded. However, at lower frequencies, less charge from the previous PD are available for the next PD because of a larger amount of charge loss and the electron generation rate is smaller when the next PD is likely to occur. Hence, τ_{stat} is greater and discharge may not start immediately after the inception field is exceeded [68]. Whilst at higher applied voltage amplitudes, τ_{stat} is expected to be smaller because of the enhanced supply of charges from the electrode. Thus, the total number of PD occurrences per cycle may be seen to increase as a function of the voltage amplitude.

The statistical time lag may vary between consecutive discharges. The delay for the

first PD occurrence may be longer than the following PD within the same cycle of the applied voltage. In a cavity that has never experienced any PD, there is a lack of free electron available. However, after the first PD occurs, there are charges accumulated on the cavity surface, which act as the source of free electrons for the following PD. Thus, the delay of free electrons available for the subsequent discharge is shorter than the first discharge. Since the surface charges accumulated on the cavity surface may decay in time, the amount of charges available for the next PD decreases. Hence, the delay between two consecutive discharges depends on the availability of free electrons and the charge decay rate [14].

2.6.3 Temperature change in the cavity due to PD events

During electron ionization, when a free electron collides with a neutral gas molecule, an electron is released from the gas molecule and heat energy is produced, resulting in an increase in the temperature of the cavity. This may cause the pressure in the cavity to increase, which in turn increases the inception field level because the inception field depends on the pressure in the cavity.

However, the heat energy generated in the cavity decreases in time as it dissipates through the material surrounding the cavity. The pressure will then recover to its initial value. The temperature decay time constant, τ_{Tdecay}, of a hot gas in the cavity depends on the size and shape of the cavity, the initial temperature of the hot gas and the material thermal properties surrounding the hot gas. A smaller size of a hot gas recovers faster because heat can dissipate faster through the surrounding material. The properties of the gas that are temperature and pressure dependent include; the thermal conductivity, mass density, specific heat per unit mass and heat transfer coefficient between the hot gas and the material [69]. From the physical properties of the gas at different temperatures, the calculated temperature decay time constant decreases with the initial gas temperature, where the hot gas temperature recovers faster to its initial value when its initial temperature is higher [70]. The heat transfer from the hot gas in the cavity to the material surrounding the cavity may be through convection, conduction or radiation.

There is a report on a model of hot gas due to an arc in a sphere gap, which uses a lumped heat capacity model, where the hot gas is assumed to resemble a spherical body [69, 70]. The temperature of the hot gas is assumed uniform in the whole gas throughout recovery and the shape of the hot gas is assumed to be always the same size. The model uses a concept where the temperature of the entire body is uniform even though it is cooled from the outside by its surroundings. The results of the temperature decay as a function of time have been compared between the simulations from the model and the measurement. Both of them are in reasonable agreement.

The effect of temperature change in the cavity on PD activity is more significant when τ_{Tdecay} is longer than the period of the applied voltage. At higher applied frequencies, the temperature change in the cavity has more significant effect on PD activity. Due to smaller time interval between consecutive discharges, there is less recovery time of pressure and temperature in the cavity towards their initial values. Consequently, the subsequent discharge occurs at higher field in the cavity because the inception field is higher. When the pressure in the cavity is too high, the inception field also becomes very high, resulting in no PD occurs at all because the inception field is never exceeded. PD activity can occur again once the inception field has reduced until it can be exceeded. Therefore, a very large increment of pressure and temperature in the cavity may be one of the reasons that results in a temporary inactive PD activity.

There is a PD model based on the Finite Difference Method (FDM) which simulates PD patterns for certain numbers of voltage cycles. The model uses a stochastic factor of a different probability distribution when determining the occurrence of PD. A lower probability of PD occurrence was used when the temperature on the cavity surface is higher than the initial temperature [71]. This has been associated with the increase in the cavity surface roughness as the temperature in the cavity keeps increasing due to aging, resulting in a higher cavity surface work function. Thus, the probability of PD occurrence becomes lower for higher surface temperatures. However, no comparison between measurement and simulation results have been reported.

2.6.4 Inception field

The inception field in the cavity, E_{inc} is the minimum field in the cavity that is required for a PD to occur. The inception field for a streamer type PD in a spherical cavity depends on the cavity geometry, pressure in the cavity, the dielectric permittivity, characteristics of ionization process in the gas and the distance between the two electrodes [13, 14, 50, 68]. In other published research, for streamer type discharge, the cavity inception field, E_{inc} has been defined as [13, 14, 50, 68]

$$E_{inc} = \left(\frac{E}{p}\right)_{cr} p\left[1 + \frac{B}{(pd)^n}\right] \tag{2.5}$$

where $(E/p)_{cr}$, B and n are parameters associated with ionization processes in the gas, p is the pressure in the cavity and d is the cavity diameter. For air, $(E/p)_{cr} = 24.2$ $\mathrm{VPa^{-1}m^{-1}}$, $n = 0.5$ and $B = 8.6$ $\mathrm{Pa^{1/2}}$ [11, 13, 30]. The derivation of Equation 2.5 is shown in Appendix D. The inception voltage obtained from the measurement, U_{incapp} is the applied voltage level at which the inception field in the cavity is exceeded.

2.7 Summary

There are many tools that have been used in PD measurement for insulation diagnosis and condition monitoring of high voltage insulation system in the past and present, including PSA, VFPRPDA, PRPDA, DAC and VLF methods. A better understanding of PD phenomena can be attained through modelling the discharge process. The well-known PD models that have been developed include three capacitance model, Pedersen's model, Niemeyer's model and FEA model. Parameters that are influencing PD activity within cavities in solid dielectric materials have been identified from PD models. These include statistical time lag, effective charge decay time constant, cavity surface time constant, temperature decay time constant and the inception field. Sources of initial free electron for a PD to occur are mainly through electron surface emission and volume ionization in the cavity. It is widely accepted that the stress conditions affecting PD behaviour in cavities are the amplitude and frequency of the applied voltage and the temperature of the material while the cavity conditions affecting PD behaviour are the cavity size, shape and location within the material.

Chapter 3

Partial Discharge Model

The PD model developed in this work is based on the Finite Element Analysis (FEA) model that was originally proposed by Cecilia Forssen. The development of a model that consists of a spherical cavity within a solid dielectric material using FEA method to model PD activity is detailed in this chapter. The two-dimensional model geometry using the FEA method, equations associated with the model and the flowcharts of the MATLAB code are explained. The PD modelling section is divided into several parts; FEA model equations, development of the model, local field enhancement, discharge process model, discharge magnitude calculation, temperature change in the cavity due to PD, surface charge decay through conduction along the cavity wall after a PD occurs and the electron generation rate. In order to simplify the simulation model, several assumptions have been made. The advantages of this model over previous models are also discussed.

The model has been used to simulate partial discharge (PD) activity in the cavity for various conditions of the stress and cavity conditions, which are the amplitudes and frequencies of the applied voltage, temperature of the material and different sizes of cavity. The obtained simulation results are then compared with measurement results to determine the critical parameters affecting PD activity and also to identify physical mechanisms affecting PD activity for different conditions. The critical parameters include the inception and extinction fields, effective charge decay time constant and the cavity surface conductivity. The physical mechanisms which can be identified from this model which are associated with PD activity are charge conduction along the cavity wall, electron generation rate process, temperature change in the cavity and the electron generation rate.

3.1 Finite Element Analysis model

The model is implemented in two-dimensional (2D) axial symmetric COMSOL software and is interfaced with MATLAB programming code [72]. The electric potential and temperature in the model are solved using Partial Differential Equations (PDE). PDE equations are rendered into Ordinary Differential Equations (ODE) and ODEs are solved. Through developing the model using 2D axial symmetric geometry, the simulation time can be reduced because of the need of less mesh elements. Two application modes are chosen to solve the problem in the model, 'Meridional Electric Current' and 'Heat Transfer by Conduction'. In the 'Model Navigator' window of COMSOL, the '2D Axial Symmetry' space dimension is chosen and the 'Quasi Statics, Electric' is selected under the 'AC/DC Module' to solve the electric field distribution and 'Conduction' under 'Heat Transfer Module' is added to the Multiphysics to solve the temperature distribution in the model.

3.1.1 Field model equation

The electric potential distribution in the dielectric is described by the field model. The basic governing equations of the field model are

$$\vec{\nabla} \bullet \vec{D} = \rho_f \tag{3.1}$$

$$\vec{\nabla} \bullet \vec{J_f} + \frac{\partial \rho_f}{\partial t} = 0 \tag{3.2}$$

where Equation 3.1 is the field model equation, Equation 3.2 is the current continuity equation, $\vec{D}$ is the electric displacement field, ρ_f the free charge density or unpaired charge density and $\vec{J_f}$ is the free current density [73]. Assuming that the dielectric model is non-dispersive, linear isotropic material with an instantaneous polarization which is exposed to slowly varying field, Equation 3.1 can be written as

$$\vec{\nabla} \bullet \vec{D} = \vec{\nabla} \bullet (\varepsilon \vec{E}) = -\vec{\nabla} \bullet (\varepsilon \vec{\nabla} V) \tag{3.3}$$

where ε is the permittivity of the material, $\vec{E}$ is the electric field and V is the electric potential. Since $\vec{J_f}$ is equal to $-\sigma\vec{\nabla}V$ and ρ_f is equal to $-\vec{\nabla}\bullet(\varepsilon\vec{\nabla}V)$ where σ is the electric conductivity, Equation 3.3 can also be written as

$$-\vec{\nabla} \bullet \left(\sigma \vec{\nabla} V\right) - \vec{\nabla} \bullet \frac{\partial}{\partial t}\left(\varepsilon \vec{\nabla} V\right) = 0 \tag{3.4}$$

FEA is used to solve Equation 3.4 and determine the electric potential in the model.

3.1.2 Heat transfer equation

To study the temperature distribution in the cavity due to a PD, the heat energy released from electron ionization during a PD is assumed to be transferred to the cavity through heat conduction, i.e. when the cavity changes its state from a non-conducting to a conducting state. Thus, the temperature distribution can be calculated using 'Heat Transfer Module by conduction' in the FEA software. The governing PDE equation is

$$\rho C \left(\frac{\partial T}{\partial t} \right) - \vec{\nabla} \bullet (k \vec{\nabla} T) = Q \tag{3.5}$$

where ρ is the density, C is the specific heat capacity, T is the temperature, k is the thermal conductivity and Q is the heat source density. The derivation of Equation 3.5 is shown in C.

3.1.3 Model geometry and mesh

Figure 3.1 to Figure 3.3 show details of the 2D axial-symmetric model geometry and the boundary line numbers of the test object that has been developed. The model consists of a homogenous dielectric material of 2.0 mm thickness and 10 mm diameter, a hemispherical cavity of 1.4 mm diameter due to the centre axis of symmetry and the cavity surface of 0.05 mm thickness to model surface charge decay through conduction along the cavity wall. The maximum cross-sectional area of the cavity centre is used to calculate dynamic current during PD for PD real charge magnitude calculation. The horizontal line in Figure 3.1 shows the centre of the cavity. A sinusoidal voltage is applied to the upper electrode while the lower electrode is always grounded. A 2D unstructured mesh with triangular elements is used. The meshes in the cavity and on the cavity surface are refined because higher accuracy is needed in electric potential calculation within these parts. The meshing in the model is shown in Figure 3.4.

3.1.4 Boundary and subdomain settings

Table 3.1 to Table 3.6 show the assigned constants, subdomain settings and boundary settings of the model that are used for the simulation.

After the boundaries and subdomains of the model have been set and assigned, the model is meshed and ready to be solved. The 'Transient, electric currents' analysis with 'Time dependent' solver is selected under the 'Solver Parameters'. The time stepping is set

at 0:0.0025:0.005. Then, the model is solved by clicking the 'Solve Problem' under the 'Solve' tab. The solution can be obtained if there is no error in the model. The electric field and temperature distributions in the model can be obtained by selecting options under the 'Postprocessing' tab in the 'Plot Parameter' window. The solved model is

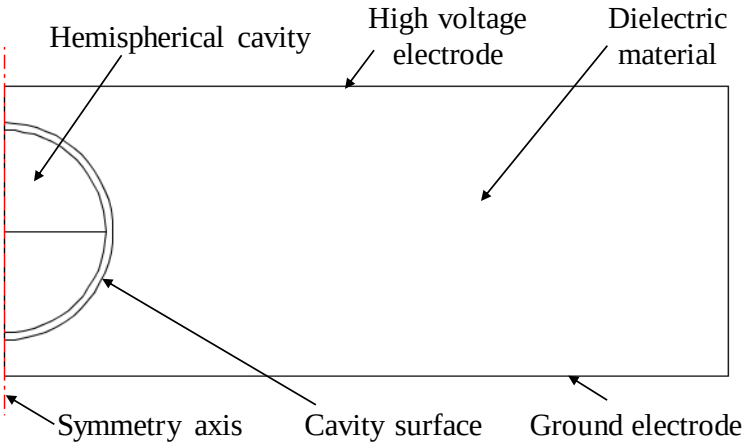

FIGURE 3.1: 2D axial-symmetric model geometry.

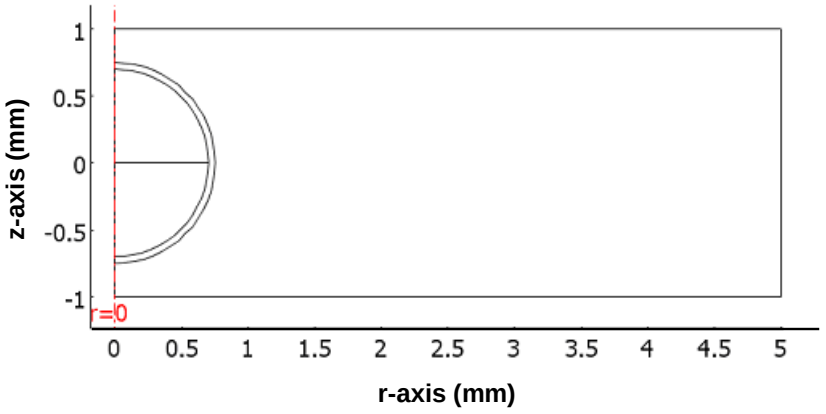

FIGURE 3.2: 2D axial-symmetric model geometry in COMSOL software.

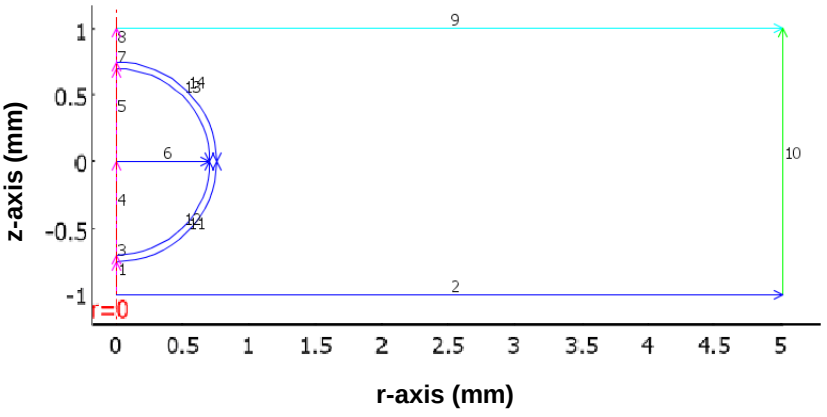

FIGURE 3.3: Model geometry with boundary line numbers.

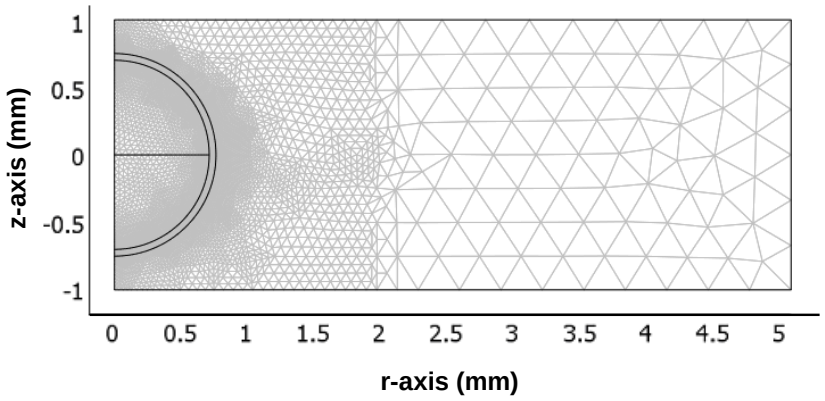

FIGURE 3.4: 2D model geometry and mesh.

Name	Expression	Description
Uapp	14 [kV]	Applied voltage amplitude
freq	50 [Hz]	Frequency of the applied voltage
Ermat	4.4	Relative permittivity of dielectric material
Ers	4.4	Relative permittivity of cavity surface
Ercav	1	Relative permittivity of the cavity
Smat	1e-13 [S/m]	Conductivity of dielectric material
Ss0	1e-13 [S/m]	Initial conductivity of cavity surface
Scav0	0 [S/m]	Initial conductivity of cavity

TABLE 3.1: Defined constants for the Meridional Electric Currents application mode

Subdomain	Relative permittivity	Electrical conductivity
Material	Ermat	Smat
Cavity Surface	Ers	Ss
Cavity	Ercav	Scav

TABLE 3.2: Subdomain settings for the Meridional Electric Currents application mode

Boundary line	Boundary condition	Expression
9	Electric potential	V=Uapp·sin(2·pi·freq·t)
10	Electric insulation	$\vec{n}\bullet\vec{J}$=0
1,3,4,5,7,8	Axial symmetry	r=0
2	Ground	V=0
All interior boundaries	Continuity	$\vec{n}\bullet(\vec{J}_1-\vec{J}_2)$=0

TABLE 3.3: Boundary settings for the Meridional Electric Currents application mode

saved as .m file so that the model can be opened and edited in MATLAB.

Name	Expression	Description
T0	300 [K]	Initial temperature
kcav	0.0258 [W/m/K]	Thermal conductivity of the cavity
kmat	0.19 [W/m/K]	Thermal conductivity of the material
Ccav	1006 [J/(kgK)]	Specific heat capacity of the cavity
Cmat	1000 [J/(kgK)]	Specific heat capacity of the material
rhcav	1.1808 [kg/mˆ 3]	Density of the cavity
rhmat	1250 [kg/mˆ 3]	Density of the material
Qcav	0 [W/mˆ 3]	Heat source density of the cavity
Qmat	0 [W/mˆ 3]	Heat source density of the material

TABLE 3.4: Defined constants for the Heat Transfer by Conduction (at 20°C, 100 kPa)

Subdomain	Thermal conductivity	Specific heat capacity	Density	Heat source density
Material	kmat	Cmat	rhmat	Qmat
Cavity Surface	kmat	Cmat	rhmat	Qmat
Cavity	kcav	Ccav	rhcav	Qcav

TABLE 3.5: Subdomain settings for the Heat Transfer by Conduction application mode

Boundary line	Boundary condition	Expression
1,3,4,5,7,8	Axial-symmetry	r=0
2,9,10	Thermal insulation	$\vec{n}\bullet(k\vec{\nabla}T)$=0
All interior boundary	Continuity	$\vec{n}\bullet(k_1\vec{\nabla}T_1-k_2\vec{\nabla}T_2)$=0

TABLE 3.6: Boundary settings for the Heat Transfer by Conduction application mode

3.2 Discharge model and charge magnitude calculation

PD is driven by the local electric field enhancement in the cavity, which is due to the applied electric field and surface charges on the cavity surface. In this model where simulation is dynamic, the electric field distribution in the cavity is calculated numerically at each time step using FEA method which solves the PDE in Equation 3.4 for the time dependent electric field. From the FEA model, in the absence of any PD and surface charge, the field distribution in a spherical cavity has been found to be uniform. However, for a spherical cavity which is quite large in diameter compared to the thickness of the material, as in Figure 3.1, the field distribution in the whole cavity is no longer uniform. The electric field on the cavity surface nearest to the electrode is slightly lower than the field at the cavity centre due to the influence of the electrode. However, the electric field in the cavity is symmetrical along the r and z-axes [74]. Because of this, FEA model is used continuously throughout the simulation to calculate the field distribution in the cavity. Symmetry of both the electric field and charge distribution in the cavity along the r and z axes is assumed before and after the occurrence of a PD. This

is achieved in FEA modelling by assuming that during a PD event, the whole cavity is affected.

There are some assumptions made to simplify the model. The discharge model does not include details of PD mechanisms, such as the motion of free electrons and ions during the electron avalanche propagation in the cavity. These parameters affect the characteristics of the cavity surface after each PD but it is difficult to determine physical parameters associated with the surface itself. For this study, it has been assumed that a simplified PD model is representative of the phenomena and this has been validated using related experimental measurements.

It is assumed that the PD in the cavity will have the characteristics of a steamer discharge. Published research has modelled streamer propagation in air by charge carriers experiencing drift and diffusion in the electric field [75]. The development of partial discharge has also been modelled by using a particle simulation, which investigate the dynamics of particles during discharge [76,77]. However, a detailed mechanism of streamer propagation is not modelled in this work because the parameters of interest are PD phase and charge magnitude only. Discharge is assumed to affect the whole spherical cavity and is assumed to occur only along the cavity symmetry axis. Therefore, only the field in the cavity centre at an instantaneous time, t, $E_{cav}(t)$ is extracted from the FEA model and it is a function of time only.

3.2.1 Cavity conductivity

When partial discharge is modelled dynamically, the discharge event can be represented by changing the state of the cavity from that of non-conducting to conducting. This can be modelled by increasing the cavity conductivity from its initial conductivity when there is no discharge, σ_{cav0} to maximum cavity conductivity, σ_{cavmax} during the discharge event. σ_{cavmax} is the cavity conductivity which causes the field in the cavity centre, $E_{cav}(t)$ to decrease until it becomes less than the extinction field, E_{ext} during the discharge process. The value for the maximum cavity conductivity during PD, σ_{cavmax}, can be estimated using the electron conductivity in the plasma because the conductivity due to ions is assumed to be negligible. The electron conductivity in the plasma, σ_e is calculated using [78]

$$\sigma_e = \frac{\alpha_e^2 N_e \lambda_e}{m_e c_e} \tag{3.6}$$

where α_e is the coefficient related to electron energy distribution and mean free path ($\sim$0.85), e is the electric charge of the electron, m_e is the electron mass, λ_e is the electron mean free path ($\sim$4 um), c_e is the electron thermal velocity ($\sim 3\times10^8$ ms^{-1}) and N_e is the electron density, which is defined as

$$N_e = \frac{q/e}{4/3\pi r^3} \tag{3.7}$$

where q/e is the number of electrons in the streamer channel, q is the total charge in the streamer channel and r is the cavity radius. For estimation of σ_{cavmax}, q in Equation 3.7 is taken as the maximum charge magnitude determined from analysis of the measurement results, q_{max}. During discharge, the current through the cavity, $I_{cav}(t)$ increases from zero until a certain maximum value but $E_{cav}(t)$ starts to decrease. After that, $I_{cav}(t)$ starts to decrease whilst $E_{cav}(t)$ keeps decreasing. Discharge stops when the field in the cavity, $E_{cav}(t)$ drops less than the extinction field, E_{ext}. After PD is over, the conductivity is reset to its initial values and current in the cavity becomes zero.

3.2.2 PD charge magnitude

In this model, since the discharge process is modelled dynamically, the charge magnitude can be calculated numerically. The real and apparent charge magnitudes, q_{PD} are calculated by time integration of current, $I(t)$ flowing through the cavity (boundary 6 in Figure 3.3) and through the ground electrode (boundary 2 in Figure 3.3) during the PD time interval, where

$$q_{PD} = \int_t^{t+dt} I(t)dt \tag{3.8}$$

The current, I, through the ground electrode is calculated by integration of current density, J over the ground electrode surface area, where J depends on the electric field distribution. Since the electric field distribution on the ground electrode is not uniform due to the presence of the cavity, the field distribution in the whole cavity and material is calculated using the FEA method to determine the PD apparent charge magnitude. Therefore, the advantage of the use of FEA over classical lumped parameter modelling is that it facilitates dynamic calculation of both real and apparent charges.

3.3 Modelling of temporal temperature and pressure change

After a PD event, the temperature in the cavity will have increased due to the electron ionization process. In other previous PD models, the influence of temperature change in the cavity on PD activity has not been considered [13, 50, 68].

3.3.1 Cavity temperature dependent using FEA model

After a PD event, the temperature in the cavity will have increased due to the electron ionization process. The hot gas due to the discharge is assumed to form a spherical shape in order to simplify the model. From the FEA model, the temperature in the whole cavity immediately after the first PD is uniform as the PD affects the whole cavity. However, a certain time after a PD has occurred, the temperature distribution in the cavity becomes non-uniform but is symmetrical along the cavity symmetry axis. The distribution is obtained from the FEA model. The temperature at the cavity centre is the highest and is the lowest at the region near the cavity surface as the heat dissipation near the cavity surface is greater through the surrounding material. Thus, the temperature in the cavity immediately after the next PD occurs is no longer uniform but symmetrical along the symmetry axis because the temperature distribution is influenced by the previous PD event. Assuming that the highest temperature is affecting the occurrence of a PD, only the temperature in the cavity centre is assumed to affect the inception field in the cavity, which is denoted as $T_{cav}(t, 0, 0)$, where (0,0) is the location of the cavity centre in the model.

In this model, all energy released from discharge is assumed to be in the form of heat energy. Thus, during a PD event, the heat source density in the whole cavity, Q_{cav} from Equation 3.5 is increased from zero while the heat source density in the material, Q_{mat} is always set to zero. The increase in Q_{cav} causes $T_{cav}(t, 0, 0)$ to increase. Discharge is modelled by changing the state of the cavity from that of non-conducting to conducting, which causes current to flow in the cavity. Since the electric field along the r-axes is very near to uniform, discharge channel can be assumed to be in the form of a cylindrical channel. Thus, Q_{cav} can be calculated using [79]

$$Q_{cav}(t) = J_{cav}(t)E_{cav}(t) \tag{3.9}$$

where $J_{cav}(t)$ is the current density in the middle of the cavity during discharge and $E_{cav}(t)$ is the field in the cavity centre. $J_{cav}(t)$ and $E_{cav}(t)$ are calculated from Equation 3.4. Equation 3.9 represents the specific heat power of heat released due to the electric current in the discharge channel. After a PD event, $Q_{cav}(t)$ is reset to zero. Therefore, the coupled equations allow the electric potentials and temperature to be determined for a set of given boundary conditions at each time step instant.

3.3.2 Temperature dependent of inception and extinction fields

During a discharge event, $T_{cav}(t_n, r, z)$ increases from its previous value, $T_{cav}(t_{n\text{-}1}, r, z)$, where n is the n-th time step and r and z are the locations in the cavity. The rise of $T_{cav}(t_n, r, z)$ may cause the pressure in the cavity, $p(t_n, r, z)$ to increase from its previous

value, $p(t_{n\text{-}1}, r, z)$. Assuming the cavity volume is constant, the changes of the number of gas molecules in the cavity after each PD is negligible and the gas in the cavity is assumed as an ideal gas, the new pressure in the cavity at the current time step t, $p(t_n, r, z)$ is calculated using

$$p(t_n, r, z) = \left[\frac{p(t_{n-1}, r, z)}{T_{cav}(t_{n-1}, r, z)}\right] T_{cav}(t_n, r, z) \tag{3.10}$$

The inception field, E_{inc} is defined as the minimum electric field in the cavity that a discharge can occur, which depends on the cavity pressure and cavity diameter. It is assumed that the inception field is dependent on the temperature in the cavity centre, $T_{cav}(t, 0, 0)$ and the initial temperature in the cavity is the same as the material temperature. Using the obtained measurement data of E_{inc} as a function of temperature in the cavity, T_{cav} in the experiment, the best fit function that can be used to represent this relationship as a function of time, t is

$$E_{inc}(t) = \kappa + \chi T_{cav}(t, 0, 0) \tag{3.11}$$

where κ and χ are constants in $\mathrm{kV{\cdot}mm^{-1}}$ and $\mathrm{kV{\cdot}mm^{-1}K^{-1}}$ respectively, determined from the experiment. Thus, $E_{inc}(t)$ changes from the initial cavity inception field, E_{inc0} when the temperature in the cavity changes with time. E_{inc0} is equal to the field in the cavity when the inception voltage level from the measurement is reached. In the model, E_{inc0} depends on the cavity diameter, d because it has been assumed that discharge only occurs along the symmetry axis of the cavity, where the distance over the cavity symmetry axis is the cavity diameter.

The pressure in the cavity may also determine the extinction field, E_{ext} because it controls the streamer propagation field, where discharge curtails at a higher field in the cavity at higher pressure [13]. Assuming that E_{ext} is approximately proportional to the cavity pressure, if E_{ext0} is the extinction field in the cavity centre at the initial cavity pressure, p_0, $E_{ext}(t)$ at an instantaneous time t is estimated as

$$E_{ext}(t) \approx E_{ext0} p(t, 0, 0)/p_0 \tag{3.12}$$

The temperature in the cavity will decay towards the initial temperature after a PD occurs. Since the temperature is calculated numerically using the FEA method, there is no need to assign any temperature decay time constant because the temperature decreases when the heat source density, $Q_{cav}(t)$ is reset to zero following a PD event. Therefore, this method can be considered as an alternative approach to a previous model which uses a lower probability of PD occurrence when the temperature on the cavity surface is higher than the initial temperature [71].

3.3.3 Thermal properties of the cavity and material

The thermal properties of the cavity can also be set as temperature and pressure dependent. Assuming the gas content in the cavity is air, the thermal properties of the cavity can be assumed to have air thermal properties. The temperature in the cavity depends on the cavity density, ρ_{cav}, specific heat capacity, C_{cav}, thermal conductivity, k_{cav} and heat source density, Q, where these parameters depends on the pressure and temperature in the cavity. Using curve fitting technique on the given data sets of air temperature, pressure, specific heat capacity, thermal conductivity and density from [80,81], the simplest functions that can be used to represent the cavity thermal properties, as a function of time, temperature and pressure are

$$\begin{aligned} C_{cav}(t,r,z) =& 1033 - 0.2799T_{cav}(t,r,z) + 1.096\times10^{-4}p(t,r,z) \\ &+ 7.429\times10^{-4}[T_{cav}(t,r,z)]^2 - 5.003\times10^{-7}T_{cav}(t,r,z)p(t,r,z) \\ &+ 1.891\times10^{-12}[p(t,r,z)]^2 - 4.19\times10^{-7}[T_{cav}(t,r,z)]^3 \\ &+ 6.184\times10^{-10}[T_{cav}(t,r,z)]^2p(t,r,z) \\ &- 4.881\times10^{-15}T_{cav}(t,r,z)[p(t,r,z)]^2 - 7.753\times10^{-20}[p(t,r,z)]^3 \end{aligned} \tag{3.13}$$

$$\begin{aligned} k_{cav}(t,r,z) =& 1\times10^{-5}\{57.88 + 9.43T_{cav}(t,r,z) + 1.049\times10^{-4}p(t,r,z) \\ &- 2.915\times10^{-3}[T_{cav}(t,r,z)]^2 - 1.726\times10^{-7}T_{cav}(t,r,z)p(t,r,z) \\ &+ 3.115\times10^{-10}[p(t,r,z)]^2\} \end{aligned} \tag{3.14}$$

$$\begin{aligned} \rho_{cav}(t,r,z) =& 3.562 - 0.03445T_{cav}(t,r,z) + 3.464\times10^{-5}p(t,r,z) \\ &+ 1.094\times10^{-4}[T_{cav}(t,r,z)]^2 - 1.13\times10^{-7}T_{cav}(t,r,z)p(t,r,z) \\ &+ 3.494\times10^{-13}[p(t,r,z)]^2 - 1.142\times10^{-7}[T_{cav}(t,r,z)]^3 \\ &+ 1.211\times10^{-10}[T_{cav}(t,r,z)]^2p(t,r,z) \\ &- 9.868\times10^{-16}T_{cav}(t,r,z)[p(t,r,z)]^2 \end{aligned} \tag{3.15}$$

where $T_{cav}(t,r,z)$ and $p(t,r,z)$ are the temperature and pressure in the cavity at an instantaneous time, t.

The mass density, specific heat capacity and thermal conductivity of the dielectric material are treated as independent of the temperature because the temperature range used in the experiment is only between 20 to 65°C. Thus, variation in the epoxy resin thermal properties can be assumed to be minimal and can be neglected in the model. From analysis using the FEA model, the temperature distribution in the cavity is not affected by

a small variation in these epoxy resin thermal properties. Since there is a wide variation of the thermal properties values for epoxy resin due to variation of epoxy components, their thermal properties are assigned using values found in [82], where those values are for the pressure and temperature of the material at 100 kPa and 20°C.

3.4 Charge decay through surface conduction

Charge decay through conduction along the cavity wall is possible as the amount of charge trapped in the cavity is time dependent. During the discharge process, when the first layer of charge arrives on the cavity surface, before being trapped, it repels oncoming charge, increasing their landing time. Thus, it can be assumed that repelled charges might remain on the cavity surface for a certain period of time or may move along the cavity wall before being trapped in a surface state. The effect will be significant if the cavity surface time constant is less than the period of the applied voltage [83].

After a PD, any charges that still remain free on the cavity surface will decay through conduction along the cavity wall before the next PD event occurs, resulting in charge recombination. This surface charge decay can be modeled using a field-dependent cavity surface conductivity, which depends on free charge movement along the cavity wall through surface conduction. The movement of these charges is assumed to be dependent on the magnitude and direction of the electric field in the cavity center, $E_{cav}(t)$ and the electric field due to the cavity surface charge, $E_s(t)$.

3.4.1 Field dependent charge movement

Figure 3.5 shows the movement of PD free charges along the cavity surface dependent on the direction of the electric field in the cavity. $E_0(t)$ is the applied field and $E_{cav0}(t)$ is the field in the cavity in the absence of surface charge. When $E_{cav}(t)$ has the opposite direction of $E_s(t)$, free charges due to previous PD that have accumulated on the cavity surface tend to move towards the center of upper and lower cavity surface at where they have been deposited by PD, as shown in Figure 3.5(a). Thus, charge movement on the cavity surface is less, resulting in charge decay through conduction along the cavity wall is less likely to happen. Thus more free charges are still left on the cavity surface by the time the next PD is likely to occur.

Under applied AC voltages, the direction of applied electric field, $E_0(t)$ can change, thus the direction of $E_{cav}(t)$ can also change. When $E_{cav}(t)$ has the same direction with $E_s(t)$, free charges due to previous PD that have accumulated on the cavity surface tend to move towards the opposite direction from where they have been deposited due to PD, as shown in Figure 3.5(b). There is charge movement on the cavity surface, thus the cavity surface conductivity is increased in the model. The movement of positive and

negative charges towards each other along the cavity wall causes charge recombination and decrement of surface charge. It is assumed that the charge distribution on the cavity wall immediately after each PD is uniform and symmetrical along the center axis. The charge movement between positive and negative charges is assumed to be identical.

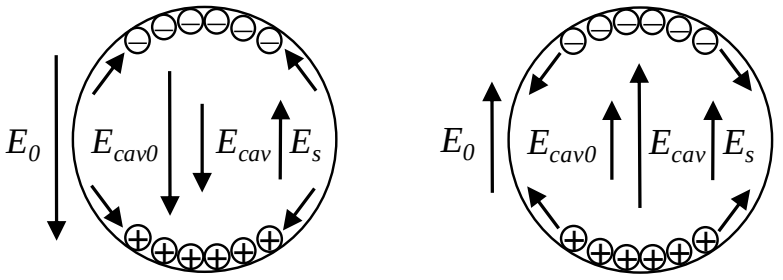

(a) E_{cav} has opposite direction of E_s (b) E_{cav} has the same direction with E_s

FIGURE 3.5: Movement of PD free charges.

When the amount of free charge on the cavity surface decreases, the magnitude of $E_s(t)$ decreases and EGR becomes lower when the next PD is likely to occur. Since this condition happens after the direction of $E_{cav}(t)$ changes after previous PD event, the 'rabbit-ear' like patterns in measurement results might also be determined by surface charge decay through conduction along the cavity wall. The effect of surface charge decay through conduction along the cavity wall on the sequence of PD events by making use of field-dependent cavity surface conductivity has not been considered in previous PD models, although many previous articles have considered the role of surface conductivity on the PD process [13, 15, 50, 68].

3.4.2 Calculation associated with charge decay

Since the charge movement along the cavity wall is modelled as dependent on the direction of field in the cavity centre, $E_{cav}(t)$ and field due to surface charge, $E_s(t)$, $E_s(t)$ needs to be calculated in the model. With reference to Figure 3.5, $E_s(t)$ is calculated using

$$E_s(t) = E_{cav}(t) - E_{cav0}(t) \tag{3.16}$$

Some PD charges will become trapped in surface states and some may remain on the cavity surface. In this model, field due to surface charge immediately after a previous PD occurrence, $E_{sPD}(t_{PD})$ is assumed as summation of field due to trapped charge, $E_{strapPD}(t_{PD})$ and field due to free surface charge, $E_{sfreePD}(t_{PD})$, where tPD is the time of the previous PD occurrence. It is further assumed that free surface charge which remains on the cavity wall do not become trapped in surface states to simplify the

model. The amount of free surface charge after a PD, $q_{sfreePD}(t_{PD})$ can be calculated from the FEA model by integration of field displacement, D over the upper cavity surface area, such that

$$q_{sfreePD}(t_{PD}) = \int_s \left[D_{z(up)}(t_{PD}) - D_{z(down)}(t_{PD})\right] dS \tag{3.17}$$

where $D_{z(up)}$ and $D_{z(down)}$ are the upper and lower side of the upper cavity surface. Therefore, the field due to free surface charge immediately after a PD event, $E_{sfreePD}(t_{PD})$ can be calculated using

$$E_{sfreePD}(t_{PD}) = \left|\frac{q_{sfreePD}(t_{PD})}{q_{PDtotal}(t_{PD})}\right| E_s(t_{PD}) \tag{3.18}$$

where $q_{totalPD}(t_{PD})$ is the total PD real charge up to time (t_{PD}) and its equivalent field is $E_{sPD}(t_{PD})$. It is calculated using

$$q_{PDtotal}(t_{PD}) = \sum_{i=1}^{m} (q_{PD})_i \tag{3.19}$$

where m is the number of PD events and $q(_{PD})_i$ is PD real charge magnitude of i-th PD event. Thus, the field due to trapped charge immediately after a PD occurs is

$$E_{strapPD}(t_{PD}) = E_{sPD}(t_{PD}) - E_{sfreePD}(t_{PD}) \tag{3.20}$$

When $E_s(t)$ reaches $E_{strapPD}(t_{PD})$ during surface charge decay, no more surface charge can decay through conduction along the cavity wall.

The surface charge decay rate through conduction along the cavity wall depends on the field on the cavity surface, $E_{ons}(t)$ and the temperature on the cavity surface, $T_{ons}(t)$ because σ_s is strongly dependent on the cavity environment and the material [84]. When $E_{ons}(t)$ and $T_{ons}(t)$ are larger, kinetic energy for surface charge is higher; the charge movement along the cavity wall faster, resulting in increased charge decay rate through charge recombination.

Therefore, when the directions of $E_{cav}(t)$ and $E_s(t)$ are the same at an instantaneous time t and $E_s(t)$ is larger than $E_{strapPD}(t_{PD})$, the surface conductivity, σ_s is increased from initial surface conducitivty value, σ_{s0} to model the charge movement through conduction along the cavity wall [85]. In the simplest case it is possible to represent the surface conductivity, $\sigma_s(t)$ at each time step using [86–89]

$$\sigma_s(t) = \sigma_{s0} \exp\left[\alpha |E_{ons}(t)| + \beta T_{ons}(t)\right] \tag{3.21}$$

where α is the stress coefficient and β is the thermal coefficient for the cavity surface conductivity. From Equation 3.21, $\sigma_s(t)$ might increase to a very high value due to the increasing $E_{ons}(t)$. In order to avoid numerical convergence problems in the simulation, $\sigma_s(t)$ is limited by a maximum cavity surface conductivity, σ_{smax}, which is defined as the maximum conductivity that can be reached by the cavity surface. However, when the direction of $E_{cav}(t)$ is opposite of $E_s(t)$, $\sigma_s(t)$ is set to initial surface conductivity, σ_{s0} as there is no charge movement along the cavity wall.

3.5 Initial electron generation

In order to initiate a PD in a cavity after the inception field has been exceeded, an initial free electron is required for electron avalanche generation. The supply of free electrons determines the characteristics of PD activity such as phase and charge magnitude of PD occurrences, the numbers of PD per cycle and the total charge magnitude per cycle. The sources of initial electron generation rate are volume ionization and surface emission [56, 90, 91].

3.5.1 Total electron generation rate

A simple term is used in the model to describe the electron generation rate equation in order to reduce the use of physical parameters of the material properties. When the field in the cavity centre, $E_{cav}(t)$ exceeds the inception field, $E_{inc}(t)$ at an instantaneous time, t, PD might occur in the cavity providing that there is a free electron in the cavity to start an avalanche. The amount of free electrons available in the cavity to start a PD is modelled using the total electron generation rate (EGR), $N_{et}(t)$ which is defined as the number of free electrons generated in the cavity per unit time. It is assumed as the sum of EGR due to surface emission, $N_{es}(t)$ and EGR due to volume ionization, N_{ev}, where

$$N_{et}(t) = N_{es}(t) + N_{ev} \tag{3.22}$$

Since discharge has been assumed to occur only along the cavity symmetry axis, $N_{et}(t)$ becomes a function of time only.

3.5.2 Electron generation rate due to surface emission

It is assumed that electron generation rate due to surface emission, $N_{es}(t)$ is dominated by charge detrapping from the cavity surface, which comes from the charge that has been trapped in the cavity surface from previous PD event. The amount of charge that

can be detrapped for a PD likely to occur is dependent on the charge magnitude of the previous PD. Thus, initially, $N_{et}(t)$ only depends on N_{ev}, which is a constant. After the first PD occurs, $N_{et}(t)$ depends on both $N_{es}(t)$ and N_{ev}.

In order to use a simple model to describe a PD behaviour, $N_{es}(t)$ is defined as the number of free electrons generated in the cavity per unit time through surface emission. If N_{es0} is the number of free electrons generated in the cavity per unit time at the initial inception field, E_{inc0}, then, the number of free electrons generated in the cavity per unit time for a PD is likely to occur due to the previous PD occurrence can be defined as

$$N_{PD} = N_{es0}|E_{cav}(t_{PD})/E_{inc0}| \tag{3.23}$$

where $E_{cav}(t_{PD})$ is the field in the cavity of the previous PD occurrence at a time t_{PD}. However, the amount of charge, N_{PD} that can be detrapped via surface emission for a PD is likely to occur after a time interval after the previous PD occurred, decays with time. The charge is assumed to decay into deeper traps exponentially with time and the decay rate is controlled by the effective charge decay time constant, τ_{dec}. Charges that have decayed no longer contribute to the initial electron generation since charges in deeper traps are harder to detrap [14,50]. Although surface charge decays, the potential due to surface charge is assumed constant because charge near to the cavity surface still contributes to the potential of the surface charge.

The electron generation rate due to surface emission has been expressed as a function that increases with increasing electric field and temperature of the material [56,91,92]. Thus, in this work, in order to avoid the use of parameters that are difficult to be determined, it is assumed that the EGR due to surface emission, $N_{es}(t)$ increases exponentially with the product of the field in the cavity, $E_{cav}(t)$ and material temperature, T_{mat}. This is based on the assumption that surface emission is enhanced by the electric field and material temperature. Therefore, the complete equation of $N_{es}(t)$ for a PD is likely to occur, by considering the charge decay effect since the previous PD occurrence and the field and temperature dependent terms, can be defined as

$$N_{es}(t) = N_{PD} \exp\left[-\frac{(t - t_{PD})}{\tau_{dec}}\right] \exp\left|\frac{E_{cav}(t)}{E_{inc0}} \cdot \frac{T_{mat}}{T_{amb}}\right| \tag{3.24}$$

where τ_{dec} is the effective charge decay time constant and T_{amb} is the ambient temperature. $E_{cav}(t)/E_{inc0}$ and T_{mat}/T_{amb} represents a simplified field and temperature dependency. For the purpose of simulation, T_{amb} is assumed to be 293 K as a reference for simulation at different material temperatures, T_{mat} and this temperature has been used to perform the measurement of PD activity in this work.

The value for N_{es0} is subdivided into N_{es0L} which is used when the polarity of $E_{cav}(t)$ changes after previous PD event and N_{es0H} when there is no polarity change between

consecutive discharges. This is based on the assumption that when the polarity of the field in the cavity, $E_{cav}(t)$ changes between PD events, the cavity surface work function is higher when detrapping electrons from a negative cavity surface charge than from a positive cavity surface charge [13, 14, 68]. N_{es0} can be defined as

$$N_{es0} = \begin{cases} N_{es0L} & \text{when } E_{PD2}/E_{PD1}<0 \\ N_{es0H} & \text{when } E_{PD2}/E_{PD1}>0 \end{cases} \tag{3.25}$$

where E_{PD1} and E_{PD2} are field in the cavity of previous and current PD event.

The exponential charge decay term in Equation 3.24 is similar to the term used in equation for surface charge decay through volume conduction in the material. If the solid dielectric is assumed to be a non-dispersive, homogenous, isotropic material, has an instantaneous polarization, a constant permittivity ε_{rmat} and a constant conductivity σ_{mat}, a simple surface charge decay model can be obtained by neglecting the space charge effects [54, 84]. Thus, from Equation 3.4, the solution obtained is

$$V(t) = V_0(t)\exp(-t/\tau_{mat}) \tag{3.26}$$

where V_0 is the potential at time zero and τ_{mat} is equal to $\varepsilon_{mat}/\sigma_{mat}$ is the material time constant. τ_{mat} determines the surface charge decay rate through volume conduction in the material.

3.5.3 Electron generation rate due to volume ionization

When there is lack of initial free electrons from the cavity surface to initiate a PD, free electrons may also come from volume ionization, which is assumed to be always available in the cavity. The EGR due to volume ionization, N_{ev} has been expressed as dependent on pressure in the cavity, cavity volume and applied voltage amplitude [13, 14]. There are many physical parameters associated with volume ionization, such as the radiative cosmic, radioactive quantum flux density and pressure reduced gas density. In this work, in order to simplify the term for N_{ev}, N_{ev} is modeled as a constant number, which represents the number of free electrons generated in the cavity per unit time through volume ionization. Its value may vary depending on the applied stress and cavity conditions.

3.5.4 Probability of a PD occurrence

In order to consider the statistical time lag effect on PD to reproduce the PD repetition rate and phase and charge magnitude distributions of the measurement results, a probability is used to determine the likelihood of a PD occurring. The probability of a PD

occurrence, P is set as proportional to the total electron generation rate, $N_{et}(t)$ and the time stepping interval during no PD event, Δt,

$$P(t) = N_{et}(t)\Delta t \tag{3.27}$$

When the field in the cavity exceeds the inception field level, P is calculated and compared with a random number, R that is between 0 and 1. Only if P is greater than R, a discharge will occur. When P is larger than 1, PD is always occur.

3.6 Design simulation program in MATLAB

3.6.1 Parameters in the model for simulation

Table 3.7 details the parameters used for all simulations at ambient temperature while Table 3.8 shows parameters that vary with the applied stresses and cavity conditions. From Table 3.7, the time step during no PD, Δt_0, is set equal to $1/500f$, where f is the frequency of the applied voltage. This value can keep the simulation time reasonable whilst keeping high precision of phase of the applied voltage. If Δt_0 is too large, the field in the cavity will change too much in one time step, resulting in a less precise indication of the phase of PD occurrence. On the other hand, if Δt_0 is set too short, the simulation time will be greatly increased for little benefit in obtained results.

The time interval during a PD event, Δt_1, is reduced to 1 ns because again if Δt_1 is less than this value, the simulation time will be greatly increased for no noticeable benefit. However, the chosen time step ensures that the precision of PD charge magnitude is maximised. If Δt_1 is set larger than 1 ns, the simulation time will be reduced but the precision of the PD charge magnitude will also be reduced because of the rate of change of the field in the cavity during PD.

The material conductivity, σ_{mat}, is set as $1{\times}10^{-13}$ Sm^{-1} because the conductivity of epoxy cast resin is reported to be $1{\times}10^{-13}$ Sm^{-1} [82, 93, 94]. Since the material is a dielectric with a non-zero DC conductivity, there will be a current flowing through the material when a voltage is applied. Through simulation using the FEA method, the electric field distribution is not affected if σ_{mat} is smaller than $1{\times}10^{-13}$ Sm^{-1}. Thus, using σ_{mat} as $1{\times}10^{-13}$ Sm^{-1} is reasonable. The cavity conductivity between PD events, σ_{cav0} is set equal to 0 Sm^{-1} because no current is flowing in the cavity during this time.

The value for the maximum cavity conductivity during a PD event, σ_{cavmax} is set equal to $5{\times}10^{-3}$ Sm^{-1}. This value is comparable to the value that is calculated using Equation 3.6 and Equation 3.7 with the measured maximum charge magnitude from the

Definition	Symbol	Value	Unit
Ambient temperature	T_{amb}	293	K
Time step during no PD	Δt_0	$1/500f$	s
Time step during PD	Δt_1	1	ns
Cavity surface thickness	h_s	0.05	mm
Material relative permittivity	ε_{rmat}	4.4	
Cavity surface relative permittivity	ε_{rs}	4.4	
Cavity relative permittivity	ε_{rcav}	1	
Material conductivity	σ_{mat}	1×10^{-13}	Sm^{-1}
Initial cavity surface conductivity	σ_{s0}	1×10^{-13}	Sm^{-1}
Cavity conductivity during no PD	σ_{cav0}	0	Sm^{-1}
Maximum cavity conductivity during PD	σ_{cavmax}	5×10^{-3}	Sm^{-1}
Thermal conductivity of the cavity	k_{cav}	0.0258	$\mathrm{Wm}^{-1}\mathrm{K}^{-1}$
Thermal conductivity of the material	k_{mat}	0.19	$\mathrm{Wm}^{-1}\mathrm{K}^{-1}$
Specific heat capacity of the cavity	C_{cav}	1006	$\mathrm{J(kgK)}^{-1}$
Specific heat capacity of the material	C_{mat}	1000	$\mathrm{J(kgK)}^{-1}$
Density of the cavity	ρ_{cav}	1.1808	kgm^{-3}
Density of the material	ρ_{mat}	1250	kgm^{-3}
Heat source density in the cavity during no PD	Q_{cav}	0	Wm^{-3}
Heat source density of the material	Q_{mat}	0	Wm^{-3}
Stress coefficient for surface conductivity	α	10	$\mathrm{mm{\cdot}kV}^{-1}$
Thermal coefficient for surface conductivity	β	1/293	K^{-1}
Effective charge decay time constant	τ_{dec}	2	ms

TABLE 3.7: Definition and symbol of parameters used for all simulations (at ambient temperature)

Definition	Symbol	Unit
Temperature of the material	T_{mat}	K
Cavity diameter	d	mm
Dielectric material thickness	h_{mat}	mm
Applied frequency	f	Hz
Applied voltage amplitude	U_{app}	kV
Initial pressure in the cavity	p_0	kPa
Maximum cavity surface conductivity	σ_{smax}	Sm^{-1}
Measured inception voltage	U_{incapp}	kV
Initial cavity inception field	E_{inc0}	kV·mm−1
Initial cavity extinction field	E_{ext0}	kV·mm−1
Higher initial EGR due to surface emission	N_{es0H}	s^{-1}
Lower initial EGR due to surface emission	N_{es0L}	s^{-1}
Electron generation rate due to volume ionization	N_{ev}	s^{-1}

TABLE 3.8: Stress and cavity condition-dependent parameters

experiment. This value is reasonable to keep the simulation time short enough but manage to avoid the field in the cavity from dropping too fast during the PD. If σ_{cavmax} is set higher than 5×10^{-3} Sm^{-1}, the field in the cavity will drop too fast and will stop at field level much lower than the extinction field, resulting in larger PD charge magnitudes.

However, if σ_{cavmax} is set lower than 5×10^{-3} Sm^{-1}, the simulation time will be greatly increased for little benefit. Using σ_{cavmax} lower than 5×10^{-3} Sm^{-1} does not significantly affect the PD charge magnitude and the field at which discharge stops, but more than 100 time steps are taken to solve a PD event. Different values of σ_{cavmax} do not influence the rate of temperature change in the cavity during a discharge.

The relative permittivity of the material, ε_{rmat} is obtained from measurement of samples manufactured in the laboratory, which has been found to be acceptable. It was found that from literature, the relative permittivity of epoxy resin is within the range of 3.5 to 5 [93]. The cavity surface permittivity, ε_{rs} and the initial cavity surface conductivity, σ_{s0} are set equal to ε_{rmat} and σ_{mat} respectively because the cavity surface is treated as part of the material. The relative permittivity of the cavity, ε_{rcav} is set equal to 1 because it is assumed that the gas in the cavity is air.

The stress-dependent coefficient for surface conductivity, α is set equal to 10 $\mathrm{mm{\cdot}kV}^{-1}$ in order to control the rate of change of σ_s. If α is set too small, σ_s will increase too slowly towards σ_{smax}, causing insufficient decrement of E_s, resulting in larger simulated maximum PD magnitudes than those of the measured data. However, if α is set too large, the increment of σ_s will be too fast, resulting in too fast a decrement of E_s. It is the same case for the thermal-dependent coefficient for surface conductivity, β, which is set equal to 1/293 K^{-1} for all simulations.

The effective charge decay time constant, τ_{dec}, is 2 ms for all simulations at room temperature. This value was based on other published literatures which use epoxy resin as a dielectric material, where the value for τ_{dec} used is between 1 to 4 ms at room temperature [13, 14, 68].

The cavity surface thickness, h_s is set to 0.05 mm. This value is reasonable as the difference in the electric field distribution on the cavity surface for different surface thicknesses is very small. However, if the thickness is too small, the simulation time is longer due to the use of more mesh elements in the model geometry.

3.6.2 Value assignment for electron generation rate parameters

Referring to Table 3.8, parameters related to electron generation rate, i.e. N_{es0H}, N_{es0L} and N_{ev} do not represent the real value of physical properties of the dielectric material. Their values are representive of the initial electron generation rate that changes with applied stress and cavity condition.

The values of N_{es0H}, N_{es0L} and N_{ev} are dependent on each other. Unsuitable choice of values will yield significant error between measurement and simulation results. For example, if the electron generation rate is set too high, the PD patterns of the simulation will not be comparable to the measured patterns and the simulated number of PDs per

cycle will be too large. However, if the electron generation rate is set too low, it will result in no PD occurring at all for many voltage cycles, consequently resulting in a very low simulated number of PDs per cycle. Therefore, a sensitivity analysis was performed to select the optimum values of N_{es0H}, N_{es0L} and N_{ev}.

The sensitivity analysis for the selection of N_{es0H}, N_{es0L} and N_{ev} values was performed using an optimization method once other parameter values in Table 3.8 had been determined. Figure 3.6 details the algorithm used for the sensitivity analysis to choose the best fit value for these parameters. For each different combination of N_{es0H}, N_{es0L} and N_{ev}, the total mean square error (MSE) between simulation and measurement of the number of PDs vs. phase distribution, $H_n(\phi)$ and total charge vs. phase distribution, $H_{qs}(\phi)$ was calculated. Initially, N_{es0H}, N_{es0L} and N_{ev} were defined with small values.

The optimization uses the initial values and N_{es0H} is increased until the global minimum from the MSE vs. N_{es0H} curve is identified. After that, the value for N_{es0L} is increased and the simulation is run again with initial value of N_{es0H}. N_{es0H} is increased until the global minimum from the MSE vs. N_{es0H} curve is identified. The value for N_{es0L}

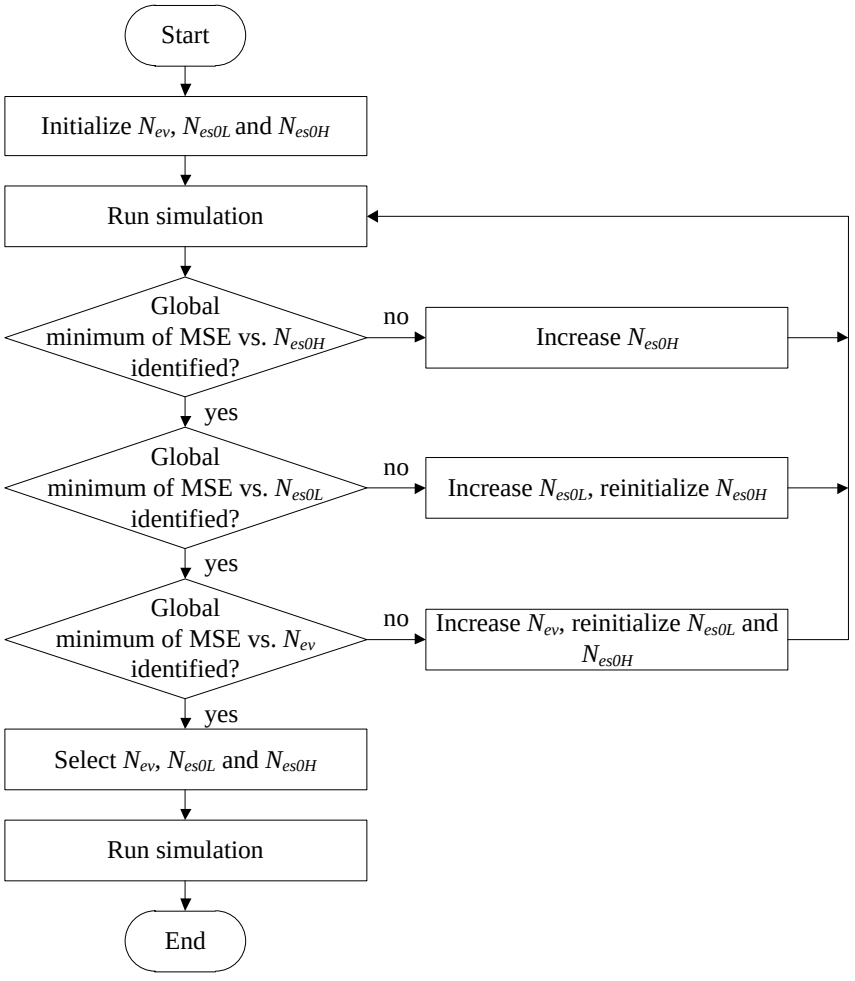

FIGURE 3.6: Flowchart of sensitive analysis for parameter values determination.

is increased again and N_{es0H} is reinitialized. The simulation is run until the global minimum from the MSE vs. N_{es0L} curve is identified. Once it has been identified, the value for N_{ev} is increased and the values for N_{es0L} and N_{es0H} are reinitialized. The whole process above is repeated and only stops once the global minimum from the MSE vs. N_{ev} curve is identified. The values for N_{es0H}, N_{es0L} and N_{ev} at that point give the best simulation results when compared to measurement data.

The selected parameter values are verified by investigating the simulation results are within the bounds of suitable acceptance criteria. Reasonable acceptance criteria have been set and they are the difference between the number of PDs per cycle between measurement and simulation must be ± 0.1 and there must be a less than 10% difference between for the total charge per cycle or maximum PD charge magnitudes.

3.6.3 Flowcharts of the test program

The FEA model is used in parallel with MATLAB programming code, which is divided into several parts; loops over time, a discharge event, calculation of initial free electron generation to start an electron avalanche, surface charge decay model, determination of temperature in the cavity, graphical user interfaces (GUI) and post-processing of simulation results. Figure 3.7 to Figure 3.9 show flowcharts of the main code and functions used in the main code. First of all, the workspace in MATLAB is cleared. Then, all constants, variables and parameters that are used in the simulation are defined and initialized. In order to create a friendly simulation environment, some GUIs are introduced before the simulation. The first GUI allows user to key in the dimensions of the cavity. The next GUI allows user to key in all input data for simulation, such as the applied frequency, applied voltage amplitude and numbers of cycles to simulate. Next, the model geometry is meshed and initialized. Boundary and subdomain settings are assigned with parameters that have been chosen. The model is then solved using initial condition values.

After that, the main loop commences. At each time step, the code interacts with the FEA model. Boundary and subdomains are updated and the model is solved for electric potential and temperature using the FEA method. The temperature in the cavity, T_{cav} is extracted from the model to update the pressure in the cavity, which is used to update the inception field, E_{inc}. The field in the cavity, E_{cav} extracted from the model is compared with the field due to surface charge, E_s. If the polarity of E_{cav} is the same with E_s, the cavity surface conductivity, σ_s, is increased to model the charge decay through surface conduction. Else, σ_s is maintained at its initial value, σ_{s0}. The cavity surface temperature is also extracted to update the value of σ_s. However, if the polarity of E_{cav} is opposite to E_s, the surface conductivity is set to its initial value. Then, E_{cav} is compared with E_{inc}. If E_{cav} is higher than E_{inc}, the total electron generation rate, N_{et} is calculated. Then a probability, P of a PD occurrence is calculated using Equation 3.27

and compared with a random number, R which lies within 0 to 1. If P is greater than R, discharge is set to occur. Otherwise, the status is set to a no discharge condition and the program proceeds to the next time step.

Once discharge is set to occur in the cavity, the electric equipotential line, electric field and temperature distributions in the model immediately before the first PD are stored. Then, the cavity conductivity is increased. The parameter values for boundary and

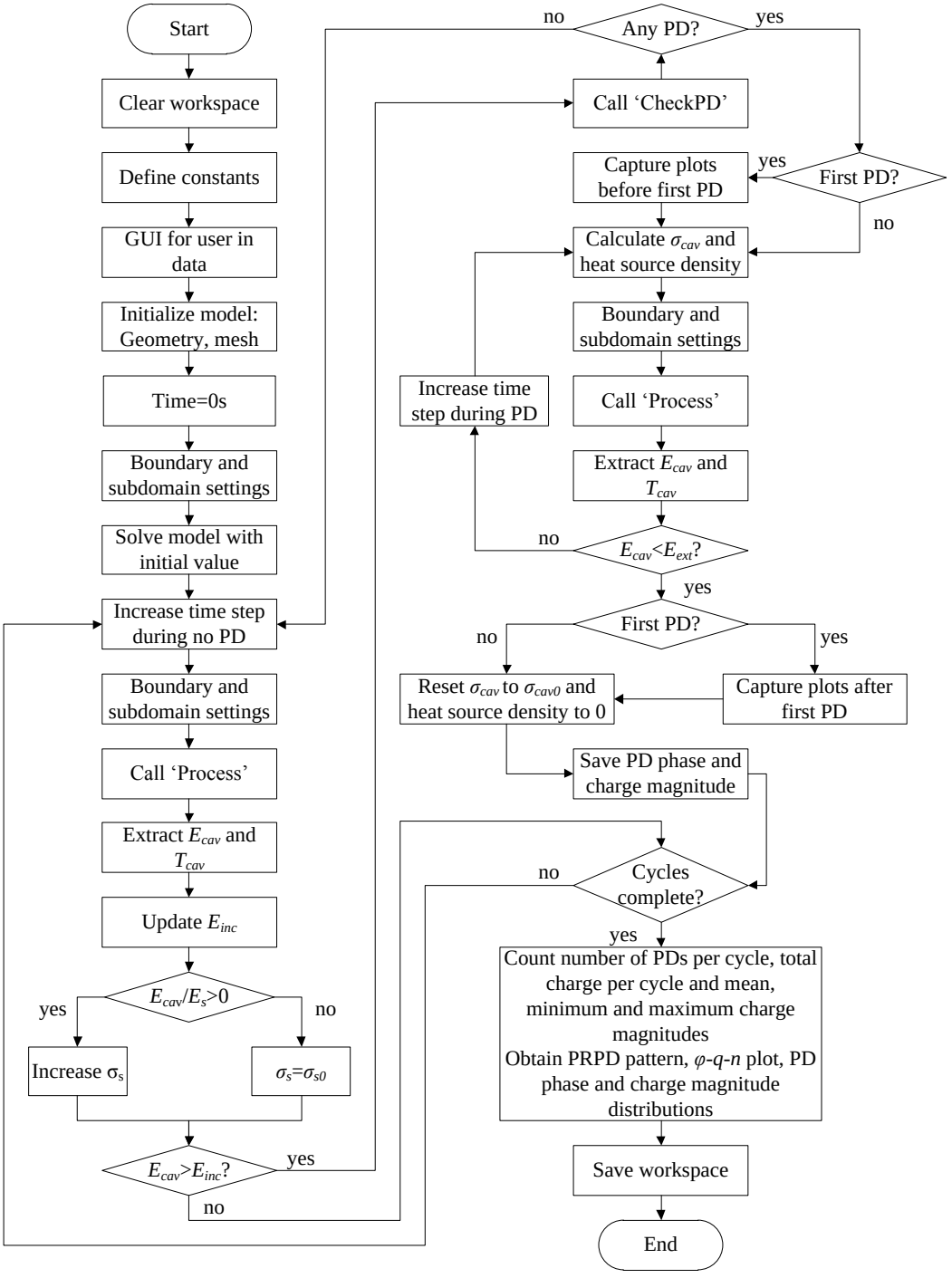

FIGURE 3.7: Flowchart of the main code in MATLAB.

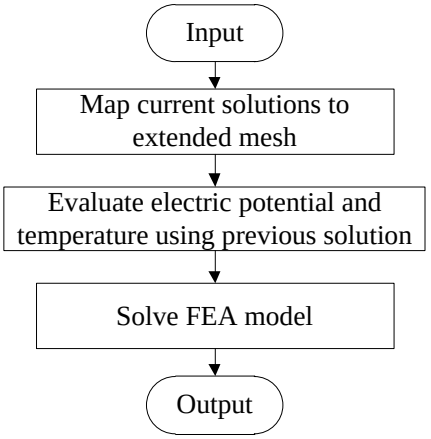

FIGURE 3.8: Flowchart of the 'Process' function.

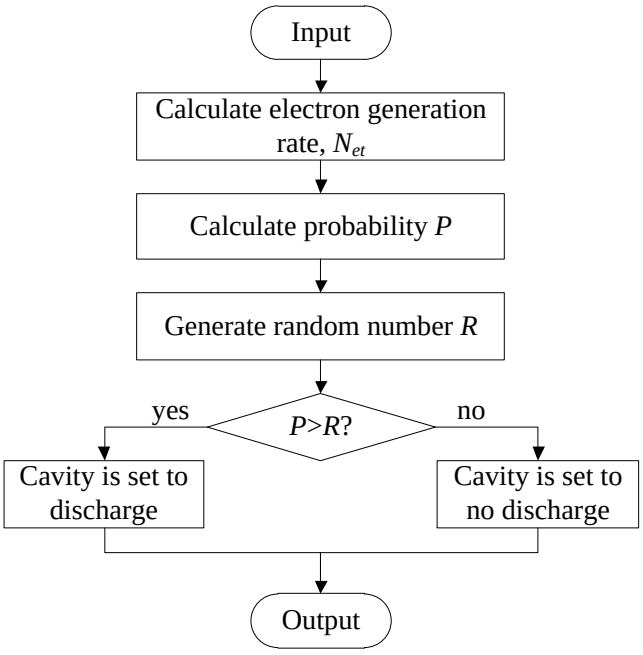

FIGURE 3.9: Flowchart of the 'CheckPD' function.

subdomains are updated and the electric field and the current are extracted from the model. At the same time, the heat source density in the cavity is increased to allow the temperature to increase. Discharge stops when E_{cav} drops below the extinction field, E_{ext}. Else, the program keeps extracting the electric field and the current at each time step during the PD. When discharge stops, the cavity conductivity and the heat source density in the cavity are reset to their initial values and the program proceeds to next time step. The phase of PD occurrence and charge magnitude are saved in the workspace. The electric equipotential line, electric field and temperature distributions in the model immediately after the first PD are also stored.

The cycle repeats until a specified number of cycles is reached. The code then calculates the number of PDs per cycle, total charge per cycle and the mean, minimum and

maximum charge magnitudes. PD phase and charge magnitude distributions, 2D PRPD pattern and 3D ϕ-q-n plot are obtained. Details of the PRPD patterns and ϕ-q-n plot are further explained in Chapter 4.

3.7 Summary

A model describing a spherical cavity within a solid dielectric material has been developed using the Finite Element Analysis (FEA) method. The advantages of this method over previous approaches are:

1. Any cavity geometry shape within a dieletric material can be modelled, especially in non-uniform electric and temperature thermal fields.
2. PD events can be modelled dynamically, where real and apparent PD charge magnitudes can be obtained from the current in the cavity and through the ground electrode during the discharge without using analytical approach.
3. The FEA has the ability of generating a 2D electric field and temperature distributions giving insight into the pre-discharge processes that are occurring.
4. Surface charge conduction along the cavity can be modelled by varying the cavity surface conductivity without the need to approximate the charge conduction along the cavity wall.
5. The temperature in the cavity can be modelled dynamically without uisng any analytical equations, which in turn enhances the precision of the model.

Chapter 4

Test Samples and Measurement Technique

This chapter focuses on the preparation of the test samples that have been used for PD measurement in this work. The setup of the experiment, which is based on the PRPDA technique and the measurement method are detailed. Different applied stress conditions for the PD experiment are applied voltage amplitudes and frequencies of the applied voltage, temperature of the material and different cavity sizes. Several ways of PD data representation are included. Results of the permittivity of the material as a function of material temperature and frequency of the applied voltage that has been used in the experiment are also presented. The obtained measurement results for different applied stresses and cavity sizes are compared with simulation results. This allows critical parameters and physical mechanisms affecting PD activity from the PD model for different stress conditions to be identified.

4.1 Test samples

4.1.1 Epoxy resin

The dielectric material used in the experiment is an epoxy resin. Epoxy resin is a highly cross-linked addition polymer. It is a thermosetting epoxide polymer that cures when mixed with a hardener. Epoxy resin is typically produced from a reaction between an alcohol or amine and an epoxide. Examples of alcohol used are glycerine, bisphenol-A and polyamine while examples of epoxide are epoxy chloride, epichlorohydrin and a bisepoxyphenol compound [95]. The reaction between these two forms an ether or amine and an alcohol, where the epoxide becomes an alcohol. Epoxy resin has a high viscosity due to the cross linking that means it cannot flow and hence it becomes a glass. When epoxy is mixed with an appropriate hardener, an exothermic process is involved

and the epoxy cures. Curing time of an epoxy resin depends on the formulation, cure temperature and the ratio of mixture between the epoxy resin and hardener.

In general, epoxy resin has excellent adhesive and mechanical properties, good chemical resistance, high strength, great impact and thermal shock resistance, high thermal stability, good corrosion resistance and dimensional stability and it is a very good electrical insulator [95]. The properties of epoxy can be improved after the post cure process, such as higher thermal insulation, electrical resistance and mechanical strength. Epoxy resin is widely used in insulation systems of electrical equipment, such as in motors, generators, transformers, switchgear and bushings.

Epoxy resin was chosen as the dielectric material of the test object ahead of other materials, such as polyethylene (PE) for several reasons. Epoxy resin is often used in the electrical insulation system of many types of equipment. Epoxy resin has a lower viscosity than PE, thus artificial voids can to be created within the epoxy resin before it cures. Since the dielectric constant of epoxy resin is higher than PE, typically in the range of 3.5 to 5 [82,93] compared to 2.25 for low density polyethylene (LDPE) [82,93,94], the inception voltage is lower than for PE samples of identical dimension. This reduces the need of higher applied voltage amplitudes to initiate PD activity. Experiments reveal that when LDPE is used as a test object, there are triple junction discharges occurring at the contact between the metal electrode, the LDPE sample and the mineral oil which affect the experiment results. Although the top and bottom surfaces of the LDPE sample have been coated with a layer of gold to increase the electrical contact between the sample and the metal electrode, triple junction discharges still occur. However, this problem does not exist when epoxy resin is used. The breakdown strengths of epoxy resin and LDPE are generally in the same range, which is approximately $20 - 160$ kV·mm^{-1}, depending on the conditions surrounding the material [96–98]. Thus, breakdown strength is not the factor which determine the selection of the material.

4.1.2 Preparation of the test samples

The epoxy resin used in this work is Araldite Rapid epoxy resin, which is manufactured by Huntsman. It is a two-part adhesive supplied in two tubes, epoxy resin and hardener tubes. To prepare the resin, the mixture ratio between the epoxy resin and its hardener is 1:1. It is a strong, powerful, high strength, long lasting adhesive, solvent free and heat, cold, water and oil resistant. It has a setting time of 10 minutes after the mixture of epoxy and hardener, gains strength over time and handling time within 2 hours at room temperature. A short setting time enables control over creation of cavities within the sample. The setting time and handling time depend on the ambient temperature. The strength of the epoxy resin can be enhanced using a post curing process, depending on the post cure time duration and the temperature.

The sample was prepared by initially using a small volume of epoxy resin and hardener in a small cylindrical mould. The equal volumes of epoxy resin and hardener were dispensed into the mould using a syringe. The syringe contains two similar size tubes of epoxy resin and hardener; both tubes have similar size of nozzles. A plunger of the syringe dispenses equal volume of epoxy resin and hardener. The plunger was pressed slowly to ensure the volume of epoxy resin and hardener dispensed was equal. The mixture was stirred slowly to prevent unwanted bubbles in the mixture and was stirred for at least two minutes to ensure all epoxy and hardener have completely mixed. Five minutes later, a controlled volume of air was injected with a precise needle into the mixture to produce an artificial spherical cavity before the mixture cures over the following three minutes. The injected bubble did not move quickly towards the top surface of the epoxy because the viscosity of the epoxy had increased as it was in the halfway of curing. There was no trace of tunnels in the epoxy after the needle was pulled out. The volume of air injected in the epoxy determined the size of the spherical cavity. A smaller block of the epoxy containing the cavity was cut 24 hours after cavity creation. The epoxy was cut so that the position of the cavity is in the middle of the epoxy block.

After an air bubble has been injected into the epoxy resin and it has cured, it cannot be guaranteed that the shape of the cavity is a perfect spherical. However, it is assumed that the shape of the cavity is close to that of perfect spherical. This assumption is based on the observation of the cavity under a microscope with light, where the largest circumference of the cavity has been found to be a perfect circle. When the cross section of the sample containing the cavity is observed by cutting the sample into two semi cylindrical, the circumference of the cavity has also been found to be a perfect circle. Hence, it is assumed that shape of the cavity obtained is close to a perfect spherical. Moreover, this is the standard way for preparing a spherical cavity of diameter larger than 1 mm in a dielectric material that has been used in previous works [13, 14, 25]. In this work, the measurement results that have been obtained using all samples that have been prepared have the similar characteristics of the measurement results from previous works.

After that, a larger volume of epoxy resin and hardener was used in a larger cylindrical mould to prepare the complete sample of the test object. The diameter of the larger mould was made sure to be larger than the diameter of the high voltage electrode that was used in the measurement to prevent any surface discharges around the edge of the material. A layer of transparent plastic of thickness 1 mm was put on the surface of the mould before the epoxy resin was dispensed on the mould to ensure that it will not stick to the mould. The mixture was stirred slowly to prevent unwanted bubbles and was stirred for at least two minutes to ensure all epoxy and hardener was completely mixed. Then, the smaller epoxy block containing the spherical cavity, which had been prepared prior to this process, was placed in the middle of the larger mould after five minutes into the cure. If a smaller epoxy block of 1.7 mm thickness was to be placed in a larger

epoxy block of 2 mm thickness, the smaller block was gripped in 0.15 mm distance from the tips of the tweezers. The smaller block was put into the larger epoxy block until the tips of the tweezers reached the bottom surface of the mould. This ensured that the smaller epoxy block was located 0.15 mm above the bottom surface of the larger epoxy block.

The smaller epoxy block may drop down a bit once it was put into the larger epoxy block before the larger block cured completely. However, due to the larger epoxy block was already in the middle of curing process, the smaller epoxy block did not drop too much into the larger epoxy block and a slight position deviation from the middle of the material does not influence the electric field distribution in the cavity. There was no gap between the smaller and larger epoxy blocks after the larger block cured. The epoxy blocks bonded strongly with each other after curing.

The whole sample was then put into a vacuum oven immediately at room temperature to remove any unwanted bubbles before the epoxy fully turned into solid. Ten minutes later, the sample was removed from the oven because the sample it had completely solidified. All unwanted bubbles that existed in the sample had moved to the top surface of the epoxy. The sample was left for 24 hours at room temperature. This completed the curing process.

When the curing process had completed, the sample was removed from the mould. Since the thickness of the sample was uneven due to uneven top surface of the sample, the top surface was filed to remove traces of bubbles that had accumulated on the top surface during curing. This ensured the uniform thickness of the sample. The acceptable range of the location of the cavity is ± 0.25 mm from the middle of the sample thickness. From the FEA simulation model, the magnitude of electric field in the middle of the cavity is still almost symmetrical within this range. After filing the surface, the whole sample was cleaned with acetone to remove dirt and charges that may have accumulated on the sample.

The process of making the sample was followed by a post-curing process, where the sample was left for 4 hours at 90°C. The aim of post-curing is to enhance the properties of the epoxy. Generally the improved properties of the epoxy after post curing process are chemical resistance, temperature stability, dimensional stability, voltage breakdown resistance and water resistance and increased in glass transition temperature, thermal conductivity, resistivity and the breakdown strength. However, these were not verified in this experiment. Post curing is normally performed at 10 to 25°C above the maximum operating temperature of the epoxy (65°C), post curing temperature was set at 90°C.

After post curing had been completed, the sample was left at room temperature for 2 hours. Then, the whole surface of the sample was cleaned with acetone. Finally, the sample was coated with a gold layer on top and bottom surfaces of the sample by using a gold sputter coated machine for four minutes at 30 mA current. The aim was to

improve the electrical contact between the electrode and the sample and to eliminate potential triple junction discharge between the electrodes, sample and oil due to poor electrical contacts. The gold-coated area was 25 mm diameter on both sides of the surface. Figure 4.1 shows the prepared samples where the deposited gold layers are approximately 32 nm thick on each sample's surface.

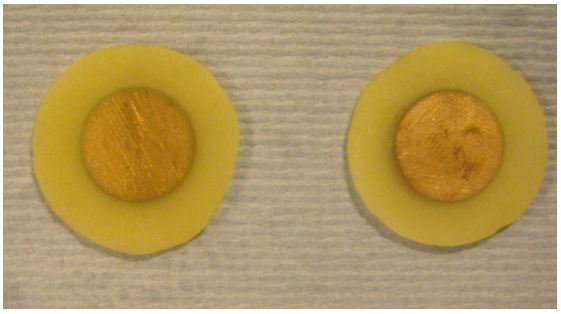

FIGURE 4.1: Gold coated epoxy samples.

4.1.3 Setup for the test samples

Figure 4.2 shows the schematic diagram of the test object which consists of a single spherical cavity of a diameter, d, placed in the middle of a cylindrical dielectric material of thickness, hmat and 38 mm diameter. The smaller rectangular block of epoxy resin containing the cavity has a thickness of h_{small} and 6 mm length and width. The cylindrical electrodes are stainless steel and diameter 25 mm. The whole test object was immersed in mineral oil to prevent surface discharges around the electrode and material boundary. The mineral oil has dielectric constant of 2.2, breakdown strength of 30 to 60 kV·mm^{-1} and a volume resistivity of 10^{11} to 10^{15} Ωm at 20°C [94, 99]. Mineral oil was used because its dielectric strength is higher than the dielectric strength of air (3 kV·mm^{-1}). An ac sinusoidal voltage was applied on the upper electrode while the lower electrode was always grounded.

Table 4.1 is a summary of the samples prepared for experiments. All samples contain a spherical cavity of diameter d located in the middle of epoxy of thickness hmat. All cavities were larger than 1 mm diameter as this is known to guarantee accumulation of charge on the cavity surface during the PD process. Thus, the effect of surface charge decay through conduction along the cavity wall can be studied experimentally. The size and shape of larger cavity were also easier to control. Sample 1 and 2 were used to study the effect of different applied voltage amplitudes and frequencies on PD activity. Samples 3 and 4 were used to study the effect of cavity diameters on PD activity and sample 5 was used in PD measurements undertaken at different material temperatures.

Figure 4.3 shows the test sample in the oil bath. The test arrangement consists of a high voltage electrode which is connected to a high voltage supply through a copper pipe, ground electrode which is connected to the ground by a black thin wire and an epoxy

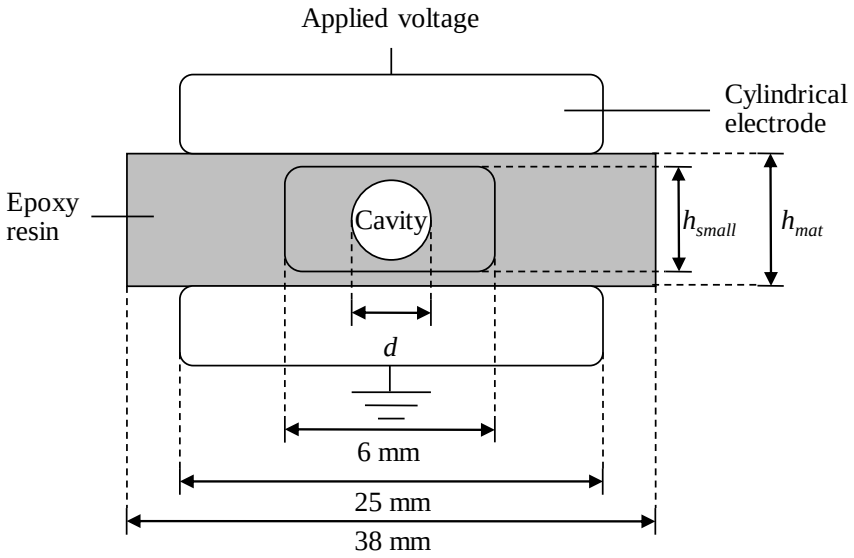

FIGURE 4.2: Schematic diagram of the test object.

Sample	**Cavity diameter, d (mm)**	**Thickness of the smaller block, h_{small} (mm)**	**Sample thickness, h_{mat} (mm)**	**Cavity location**
1	1.4	1.7	2.0	Middle of the epoxy
2	1.55	1.7	2.0	Middle of the epoxy
3	1.1	2.0	3.0	Middle of the epoxy
4	2.35	2.7	3.0	Middle of the epoxy
5	1.7	2.0	2.5	Middle of the epoxy

TABLE 4.1: Samples prepared for experiments.

resin sample placed between the two electrodes. The electrodes and sample are placed between two sheets of paxolin, which are held by a plastic leg at each corner. The whole arrangement is immersed in mineral bath.

4.2 The experiment

4.2.1 Phase resolved partial discharge analysis (PRPDA)

The PD measurement analysis technique that is generally adopted is Phase-Resolved Partial Discharge Analysis (PRPDA). Generally, PRPDA measurement equipment measures the apparent charge magnitude and phase of each PD occurrence and the PRPD pattern is obtained by sorting and counting each charge magnitude, q_j occurring at phase, ϕ_j of the applied voltage into a discretized two-dimensional (2D) counter array, C(ϕ_m,q_m) where $\phi_n \leq \phi_j \leq \phi_{n+1}$ and $q_m \leq q_j \leq q_{m+1}$. The PRPDA measurement equipment maps certain numbers of voltage cycles over a single voltage cycle and the phase of PD occurrence is discretized into X channels, over a range of 0 to 360. The magnitude

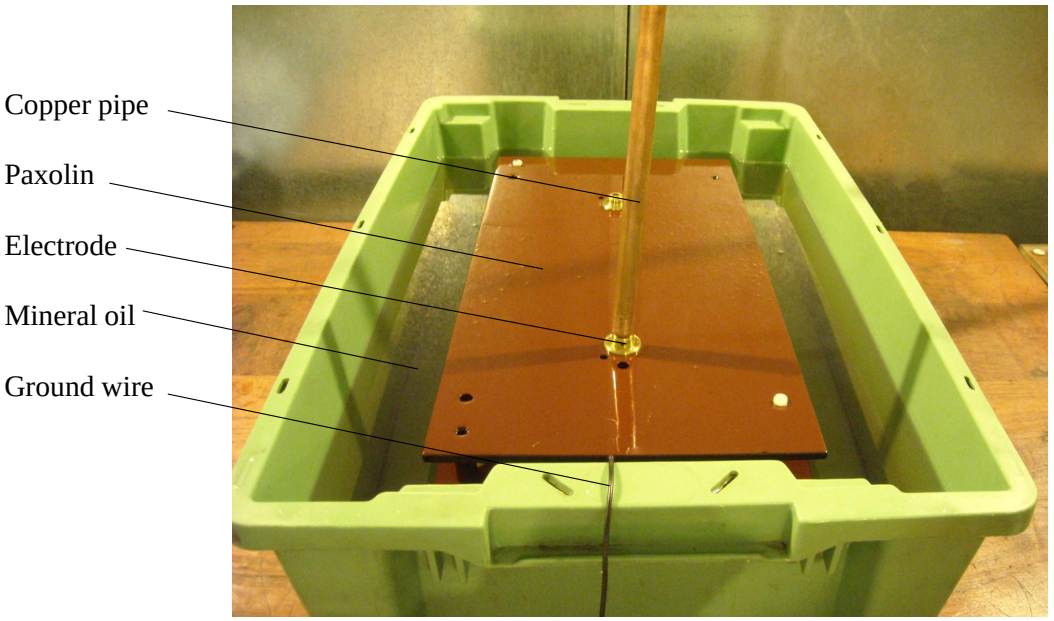

FIGURE 4.3: Test sample in an oil bath.

of PD is discretized with Y channels, where there are Y/2 channels each for positive and negative PD. The number, C(ϕ_n,q_m) are the counts of the discharge occurring at phase, ϕ_n with the apparent charge magnitude, q_m.

In 2D PRPD patterns, the x-axis is for the phase channel and the y-axis is for the charge magnitude channel. Each element in (x,y) is the number of discharges having a defined range of magnitude and occuring over a defined phase interval. This number is represented by differing levels of color intensity, where the higher the colour intensity of (x,y), the larger the number of events. In three-dimensional (3D) histograms, the PD pattern is known as ϕ-q-n plot, where ϕ on the x-axis is the PD phase of the applied voltage, q on the y-axis is the apparent charge magnitude and n on the z-axis is the number of PDs of a certain range of charge magnitude that occurs at a specific phase of the applied voltage. Figure 4.4 shows the mapping and sorting of each individual PD into X $\times$ Y channels and Figure 4.5 shows an example of 2D PRPD pattern and 3D ϕ-q-n plot. The advantage of using 2D PRPD pattern is the phase and charge magnitude of PD pattern can be clearly seen. However, the height of each PD count cannot be clearly seen, this is more obvious with the 3D ϕ-q-n plot. Thus, the user has to rely on the colourbar provided in the diagram. The numbers of phase and charge magnitude channels depend on the measurement system, 200 $\times$ 200 channels have been used for ϕ-q-n plots included in this thesis.

Figure 4.6 shows the flowchart to obtain a PRPD pattern and ϕ-q-n plot. First, all phase, ϕ_j and charge magnitude, q_j of PD occurrences are extracted. Then, the counter, C(ϕ_n,q_m), which is 200 $\times$ 200 channels, is initialized to zero and the maximum charge magnitude, q_{maxd}, for charge discretization, q_{maxd} is set equal to or higher than the maximum charge magnitude of q_j. Each of ϕ_j and q_j are discretized onto 200 channels

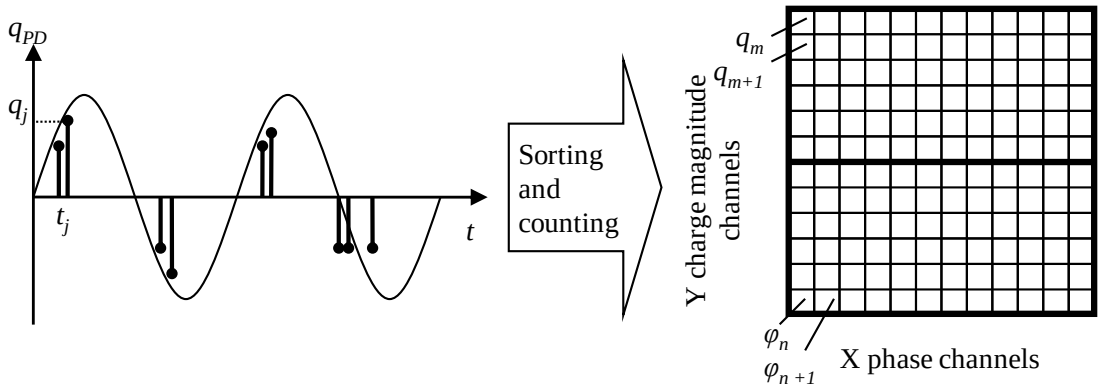

FIGURE 4.4: Mapping of each PD event into X × Y channels.

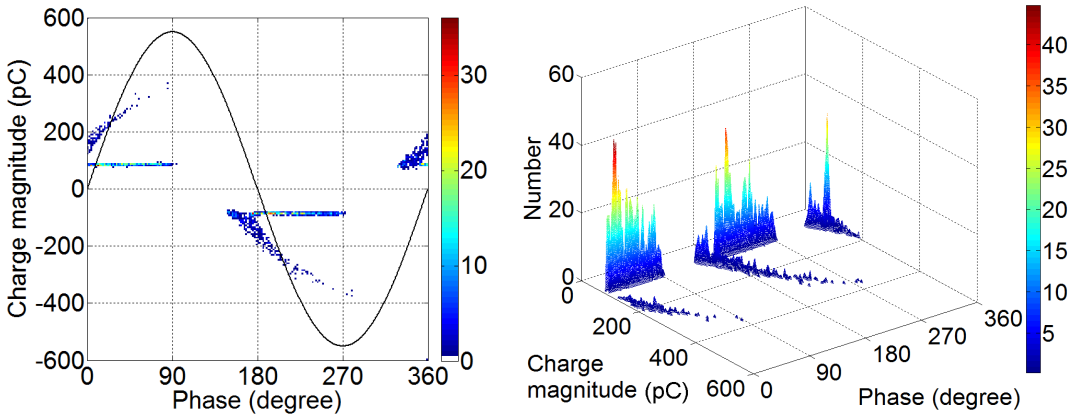

(a) 2D PRPD pattern

(b) 3D ϕ-q-n plot

FIGURE 4.5: Example of a PD pattern.

of phase, ϕ_n and 200 channels of charge magnitude, q_m. The number on each channels are counted and stored into C(ϕ_n,q_m). Finally, the PRPD pattern and ϕ-q-n plot are obtained.

4.2.2 Experimental setup

The equipment used for PD measurement is the mtronix MPD 600 system, which is manufactured by OMICRON. The mtronix MPD 600 system is a fully digital system which is suitable for laboratory and on-site measurement of PD activity in high voltage equipment. This setup provides many advantages over previous detection systems used for PD research. Previously, a Robinson PD detector and an associated with a digital signal oscilloscope (DSO), where the PD detector detects PD pulses from the test object and the DSO is used to display, monitor and save the PD pulses captured from the PD detector was used in the Tony Davies High Voltage Laboratory. The advantages of MPD 600 system are explained in the next sections.

Figure 4.7 shows the schematic diagram of the experiment that has been used to measure

PD activity. The experiment consists of a high voltage supply, a high voltage filter, a coupling capacitor C_k, a test object, a coupling device, a PD detector and a USB controller which is connected to a personal computer (PC) via fiber optic cables. The operating frequency range for the overall setup is 0.1 Hz to 2.5 kHz. The system supports for any detected PD signal of center frequency in the range of 0 Hz to 32 MHz with bandwidth range of 9 kHz to 3 MHz. The system noise is less than 15 fC. The PD event time resolution is less than 2 ns, which makes the detected pulse very precise.

A high voltage source is supplied from a low-voltage function generator signal, which has output frequency range of 0.1 mHz to10 MHz and output voltage range of 5 mV to 20 V AC peak-to-peak with a 1 mV resolution. The low-voltage signal is amplified by a high voltage amplifier of 1V/2000V gain and a maximum output voltage of 20 kV. Its input voltage range is 0 to 20 V AC peak-to-peak and input impedance is 25 kΩ nominal. A

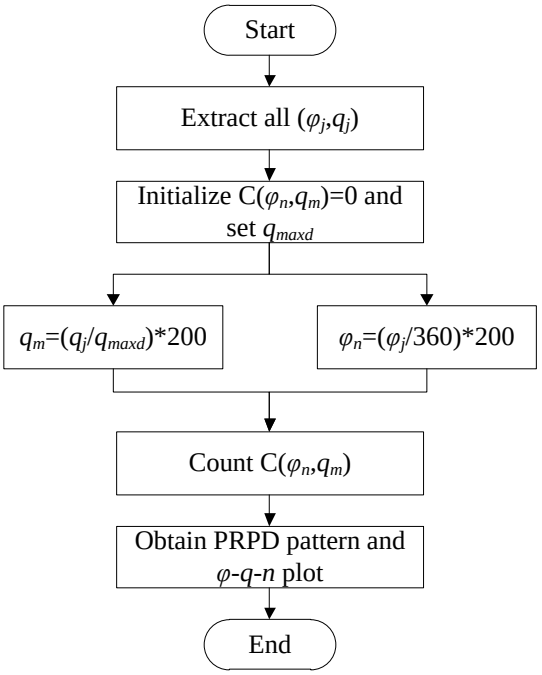

FIGURE 4.6: Flowchart to obtain PRPD histogram and ϕ-q-n plot.

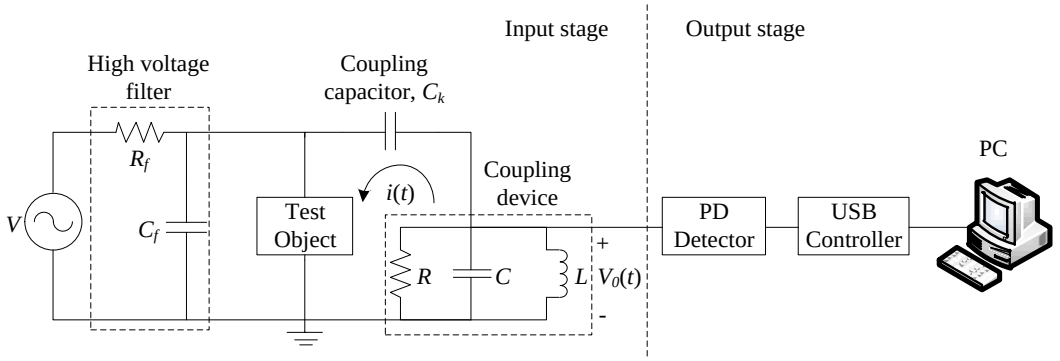

FIGURE 4.7: Schematic diagram of the experiment.

high voltage filter is used to reduce high frequency noise from the input signal amplified by the high voltage amplifier into the setup and also to eliminate high frequency surface discharge signals between the tip of the amplifier output and the ground shield of its insulation.

The low pass filter consists of three capacitors, C_f of 150 pF and voltage rating of 15 kV each which are connected in parallel and two resistors, R_f of 22 kΩ and voltage rating of 2.2 kV connected in series. C_f and R_f are connected between the high voltage amplifier and the test object. The setup of this low pass filter is chosen because it manages to eliminate unwanted high frequency signals into the measurement system. Although noise signals below 50 pC are unable to be filtered, it practically does not affect the PD experiment results because the detected minimum PD charge magnitude from the test object is larger than 50 pC. If higher resistance is used in the filter, the maximum effective RMS value of the high voltage output will be reduced while if higher capacitance is used, the sine waveform from the high voltage supply will be distorted when the applied voltage amplitude is larger than 10 kV RMS.

The voltage rating of the capacitor is chosen based on the maximum applied voltage amplitude that is used in the measurement, which is 14 kV peak-to-peak while the voltage rating of the resistor is chosen lower than 14 kV. This is because the capacitor voltage rating is already sufficient. However, if the test object breaks down during experiment, the resistors could be damaged due to short circuit but this is unlikely to occur because the breakdown strength of the test object is higher than 14 kV applied voltage. The value of coupling capacitor, C_k used is 1 nF and has a blocking voltage of 50 kV. It is connected in series with the coupling device and in parallel with the test object. The reason of this connection rather than connecting C_k in parallel with a serial connection of the coupling device and the test object is the PD detector is protected by C_k if the test object breaks down.

The concept of the PD detection system is based on measuring the current pulse across the test object. When a discharge happens in the test object, charges are transferred from the coupling capacitor, C_k to the test object to compensate the voltage drop across the test object. As a result, a current pulse, $i(t)$ of short duration, which is within nanoseconds range flows in the circuit and a voltage pulse, $V_0(t)$ is generated across the coupling device. The amount of charge transferred is called the apparent charge. The apparent charge magnitude is determined by the induced number of dipole moments of the real charge from PD in the cavity that produces a sudden change of the test object capacitance and their interaction with the electrodes of the system [30, 100].

The coupling device or CPL 542 measuring impedance measures the short-duration voltage pulse, $V_0(t)$ when a PD occurs. The output frequency of this equipment is in the range of 20 kHz to 6 MHz. A simplified parallel RLC circuit in the coupling device forms a wide-band PD measuring system. The value of each component in the coupling

device is not provided by the supplier. Referring to Figure 4.7, the coupling device is the end of the input stage of the measuring system.

The PD detector detects the magnitude of discharge pulse through its PD impulse input and the applied voltage amplitude through its voltage input. The PD impulse input frequency range of the device is 0 Hz - 20 MHz and the maximum PD impulse input voltage is 60 V rms. Referring to Figure 4.8, which shows the graphical user interface (GUI) of the mtronix software that is associated with the measurement devices, the center frequency used for charge integration setting is 350 kHz and the bandwidth is 300 kHz. This setting is chosen based on the IEC 60270 standard, where frequency range is 30 kHz to 100 kHz for lower limit, 500 kHz for upper limit and 100 to 400 kHz for bandwidth [30].

The output signals from the PD detector are connected to the USB controller via fibre optic cables and the data is sent to the PC for user to display, store and analyse PD events. The USB controller provides an interface between data transferred from the PD detector and the PC. The advantage of using fiber optic cables ahead of conventional cables, as where used in the previous PD measurement, is that it guarantees complete galvanic isolation between the PD detector and the USB controller. The elimination of ground loops reduces interference and improves the signal-to-noise ratio which in turn increases the sensitivity of the system. The system has 500 channels for phase and 400 channels for discharge magnitude, where 200 channels each for positive and negative discharge.

4.2.3 System calibration

Every time after the mtronix software is restarted, the system needs to be calibrated. The MPD 600 system allows charge calibration to be done digitally. A CAL 542 charge calibrator is connected in parallel with test object during calibration, where a calibration charge is injected to the electrode. The range of calibration charge is 1 to 100 pC, where 1 pC is equivalent to 1 mV pulse. Referring to Figure 4.8, the target value of the charge in 'Calibration Settings' is set equal to the target charge value of the calibrator and the 'Compute' button is pressed to complete the charge calibration. The calibrator is then removed from the system. This method ensures the charge calibration can be done more precise and straightforward manner. The calibration of the previous system was performed using a calibration pulse generated in the PD detector and is compared with the pulse injected by the calibrator. The pulse generated in the PD detector is adjusted until its magnitude is very close to the calibrator pulse magnitude. This method may not give a precise calibration and is dependent on the expertise of the operator.

The equipment also allows calibration for the applied voltage amplitude. This is done by applying a specific value of voltage amplitude on the system and the voltage is calibrated

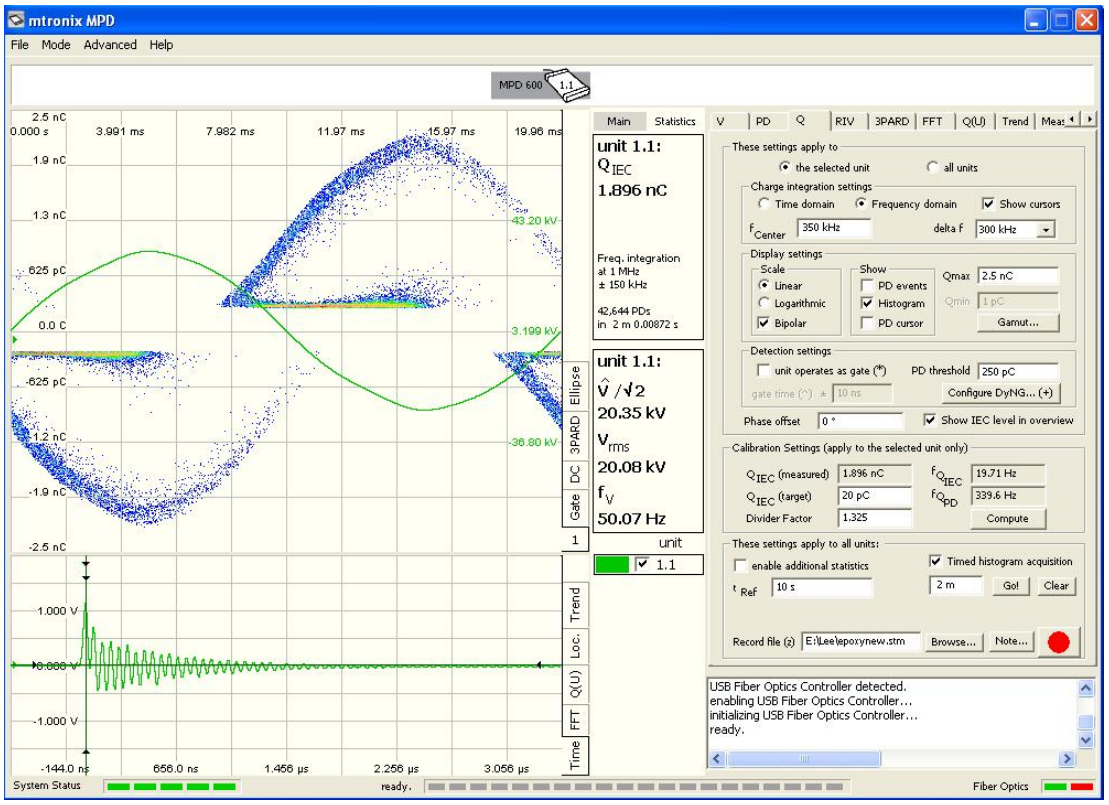

FIGURE 4.8: The graphical user interface (GUI) of mtronix software.

in similar way with the charge calibration but under the 'V' tab in the mtronix GUI, by referring to Figure 4.8. The high voltage voltmeter can be removed from the setup after the voltage calibration. This ensures that the setup is PD-free from the high voltage voltmeter. The waveform and amplitude of the applied voltage can be observed from the GUI. The GUI allows interactive display for users, allowing the users to view PRPD pattern, ϕ-q-n plot and PD pulse signals at the instance, which are unavailable in the previous system.

4.2.4 Amplifier gain setup

When PD measurement is performed using the Robinson PD detector and DSO, the common difficulty found is setting the amplifier of the equipment. Since different conditions of the cavity and stress yield in different range of discharge magnitude, the amplifier gain needs to be adjusted manually based on the discharge magnitude range. If the amplifier gain is set too low, the detected PD pulse magnitude may be lower than the noise level and this causes difficulty in segregating between PD pulses and noise. However, if the gain is set too high, PD pulse magnitude may be larger than the dynamic range of the amplifier and PD pulse could not be detected. This problem may be more difficult to overcome if the range of PD pulse magnitudes is very large. However, the amplifier gain of the MPD 600 system can be set to auto gain in the mtronix GUI, where the gain

responds automatically corresponding to the discharge magnitude. Thus, this reduces the burden of setting the amplifier every time measurements are performed.

Figure 4.9 shows the actual measurement setup, which consists of the test object and the coupling capacitor, which are connected to the high voltage supply with copper pipes.

FIGURE 4.9: The actual experiment setup.

4.3 Measurement Methods

4.3.1 Pre-measurement

It is important to make sure that the oil is bubble free because any bubbles in the oil might affect the measurement results. Sharp edges are also avoided to ensure no corona discharge occurs. Prior to any measurement, the test arrangement was tested to ensure that it was PD free. It was found to be PD-free up to 30 kV.

In this experiment, when a new sample is tested, the voltage level of the first discharge may not be the real inception voltage because there may be a delay due to the lack of an initial free electron in a cavity which has never experienced PD yet. Thus, the required applied voltage amplitude is left on for five minutes to introduce surface charges on

the cavity surface, which will act as initial free electron for PD. After that, the applied voltage is turned off before being reapplied one minute later. The supply voltage is increased slowly until the first discharge appears and that voltage level is recorded as the measured inception voltage. If the supply voltage is increased too fast, the true inception voltage could be easily missed. However, it has been reported that the voltage ramp rate does not significantly affect the inception voltage [17]. The voltage is then increased until it reaches the required value.

After the voltage is applied to the test object, the sample is stressed for 2 hours to ensure a quasi-static condition is reached. This is because within the first 30 minutes of testing, the number of PDs per cycle and the maximum charge magnitude are seen to decrease. However, after 2 hours, the number of PDs per cycle and the maximum charge magnitude are almost constant. Therefore, all new samples are pre-stressed for 2 hours using a 50 Hz applied voltage before any measurement results are obtained. This is done to ensure a consistent measurement procedure is taken because different stress times might yield different results making comparison difficult. Measurements are taken for several voltage cycles to ensure adequate data is captured and are repeated three times for consistency.

4.3.2 Variable applied frequency measurement

The sample which consists of a spherical cavity of diameter 1.5 mm has been tested using a descending and ascending sequence of applied frequencies continuously. The order of applied frequencies was 50, 20, 10, 5, 1, 5, 10, 20 and 50 Hz and this allowed observation of whether the sequence affected the PD measurement. The test was started with the highest applied frequency in order to minimize the time required for the first electron to become available to generate the first discharge. The minimum frequency was chosen to be 1 Hz because the PD detector system is not stable at frequency below 1 Hz. The maximum frequency was 50 Hz because the high voltage amplifier output became distorted for higher frequencies due to the high voltage filter.

The sample was initially stressed at 50 Hz 14 kV for 2 hours. Then the sample was left for an additional 30 minutes at the desired frequency before any measurement results were taken. Measurement results were obtained for 500 cycles at each frequency. The tests were undertaken continuously in order to provide a consistent stress condition on the test object as any interruption between two consecutive applied frequencies might affect the measurement results. It was observed that when the applied voltage was removed from the system and then reapplied 1 hour later, the PRPD pattern of the sample reverted to its initial pre-stressing pattern immediately. The test time to capture data for all of the applied frequencies is around 8 hours.

4.3.3 Variable applied voltage amplitude measurement

For measurements of PD activity under different applied voltages, the applied voltage sequence was 14, 16, 18, 20, 18, 16 and 14 kV at frequency 50 Hz and this allowed observation of whether the sequence affected the PD measurement. The test object was stressed for 2 hours at 14 kV 50 Hz before measurements were taken. After the voltage was altered, the test object was stressed for 15 minutes before any measurement was taken to ensure that quasi-static conditions were achieved. The choice of 15 minutes was based on the assumption that far less settling time was required compared to when the frequency was altered. The average time interval between two consecutive discharges is almost constant when the applied voltage amplitude is changed and the frequency is constant. Thus any changes in local condition of the cavity and the cavity surface are relatively small.

Although starting the test at the lowest applied voltage increases the time delay for the first electron to become available, it also limits any cavity surface degradation. Higher applied voltages will have higher PD repetition rate which may increase degradation and influence the PD patterns at the next applied voltage amplitude. The experimental arrangement is similar to that shown in Figure 4.7 except that the high voltage source and filter were replaced with a step-up transformer capable of supplying 60 kV rms. The total test time for the sequence of applied voltages is around 5 hours.

4.3.4 Variable cavity size measurement

For PD measurements of different spherical cavity sizes, each sample was stressed at 50 Hz 18 kV for 2 hours before the measurements of 500 applied voltage cycles were taken. Then, the applied voltage was increased to 20 kV and measurements were taken 30 minutes later. This was done to observe the effect of applied voltage amplitude for different cavity sizes on PD activity. The experimental arrangement is the same as the measurement for different applied voltage amplitudes.

4.3.5 Variable material temperature measurement

The effect of temperature of the material on PD activity was studied by applying a temperature sequence of 20, 35, 50, 65, 50, 35 and 20°C at 50 Hz, 20 kV. The maximum temperature of the material was selected at 65°C because the maximum operating temperature of the material is higher than 65°C after post cure. A smaller paxolin sheet holding the electrode and the material was used and was immersed in mineral oil in a beaker instead of in oil bath. First, the sample was tested at 20°C at 50 Hz 20 kV for two hours before measurements were taken. Then, the beaker containing the test object was disconnected from the whole experiment setup and was transferred

into a fan oven to increase the temperature of the material. The beaker was left for 30 minutes at 35°C in the fan oven to ensure that the temperature of the test object was uniform. Then, the beaker was taken out from the fan oven and the whole beaker was insulated with polystyrene sheets. This was done to ensure the temperature of the mineral oil and the test object remained at a specific temperature for a longer period of time. The temperature only decreased 0.3°C in 30 minutes. This method was used because there is difficulty of connecting the high voltage supply to the test object when using a temperature chamber.

After that, the insulated beaker was reconnected to the measurement system and the voltage was reapplied. Measurements were taken 10 minutes after the voltage was reapplied in order to allow the test object to reach quasi-static condition at the new temperature. The insulated beaker containing the test object was then removed from the system again and the polystyrene sheets covering the beaker were removed before the beaker was placed into the oven again to increase the temperature. These processes were repeated until the whole sequence of the temperature was completed. The experiment took between 7 to 8 hours.

4.4 Data Representation

The GUI of the mtronix software has an 'Export Function' option for data acquisition, which allows the user to export PD data to MATLAB. The data is exported when the recorded sequence of PD events is replayed in the mtronix software. Thus, the user can process and analyse data for other meaningful purposes, such as evaluating the sequence of discharge events and obtaining PD phase and charge magnitude distributions. However, the exported data from mtronix cannot be read directly by MATLAB because it is recorded as a binary file. Therefore, MATLAB code has been written to read the data. The well-known PD characteristics usually used to represent PD measurement results without interpreting the PD patterns are the number of PDs per cycle, total apparent charge per cycle, mean charge and maximum charge magnitude.

4.4.1 Phase distributions

PRPD pattern and ϕ-q-n plot can be represented by various PD phase distributions. The commonly used PD phase distributions are:

$H_n{}^+(\phi)$ and $H_n{}^-(\phi)$ - Positive and negative number of PDs per cycle against phase distribution respectively, where

$$H_n^{\pm}(\phi_i) = \frac{1}{N}\sum_{j=1} n(\phi_i, q_j^{\pm}) \tag{4.1}$$

$H_{qs}{}^{+}(\phi)$ and $H_{qs}{}^{-}(\phi)$ - Positive and negative total apparent charge magnitude per cycle against phase distribution respectively, where

$$H_{qs}^{\pm}(\phi_i) = \frac{1}{N}\sum_{j=1} q_j^{\pm} n(\phi_i, q_j^{\pm}) \tag{4.2}$$

$H_{qn}{}^{+}(\phi)$ and $H_{qn}{}^{-}(\phi)$ - Positive and negative mean charge magnitude against phase distribution respectively, where

$$H_{qn}^{\pm}(\phi_i) = \frac{H_{qs}^{\pm}(\phi_i)}{H_n^{\pm}(\phi_i))} \tag{4.3}$$

$H_{qm}{}^{+}(\phi)$ and $H_{qm}{}^{-}(\phi)$ - Positive and negative maximum charge magnitude against phase distribution respectively, where

$$H_{qm}^{\pm}(\phi_i) = \max\left|q_j^{\pm}(\phi_i)\right| \tag{4.4}$$

where ϕ_i is i-th element of the phase, q_j is j-th element of the charge magnitude and N is the number of cycles.

Each phase distribution above indicates the behaviour of PD activity in terms of phase of discharge occurrence. The $H_n(\phi)$ distribution indicates how frequent discharges occur at each phase of the applied voltage per cycle. The $H_{qs}(\phi)$ distribution shows the total apparent charge per cycle at each phase of the applied voltage. The $H_{qn}(\phi)$ distribution is the average of how frequent discharge events at each phase while the $H_{qm}(\phi)$ distribution indicates the trend of maximum charge magnitude with respect to each phase of the applied voltage.

The least mean square error (MSE) of PD phase, $(\text{MSE})_\phi$ and charge magnitude, $(\text{MSE})_q$ distributions between measurement and simulation results are calculated using

$$(MSE)_\phi = \frac{1}{360}\sum_{i=1}^{360}\left[H_n(\phi_i)_M - H_n(\phi_i)_S\right]^2 \tag{4.5}$$

$$(MSE)_q = \frac{1}{360}\sum_{i=1}^{360}\left[H_{qs}(\phi_i)_M - H_{qs}(\phi_i)_S\right]^2 \tag{4.6}$$

where $H_n(\phi_i)$ and $H_{qs}(\phi_i)$ are the number of PDs and charge mangitude per cycle against phase distributions while M and S are the measurement and simulation data respectively.

4.4.2 Other PD data

The PD charge magnitude distribution is the number of PDs occurring with specific charge magnitude. The cycle to cycle behaviour of PD events can be analysed by using graphs of charge magnitude and applied voltage amplitude of PD events against phase of the applied voltage for certain voltage cycles.

4.5 Measured permittivity of the material

The permittivity of a dielectric material is known to be temperature and frequency dependent [50]. Figure 4.10 shows the measured real and imaginary permittivity of the dielectric material used in the experiment as a function of material temperature and frequency of the applied voltage. When the material temperature is increased, the apparent dielectric loss factor increases. Higher temperature enhances the transition of the dielectric from glassy to rubber form. When this happens, the electron mobility of the polymer is enhanced, dipole self-organization is facilitated and the orientational polarization becomes easier. Thus, the permittivity of the material increases with the temperature [101]. However, when the applied frequency is increased, the permittivity of the material decreases because dipole orientation in the material does not respond as fast as with the change of the electric field magnitude.

4.6 Summary

The material that has been chosen for the experiment in this work is Araldite Rapid epoxy resin. Samples with a spherical cavity within the epoxy resin have been prepared for PD measurement of different stress conditions and cavity sizes. The stress conditions are the applied voltage amplitudes and frequencies of the applied voltage, temperature of the material and different cavity sizes. The setup of the experiment is based on the mtronix PD detector system which is adopted from the PRPDA technique. The well-known ways of representing PD activity patterns are through ϕ-q-n plots, PRPD patterns and phase and charge magnitude distributions. Without treating the sequence of PD events, PD data is usually represented by the number of PDs per cycle, total charge per cycle and mean and maximum charge magnitudes. From the measurement, the permittivity of the epoxy resin used in the experiment increases with material temperature but decreases with frequency of the applied voltage. The comparison between measurement and simulation results for different applied stresses and cavity sizes are detailed in Chapters 7 and 8. This allows critical parameters and physical mechanisms affecting PD activity from the PD simulation model for different stress conditions can be identified.

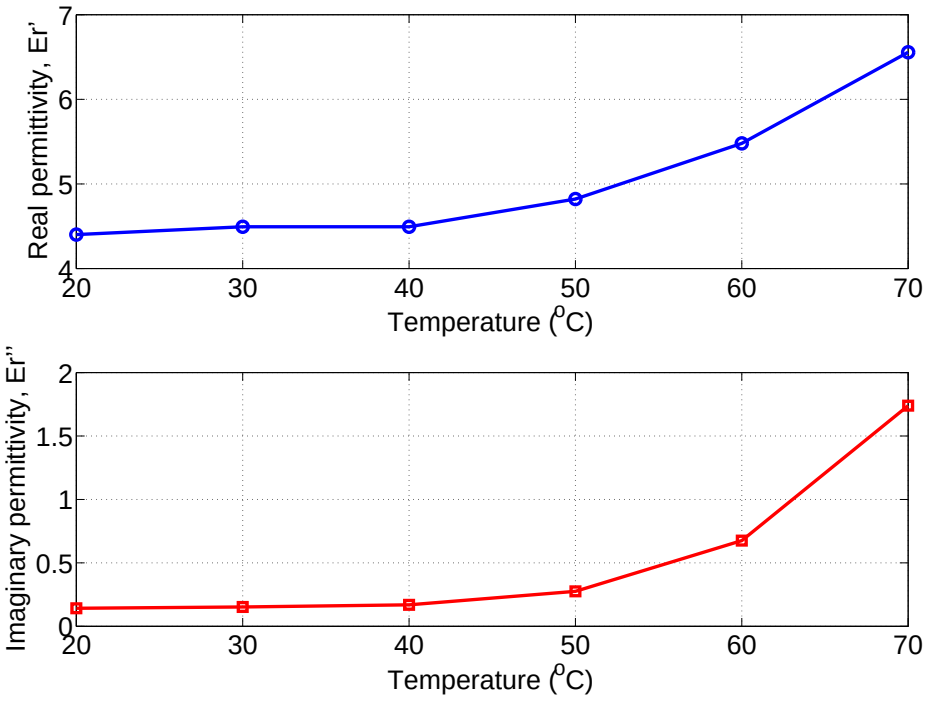

(a) Applied frequency is 50 Hz

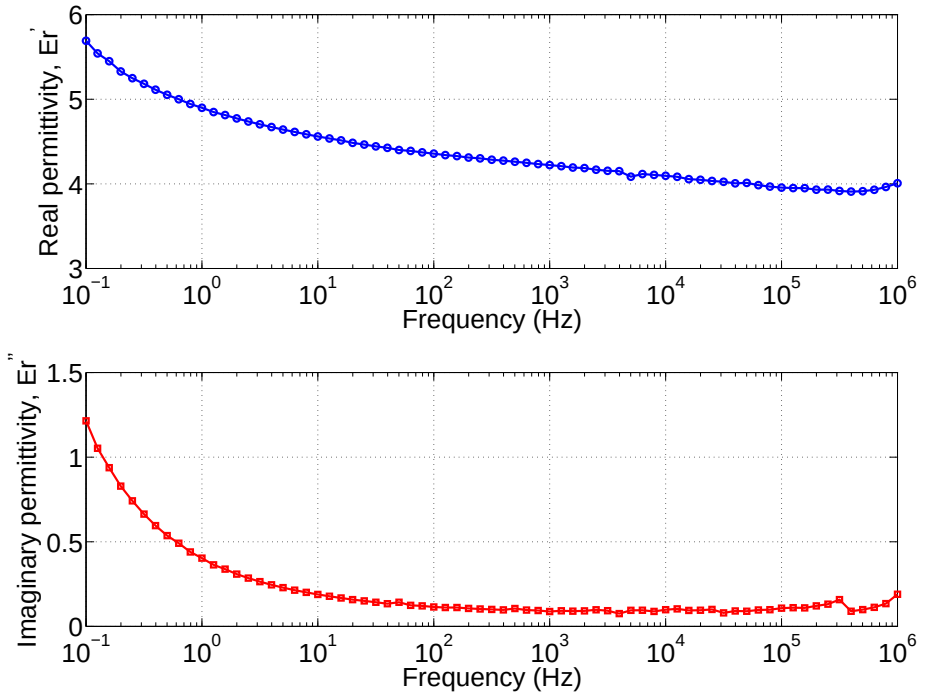

(b) Material temperature is 20°C

FIGURE 4.10: Measurement of real and imaginary relative permittivity of epoxy resin.

Chapter 5

Partial Discharge Measurement Results

PD measurement results are presented in this chapter. PD measurements have been performed for different applied voltage amplitudes and frequencies, spherical cavity sizes and material temperatures. Results of PD events for numerous voltage cycles are summarized through PRPD patterns, ϕ-q-n plots and phase and charge magnitude distributions. The number of PDs per cyle, total charge magnitude per cycle and mean and maximum charge magnitude as a function of different stress conditions and cavity sizes are also presented.

5.1 PD activity against time of the applied voltage

The test object for this experiment consisted of a spherical cavity of diameter 1.4 mm located in the middle of a dielectric material of thickness 2 mm. Figure 5.1 shows the measured number of PDs per cycle, total charge magnitude per cycle, mean charge and maximum charge magnitude while Figure 5.2 shows the measured ϕ-q-n plots at different times during which a 50 Hz, 14 kV ac applied voltage was present. In the first 1.5 hours, the number of PDs per cycle and the total charge magnitude per cycle decrease significantly and from the ϕ-q-n plots in Figure 5.2, the number of PDs occurring near the minimum charge magnitude also decrease. This might be due to the change of the cavity surface properties, such as an increase in the cavity surface conductivity, which reduces the electron generation rate. There is no significant change in the mean charge and maximum charge magnitudes with time. However, after 1.5 hours, the number of PDs per cycle, the total charge magnitude per cycle and the number of PDs occurring near the minimum charge magnitude in the ϕ-q-n plots are fairly constant. Thus, the test object is assumed to achieve a quasi-static condition 2 hours after the voltage has been applied, where the measured PD data has become stable and do not change significantly

with time of the applied stress. Therefore, each new test object was stressed for 2 hours at the specific applied voltage before any measurement was recorded. Overstressing (i.e. for more than a few hours) could cause aging to take place in the cavity and the PD patterns might change drastically [102, 103].

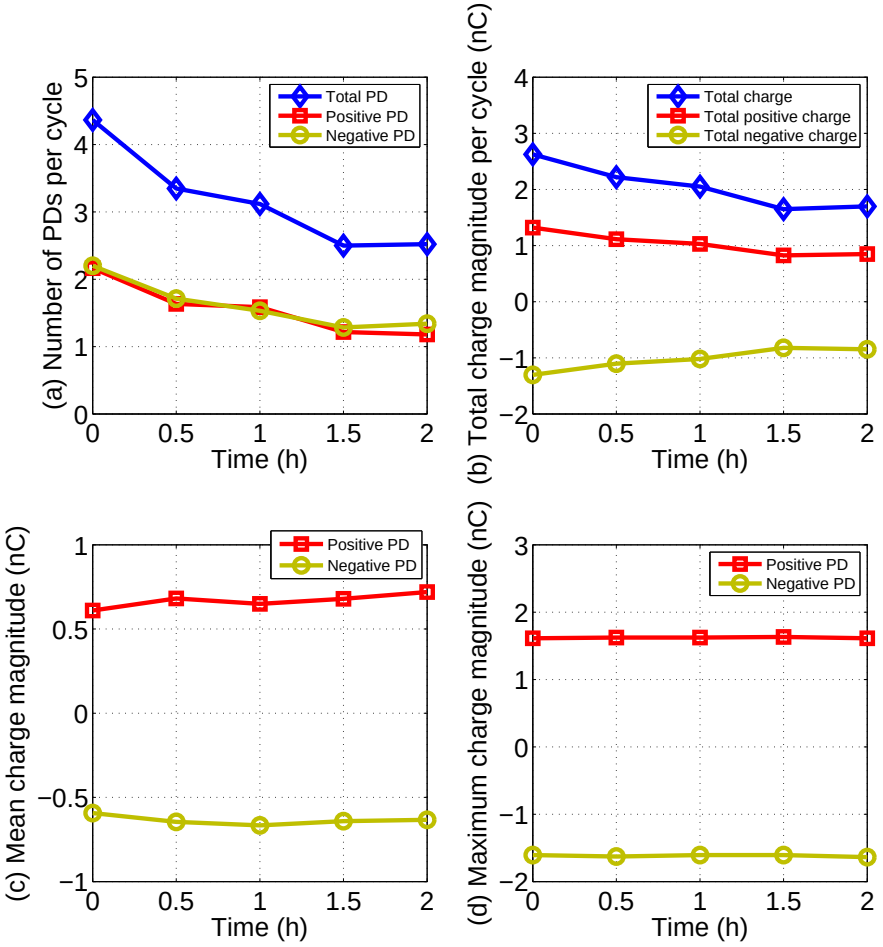

FIGURE 5.1: PD data as a function of time of the applied voltage from the measurement (50 Hz, 14 kV applied voltage).

5.2 Influence of applied voltage amplitude on PD activity

The PD data obtained for a spherical cavity of diameter 1.4 mm in a dielectric material of thickness 2 mm as a function of 50 Hz applied voltage amplitude, U_{app} is shown in Figure 5.3. For increasing voltage, the number of PDs per cycle, the total charge magnitude per cycle and the maximum discharge magnitude increase but the mean charge magnitude decreases. Discharges show a symmetrical behaviour between positive and negative discharges. This is because the cavity is located near to the middle of the material, thus the electric field distributions on the upper and lower cavity surface are the same. Only the ascending order of the applied voltage is shown here, very similar results were obtained as the voltage was reduced. When the applied voltage is

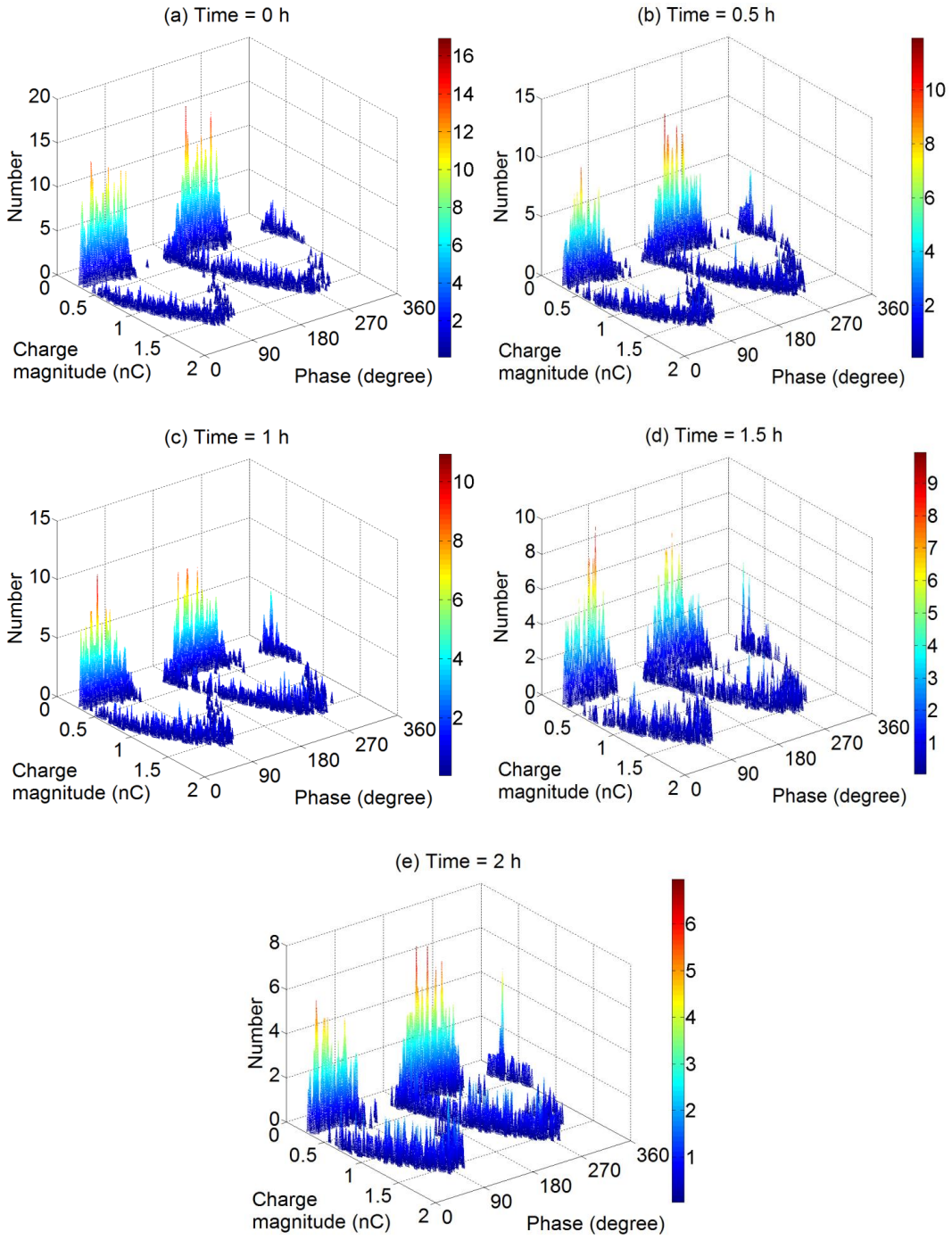

FIGURE 5.2: Measured ϕ-q-n plots at different times during the experiment.

increased, the electric field is enhanced and the electron generation rate is increased, which corresponds to a larger number of initial free electrons in the cavity. Therefore, the statistical time lag decreases, resulting in more PDs occurring earlier in the phase of the applied voltage. Consequently, there are more PDs per cycle as the applied voltage amplitude is increased [104].

The total charge per cycle also increases with increasing voltage because of the higher PD repetition rate. However, the mean charge magnitude decreases as the applied voltage

is increased because the increase in the number of PDs per cycle is greater than the increase in total charge per cycle. The reduction of statistical time lag as the applied voltage is increased causes more PDs per cycle but they have lower charge magnitudes. The maximum charge magnitude increases with increasing applied voltage because the higher applied voltage ensures a larger voltage drop across the cavity when a PD occurs.

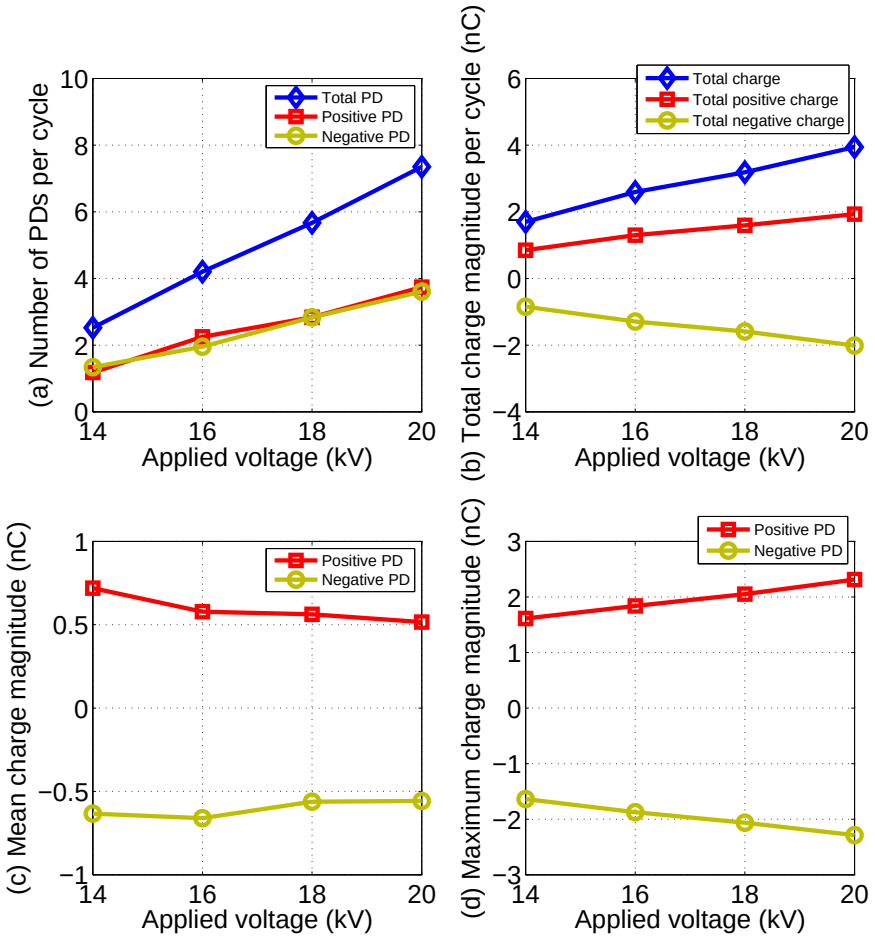

FIGURE 5.3: PD data as a function of applied voltage amplitude from the measurement.

Figure 5.4 shows the measured PRPD patterns for different applied voltage amplitudes. The 'rabbit-ear' like curves where PDs occur with higher charge magnitude and broad 'straight-line' curve patterns where PDs occur with a lower charge magnitude are clearly seen. When increasing the applied voltage, the PD patterns do not change significantly but the curve of the 'rabbit-ear' like patterns is larger and the density of PDs near the minimum charge magnitude increases. Higher applied voltages increase the maximum voltage across the cavity, resulting in a larger maximum PD charge magnitude.

PRPD patterns shown in Figure 5.4 can be further analysed using the 2D plots shown in Figure 5.5, which clearly illustrate the effect of applied voltage on PD activity. The shapes of each phase distribution for different applied voltages are similar to each other. Each plot shows that when the applied voltage is increased, the number of PDs per cycle, total charge magnitude per cycle and maximum charge magnitude increase but

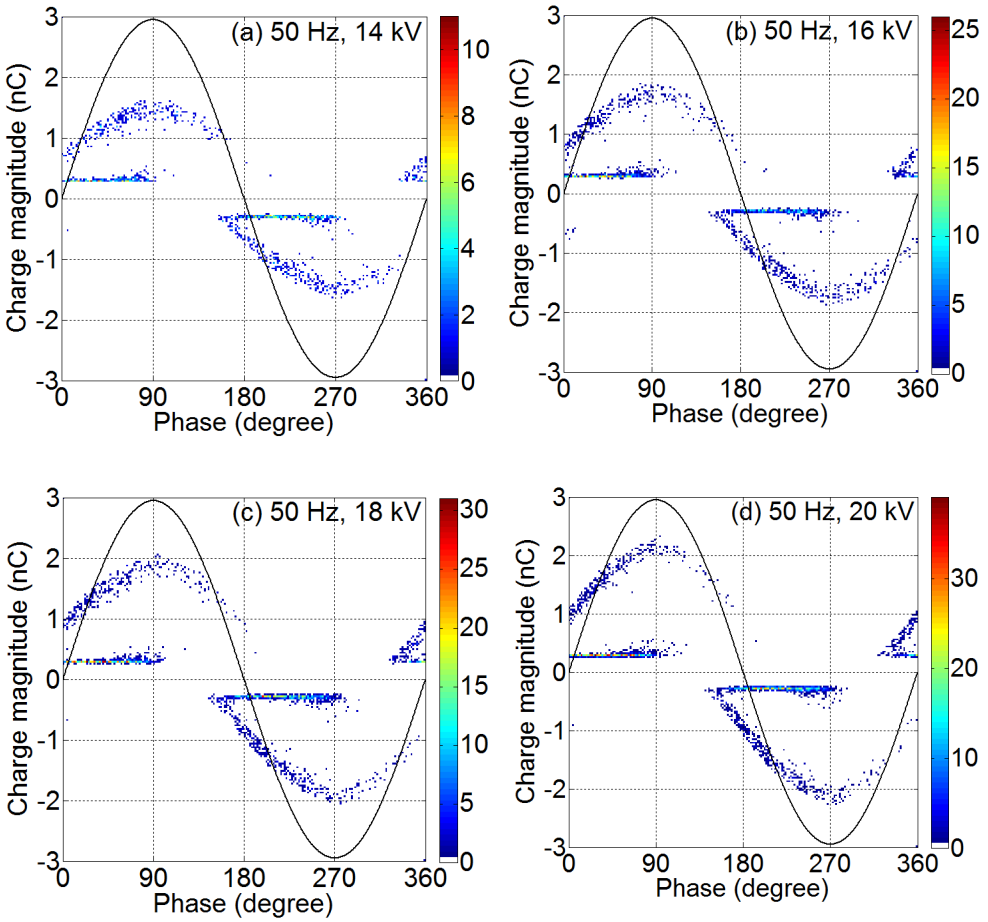

FIGURE 5.4: PRPD patterns as a function of applied voltage amplitude.

mean charge magnitude decreases at generally across the whole phase of the applied voltage. Referring to Figure 5.5(a), most of discharges occur at the rising edge of the applied voltage and less discharges occur at the end of the falling edge of the applied voltage as the electron generation rate is higher at the rising edge. The earliest phase of PD occurrence is shifted forward in phase when the applied voltage is increased due to an enhanced electron generation rate.

In Figure 5.5(b), the $H_{qs}(\phi)$ distribution has a right-skewed distribution. Since more PDs occur earlier, at the rising edge rather than at the peak of the applied voltage, the total charge magnitude per cycle is also higher over that region. Dividing $H_{qs}(\phi)$ by $H_n(\phi)$ gives the $H_{qn}(\phi)$ distribution shown in Figure 5.5(c). The mean charge magnitude is higher in the second and fourth quadrants of the applied voltage because less PDs per cycle occur in those regions. From Figure 5.5(d) which shows the $H_{qm}(\phi)$ distribution, the maximum charge magnitude is largest at the peak applied voltage amplitude (90 and 270 degrees) because the voltage across the cavity is also at a maximum.

PD charge magnitude distribution for different applied voltage amplitudes is shown in Figure 5.6. For increasing applied voltage, the number of PDs occurring with lower charge magnitude is higher but PDs occurring with larger charge magnitude is lower.

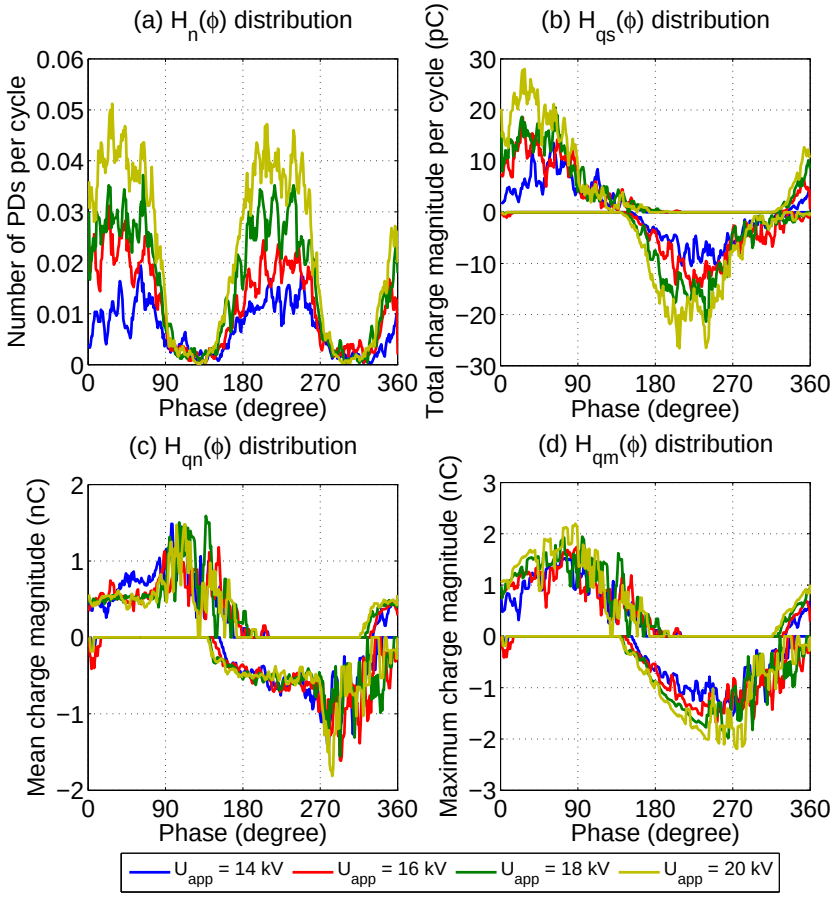

FIGURE 5.5: PD phase distributions as a function of applied voltage amplitude.

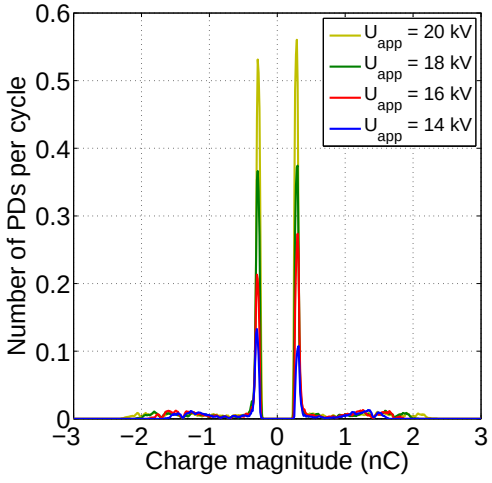

FIGURE 5.6: PD charge magnitude distribution as a function of applied voltage amplitude.

Since a higher applied voltage enhances the electron generation rate, the statistical time lag is reduced, resulting in PDs to occur near to the inception voltage. Thus, the voltage drop across the cavity is smaller when a PD occurs and lower PD charge magnitudes result.

5.3 Influence of applied frequency on PD activity

The PD data of the measurement results as a function of frequency, f is shown in Figure 5.7. The spherical cavity diameter is 1.55 mm and is located within a dielectric material of thickness 2 mm. The applied voltage amplitude is 14 kV ac. When the frequency is decreased, the number of PDs per cycle and the total charge per cycle decrease but the maximum PD magnitude remains constant whilst the mean charge magnitude increases. During the experiment, the obtained results indicated that the order of applied frequency did not affect PD activity. Thus only the descending order of the applied frequency is displayed here.

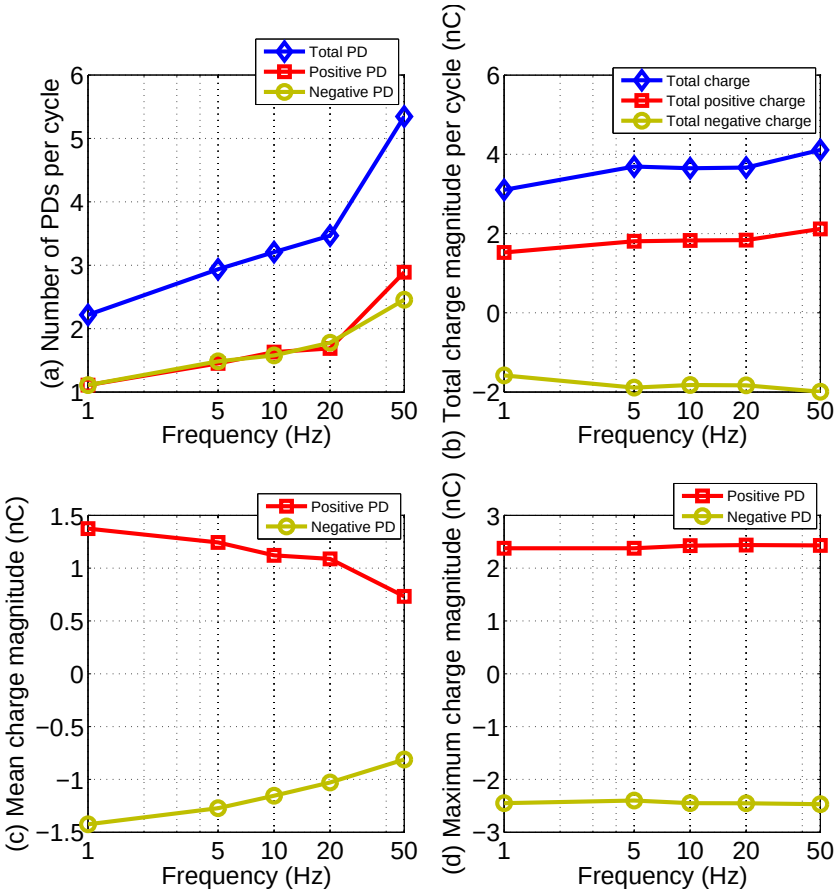

FIGURE 5.7: PD data as a function of applied frequency from the measurement.

The number of PDs per cycle increases with increasing applied voltage frequency because the cavity surface charge decay between consecutive discharges is less significant [104]. At higher frequencies, there is more charge on the cavity surface and available in local shallow traps when the next PD is likely to occur. Thus the electron generation rate is higher and PD occurs almost immediately after the inception voltage level is exceeded, resulting in a higher PD repetition rate for higher applied frequencies. These results are consistent with other measurement results for a spherical cavity where the number of PDs per cycle is higher with increased applied frequency [68].

The total charge magnitude per cycle slightly increases when the frequency is increased because the number of PDs per cycle increases, resulting in higher total charge magnitude per cycle. However, the increase in total charge magnitude per cycle is small because there is a corresponding decrease in the number of discharges with higher charge magnitudes. At lower frequency, the effect of surface charge decay is more significant, reducing the electron generation rate and increasing statistical time lag. Hence, more PDs occur at voltages higher than the inception voltage, resulting in a reduced number of PD events but with larger individual PD charge magnitudes.

The mean charge magnitude decreases with increasing frequency because there are more discharges having lower magnitudes. The maximum charge magnitude is independent of frequency because the applied voltage amplitude is unaltered, resulting in the same maximum voltage drop across the cavity when PD occurs.

Figure 5.8 shows the measurement of ϕ-q-n plots as a function of frequency of the applied 14 kV voltage. For a frequency of 50 Hz, the 'rabbit-ear' like curves due to higher magnitude events are clearly separated from lower magnitude PDs. However, as the applied frequency is decreased the 'rabbit-ear' curves disappear and the characteristic 'turtle' like pattern can be observed, especially at very low frequencies [68]. As the applied frequency is decreased, there are less lower charge magnitude PD events. However, the number of PDs occurring on the rising edge of the 'rabbit-ear' curve slightly increases as the applied frequency decreases. This may be due to the surface charge decay effect between consecutive discharges that is more significant over the longer period of the applied voltage. This effectively decreases the electron generation rate, resulting in an increased statistical time lag and hence discharges continue to occur at voltage levels higher than the inception voltage.

The PD phase distributions of PRPD patterns in Figure 5.8 are shown by Figure 5.9. From the $H_n(\phi)$ distribution in Figure 5.9(a), there are more PDs occurring in the first and third quadrants than the second and fourth quadrants of the applied voltage. When the applied frequency is decreased, there are less PDs per cycle at almost each phase of the applied voltage and the earliest phase of PD occurrence is shifted forward. From the $H_{qs}(\phi)$ distribution shown in Figure 5.9(b), the total charge magnitude per cycle at each phase does not change significantly with the applied frequency. However, at 180 and 360 degrees, the total charge magnitude per cycle decreases at lower applied frequency because less PDs occur at the earlier phase of the applied voltage due to the longer statistical time lag. At lower applied frequencies, the effect of surface charge decay on PD activity is more significant. The charge magnitude per cycle in the second and fourth quadrants is smaller than in the first and third quadrants of the applied voltage because more PDs occur on the rising edge of the applied voltage. The $H_{qn}(\phi)$ distribution shows the mean charge magnitude increases across the whole phase range with decreasing applied frequency (Figure 5.9(c)). The $H_{qm}(\phi)$ distribution in Figure 5.9(d) shows that the maximum charge magnitude distribution does not change significantly with the

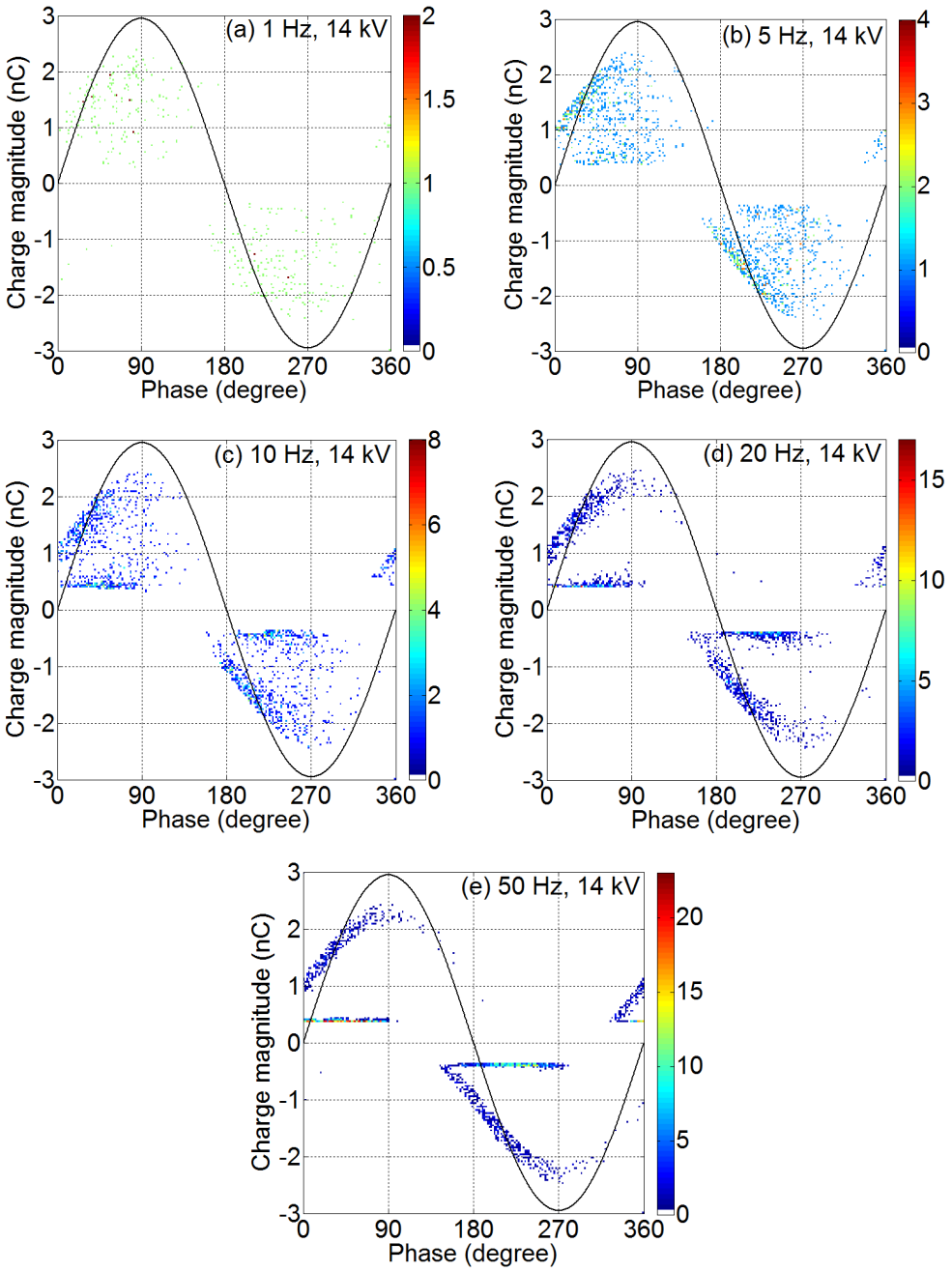

FIGURE 5.8: PRPD patterns as a function of applied frequency.

applied frequency because the applied voltage amplitude is always 14 kV.

Referring to Figure 5.10, when the applied frequency is decreased, the number of PDs occurring near the minimum charge magnitude decreases [105]. Since the surface charge decay effect between consecutive discharges is more significant at lower frequencies, the electron generation rate is lower, increasing the statistical time lag and less PDs occur with lower charge magnitudes.

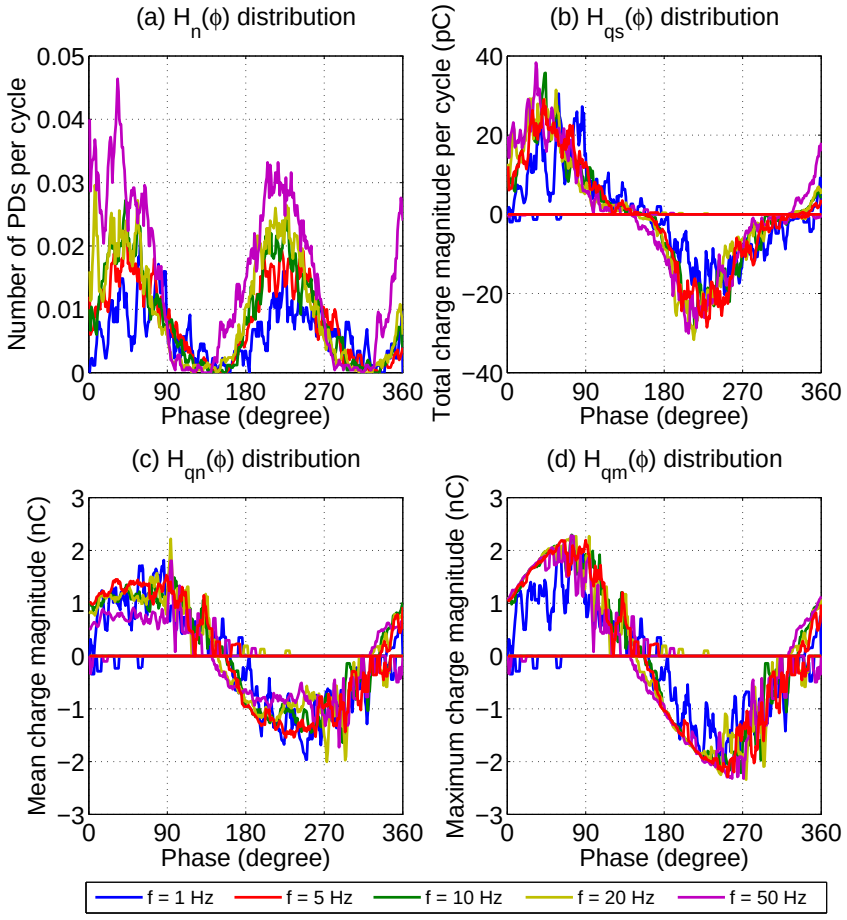

FIGURE 5.9: PD phase distributions as a function of applied frequency.

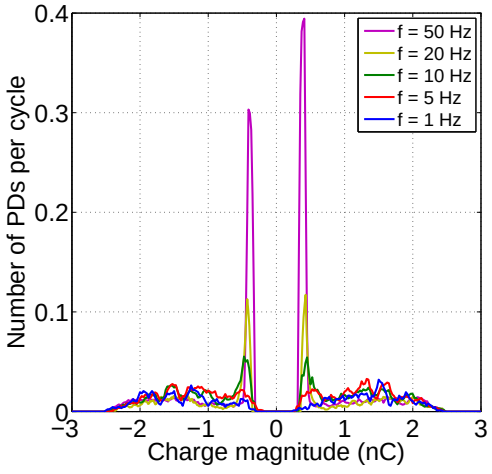

FIGURE 5.10: PD charge magnitude distribution as a function of applied frequency.

5.4 Influence of spherical cavity diameter on PD activity

Table 5.1 shows the measured PD data for spherical cavities of diameter 1.1 mm and 2.35 mm within a dielectric material of thickness 3 mm at 50 Hz, 18 and 20 kV ac

sinusoidal applied voltages. The number of PDs per cycle is higher but the total charge magnitude per cycle and the mean charge, maximum and minimum charge magnitudes are lower for the smaller cavity than the larger cavity. A lower number of PDs per cycle obtained for the larger spherical cavity contradicts with PD measurement results for a cylindrical cavity in a polycarbonate at variable applied frequency [43, 104]. The results reported that the number of PDs per cycle is higher in a larger cylindrical cavity diameter. In a larger cylindrical cavity, simultaneous discharges can occur. However, in a spherical cavity, simultaneous discharges are less likely to occur. Since there may be more free charges on the larger cavity surface after a discharge, surface charge decay through conduction along the cavity wall could be more significant than the smaller cavity, resulting in a lower electron generation rate and less PDs per cycle. There is more inactive time observed from the measurements in the larger cavity size, where no PD occurs at all and this may be due to very low electron generation rate. Therefore, PD activity is not only influenced by the size of the cavity but also the shape of the cavity as well.

Referring to Table 5.1, each PD measured is higher for the 20 kV than the 18 kV applied voltage, except for the mean charge magnitude of the smaller cavity, which is lower at the higher applied voltage. For the smaller cavity, the difference in the number of discharges occurring with lower charge magnitude and higher charge magnitude is very large between 20 kV applied voltage and 18 kV applied voltage, resulting in a lower mean charge magnitude. However, for the larger cavity diameter, the difference in the number of discharges occurring with lower charge magnitude and higher charge magnitude between 20 kV applied voltage and 18 kV applied voltage is not as much, thus mean charge magnitude increases with the applied voltage.

Spherical cavity diameter (mm)	1.1		2.35	
Applied voltage (kV)	18	20	18	20
Measured inception voltage, U_{incapp} (kV)	7.5	7.5	7.0	7.0
Total number of PDs per cycle	6.5	8.6	2.5	3.4
Total apparent charge per cycle (pC)	651	809	5420	8552
Mean charge magnitude (pC)	101	94	2165	2509
Maximum PD magnitude (pC)	373	344	4763	5550
Minimum PD magnitude (pC)	80	80	938	938

TABLE 5.1: Comparison of measured PD data between two different cavity sizes

The obtained results in Table 5.1 are in agreement with the other reported measurements of PD activity in spherical cavities [25, 106–109]. The charge magnitude increases with cavity diameter because the cavity diameter determines the maximum propagation length of the avalanche parallel with the applied field and the size of avalanche head perpendicular to the applied field [110]. Thus, in a larger spherical cavity, the avalanche head can grow larger, resulting in a larger PD charge magnitude and higher total charge

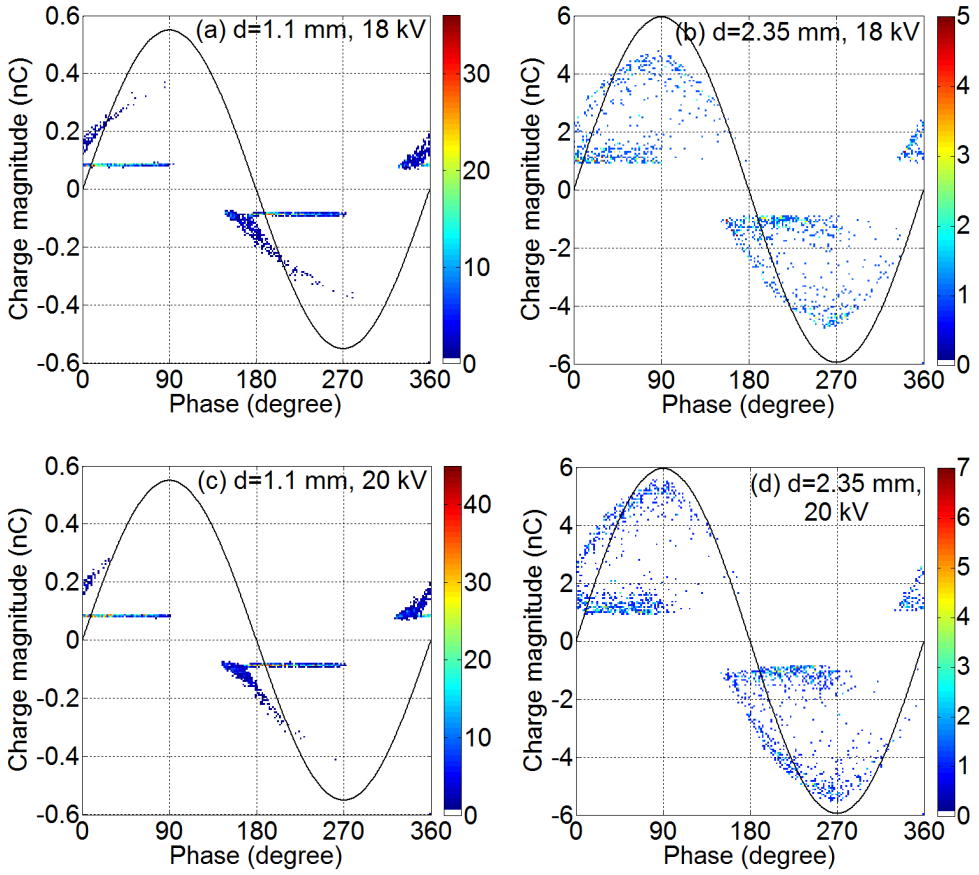

FIGURE 5.11: PRPD patterns for different cavity diameters (50 Hz, 18 and 20 kV).

per cycle [71].

The measured inception voltage, U_{incapp}, is higher for the smaller cavity than the larger cavity. The cavity wall that is parallel with the applied field may influence the inception field, E_{inc}, where smaller cavity diameter increases the contact between avalanche head and the cavity wall, thus increasing E_{inc} [109]. There is a work reported that higher inception field in a smaller cavity is also due to the reduction of initial electron generation rate, resulting in longer statistical time lag and discharge occurs at higher voltage level [55]. In a dielectric-electrode bounded cavity, the inception field of a streamer is reported to decrease when the electrode surface is larger [111]. A PD measurement using CIGRE-II electrode system also shows that the measured inception voltage decreases when the diameter of the cavity in a polyethylene is larger [112].

PRPD patterns obtained from experiments are presented in Figure 5.11. It can be seen that the tail of the 'rabbit-ear' curve in the smaller cavity peaks at the 90 and 270 degree phase angles of the 18 and 20 kV 50 Hz ac applied voltage. In the larger cavity, large discharge events occur across the whole ac cycle. Increasing the applied field results in advancing the phase angle at which PD activity starts to occur, and, if the field is sufficiently high, PD events will occur prior to the zero crossing points.

The $H_n(\phi)$ distribution in Figure 5.12(a) represents the average number of PD events occurring at each phase angle of the applied voltage. In the first and third quadrants, more PDs occur in the smaller cavity than in the larger. In both, the largest numbers of PD occur immediately after polarity reversal. Analysis of the total charge magnitude per cycle, as a function of phase angle, $H_{qs}(\phi)$ (Figure 5.12(b)) reveals that the apparent charge magnitude is greater for the larger cavity. In the larger cavity the phase angles at which the largest total charge per cycle occur move away from the zero crossing points towards the peak voltage phase angles of 90 degrees and 270 degrees. The $H_n(\phi)$ plot in Figure 5.12(c) illustrates the effect of cavity size on PD behaviour; the smaller cavity has a nearly constant mean charge magnitude over the first and third quadrants, whereas the larger cavity mean charge magnitude is greatest at the applied voltage peaks. Furthermore, PD activity occurs across the whole cycle in the larger cavity. Figure 5.12(d) shows the maximum PD magnitude ($H_{qm}(\phi)$) distribution, which the peak for the larger cavity is at 90 degrees and 270 degrees but the peak for the smaller cavity is slightly before 90 degrees and 270 degrees.

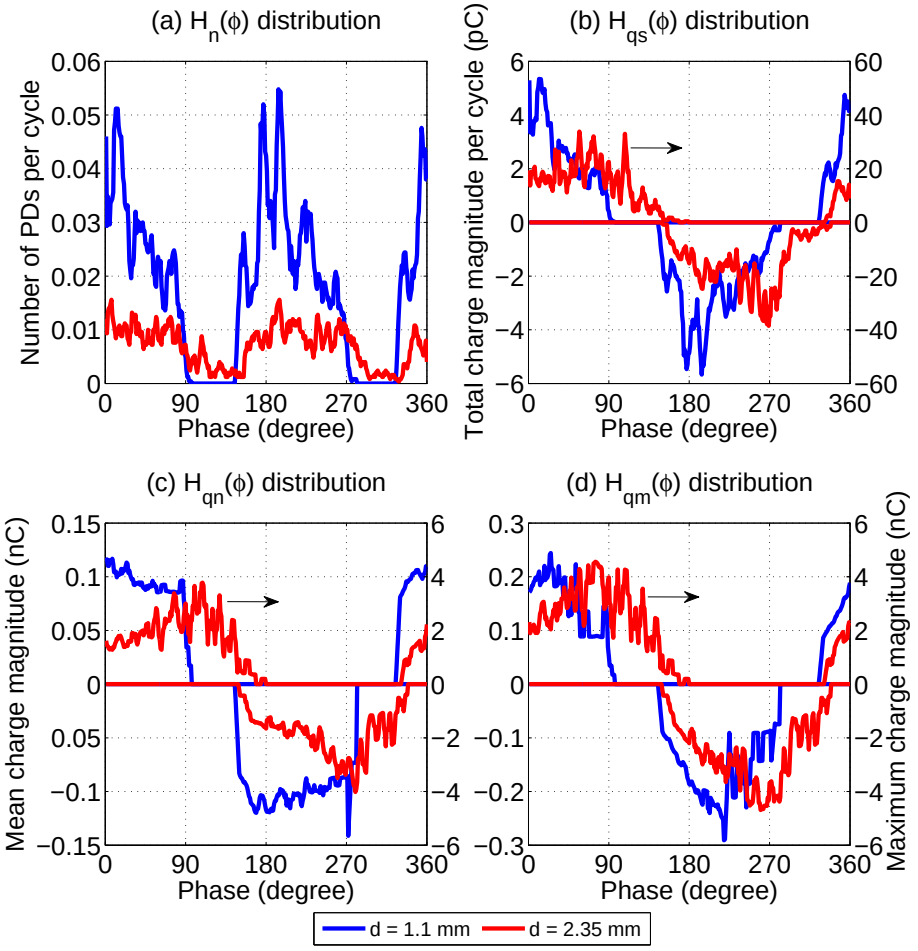

FIGURE 5.12: PD phase distributions for different spherical cavity diameters (50 Hz, 18 kV).

From Figure 5.13(a), the density of the distribution for the smaller cavity is very high near the minimum charge magnitude compared to higher charger magnitude. However, for the larger cavity, as shown in Figure 5.13(b), the charge distribution is less concentrated at the minimum charge magnitude. The number of PDs per cycle is the lowest in the region between the minimum and maximum charge magnitude. Due to the surface charge decay effect, there are many PDs occurring with higher charge magnitudes in the larger cavity.

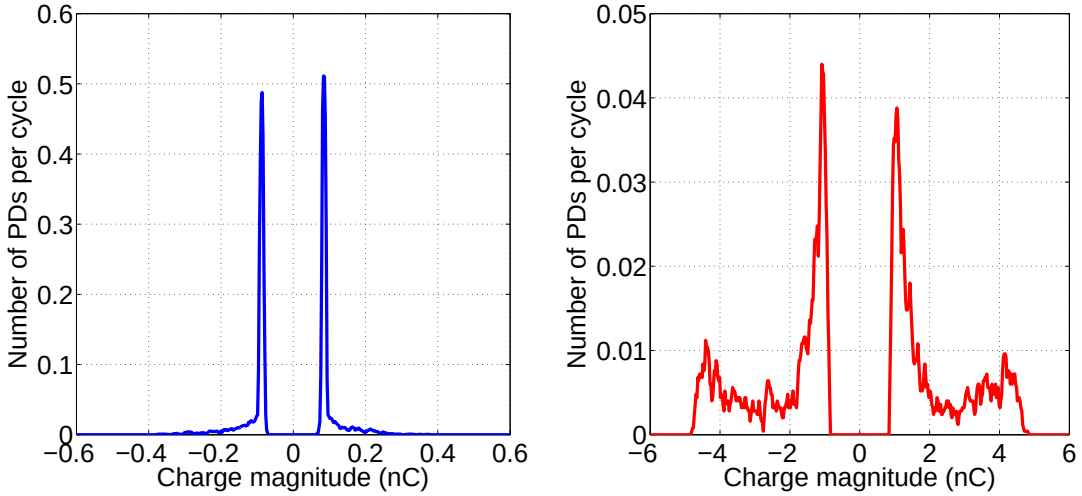

(a) d = 1.1 mm

(b) d = 2.35 mm

FIGURE 5.13: PD charge magnitude distributions for different spherical cavity diameters (50 Hz, 18 kV).

5.5 Influence of temperature of the material on PD activity

The PD measurement results as a function of temperature are shown in Figure 5.14. At higher temperatures, the number of PDs per cycle, the total charge per cycle and the minimum charge magnitude increase but the maximum charge magnitude decreases while there is no clear tread for the mean charge magnitude. Previous work has reported that the number of PDs per cycle is lower at higher temperatures of the material due to the higher cavity surface work function, which reduces the electron generation rate, resulting in a lower PD repetition rates [50,113,114]. However, in this work, higher PD repetition rate at higher temperatures may be due to a higher electron generation rate, which increases the PD repetition rate and total charge per cycle.

The minimum charge magnitude increases with temperature because the initial pressure in the cavity increases with temperature. Thus, the inception voltage becomes higher, resulting in a larger voltage drop across the cavity when a PD occurs. However, the maximum PD magnitude decreases with temperature because the electron generation

rate increases, reducing the statistical time lag and hence more PDs occur almost immediately after the inception voltage has been exceeded, resulting in lower maximum charge magnitudes.

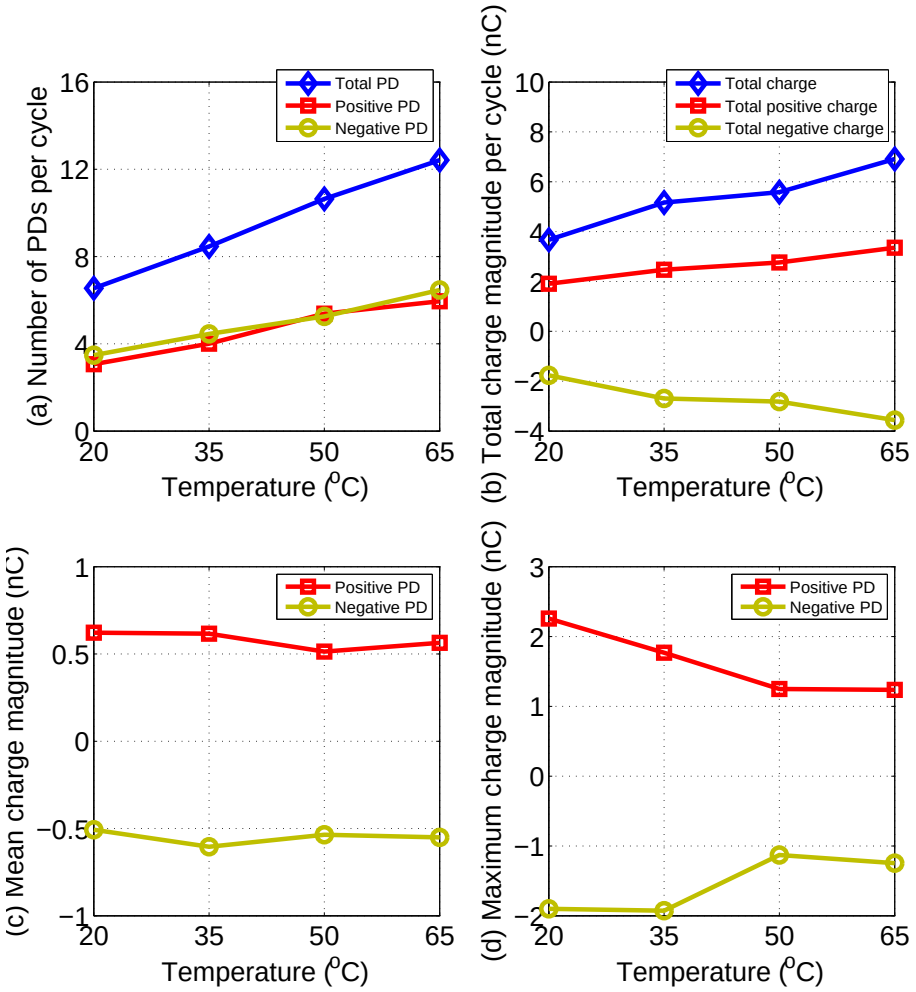

FIGURE 5.14: PD data as a function of material temperatures from the measurement (50 Hz, 20 kV).

Referring to Figure 5.15, when the temperature is increased, the 'rabbit-ear' like curve of PRPD patterns ends at an earlier point in term of phase and the end of the curves become sharper while the density of PDs near the minimum charge magnitude increases. Since the electron generation rate is enhanced by higher temperatures of the material, this generates more PDs with lower charge magnitudes. Due to higher pressure in the cavity at higher temperature, the inception voltage becomes larger. Thus, the minimum charge magnitude increases and the earliest phase of PDs occurring before the zero point crossing also increases.

PD phase distributions for Figure 5.15 as a function of temperature are shown in Figure 5.16. The $H_n(\phi)$ distribution (Figure 5.16(a)) shows that when at higher temperature, the number of PDs per cycle at across the phase range is higher. The earliest phase

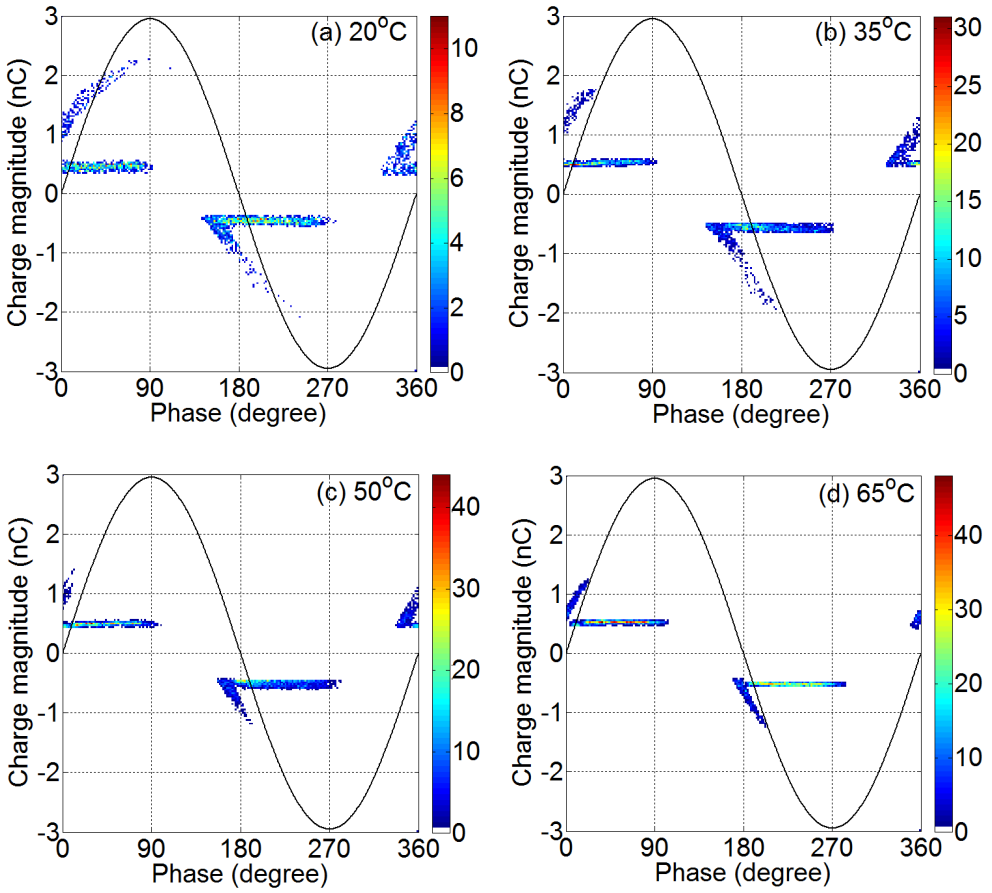

FIGURE 5.15: PRPD patterns for different temperatures of the material (50 Hz, 20 kV).

of PD occurrence can be seen to be increased at higher temperatures. Figure 5.16(b) shows the $H_{qs}(\phi)$ distribution, where charge magnitude per cycle is higher at almost each of the phase. The peak of the distribution is shifted forward in phase at higher temperatures because the peak of $H_n(\phi)$ distribution is also shifted forward in phase. The peak of $H_{qs}(\phi)$ distribution is near to 0 and 180 degree as many PDs are occurring around these phase positions.

Referring to Figure 5.16(c), the $H_{qn}(\phi)$ distribution increases sharply from 0 nC to a maximum mean charge when the phase is approaching 0 and 180 degree phases but it remains almost constant after 0 and 180 degrees. This is because the $H_{qn}(\phi)$ distribution is the ratio between $H_{qs}(\phi)$ and $H_n(\phi)$. Finally, it can be seen that the peak of the maximum charge magnitude is shifted forward in phase at higher temperatures, as shown in Figure 5.16(d).

Figure 5.17 shows PD charge magnitude distribution as a function of temperature. At increased temperatures, the number of PDs with higher charge magnitudes reduces but there are more PDs near the minimum charge magnitude. Due to enhanced electron generation rates at higher temperatures, the statistical time lag is reduced, resulting in PDs that occur near the inception field, yielding lower PD charge magnitudes overall.

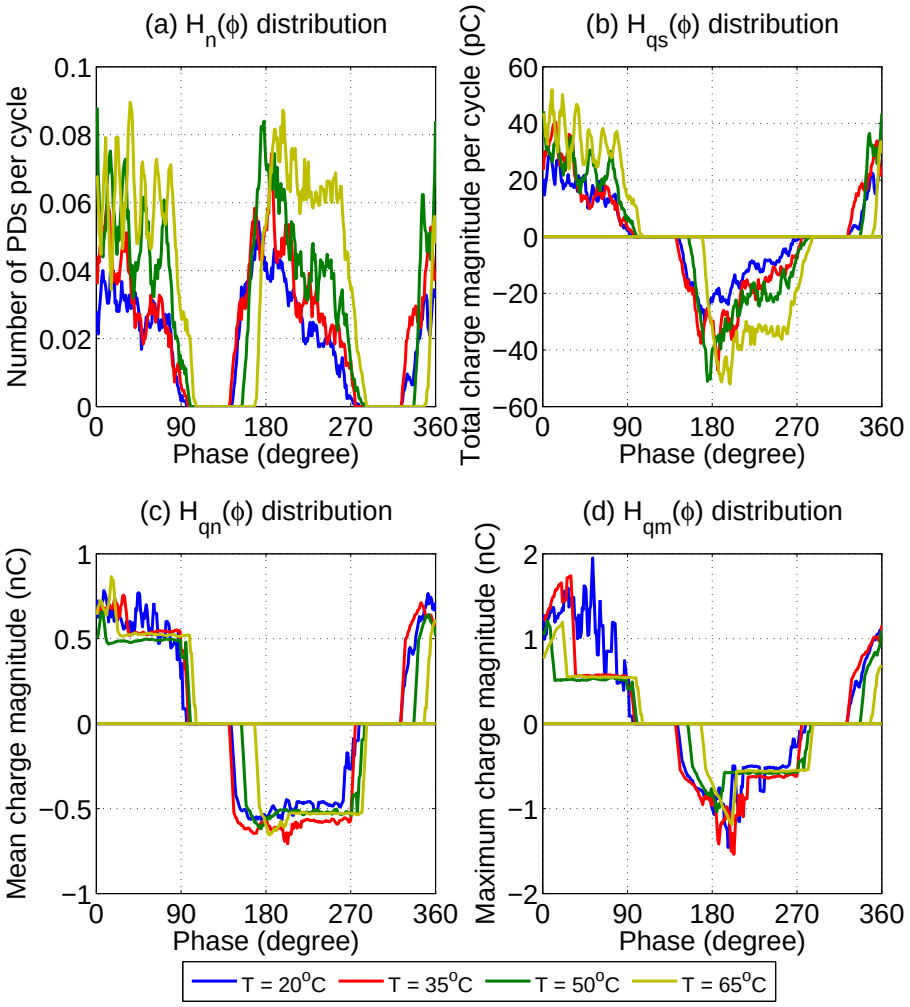

FIGURE 5.16: PD phase distributions for different temperatures of the material.

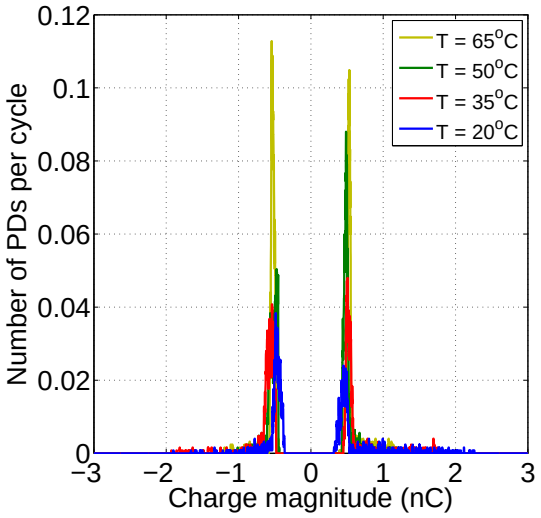

FIGURE 5.17: PD charge magnitude distribution for different material temperatures.

5.6 Summary

From analysis of the measurement results, there are clear 'rabbit-ear' like patterns and patterns where PDs occur near the minimum charge magnitude from the PRPD patterns. When the applied voltage amplitude is increased, the maximum charge magnitude increases and the 'rabbit-ear' like curve becomes wider. The 'rabbit-ear' like curve turns into a 'turtle' like pattern when the applied frequency is decreased. The 'rabbit-ear' like curve is more dispersed for the larger cavity compared to the smaller cavity. When the temperature of the material increases, the maximum charge magnitude decreases, resulting in shorter 'rabbit-ear' like curves. Overall, the number of PDs per cycle and total charge per cycle increase with the applied voltage amplitude, frequency of the applied voltage and temperature of the material. This could be due to an enhanced electron generation rate, causing shorter statistical time lags, resulting in a higher number of PDs per cycle and total charge per cycle. However, the number of PDs per cycle is lower for the larger cavity, which may be due to the more significant effect of charge conduction along the cavity wall and lower electron generation rate than the smaller cavity. The total charge per cycle is higher for the larger cavity than the smaller cavity. From the PD charge magnitude distributions for different stress conditions and cavity sizes, more PDs occur near the minimum charge magnitude than at higher charge magnitude. From the phase of PD occurrence distributions, there are more PDs occuring at the rising edge of the ac applied voltage than at the falling edge. The obtained measurement results are repeatable and can be compared with the simulation results, which are detailed in Chapters 7 and 8.

Chapter 6

Results from the Finite Element Analysis Model

This chapter details the result of the electric field and temperature distributions generated using the FEA model. The electric field and temperature distributions before, immediately and after a PD event are detailed and discussed. The effect of charge decay through surface conduction along the cavity wall on the electric field distribution and effect of temperature decay in the cavity on the temperature distribution are described. The influence of the cavity location within the dielectric material on the electric field distribution is also considered.

6.1 Electric field distributions in the FEA model

The simulated electric equipotential lines and the electric field distribution from the Finite Element Analysis (FEA) model before and after the first discharge are shown in Figure 6.1. The model consists of a spherical cavity of diameter 1.4 mm within the dielectric material of thickness 2 mm that experiences a 50 Hz, 18 kV ac applied voltage. These plots agrees with the simulation results obtained from a model of a spherical cavity in a polyethylene cable [115]. Other published work has used FEA software to plot the distributions of electric field within a spherical cavity in an epoxy resin of a CIGRE II test cell [116] and a twisted-pair sample simulating the coil to coil insulation of a low voltage stator windings [117]. Figure 6.2 shows the cross-section plots of the electric field magnitude along the z and r-axes from the FEA model in Figure 6.1 before and after a PD occurs in the cavity.

In Figure 6.1(a), the electric field before the first PD is higher in the cavity than in the surrounding dielectric material, since the relative permittivity of the cavity is lower than that of the solid dielectric. This is consistent with the light blue colour scale and the

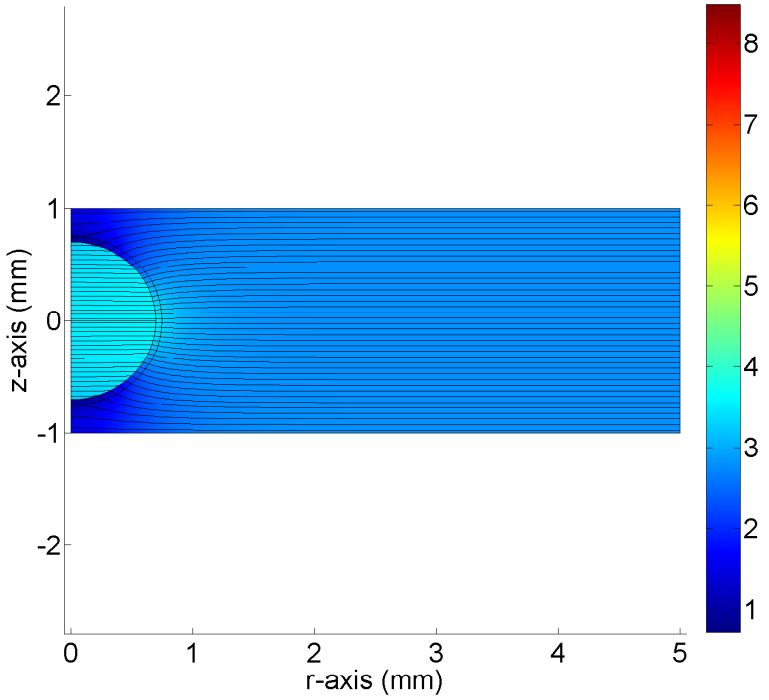

(a) Before the first PD occurs

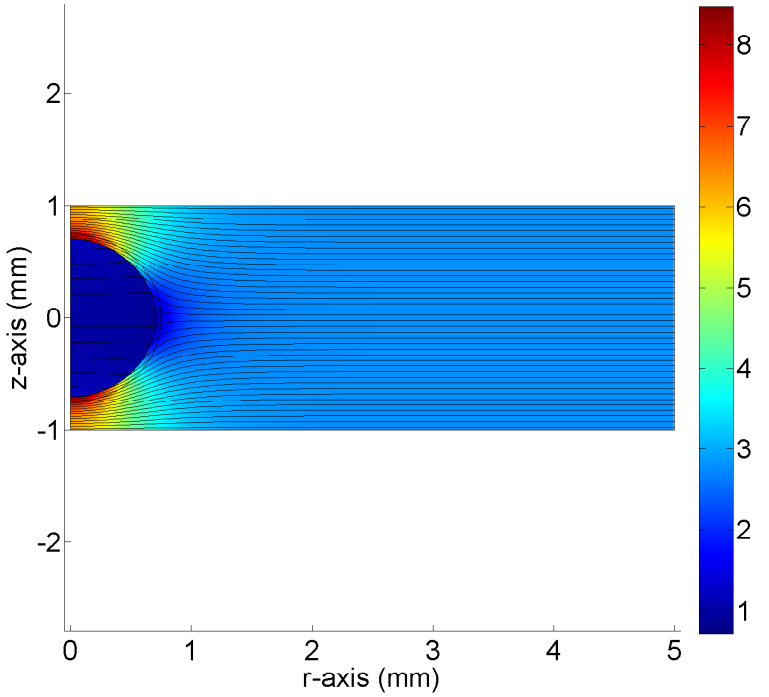

(b) After the first PD occurs

FIGURE 6.1: Simulation of electric field distribution (surface plot in kV·mm^{-1}) and electric equipotential lines (contour plot) in the FEA model (Applied field, E_0 = 9 kV·mm^{-1}, applied frequency, f = 50 Hz, inception field, E_{inc} = 3.4 kV·mm^{-1}, extinction field, E_{ext} = 1 kV·mm^{-1}).

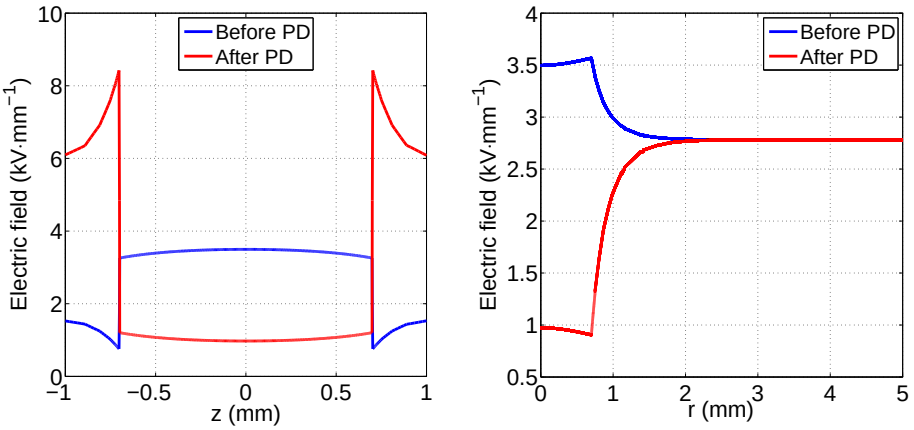

(a) Along the z-axis

(b) Along the r-axis

FIGURE 6.2: Cross-section plots of the electric field magnitude from the FEA model in Figure 6.1 before and after the first PD.

more closely packed equipotential lines within the cavity. However, the electric field is lowest on the cavity surface areas closest to the electrodes because the applied field is almost perpendicular to the cavity surface. This can also be seen from the cross-section plotf of the electric field magnitude along the z-axis of the FEA model in Figure 6.2(a). The field magnitude along the z-axis is not uniform but symmetrical because the cavity size is quite large compares to the material thickness. Thus, the field in the cavity nearest to the electrode is affected by the electrode, resulting in the field in those region to be lower than the middle of the cavity. The cross-section plot of the electric field magnitude along the r-axis shown in Figure 6.2(b) differs from Figure 6.2(a) because the field is parallel to the cavity wall.

Immediately after a PD occurs the electric field distribution in the cavity is significantly altered, as shown in Figure 6.1(b), assuming that the whole cavity is affected. Due to dynamic charge movement across the cavity, the cavity field is significantly reduced (represented as the dark blue region in the surface plot of Figure 6.1(b)). However, at the same time the electric field on the upper and lower cavity surface is significantly increased. This is also apparent from the cross-section plot of the electric field magnitude along the z-axis from the FEA model, as shown in Figure 6.2(a). Charge from PD activity accumulates on the cavity surface, and produces an opposing electric field which reduces the electric field in the cavity. Less charge accumulates on the cavity wall, i.e., quasi-parallel to the applied field, and consequently the electric field magnitude along the r-axis after a PD occurrence is greatest within the solid dielectric distant from the cavity wall (Figure 6.2(b)). Therefore, immediately after a PD the electric field strength on the upper and lower cavity surface is higher than that in the dielectric, and this will directly affect the characteristics of the next PD event.

After the first PD occurs, the electric field in the cavity increases again due to the increase in the applied voltage. A PD can occur again if the field in the cavity exceeds

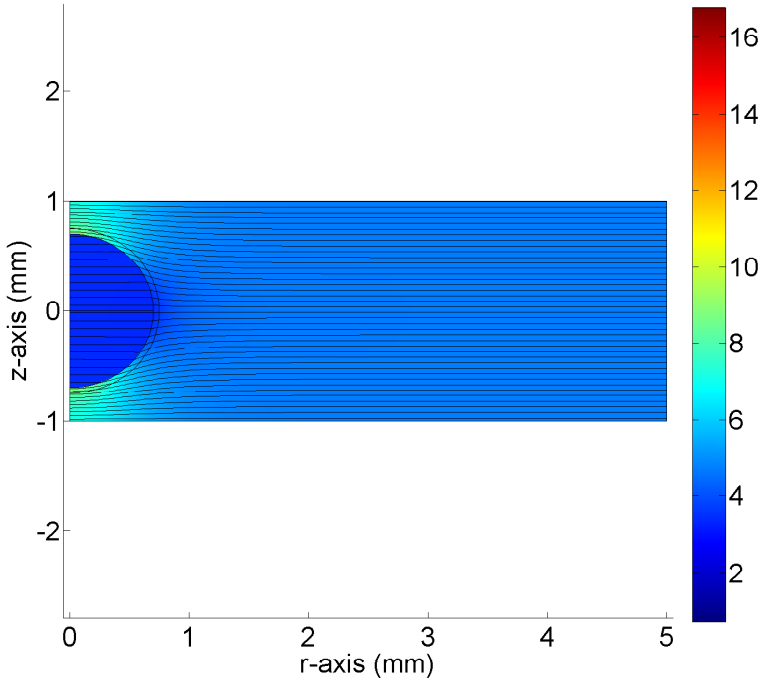

(a) Before the second PD occurs

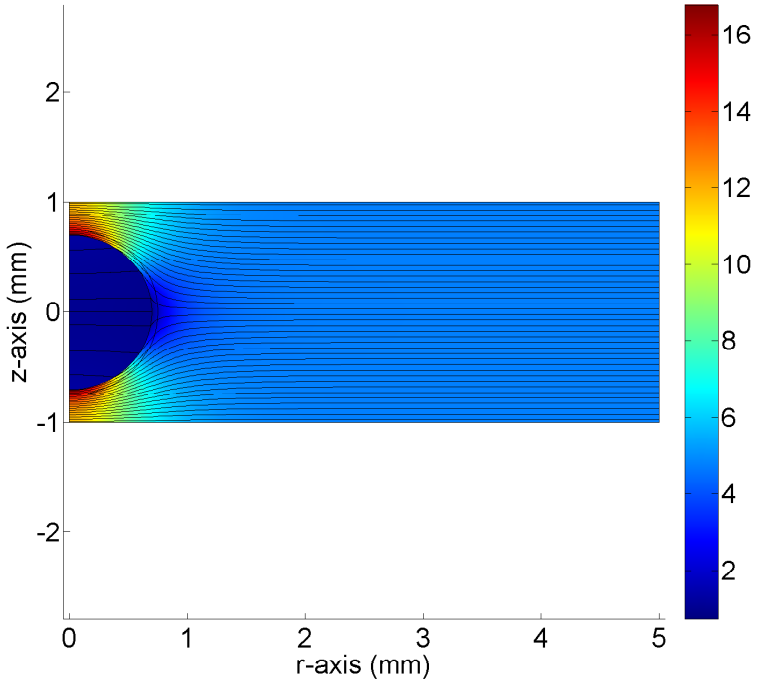

(b) After the second PD occurs

FIGURE 6.3: Simulation of electric field distribution (surface plot in kV·mm^{-1}) and electric equipotential lines (contour plot) in the FEA model.

the inception field. The electric field in the cavity decreases again after the second PD occurs, which can be seen in Figure 6.3(b). From Figure 6.4, the cross-section plots of the electric field magnitude along the r and z-axes from the FEA model before and after

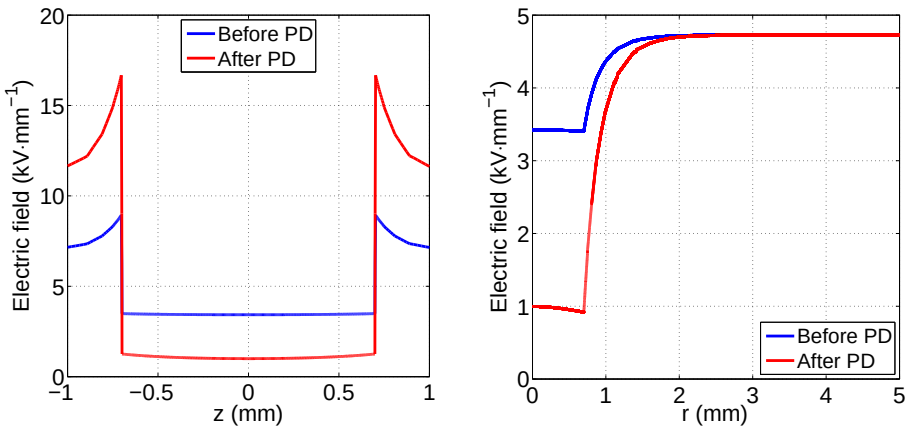

(a) Along the z-axis

(b) Along the r-axis

FIGURE 6.4: Cross-section plots of the electric field magnitude from the FEA model in Figure 6.3 before and after the second PD.

the second PD have similar trends, except that the electric field in the cavity after the discharge is lower. However, the electric field magnitude on the cavity surface after the discharge is higher than before the discharge, which can be seen in Figure 6.4(a) (at points z = -0.7 and 0.7 mm). Since charges from the first PD still remain on the cavity surface when the second PD occurs, the amount of surface charges increases after the second PD. Hence, the electric field on the cavity surface becomes higher.

6.2 Simulation of field against time of the applied field

Figure 6.5 shows the simulation of the field in the cavity in the absence of PD event, E_{cav0}, field in the cavity, E_{cav}, field due to surface charge, E_s, and the inception field, E_{inc} against time of the applied field. Initially, E_{cav} is equal to E_{cav0} in the absence of surface charge. After the first PD has occurred at 1.3 ms, E_{cav} decreases sharply due to charge accumulation on the cavity surface, E_s, which is of opposite polarity to E_{cav}. When the polarity of E_{cav} changes and is the same with E_s at 7.5 ms, E_{cav} is enhanced by E_s. Hence the maximum E_{cav} can be larger than the maximum value of E_{cav0}. Thus, when the polarity of the field in the cavity changes from the previous PD event, PD can happen at a higher level of E_{cav}, resulting in a larger charge magnitude due to a larger field drop in the cavity. This can be seen at time 11, 23.5 and 29 ms in Figure 6.5. Therefore, a larger PD charge magnitude is obtained when there is polarity change of E_{cav} between consecutive discharges, which actually yields in the 'rabbit-ear' like curve in PRPD patterns. A smaller PD charge magnitude is obtained when there is no polarity change of E_{cav} between consecutive discharges. Hence, a pattern of PDs near the minimum charge magnitude, which appears as a broad 'straight-line' pattern, is obtained.

With reference to region B in Figure 6.5, when the polarity of E_{cav} is the same as that of E_s, surface charge decays through conduction along the cavity wall because the charge movement is assumed to be field-dependent, resulting in E_s starting to decrease. The cavity surface conductivity is increased from its initial value during this interval to a maximum surface conductivity, σ_{smax} to model the surface charge movement along the cavity wall. Surface charge decay will affect the electron generation rate, which in turn affects the occurrence of next PD event. When the polarity of E_{cav} is opposite to E_s as shown in region C of Figure 6.5, surface charges do not decay through surface conduction. Thus in the model the surface conductivity is reset to its initial value.

With reference to Figure 6.5, when there is no polarity change of E_{cav} after a previous PD occurrence, e.g. at 1.3 and 2 ms, the effect of surface charge decay is less significant due to the shorter time interval between two PD events. Thus, the total electron generation rate, N_{et} is higher at the point when the next PD is likely to occur, resulting in a shorter statistical time lag, τ_{stat} and PD occurs almost immediately once E_{inc} is exceeded. However, when there is a polarity change of E_{cav} after the previous PD, e.g. between 3 to 11 ms, surface charge decay is more significant due to the long time interval between events. Thus, N_{et} is smaller when the next PD is likely to occur, resulting in longer τ_{stat}. PD then occurs at higher field than E_{inc}, yielding larger PD charge magnitudes.

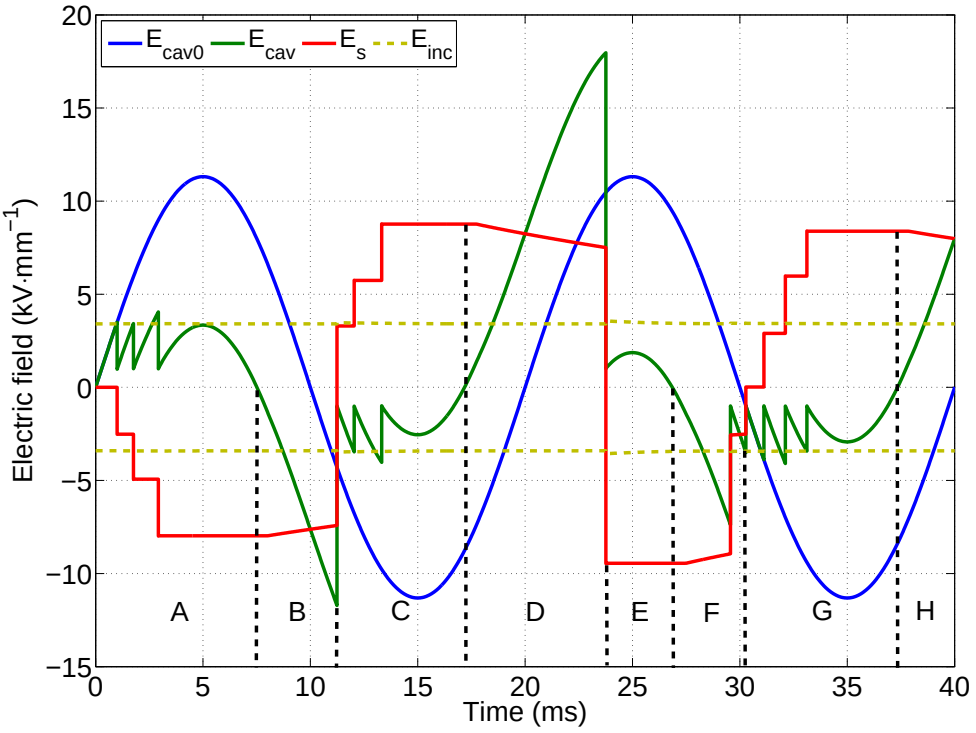

FIGURE 6.5: Simulation of field against time for the first two cycles from the FEA model (All parameters are the same as for Figure 6.1 and maximum surface conductivity, σ_{smax} = 5×10^{-9} Sm^{-1}).

Figure 6.6 shows simulation of field due to surface charge, E_s using a different maximum cavity surface conductivity, σ_{smax} to model surface charge decay through conduction

along the cavity wall in the FEA model. In this figure, E_s starts decaying from 7.5 ms, when the polarity of the field in the cavity is the same with the field due to surface charge. For each σ_{smax}, PD is set to occur at time 5 ms. It can be seen that the decrement rate of E_s is faster when the maximum cavity surface conductivity is higher, which causes faster surface charge decay rate through conduction along the cavity wall.

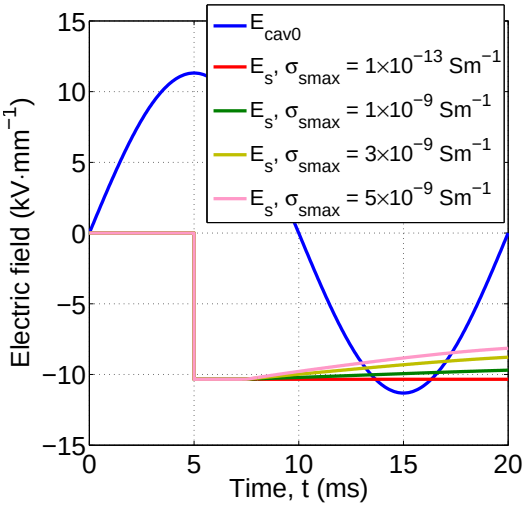

FIGURE 6.6: Simulation of field due to surface charge using different cavity surface conductivity in the FEA model, where E_{cav0} is the field in the cavity in the absence of surface charge.

6.3 Temperature distributions in the FEA model

The temperature distributions in the cavity before and after a PD event obtained from the FEA model are shown in Figure 6.7 while the corresponding cross-section plots of the temperature along the r and z-axes are shown in Figure 6.8. Initially, the temperature in the whole cavity is uniform and equal to the initial temperature, which is set to 293 K. After the first discharge, the temperature in the cavity becomes higher than the surrounding material because the heat source density in the cavity is assumed to increase from zero during the PD process. The temperature rise in the cavity is due to heat energy dissipation from electron ionization. The whole temperature in the cavity immediately after the first PD occurs is uniform.

After the second discharge occurs, the temperature distribution in the cavity is different to that obtained after the first discharge, which can be seen in Figure 6.9(b). The temperature in the cavity decays towards an initial value after the first discharge. Hence, the temperature in the cavity becomes non-uniform before the second PD occurs, where the temperature is assumed to be largest in the middle of the cavity, as shown in Figure 6.10. The temperature distribution is symmetrical along the symmetry axis. The heat in the cavity near the cavity surface dissipates faster through the surrounding material than in

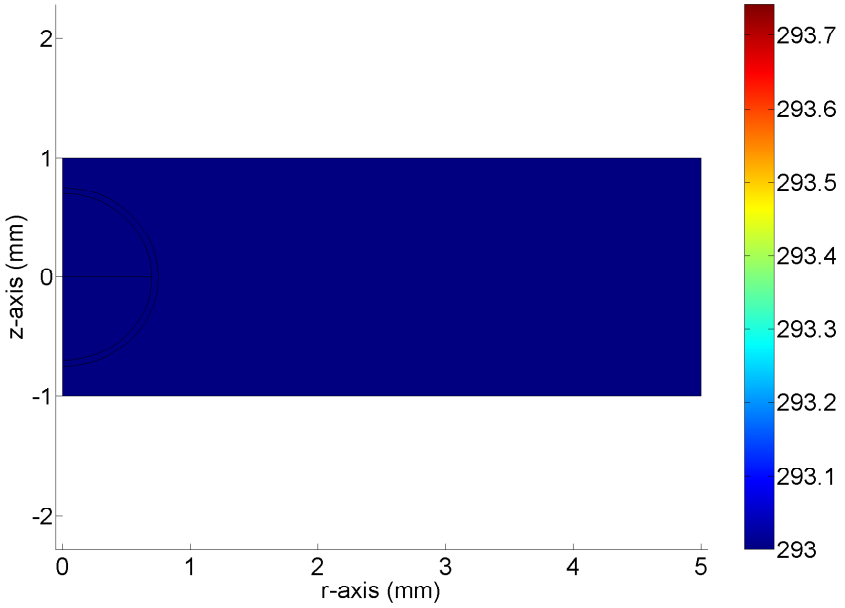

(a) Before the first PD occurs

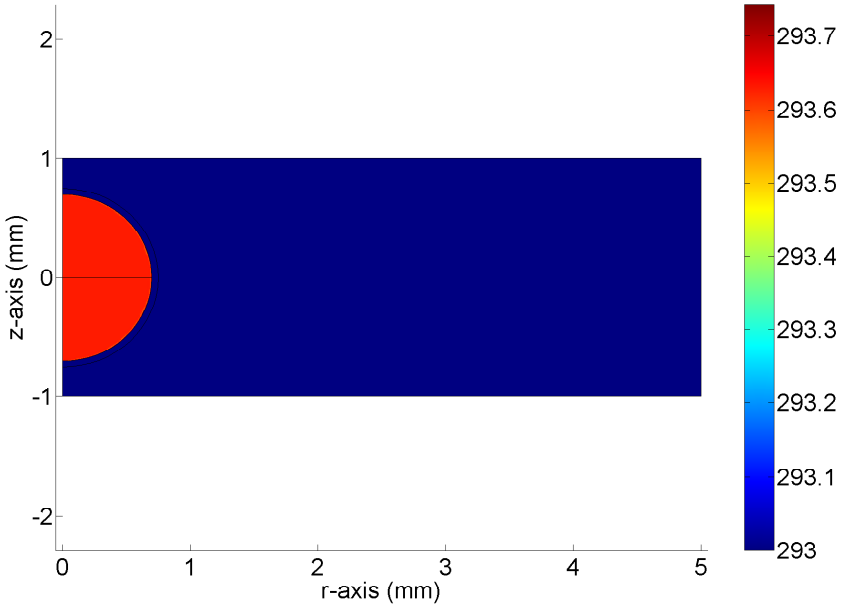

(b) After the first PD occurs

FIGURE 6.7: Simulation of temperature distributions (surface plot in K) in the FEA model (All parameters are the same as for Figure 6.1).

the middle of the cavity, resulting in higher temperature in the middle of the cavity. The temperature distribution in the cavity immediately after the second discharge follows the temperature distribution before the second PD occurs.

The simulation of the temperature in the middle of the cavity with time is shown in

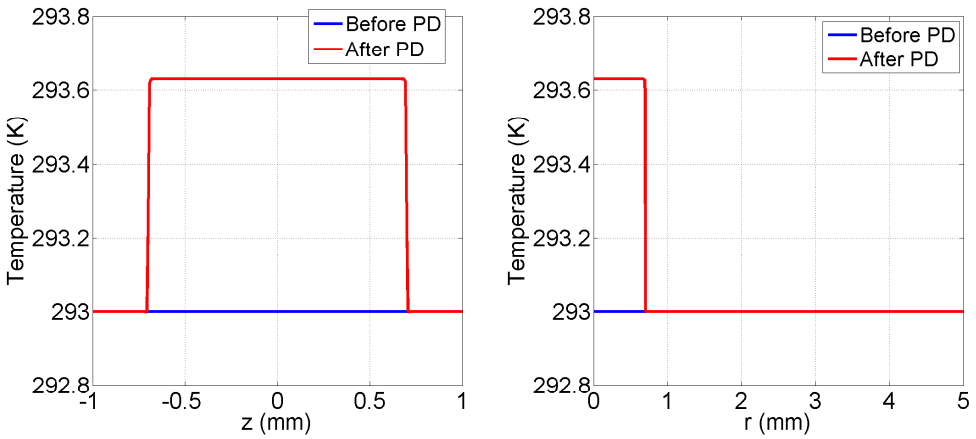

(a) Along the z-axis

(b) Along the r-axis

FIGURE 6.8: Cross-section plots of the temperature from the FEA model in Figure 6.7 before and after the first PD.

Figure 6.11. When the temperature starts to decay, it decays almost exponentially with time towards the initial temperature, T_0. Thus, the temperature decay time constant is determined by assuming an exponential decay of the temperature. This decay rate is assumed similar to the voltage recovery characteristic of a hot gas due to an arc [69,70]. The temperature does not decay immediately because the temperature in the cavity centre decreases slower than at the region nearer to the cavity surface boundary. In the model developed, the temperature distribution in the cavity is symmetrical along the symmetry axis when it starts to decay, where it is the highest in the cavity centre.

It is possible to relate the temperature increment in the cavity and the heat source during a PD occurrence. Figure 6.12 shows the simulation of temperature increment as a function of heat source obtained from the FEA model. It can be seen that the temperature increment in the cavity is linearly proportional to the heat source density, Q from a PD event.

6.4 Simulation of electric field and temperature against time of the applied field

Figure 6.13 shows measurement of inception field, E_{inc} as a function of cavity temperature, T_{cav} for each sample that has been created, as summarised in Table 4.1 in Chapter 4. From the measurement, T_{cav} is assumed to be the same with the material temperature. Therefore, the values of κ and χ in Equation 3.11 in Chapter 3 can be determined using Figure 6.13. For the range of temperature between 293K and 338K, it was found that κ and χ vary for each sample. These values were used in the simulation.

Figure 6.14 shows simulation of the field, the inception field, E_{inc}, PD real charge mag-

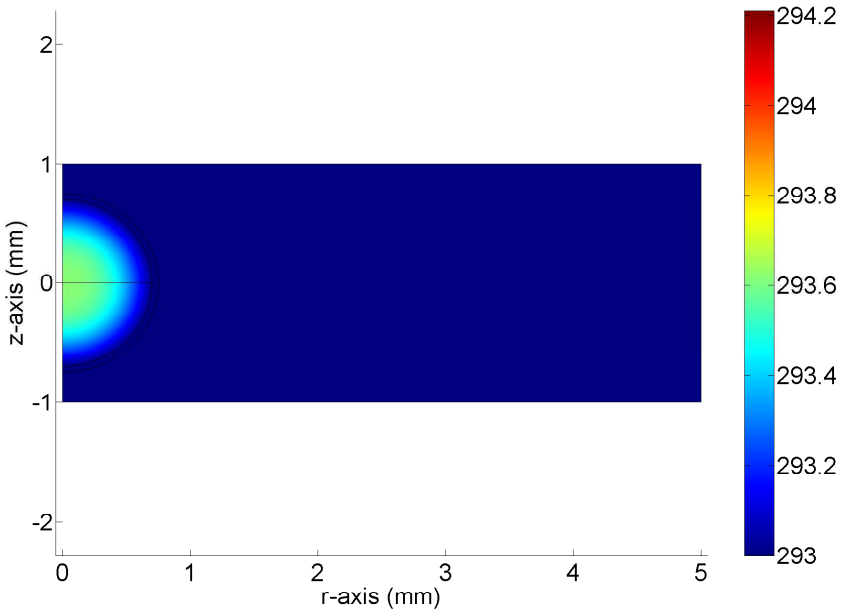

(a) Before the second PD occurs

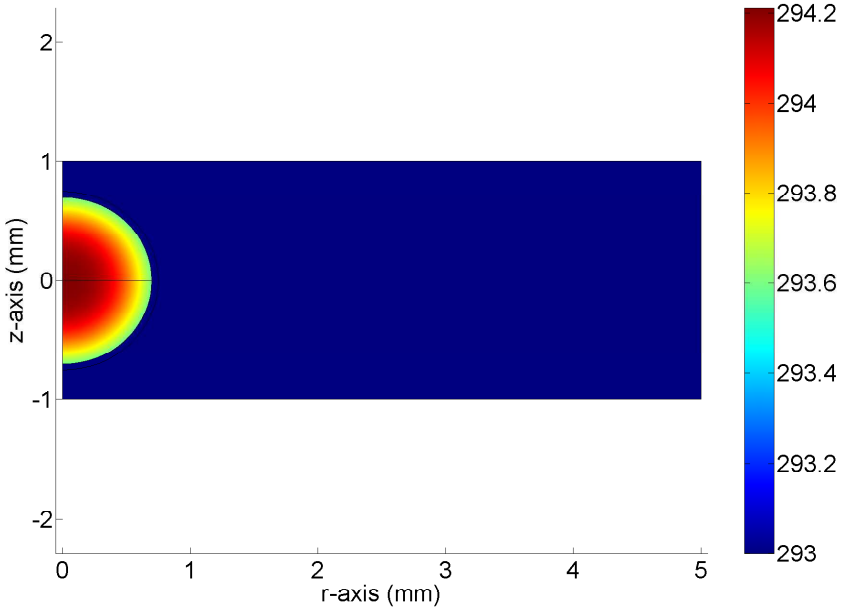

(b) After the second PD occurs

FIGURE 6.9: Simulation of temperature distributions (surface plot in K) in the FEA model.

nitude and temperature in the cavity centre, T_{cav} against time of the applied field for the model geometry in Figure Figure 6.1. Immediately after a PD, the temperature in the cavity increases, resulting in the increase of the inception field, as shown in Figure 6.14(a). A higher inception field will delay the next PD occurrence. When the temperature decays with time and recovers towards initial temperature, T_0 (Figure 6.14(b)),

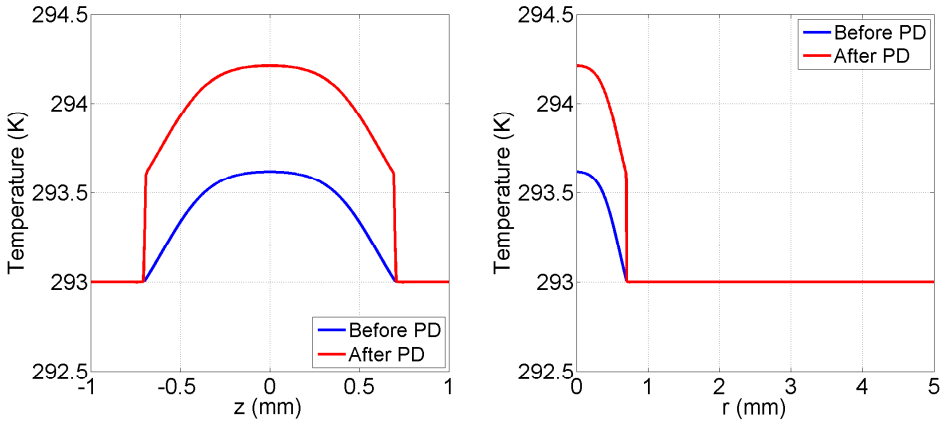

(a) Along the z-axis (b) Along the r-axis

FIGURE 6.10: Cross-section plots of the temperature from the FEA model in Figure 6.9 before and after the second PD.

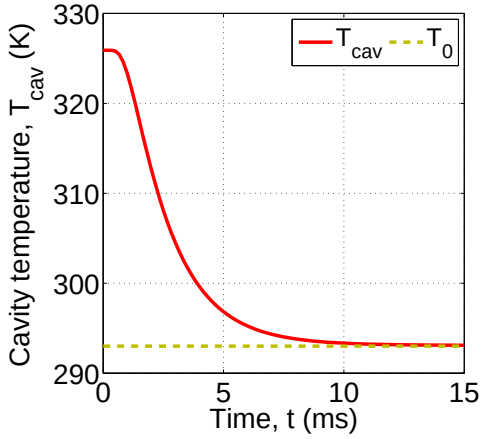

FIGURE 6.11: Simulation of the temperature in the cavity against time after a PD.

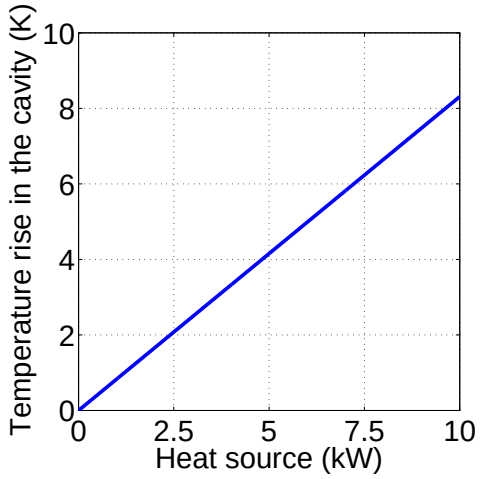

FIGURE 6.12: Temperature increment in the cavity as a function of heat source during a PD event.

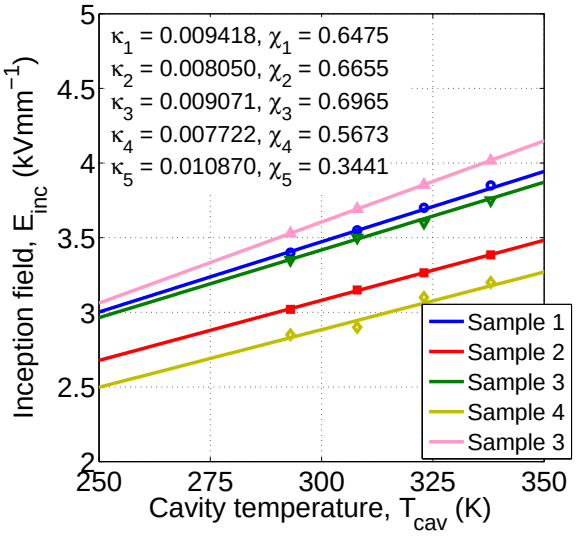

FIGURE 6.13: Measurement of inception field, E_{inc} as a function of cavity temperature, T_{cav} for different sample geometries.

the inception field also decreases. A larger field change in the cavity during a PD causes a larger PD charge magnitude and also higher temperature rise in the cavity.

Referring to Figure 6.14, the average temperature increase in the cavity centre per PD event is around 2.6K, the maximum temperature increase in the cavity is 24K and the average temperature decay time constant, τ_{Tdecay} is 2 ms. Since the period of the applied voltage is longer than τ_{Tdecay}, this suggests that the effect of instantaneous temperature change in the cavity due to PD events does not have a significant impact on the sequence of PD behaviour. The increment of the inception field Figure 6.14(a) is also very small, which may have little influence on the seqeunce of PD occurrence. Thus, the temperature variation in the cavity due to PD events and Equation 3.9 to Equation 3.15 in Section 3.3 (Chapter 3) can be neglected for the whole simulation. Hence, the model can be further simplified and the simulation time can be reduced. For comparison, the simulation has been performed using models which consider and neglect temperature changes in the cavity.

6.5 Simulation of PD current pulse in the cavity

When the FEA method is used, it is possible to model the PD current in the cavity. Figure 6.15 shows an example of the current in the cavity, I_{cav}, field in the cavity, E_{cav}, real PD charge magnitude and temperature in the cavity, T_{cav} as a function of time during a discharge from the simulation. When a discharge occurs, the current in the cavity increases sharply from zero until a maximum value. The real charge magnitude and temperature in the cavity also increase because of the current flowing through the cavity. This causes the field in the cavity to start to decrease from the field level at

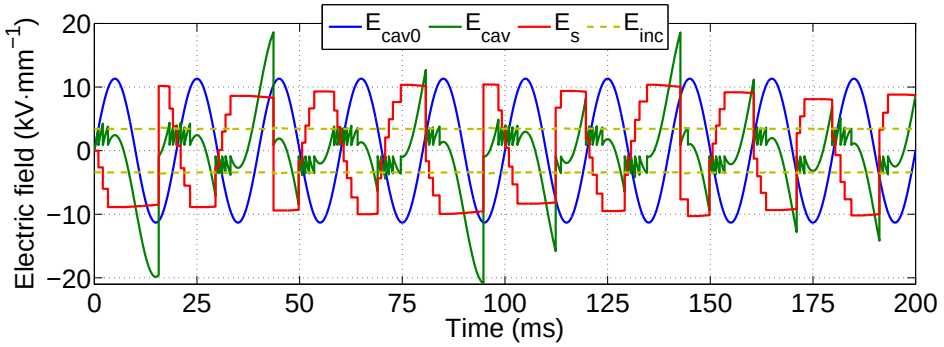

(a) Electric field and inception field

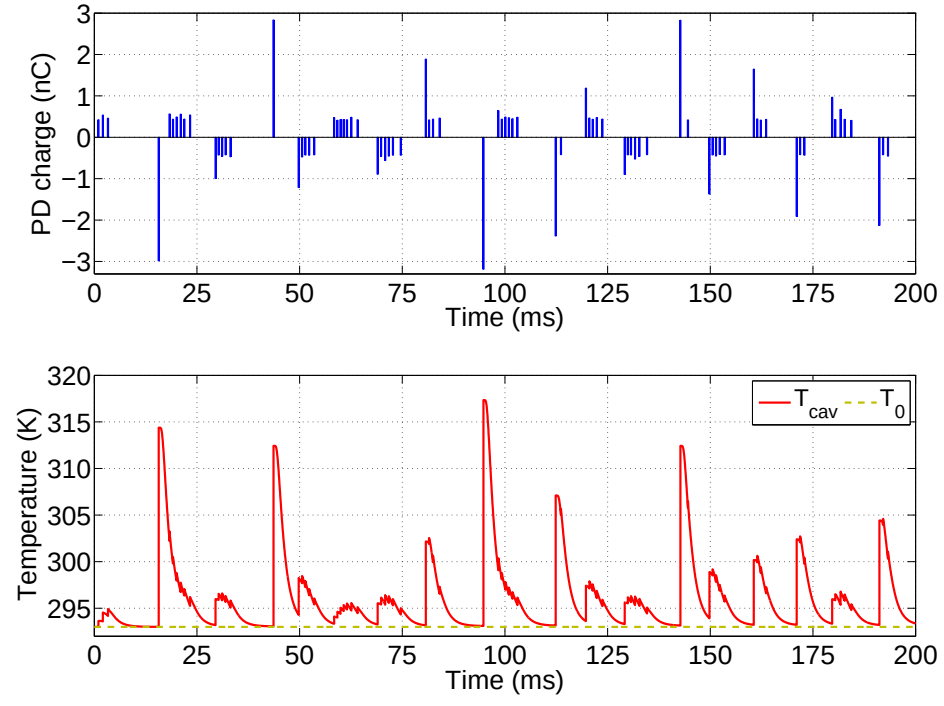

(b) PD real charge magnitude and cavity temperature

FIGURE 6.14: Simulation of electric field, inception field, PD charge magnitude and cavity temperature against time for 10 cycles of the applied field (All parameters are the same as for Figure 6.1 and maximum surface conductivity, $\sigma_{smax} = 1\times10^{-9}$ Sm^{-1}).

which the discharge occurs. After that, the current starts to decrease whilst the field in the cavity keeps decreasing. However, the charge magnitude and temperature in the cavity keeps increasing but at a slower rate because the PD current is decreasing. E_{cav} decreases until it becomes lower than the extinction field, E_{ext}, discharge then stops E_{cav} stops to decrease and no further current flows in the cavity.

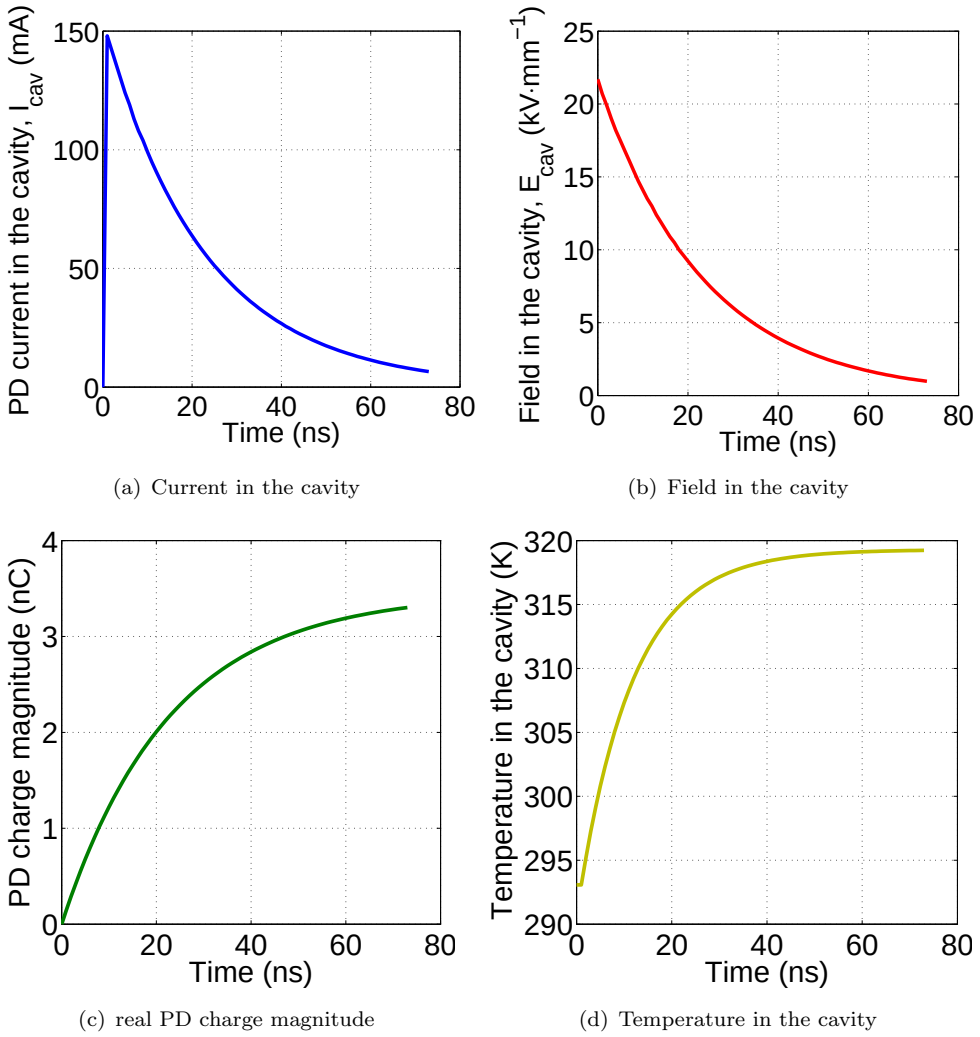

(a) Current in the cavity

(b) Field in the cavity

(c) real PD charge magnitude

(d) Temperature in the cavity

FIGURE 6.15: Simulation as a function of time during PD occrrence.

6.6 Electric field within different cavity locations in a material

The simulation of electric field magnitude at 5 ms of the 50 Hz 18 kV applied voltage in the centre of a spherical cavity, E_{cav} in the absence of any PD, against its location in a dielectric material is shown in Figure 6.16. The cavity diameter is 1 mm and the material thickness is 3 mm. When the cavity is situated closer to the electrode, the electric field in the cavity center decreases because the electric field on the cavity surface

that is nearer to the electrode is reduced. Hence, the net electric field in the cavity is reduced.

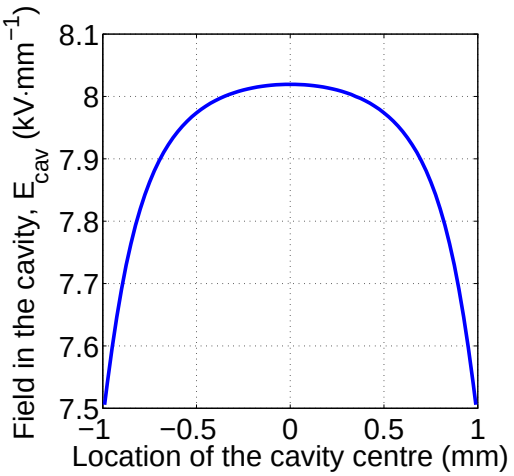

FIGURE 6.16: Electric field magnitude in the cavity against location of the cavity in the material (50 Hz, 18 kV applied voltage).

Figure 6.17 shows cross-section plot of the electric field magnitude along the z-axis in the FEA model for different location of the cavity centre, L in the material. The electric field magnitude along the z-axis in the cavity is uniform and symmetrical when the cavity is located in the middle of the material (at L = 0 mm). The electric field distribution is not uniform when the cavity is not located exactly in the middle of the material because the electric field in the cavity closer to one electrode is influenced by that electrode. However, positive and negative discharge polarities on the PD pattern may be symmetrical because the electric field distribution in the cavity is nearly symmetrical. However, when the cavity is located against the electrode (at L = -1 and 1 mm), the electric field magnitude along the z-axis in the cavity is totally asymmetrical. After a PD occurs in the cavity, charges accumulated on the electrode can decay faster. Thus, charge distribution on the cavity surface becomes non uniform and asymmetrical and this may results in asymmetrical behaviour of PD pattern between positive and negative discharges [43, 118, 119].

6.7 Summary

From the FEA model, before any PD occurs, the electric field in the cavity is higher than the dielectric material due to its lower permittivity while the temperature distribution in the whole cavity and material is uniform. However, after a PD occurs, the electric field in the cavity is lower than the material due to charge accummulation on the cavity surface but the temperature in the cavity becomes higher than the material. Heat energy released in the cavity during PD event, causes the temperature of the cavity to increase. This may cause the pressure in the cavity and the inception field level to increase. After a

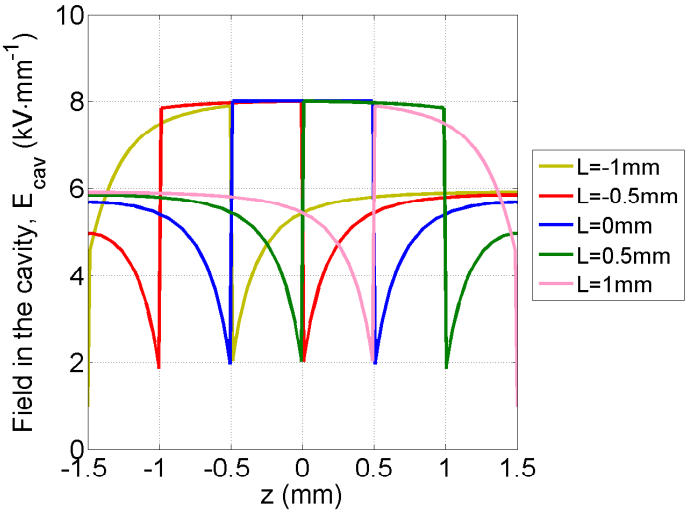

FIGURE 6.17: Cross-section plots of the electric field magnitude along the z-axis in the cavity of diameter 1 mm in the FEA model for different location in the cavity.

certain time, the temperature in the cavity decreases, where heat dissipates through the surrounding material, resulting in the temperature in the cavity becoming non-uniform. It has also been found that the temperature increase in the cavity due to PD events is very small and this may suggest that the temperature change in the cavity has very little influence on the sequence of PD events. The surface charge that has accummulated on the cavity surface may decay with time through surface conduction along the cavity wall, causing charge recombination, resulting in a reduction of the electric field due to surface charge and the amount of surface charge. From the simulation of electric field for different locations of the cavity within the material, the electric field distribution is no longer symmetrical along the symmetry axis when the cavity is not located at the exact centre of the material. This is due to the influence of the nearer electrode on the electric field on the cavity surface nearest to it.

Chapter 7

Comparison between Simulation and Measurement Results: Effect of applied voltage and frequency on PD activity

The comparison of PD activity measurement and simulation results has been made for different applied voltage amplitudes and frequencies of the applied voltage to study PD behaviour under these conditions. From the comparison, variation in certain model parameters allows the critical parameters and physical mechanisms affecting the sequence of PD events for different applied voltage amplitude and frequency of the applied voltage to be identified. Comparisons are mainly made using the ϕ-q-n plots, number of PDs per cycle, maximum charge magnitude and minimum charge magnitude. Simulation of field against time of the applied field, PD charge magnitude and temperature in the cavity have been completed to study the sequence of PD events for different amplitudes and frequencies of the applied voltage.

7.1 Effect of applied voltage amplitude on PD activity

7.1.1 Comparison of PD patterns

Figure 7.1 shows ϕ-q-n plots of measurement and simulation results of PD activity as a function of amplitude of the applied 50 Hz ac sinusoidal voltage for 500 cycles. The simulation results shown in Figure 7.1 are obtained from the model when the temperature change in the cavity due to PD events is considered. This is because the simulation results from the model when the temperature change in the cavity is neglected are almost

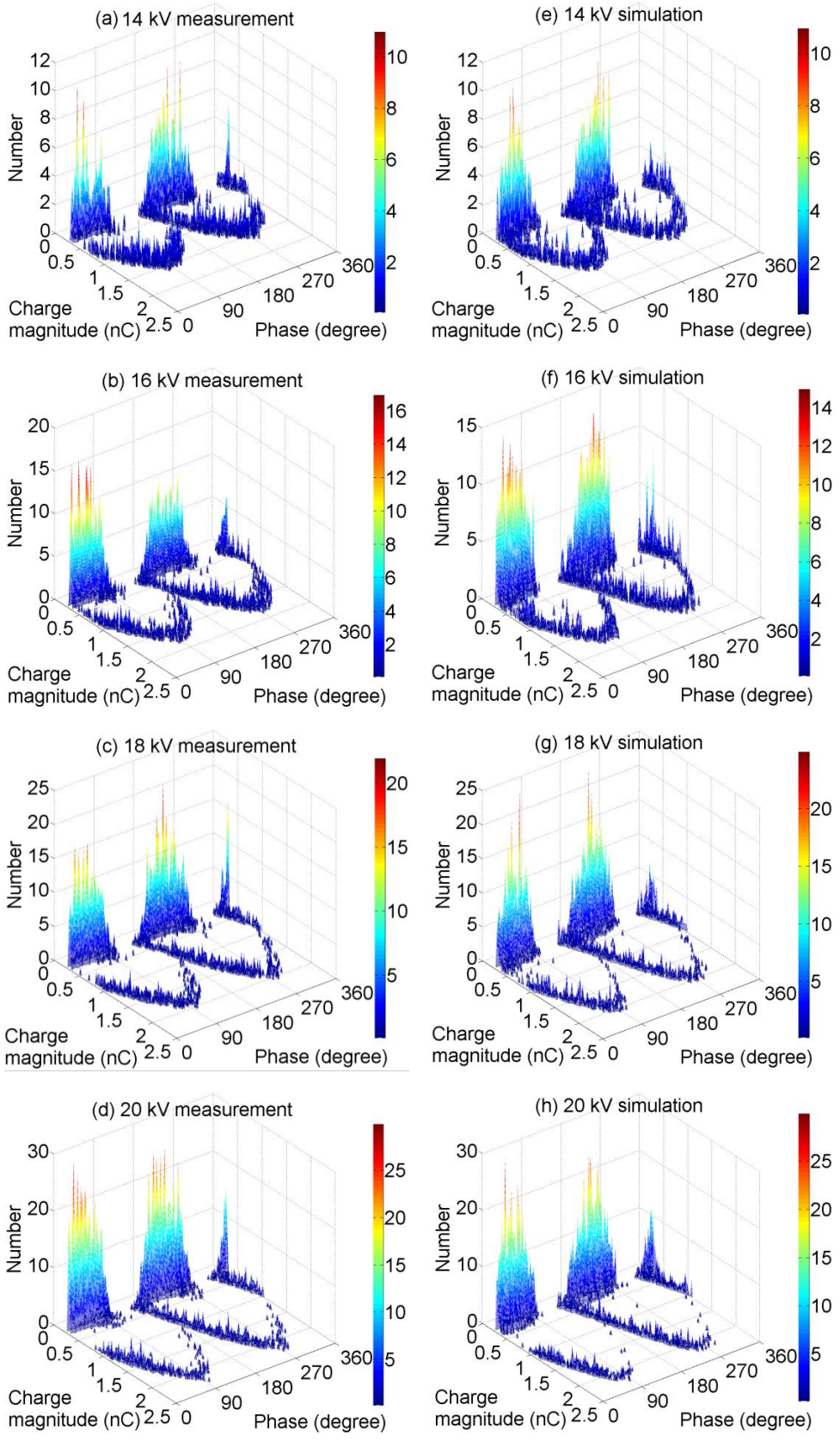

FIGURE 7.1: ϕ-q-n plots of the measurement and simulation results for different applied voltages (Simulation when the temperature change in the cavity is considered).

similar to that of the model when the temperature change is considered. The sample consists of a spherical cavity of diameter 1.4 mm within a dielectric material of thickness 2.0 mm. Table 7.1 to Table 7.3 compares the measurement and simulation results, when the temperature change in the cavity due to PD events in the model is neglected and considered. Comparison between measurement and simulation results clearly indicates that the simulation results are in reasonable agreement with the measurement results for all applied voltages. From the ϕ-q-n plots, referring to the charge magnitude-phase axes, the 'rabbit-ear' like curves where PDs occur with higher charge magnitude and broad 'straight-line' patterns where PDs occur with a lower charge magnitude are clearly seen. The simulation of ϕ-q-n plots shown here are only for the model considering the temperature change in the cavity due to PD events because the simulation by neglecting the temperature change in the cavity also yields the similar patterns. This is due to the temperature change in the cavity only influences PD events that occur near the inception field level, i.e. it only influences PDs occuring near the minimum charge magnitude but not the 'rabbit-ear' like patterns, by referring to the charge magnitude-phase axes in the ϕ-q-n plots.

Applied voltage (kV)	14	16	18	20
Number of PDs per cycle	2.5	4.2	5.7	7.3
Total charge per cycle (pC)	1698	2591	3186	3940
Mean charge magnitude (pC)	674	616	562	536
Maximum PD magnitude (pC)	1625	1856	2056	2250
Minimum PD magnitude (pC)	263	263	263	263

TABLE 7.1: Measurement results for different applied voltages

Applied voltage (kV)	14	16	18	20
Number of PDs per cycle	2.5	4.2	5.7	7.3
Total charge per cycle (pC)	1404	2278	3114	3924
Mean charge magnitude (pC)	552	546	546	537
Maximum PD magnitude (pC)	1626	1857	2076	2288
Minimum PD magnitude (pC)	263	263	263	263

TABLE 7.2: Simulation results for different applied voltages (When the temperature change in the cavity is neglected)

Applied voltage (kV)	14	16	18	20
Number of PDs per cycle	2.5	4.2	5.7	7.3
Total charge per cycle (pC)	1390	2309	3154	3964
Mean charge magnitude (pC)	565	552	554	545
Maximum PD magnitude (pC)	1625	1861	2082	2253
Minimum PD magnitude (pC)	263	264	263	264

TABLE 7.3: Simulation results for different applied voltages (When the temperature change in the cavity is considered)

From the simulation, the 'rabbit-ear' like patterns are created by the PDs that occur after a change in polarity of the field in the cavity from the previous PD, which has been detailed in Chapter 6 [120]. When the field in the cavity changes between consecutive PD events, the magnitude of the field in the cavity is enhanced. This increases the charge magnitude of the next PD event. Whilst the broad 'straight-line' patterns are obtained when there is no polarity change of field in the cavity between consecutive discharges. There are PDs occurring before zero-volt crossing of the applied voltage (at 180 and 360 degrees) due to an enhanced electron generation rate at higher applied voltages and the field due to surface charge in the cavity.

7.1.2 Parameter values for the simulation

Table 7.4 shows the definition of parameters used in the simulation for different applied voltage amplitudes. From this table, constant parameter values are used for all applied voltages except for the maximum cavity surface conductivity, σ_{smax} and electron generation rate (EGR) due to volume ionization, N_{ev}. At higher applied voltages, σ_{smax} is increased to obtain the measured maximum charge magnitude seen on the measurement 'rabbit-ear' like curves. Else, the simulated maximum charge magnitude will be higher than the measured data if σ_{smax} is not increased for higher applied voltages. Since the cavity surface conductivity is field-dependent, higher applied voltage increases σ_{smax}, which indicates that surface charge decay through conduction along the cavity wall may be more significant [86, 87]. A higher surface conductivity causes a reduction in the maximum field in the cavity, resulting in lower maximum charge magnitude. From experimental data where the applied field, E_0 is varied, it is possible to select σ_{smax} in the simulation to provide closest match between experimental data and simulation results. Analysis yields Figure 7.2(a). From this, it is possible to estimate σ_{smax} as a dependent variable of E_0 using

$$\sigma_{smax} = \alpha exp(\beta E_0) \tag{7.1}$$

where α is 6.526×10^{-13} Sm^{-1} and β is 0.8047 $\mathrm{mm{\cdot}kV}^{-1}$.

The initial inception field, E_{inc0} are extracted from the FEA model when the amplitude of the applied voltage is equal to the measured inception voltage, U_{incapp}. The obtained U_{incapp} is around 5.06 kV from the experiment and this value is used to determine E_{inc0}, which is calculated using Equation 2.5. The initial pressure, p_0 in the cavity is assumed to be 101 kPa. U_{incapp} is assumed to be applied voltage independent because it has been reported that the ramp rate does not influence the inception voltage [121]. The initial extinction field, E_{ext0} is chosen based on the minimum PD charge magnitude from the measured ϕ-q-n plots because the field drop in the cavity after a PD determines the PD charge magnitude. It is assumed to be constant for all applied voltages because from

the measurement, the minimum charge magnitude is independent of the applied voltage. The extinction field has been expected to be lower than the inception field [106].

Once E_{inc0}, E_{ext0} and σ_{smax} have been determined, the values for N_{es0H}, N_{es0L} and N_{ev} were chosen by using sensitivity analysis through an optimization method which yields the global minimum of mean square error (MSE) between the measurement and simulation results for all applied voltages. These values determine the density of PDs near the minimum charge magnitude and on the 'rabbit-ear' like pattern of the simulated ϕ-q-n plots. N_{es0H} and N_{es0L} are constant for all applied voltages because the total electron generation rate is controlled by the exponential term, $\exp(E_{cav}(t)/E_{inc})$ in Equation 3.24. The effective charge decay time constant, τ_{dec}, is independent of the applied voltage because it is assumed that charge decay of the trapped charges is only influenced by the thermal process.

Referring to Figure 7.2(b), N_{ev} is increased with the applied voltage because there is no field dependent term in N_{ev}. Higher volume ionization may be due to more background ionizations occurring under higher electric field magnitudes. However, the increment rate of N_{ev} is slower with increasing applied voltage, which may be due to volume ionization being limited by the cavity volume. From this, it is possible to estimate N_{ev} as a dependent variable of the applied field, E_0 using

$$N_{ev} = \alpha \left[1 - (E_0/\beta)^{-\gamma}\right] \tag{7.2}$$

where α is 99.42 s^{-1}, β is 5.446 $kV{\cdot}mm^{-1}$ and γ is 3.2. E_0 is expressed as U_{app}/h_{mat}, where U_{app} is the applied voltage amplitude and h_{mat} is the material thickness used for this experiment (h_{mat} = 2 mm).

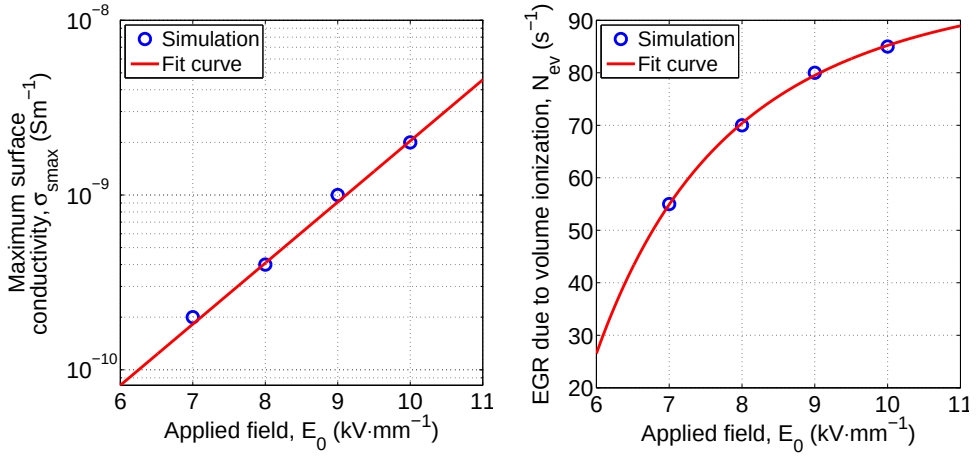

(a) Maximum surface conductivity, σ_{smax} (b) EGR due to volume ionization, N_{ev}

FIGURE 7.2: Simulation of model parameters as a function of applied voltage amplitude.

Definition	Symbol	Value	Unit
Cavity diameter	d	1.4	mm
Material thickness	h_{mat}	2.0	mm
Applied voltage amplitude	U_{app}	14, 16, 18, 20	kV
Initial temperature in the cavity	T_0	293	K
Initial pressure in the cavity	p_0	101	kPa
Initial inception field	E_{inc0}	3.35	kV·mm^{-1}
Initial extinction field	E_{ext0}	0.89	kV·mm^{-1}
Effective charge decay time constant	τ_{dec}	2	ms
Initial electron generation rate	N_{es0H}	3000	s^{-1}
due to surface emission	N_{es0L}	150	s^{-1}
Electron generation rate due to volume ionization	N_{ev}	$99.42[1-(E_0/5.446)^{-3.2}]$	s^{-1}
Maximum surface conductivity for charge decay	σ_{smax}	$0.6526\exp(0.8047E_0)$	pSm^{-1}

TABLE 7.4: Definition of parameters used in the simulation at different applied voltages

7.1.3 Simulation using different cavity surface conductivity values

Table 7.5 shows the results obtained for different maximum cavity surface conductivities, σ_{smax} for an 18 kV applied voltage. The simulation results are dependent on σ_{smax}. When σ_{smax} is set lower than 1×10^{-9} Sm^{-1}, the simulated number of PDs per cycle and the maximum charge magnitude are larger than the measured data. However, these data are lower than the measured data when σ_{smax} is set higher than 1×10^{-9} Sm^{-1}. The surface conductivity value controls the surface charge decay rate through conduction along the cavity wall, where higher surface conductivity reduces the amount of surface charge and the electron generation rate. Hence, the obtained maximum PD charge magnitude and the number of PDs per cycle are lower. This is the reason why the cavity surface conductivity is increased from its initial value up to a certain value to model charge decay through surface conduction when the polarity of field in the cavity and field due to surface charge are the same [122].

Surface conductivity, σ_{smax} (Sm^{-1})	**1×10^{-13}**	**1×10^{-9}**	**1×10^{-8}**	**Measured**
Total PDs per cycle	6.1	5.7	5.3	5.7
Total charge per cycle (pC)	3333	3154	2818	3186
Mean charge magnitude (pC)	545	554	528	562
Maximum charge magnitude (pC)	2141	2082	1921	2056
Minimum charge magnitude (pC)	264	263	264	263

TABLE 7.5: Results for different surface conductivity (50 Hz, 18 kV)

7.1.4 Simulation for 10 applied voltage cycles

Figure 7.3 and Figure 7.4 show simulation of electric fields, inception field, PD charge magnitude and temperature in the cavity against time for the first 10 cycles of 14 and 20 kV applied voltages. From Figure 7.3(b) and Figure 7.4(b), the temperature decay time constant,τ_{Tdecay} varies between consecutive discharges because it depends on the temperature when it starts to decay. τ_{Tdecay} is smaller when the temperature after a PD is larger, where the temperature decays faster when the initial temperature is higher. Assuming the temperature decays exponentially, the average τ_{Tdecay} is around 2 ms. The average temperature rise per PD event is 3.1K and 3.8K for 14 kV and 20 kV applied voltage while the maximum temperature rise due to PD events is 14K for 14 kV and 27K for 20 kV applied voltage. It is higher for 20 kV because the total charge per cycle is larger than for 14 kV. After a PD occurs with large charge magnitude, the temperature in the cavity does not recover immediately to its initial temperature when the next PD occurs because the temperature in the cavity is higher. Thus, the inception field is higher when the next PD is likely to occur after a previous PD occurs with large charge magnitude. However, the average temperature rise in the cavity for both applied voltage is small and the temperature can be seen to decay rapidly between consecutive discharges. Thus, this may suggest that the temperature change in the cavity due to PD events have little influence on PD occurrences.

7.1.5 Simulation for 12 and 22 kV applied voltages

The PD activity for 50 Hz, 12 and 22 kV applied voltage can also be simulated using parameter values in Table 7.4 if those values are assumed to be applicable for 12 and 22 kV. Figure 7.5 and Figure 7.6 show the simulated PD data and ϕ-q-n plots for 12 and 22 kV applied voltages. The simulation results can be said to be reasonable compared to the measurement because the number of PDs per cycle and total charge magnitude per cycle increase with the applied voltage. Referring to Figure 7.6(a), for 12 kV simulation, the density of PDs near the minimum charge magnitude is lower but the intensity of PDs on the 'rabbit-ear' like pattern is higher than 14 kV applied voltage (Figure 7.1). At lower applied voltages, the electron generation rate is lower, increasing the statistical time lag, resulting in more PDs occurring at higher field than the inception field. Thus, the number of PDs with larger charge magnitude increases. However, at 22 kV, the intensity of PDs near the minimum charge magnitude is higher than 20 kV (Figure 7.1) because of the higher electron generation rate, resulting in more PDs with lower charge magnitude.

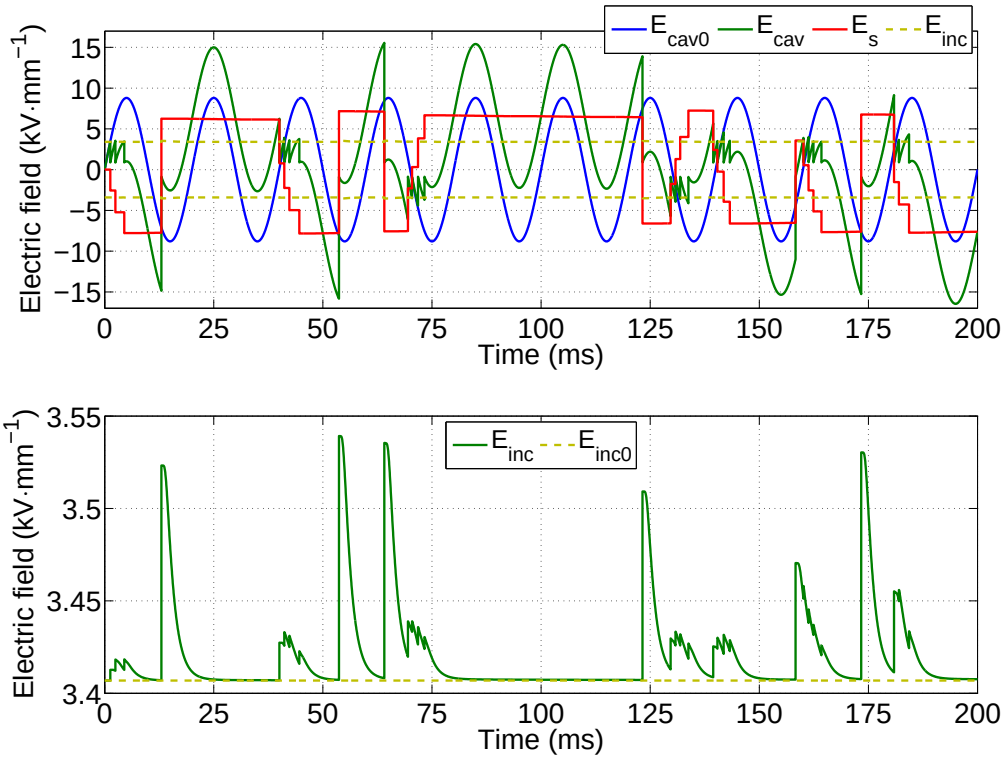

(a) Electric fields and inception field

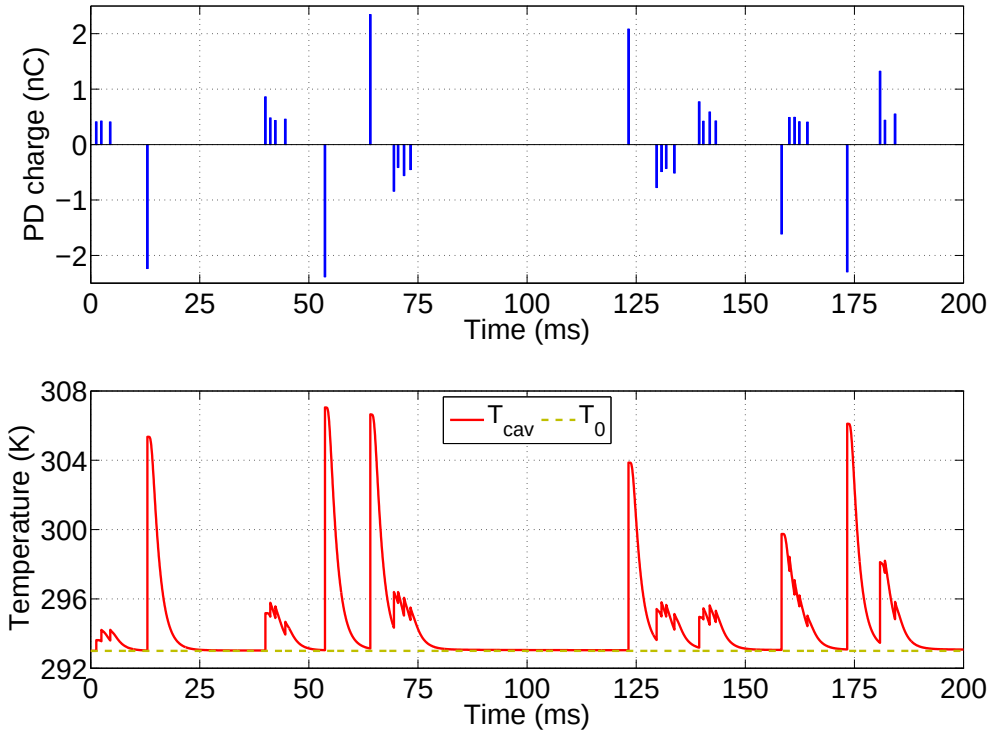

(b) PD charge magnitude and temperature

FIGURE 7.3: Simulation of electric fields, inception field, PD charge magnitude and temperature in the cavity against time for 50 Hz 14 kV applied voltage.

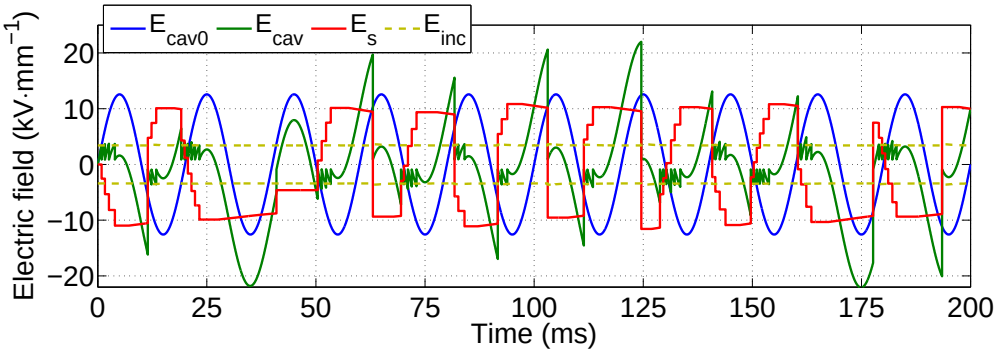

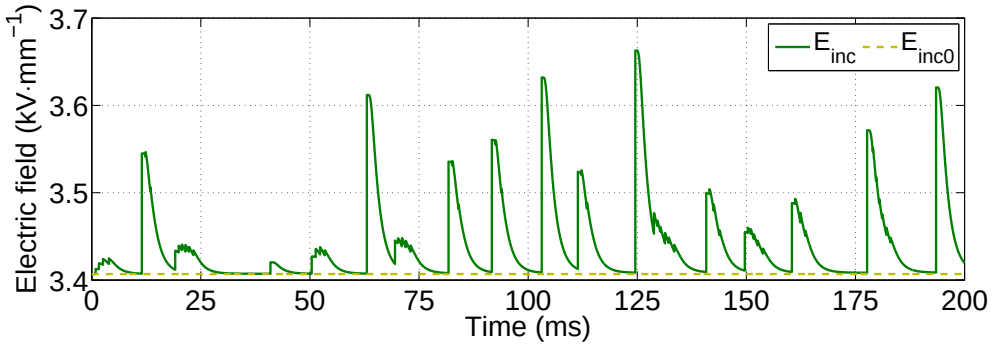

(a) Electric fields and inception field

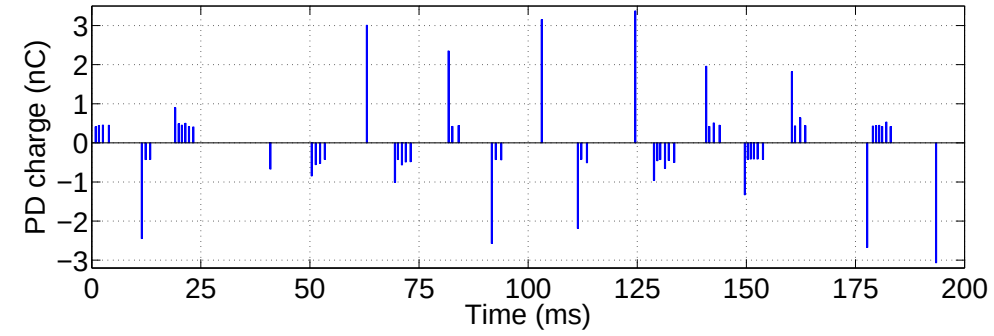

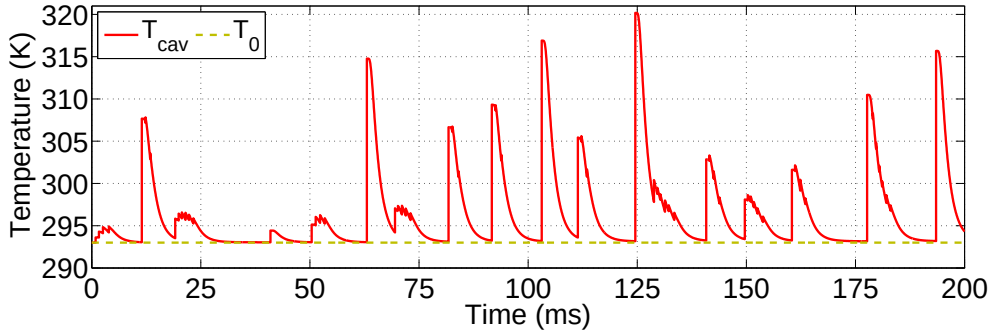

(b) PD charge magnitude and temperature

FIGURE 7.4: Simulation of electric fields, inception field, PD charge magnitude and temperature in the cavity against time for 50 Hz 20 kV applied voltage.

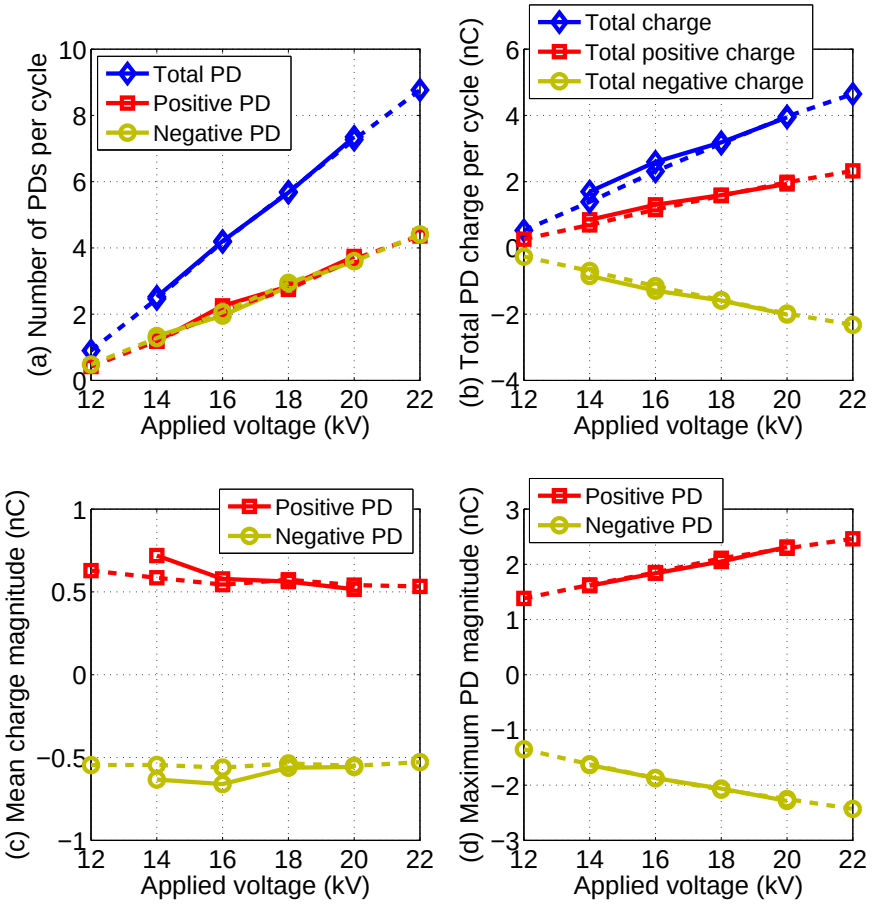

FIGURE 7.5: Simulation (dotted line) and measurement (solid line) results for different applied voltages.

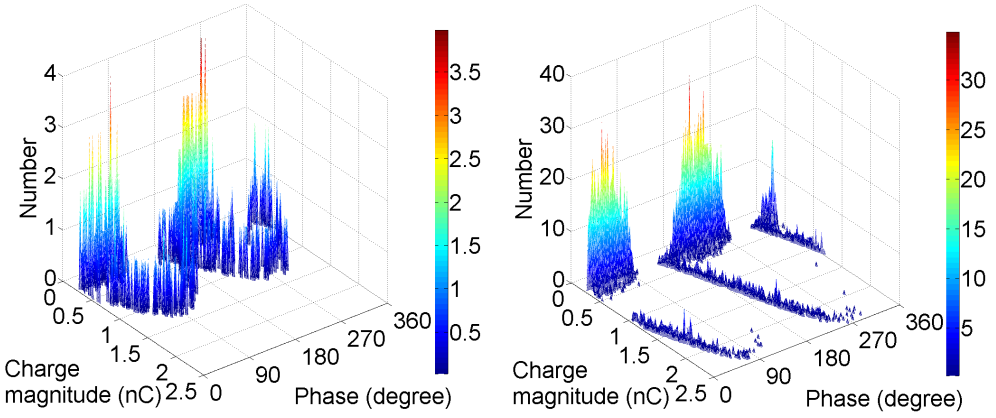

(a) 12 kV applied voltage

(b) 22 kV applied voltage

FIGURE 7.6: ϕ-q-n plots of simulation (Temperature change in the cavity is considered).

7.1.6 Comparison between models neglecting and considering temperature change in the cavity

The simulation as a function of applied voltage amplitude has also been undertaken by neglecting the temperature change in the cavity to observe the difference compared to when it is considered in the model. Table 7.6 and Table 7.7 show the least mean square error (MSE) of PD phase and charge magnitude distributions between measurement and simulation results for the model which neglects (S1) and considers (S2) the temperature change in the cavity after a PD event. From these tables, the least MSE are slightly smaller for S2 than S1. This indicates that the error between the measurement and simulation can be reduced, although very small, when the temperature change in the cavity is considered, which therefore slightly improves the model.

Applied voltage, U_{app} (kV)	**14**	**16**	**18**	**20**
Least MSE for S1	9.0278	12.3472	20.6167	29.7611
Least MSE for S2	8.6472	11.0861	15.3417	26.3917
Difference between S1 and S2	0.3806	1.2611	5.2750	3.3694
Reduction in S2 from S1 (%)	4.2159	10.2137	25.5861	11.3215

TABLE 7.6: Least MSE for PD phase distribution between measurement and simulation results for different applied voltages

Applied voltage, U_{app} (kV)	**14**	**16**	**18**	**20**
Least MSE for S1 ($\times 10^{-18}$)	2.5727	3.8703	5.0292	7.1272
Least MSE for S2 ($\times 10^{-18}$)	2.3878	3.8524	4.0335	6.9826
Difference between S1 and S2 ($\times 10^{-18}$)	0.1849	0.0180	0.9957	0.1446
Reduction in S2 from S1 (%)	7.1852	0.4638	19.7676	2.0282

TABLE 7.7: Least MSE for PD charge magnitude distribution between measurement and simulation results for different different applied voltages

7.2 Effect of applied frequency on PD activity

7.2.1 Comparison of PRPD patterns

A sample of a spherical cavity of diameter 1.55 mm within a dielectric material of 2 mm thickness has been used for PD measurement under different frequencies of the applied voltage. Figure 7.7 and Figure 7.8 shows the measurement and simulation ϕ-q-n plots as a function of frequency of the applied 14 kV voltage for 500 cycles. The simulation results shown here are only for the model which considers the temperature change in the cavity due to PD event because the simulation results when the temperature change in the cavity is neglected are almost similar. Table 7.8 to Table 7.10 details the comparison between the measurement and simulation results for different applied frequencies when

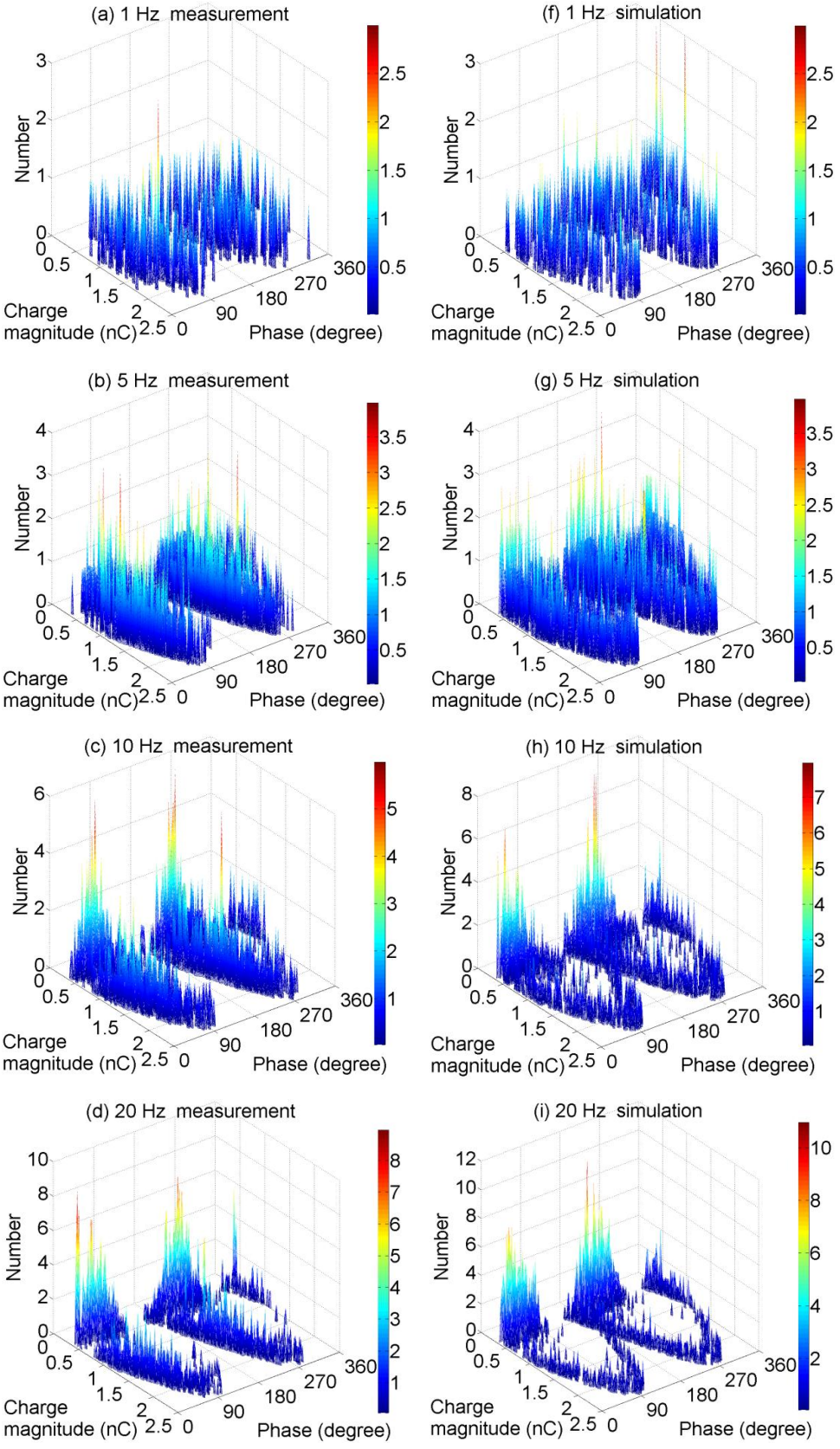

FIGURE 7.7: ϕ-q-n plots of the measurement and simulation results for different frequency of the applied voltage (1, 5, 10 and 20 Hz) (Continue to Figure 7.8).

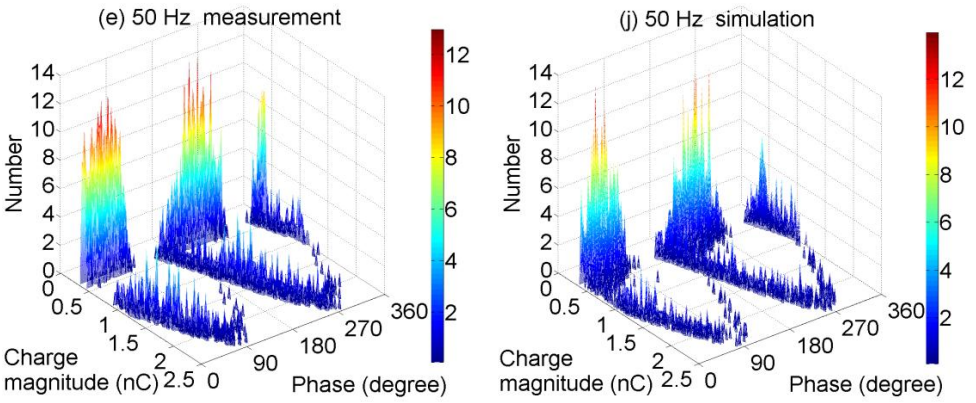

FIGURE 7.8: ϕ-q-n plots of the measurement and simulation results for different frequency of the applied voltage (50 Hz) (Simulation when the temperature change is considered).

Frequency (Hz)	**1**	**5**	**10**	**20**	**50**
Total PDs per cycle	2.2	2.9	3.2	3.5	5.3
Total charge per cycle (pC)	3102	3693	3648	3665	4111
Mean charge (pC)	1399	1258	1137	1057	769
Maximum charge magnitude (pC)	2450	2400	2450	2453	2450
Minimum charge magnitude (pC)	375	375	375	375	375

TABLE 7.8: Measurement results for different applied frequencies

Frequency (Hz)	**1**	**5**	**10**	**20**	**50**
Total PDs per cycle	2.2	2.9	3.2	3.5	5.3
Total charge per cycle (pC)	2700	3204	2968	2788	3762
Mean charge (pC)	1233	1113	927	786	704
Maximum charge magnitude (pC)	2407	2421	2436	2443	2444
Minimum charge magnitude (pC)	375	375	375	375	374

TABLE 7.9: Simulation results for different applied frequencies (When the temperature change in the cavity is neglected)

Frequency (Hz)	**1**	**5**	**10**	**20**	**50**
Total PDs per cycle	2.2	2.9	3.2	3.6	5.3
Total charge per cycle (pC)	2803	3139	2978	2852	3728
Mean charge (pC)	1254	1098	920	790	709
Maximum charge magnitude (pC)	2428	2422	2429	2443	2444
Minimum charge magnitude (pC)	375	376	375	376	375

TABLE 7.10: Simulation results for different applied frequencies (When the temperature change in the cavity is considered)

the temperature change in the cavity due to PD events are neglected and considered. With reference to these tables, there is good agreement between the simulation and experimental data, except for some data in the total charge magnitude per cycle.

Referring to the charge magnitude-phase axes of the ϕ-q-n plots in Figure 7.7 and Figure 7.8, when the applied frequency is decreased from 50 Hz to 1 Hz, the 'rabbit-ear' like curves disappear whilst the density of PDs near the minimum charge magnitude and on the 'rabbit-ear' like curve become almost the same. This can be seen because the number of PDs occurring with lower charge magnitude decrease at lower applied frequency.

From the simulation, this characteristic is obtained because the surface charge decay effect is more significant at lower applied frequency [15]. For increasing period of the applied voltages, more charges from previous PD will have decayed when the next PD is likely to occur. The lower availability of initial free electron increases the delay of a PD. Hence, more PD will occur with larger charge magnitude because the field drop in the cavity due to a PD is higher. When this occurs, by referring to the charge magnitude-phase axes in the ϕ-q-n plots, the clearly separated 'rabbit-ear' like curve from the PDs that occur with lower charge magnitude at 50 Hz (Figure 7.8(e)) diminishes when the applied frequency is decreased towards 1 Hz (Figure 7.7(a)).

7.2.2 Parameter values for the simulation

Table 7.11 details the definition of parameters used in the simulation for different applied frequencies and Figure 7.9 shows plots of parameter values as a function of applied frequency. The permittivity values obtained from the measurement are used in the simulation, as shown in Figure 4.10(b) in Chapter 2. The material used in this work has decreasing permittivity with frequency. For the applied frequency, f of 1 to 100 Hz, the material permittivity, ε_{rmat} that has been obtained from the measurement can be represented with

$$\varepsilon_{rmat} = (1.7189/f)^{0.1574} + 3.819 \text{ for } 1 \leq f \leq 100 \text{ Hz} \tag{7.3}$$

The initial inception field, E_{inc0} is extracted from the FEA model when the applied voltage amplitude is equal to the measured inception voltage, U_{incapp} in the model. The measured U_{incapp} for 50 Hz is 5.0 kV and the initial pressure in the cavity, p_0 is assumed to be atmosphere pressure (101 kPa). According to Paschen's curve, for the cavity geometry of the test sample used in the measurement, it is impossible to obtain a cavity pressure which is lower than 70 kPa. It is assumed that the inception field is independent of the frequency of the applied voltage, where E_{inc0} for 50 Hz is used for all applied frequencies in the simulation [105]. Since the measurement is done in continuous sequence between different applied frequencies, the measured inception voltage at each frequency is not determined. Previous research measured PD inception voltages for an insulated cylindrical cavity in polyethylene over a range of frequencies and did not identify any frequency dependent behaviour [55].

Definition	Symbol	Value	Unit
Cavity diameter	d	1.55	mm
Material thickness	h_{mat}	2.0	mm
Initial temperature in the cavity	T_0	293	K
Applied voltage amplitude	U_{app}	14	kV
Applied frequency	f	1, 5, 10, 20, 50	Hz
Material permittivity	ε_{rmat}	$(1.7189/f)^{0.1574} + 3.819$	
Initial pressure in the cavity	p_0	101	kPa
Initial inception field	E_{inc0}	3.02	$\mathrm{kV{\cdot}mm^{-1}}$
Initial extinction field	E_{ext0}	$(0.0355/f)^{0.1305}$+0.2474	$\mathrm{kV{\cdot}mm^{-1}}$
Effective charge decay time constant	τ_{dec}	2	ms
Initial electron generation rate	N_{es0H}	2100	$\mathrm{s^{-1}}$
due to surface emission	N_{es0L}	300	$\mathrm{s^{-1}}$
Electron generation rate due to volume ionization	N_{ev}	$(8.8492f)^{0.7852}$−0.2386	$\mathrm{s^{-1}}$
Maximum surface conductivity for charge decay	σ_{smax}	$0.3177f^{0.1499}$+0.04201	$\mathrm{nSm^{-1}}$

TABLE 7.11: Definition of parameters used in the simulation for different applied frequencies

The initial extinction field, E_{ext0} is chosen based on the minimum charge magnitude for each applied frequency from the measurements. Since the measured minimum charge magnitude is frequency independent, the decrease in the measured permittivity with increasing applied frequency results in the decrease of E_{ext0}. Figure 7.9(c) shows E_{ext0} as a function of frequency, which can be written as

$$E_{ext0} = (0.0355/f)^{0.1305} + 0.2474 \ [\mathrm{kV{\cdot}mm^{-1}}] \text{ for } 1 \leq f \leq 100 \ \mathrm{Hz} \tag{7.4}$$

From the measurement, the maximum charge magnitude seems to be frequency independent and it is used to determine the values of σ_{smax} for each applied frequency. From Figure 7.9(d), the simulated σ_{smax} is found to increase with the applied frequency because higher applied frequency causes the field in the cavity to change faster, resulting in faster charge movement along the cavity wall. However, this does not reduce the maximum charge magnitude at higher applied frequency because fewer amounts of charge decay through surface conduction due to a smaller time interval between consecutive discharges. σ_{smax} can be expressed as a function of frequency using

$$\sigma_{smax} = 0.3177 f^{0.1499} + 0.04201 \ [\mathrm{nSm^{-1}}] \text{ for } 1 \leq f \leq 100 \ \mathrm{Hz} \tag{7.5}$$

Parameters relating to electron generation rate (N_{es0H}, N_{es0L} and N_{ev}), which determine the PD repetition rate and the PD patterns on the ϕ-q-n plots were chosen by using sensitive analysis. N_{es0H} and N_{es0L} are applied frequency independent because the

electron generation rate (EGR) due to surface emission for the next PD to occur is determined by the term $\exp(-t/\tau_{dec})$ in the EGR equation, where τ_{dec} effective charge decay time constant and t is the time elapsed since previous PD event. Since τ_{dec} is frequency independent, N_{es0H} and N_{es0L} are constant. However, N_{ev} increases with the applied frequency. It is assumed that the number of free electrons generated in the cavity through volume ionization in one voltage cycle is the same for all applied frequencies. Thus, the number of free electron generated per one second is larger at higher applied frequencies. N_{ev} can be estimated as a dependent variable of the applied frequency, f using

$$N_{ev} = (8.8492f)^{0.7852} - 0.2386\ [\mathrm{s}^{-1}] \text{ for } 1 \leq f \leq 100\ \mathrm{Hz} \tag{7.6}$$

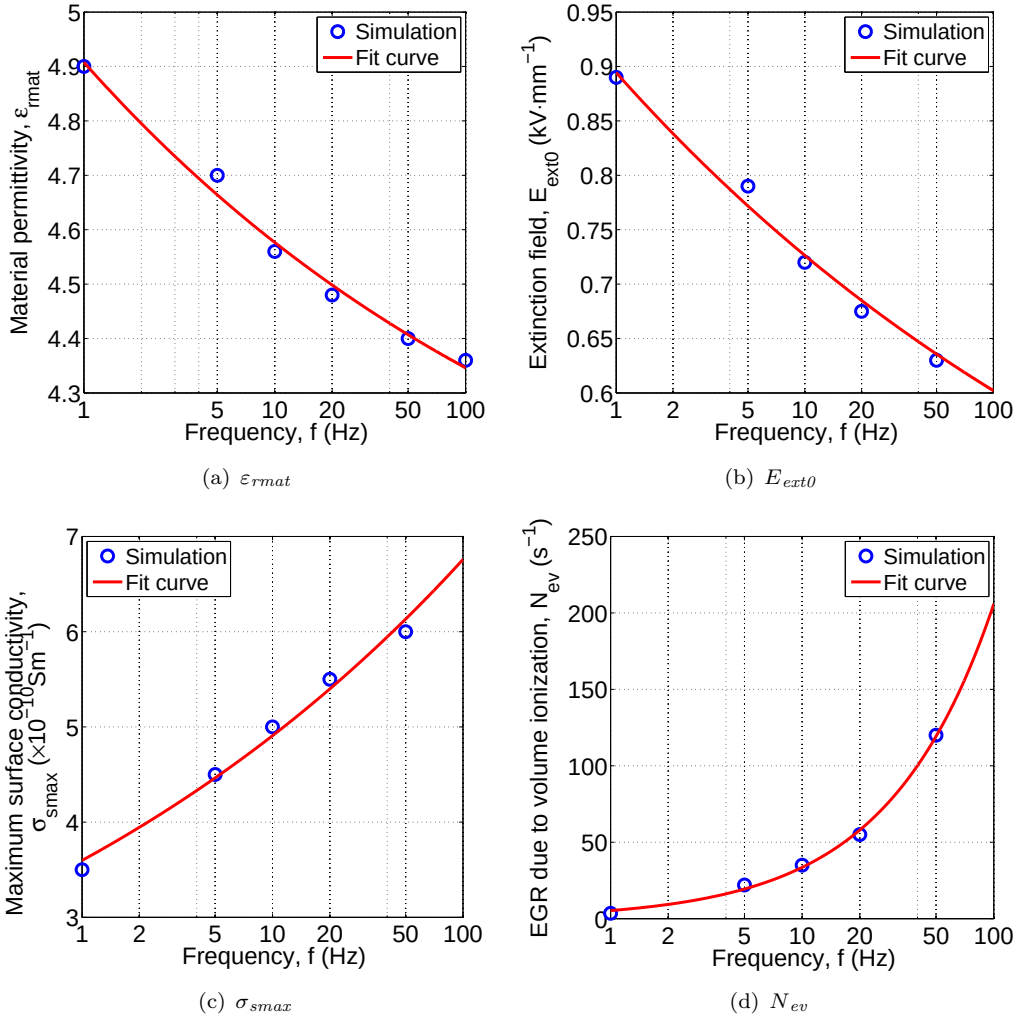

(a) ε_{rmat} (b) E_{ext0}

(c) σ_{smax} (d) N_{ev}

FIGURE 7.9: Simulation of model parameters as a function of frequency of the applied voltage.

7.2.3 Simulation for 10 applied voltage cycles

The simulation of electric field, inception field, PD charge magnitude and temperature in the cavity against time of 1 and 50 Hz 14 kV applied voltage are shown in Figure 7.10 and Figure 7.11. Assuming the temperature decays exponentially, the temperature decay time constant, τ_{Tdecay} for both frequencies are around 2.2 ms, which is independent of the applied frequency. However, the average temperature rise per PD is 4.8K for 1 Hz and 2.6K for 50 Hz. This is due to more PDs with larger charge magnitude occurring at 1 Hz, consequently average temperature rise per PD event is higher. The maximum temperature rise due to PD events is 14K for 1Hz and 16K for 50 Hz applied frequency. There is no significant difference in the maximum temperature between these two frequencies. From Figure 7.10(b) and Figure 7.11(b), it can be seen that at frequency 1 Hz, the temperature in the cavity after a PD occurs recovers towards the initial temperature before the next PD occurs. However, at frequency 50 Hz, the temperature in the cavity does not recover towards the initial temperature between two consecutive discharges at certain time. Therefore, the temperature change in the cavity may have higher influence on the sequence of PD events at higher applied frequencies.

7.2.4 Simulation for 100 Hz applied frequency

The PD activity for frequency 100 Hz, 14 kV applied voltage can be simulated by using parameters in Table 7.11, by assuming those values are applicable for 100 Hz. The applied frequency lower than 1 Hz is not simulated because the change of the measured permittivity of the material is quite large below 1 Hz. Thus, parameter values in Table 7.11 may not be applicable for frequency less than 1 Hz. Figure 7.12 and Figure 7.13 show the simulated PD data and the ϕ-q-n plot for 100 Hz 14 kV applied voltage. The simulation results for 100 Hz seem to be reasonable compared to the measurement results because it fits the trend of the measurement data, i.e. the number of PDs per cycle and the total charge magnitude per cycle increase with the applied frequency. At higher applied frequency, the total electron generation rate is higher, reducing the statistical time lag and resulting in more PDs per cycle than 50 Hz [15,68]. The maximum PD charge magnitude is lower for frequency 100 Hz because of shorter time lag causes discharge to occur at lower field in the cavity, resulting in lower maximum charge magnitude. Thus, more PDs with lower charge magnitude are obtained and the 'rabbit-ear' like curve can be seen obviously on the charge magnitude-phase axes in Figure 7.13.

From the simulation results, at decreasing applied frequency, the surface charge decay effect is more significant between consecutive discharges due to the longer period of the applied voltage [56]. This allows more charges on the cavity surface to decay, resulting in a lower electron generation rate and the number of PDs per cycle is lower. This can

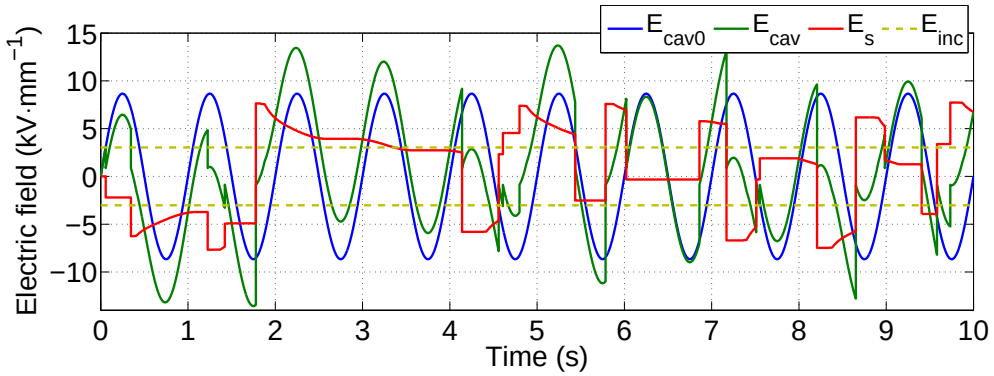

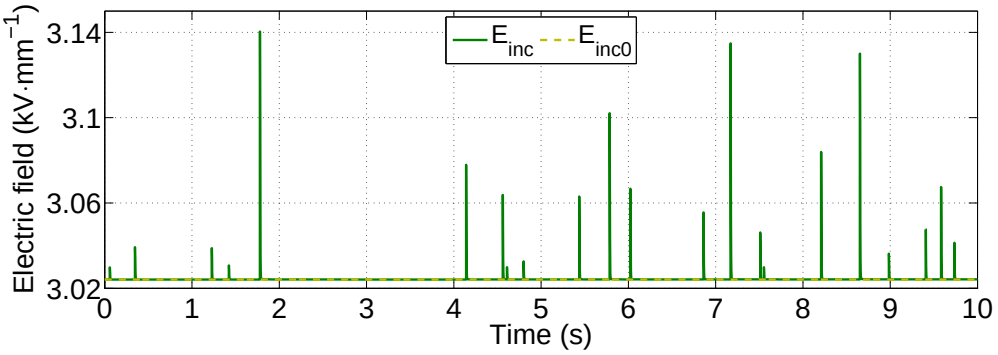

(a) Electric field and inception field

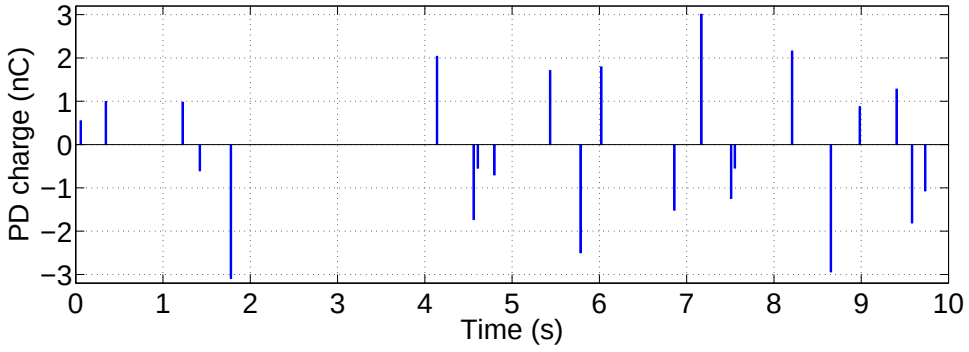

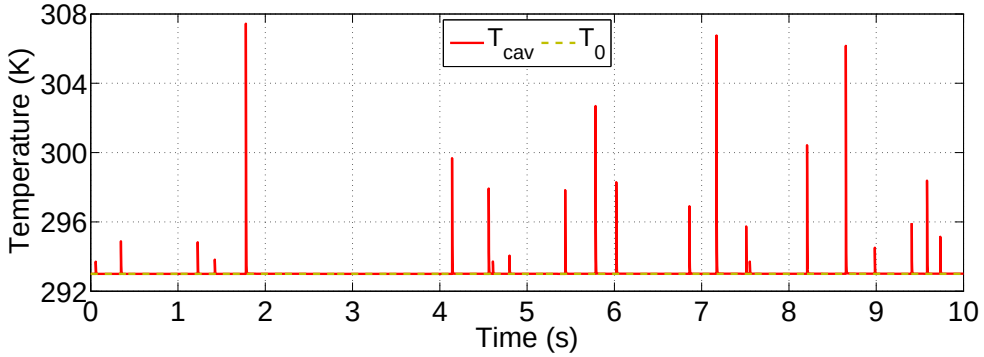

(b) PD charge magnitude and temperature

FIGURE 7.10: Simulation of electric field, inception field, PD charge magnitude and temperature in the cavity against time for 1 Hz 14 kV applied voltage.

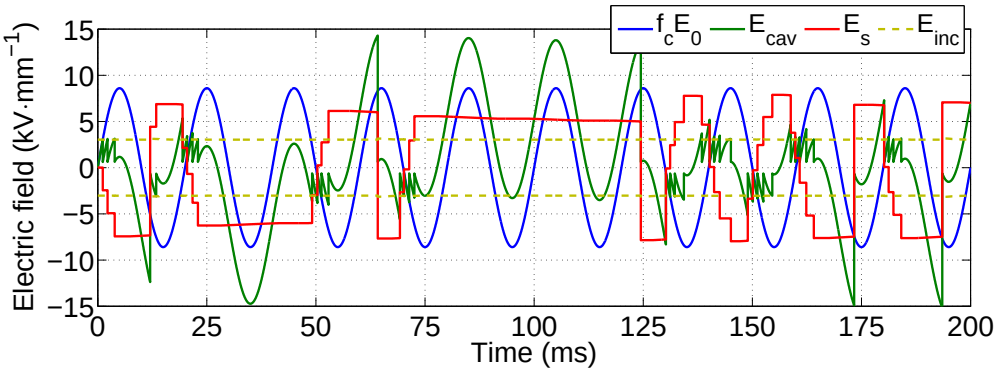

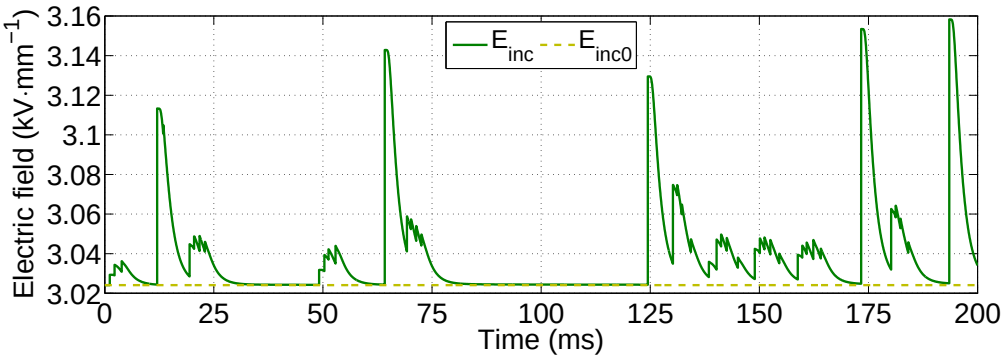

(a) Electric field and inception field

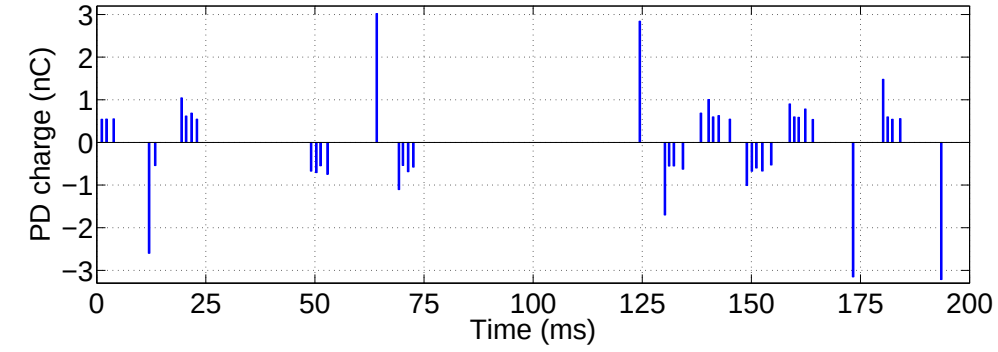

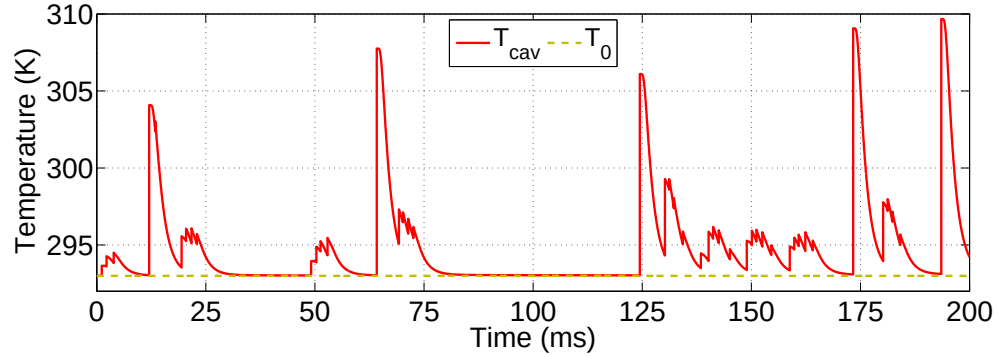

(b) PD charge magnitude and temperature

FIGURE 7.11: Simulation of electric field, inception field, PD charge magnitude and temperature in the cavity against time for 50 Hz 14 kV applied voltage.

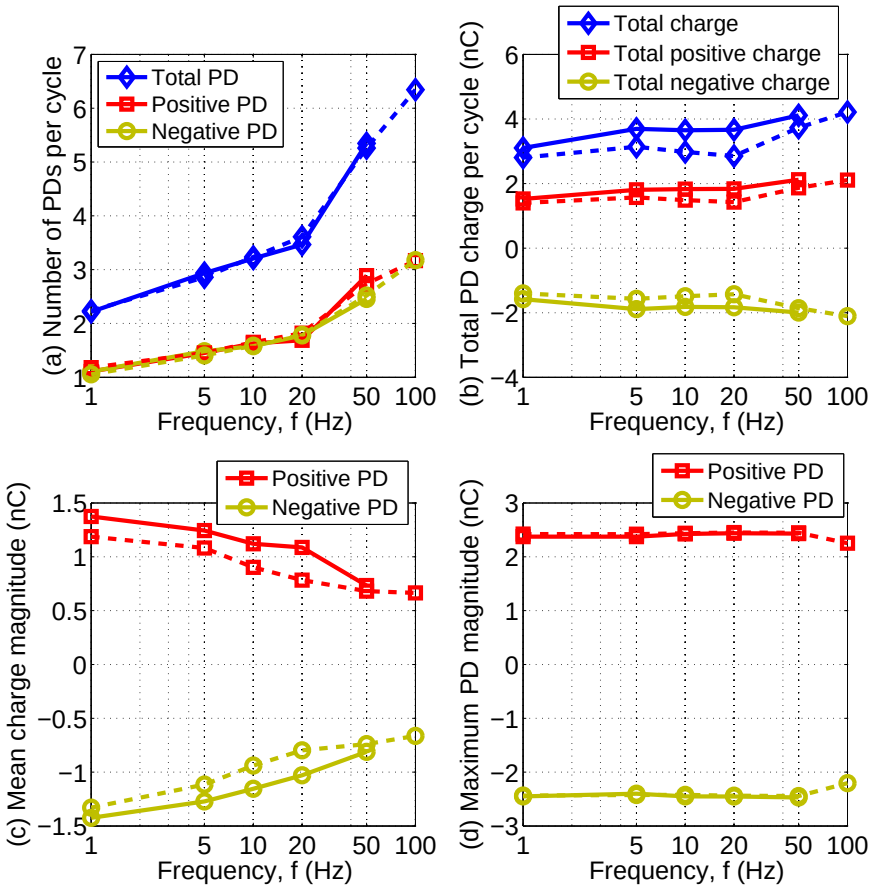

FIGURE 7.12: Simulation (dotted line) and measurement (solid line) results as a function of applied frequency.

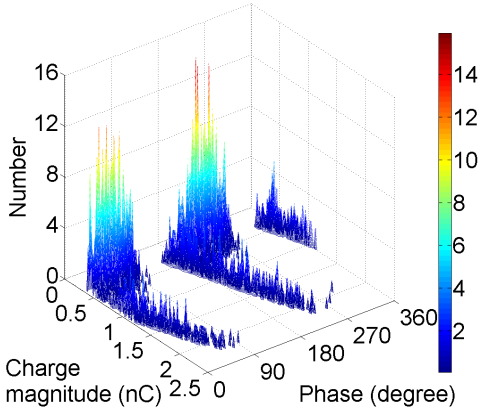

FIGURE 7.13: ϕ-q-n plot for 100 Hz, 14 kV applied voltage.

be seen at frequency 1 Hz of the measured ϕ-q-n plot, where the 'rabbit-ear' like curve diminishes completely due to the significant surface charge decay effect, reducing the number of PDs per cycle. Surface charge decays through charge movement into deeper traps or in the material and through conduction along the cavity wall.

7.2.5 Comparison between models neglecting and considering temperature change in the cavity

Table 7.12 and Table 7.13 show the least mean square errors (MSE) of PD phase and charge magnitude distributions between measurement and simulation when the temperature change in the cavity is neglected (S1) and considered (S2) in the model. At lower applied frequencies, the difference of least MSE between S1 and S2 is negligible but at higher applied frequencies, the difference is slightly higher. This is associated with the temperature change in the cavity may have more effect on PD activity at higher applied frequency. Thus, at higher frequency, the simulation results can be slightly improved with the inclusion of temperature change in the cavity due to PD events although the difference is very small.

Applied frequency (Hz)	**1**	**5**	**10**	**20**	**50**
Least MSE for S1	2.9278	12.4722	11.8083	15.3222	17.6556
Least MSE for S2	2.9083	12.0694	11.4833	10.9500	15.1778
Difference between S1 and S2	0.0195	0.4028	0.3250	4.3722	2.4778
Reduction in S2 from S1 (%)	0.6660	3.2296	2.7523	28.5351	14.0341

TABLE 7.12: Least MSE for PD phase distribution between measurement and simulation results for different applied frequencies

Applied frequency (Hz)	**1**	**5**	**10**	**20**	**50**
Least MSE for S1 ($\times 10^{-18}$)	2.7689	10.0630	10.0680	12.5560	7.8413
Least MSE for S2 ($\times 10^{-18}$)	2.8823	9.5603	10.7250	10.5090	7.2341
Difference between S1 and S2 ($\times 10^{-18}$)	-0.1134	0.5027	-0.6570	2.0470	0.6072
Reduction in S2 from S1 (%)	-4.0955	4.9955	-6.5256	16.3030	7.7430

TABLE 7.13: Least MSE for PD charge magnitude distribution between measurement and simulation results for different different applied frequencies

7.3 Summary

The measurement and simulation results have been compared and they are in agreement. When the applied voltage amplitude is increased, the total electron generation rate increases, resulting in higher number of PDs per cycle. The electron generation rate due to volume ionization increases with the applied voltage amplitude. However, the effect of surface charge decay through conduction along the cavity wall increases. It is due to the fact that the cavity surface conductivity is a field-dependent parameter, where higher applied field causes the cavity surface conductivity to become higher, resulting in charge to move faster along the cavity wall and causing charge recombination. The effect of temperature change in the cavity on the sequence of PD events is larger for

higher applied voltage amplitude due to the higher number of PDs that occur per cycle.

When the frequency is increased, the number of PDs per cycle increase because the total electron generation rate is higher. The effect of charge decay is less significant at higher applied frequencies because of the shorter time interval between consecutive discharges. This shortens the statistical time lag, causing many PDs to occur almost immediately after the inception voltage has been exceeded. However, charge movement along the cavity wall is faster at higher frequencies because of the shorter period of the applied voltage. The effect of temperature change in the cavity on the sequence of PD events is larger at higher applied frequencies because when the time interval between consecutive PDs is shorter, the temperature has a shorter time to recover to its initial value when the next PD is likely to occur.

Therefore, from comparison between measurement and simulation results, the critical parameters affecting the sequence of PD events for different applied voltage amplitude and frequency of the applied voltage have been identified. These include the inception field, extinction field, cavity surface conductivity, temperature decay time constant and the effective charge decay time constant. Physical mechanisms affecting PD behaviour are the electron generation rate due to surface emission and volume ionization, charge decay through charge trapping and charge conduction along the cavity wall and temperature variation in the cavity.

Chapter 8

Comparison between Simulation and Measurement Results: Effect of cavity size and temperature on PD activity

This chapter details the comparison between measurement and simulation results of PD activity for different spherical cavity sizes and ambient temperature of the dielectric material. Critical parameters affecting PD behaviour for these conditions can be identified from the simulation model. In addition, physical parameters influencing PD activity for different cavity sizes and temperature of the material can also be identified. Cycle to cycle behaviour of PD events is studied through plots of PD charge magnitude and applied field level of PD events against time of the applied voltage. The comparison of cycle to cycle PD behaviour between measurement and simulation results have been made, which can be used to support the assumptions made within the simulation mode.

8.1 Effect of spherical cavity diameter on PD activity

8.1.1 Comparison of PD patterns

Two samples have been used in the PD experiment for different spherical cavity size, where the diameters of the cavity are 1.1 and 2.35 mm located within the material samples of thickness 3 mm. Table 8.1 compares the measurement (M) and simulation results, when the temperature change in the cavity due to PD events in the model is neglected (S1) and considered (S2). Both of them are in reasonable agreement compared to the measurement results. Figure 8.1 shows the ϕ-q-n plots from the measurement and simulation of PD activity for different spherical cavity diameters at 50 Hz of 18 kV applied

voltage. Only simulation patterns for the model considering the temperature change in the cavity due to PD events are shown here because the simulation by neglecting the temperature change in the cavity also yields the similar patterns.

Cavity diameter (mm)	**1.1**			**2.35**		
	M	**S1**	**S2**	**M**	**S1**	**S2**
Number of PDs per cycle	6.5	6.5	6.5	2.5	2.5	2.5
Total charge per cycle (pC)	651	660	665	5420	5439	5456
Mean charge magnitude (pC)	101	101	102	2165	2138	2212
Maximum PD magnitude (pC)	373	347	368	4763	4761	4785
Minimum PD magnitude (pC)	80	83	83	938	938	939

TABLE 8.1: Comparison between measurement (M) and simulation (S1 and S2) results for different cavity diameters

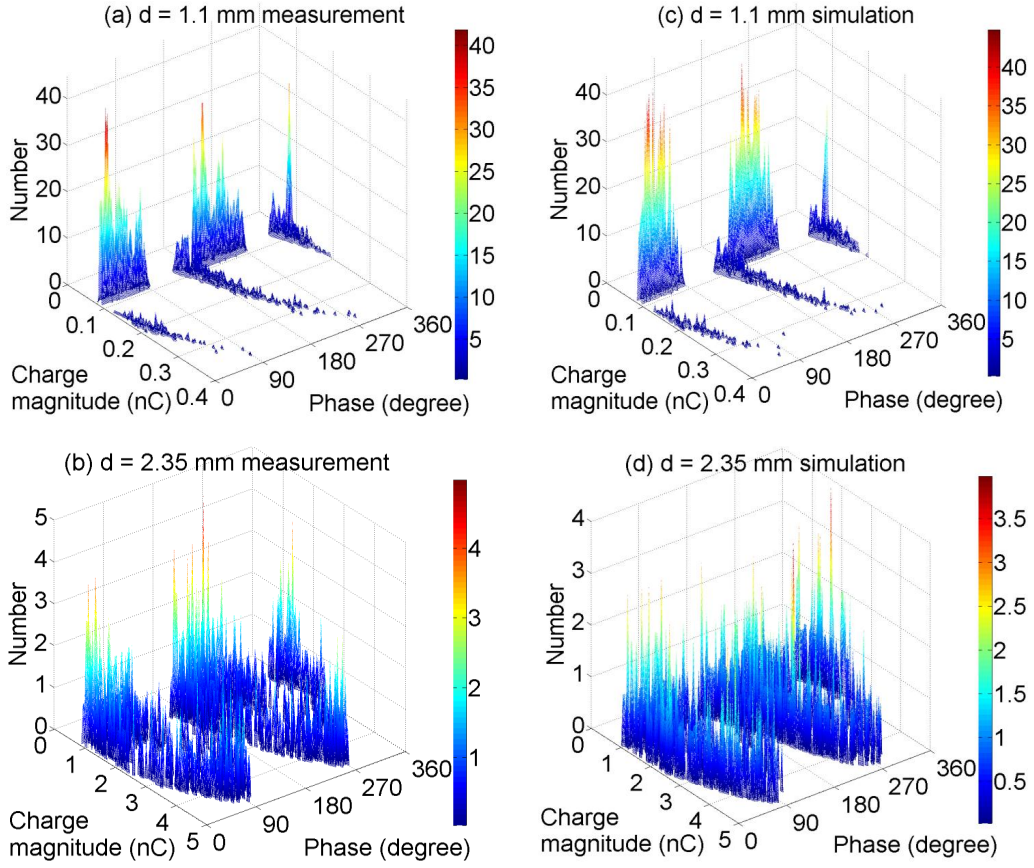

FIGURE 8.1: ϕ-q-n plots of the measurement (a-b) and simulation (c-d) results for different cavity sizes (Simulation when the temperature change in the cavity is considered).

8.1.2 Parameter values for the simulation

Table 8.3 shows the definition of parameters used in the simulations for different cavity diameters. From this table, the initial electron generation rates due to surface emission

(N_{es0H} and N_{es0L}) are higher but the electron generation rate due to volume ionization, N_{ev} and the maximum cavity surface conductivity, σ_{smax} are lower for the smaller cavity than the larger cavity. N_{es0H}, N_{es0L} and N_{ev} were obtained through sensitive analysis, where the combination of their values yields in the lowest mean square error between the simulation and measurement results.

From the simulation, higher N_{es0H} and N_{es0L} yield more PDs per cycle for the smaller cavity than the larger cavity and it also results in the 'rabbit-ear' curves that are clearly separated from PDs with lower charge magnitude, as shown in Figure 8.1(a). In a larger cavity, there may be more free charges accumulated on the cavity surface than charge trapping in surface state. This reduces the amount of charge detrapping from the cavity surface, which act as initial free electrons for the next PD. Therefore, this is the reason why lower initial electron generation rate due to surface charge is obtained in the simulation. However, the electron generation rate due to volume ionization, N_{ev} is higher for the larger cavity size because there may be more free electrons generated from background radiation in a larger cavity volume.

The maximum surface conductivity, σ_{smax} is found to be higher for the larger cavity size. Since the cavity surface conductivity is a field dependent parameter, larger σ_{smax} is obtained for the larger cavity in order to match the measured and simulated maximum PD charge magnitude. Hence, free surface charge decay through conduction along the cavity wall is more significant for the larger cavity size. There may be high amount of charges accumulated on the cavity surface, which decays through surface conduction with time. This could be the reason why the 'rabbit-ear' like curve of ϕ-q-n plot has a dispersed pattern, compared to the 'rabbit-ear' like curve for the smaller cavity.

The analysis of the average PD inception phase from the ϕ-q-n plots that have been obtained for the smaller and larger cavities is detailed in Table 8.2. It was found that both average positive and negative PD inception phases are higher for the larger cavity than the smaller cavity. This may indicate that for the larger cavity, the average statistical time lag is longer, which is due to lower electron generation rate. Thus, the number of PDs per cycle is less for the larger cavity than the smaller cavity and this is why lower N_{es0H} and N_{es0L} are assigned for the larger cavity.

Cavity diameter (mm)	**Average positive PD inception phase (degree)**	**Average negative PD inception phase (degree)**
1.1	-3.4400	178.2208
2.35	27.0760	216.9807

TABLE 8.2: PD inception phase for the smaller and larger cavities

It is assumed that charge decay rate through surface conduction is faster for the larger cavity than the smaller cavity. When charge decay rate is faster, the maximum field in the cavity centre, $E_{cav}(t)$ is lower than the case when the charge decay rate is slower.

This results in the electron generation rate due to surface emission, $N_{es}(t)$ (from Equation 3.24) becomes lower, resulting in a longer statistical time lag. Thus, the number of PDs per cycle is lower for the larger cavity than the smaller cavity.

The initial extinction field, E_{ext0} is set according to the minimum charge magnitude for each cavity size. E_{ext0} is found to be lower for the larger cavity than the smaller cavity size. This corresponds to the streamer propagation length across the cavity. Longer streamer propagation lengths are extinguished at lower fields in the cavity [13].

Definition	Symbol	Value	Value	Unit
Cavity diameter	d	1.1	2.35	mm
Material thickness	h_{mat}	3.0	3.0	mm
Initial pressure in the cavity	p_0	101	101	kPa
Initial inception field	E_{inc0}	3.35	2.83	kV·mm^{-1}
Initial extinction field	E_{ext0}	0.31	0.24	kV·mm^{-1}
Effective charge decay time constant	τ_{dec}	2	2	ms
Initial electron generation rate	N_{es0H}	12000	240	s^{-1}
due to surface emission	N_{es0L}	6000	120	s^{-1}
Electron generation rate due to volume ionization	N_{ev}	10	100	s^{-1}
Maximum surface conductivity for charge decay	σ_{smax}	5×10^{-13}	9×10^{-9}	Sm^{-1}

TABLE 8.3: Definition of parameters used in the simulation (S1 and S2) for different spherical cavity diameters

8.1.3 Inception field as a function of cavity size

The initial inception field, E_{inc0}, is set according to the measured inception voltage, U_{incapp} from the experiment. The measured U_{incapp} for the smaller cavity is around 7.5 kV, which yields in E_{inc0} equals to 3.35 kV·mm^{-1} from the simulation while U_{incapp} for the larger cavity is around 7 kV, where E_{inc0} is found to be equal to 2.83 kV·mm^{-1} [123]. The initial pressure, p_0 in both cavity sizes has has been assumed to be around 101 kPa. The inception field in a cavity is determined by its size, which is explained as follows.

Figure 8.2 shows simulation of electric field magnitude in the cavity centre as a function of cavity diameter in the middle of a material of 3.0 mm thickness at 50 Hz, 18 kV applied voltage. The electric field is cavity size-independent because the ratio between the axial and radial dimension of the cavity is the same for any diameter. Thus the field enhancement factor in a spherical cavity is size-independent [11]. However, when the cavity diameter is larger than 1.5 mm, there is a slight decrease in the electric field magnitude in the cavity because the field is influenced by the electrode.

Since the electric field in the cavity is size-independent when the cavity diameter is smaller than 1.5 mm, the measured inception voltage, U_{incapp} (or the applied inception

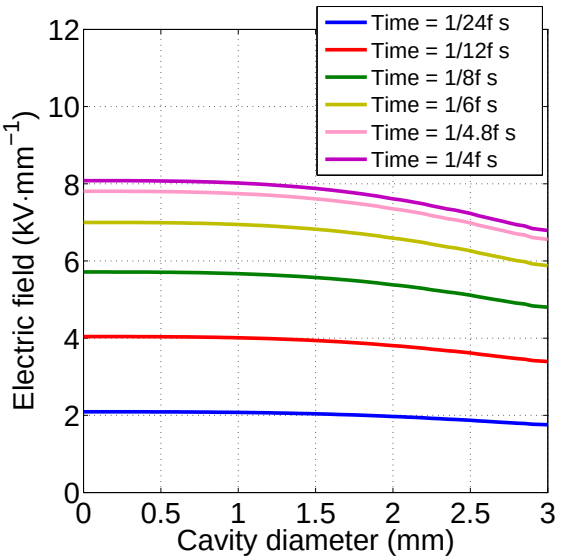

FIGURE 8.2: Simulation of electric field magnitude as a function of spherical cavity diameter (f = 50 Hz, 18 kV).

voltage) U_{incapp} is only dependent on the inception field, E_{inc}. Using Equation 2.5 in Section 2.6.4 to calculate E_{inc}, it is found that E_{inc} decreases with increasing cavity diameter. Therefore, a lower U_{incapp} is required for the larger cavity diameter to reach the inception field, as shown in Figure 8.3. When the cavity diameter is smaller than 0.1 mm, the inception field could not be exceeded by the maximum applied voltage amplitude.

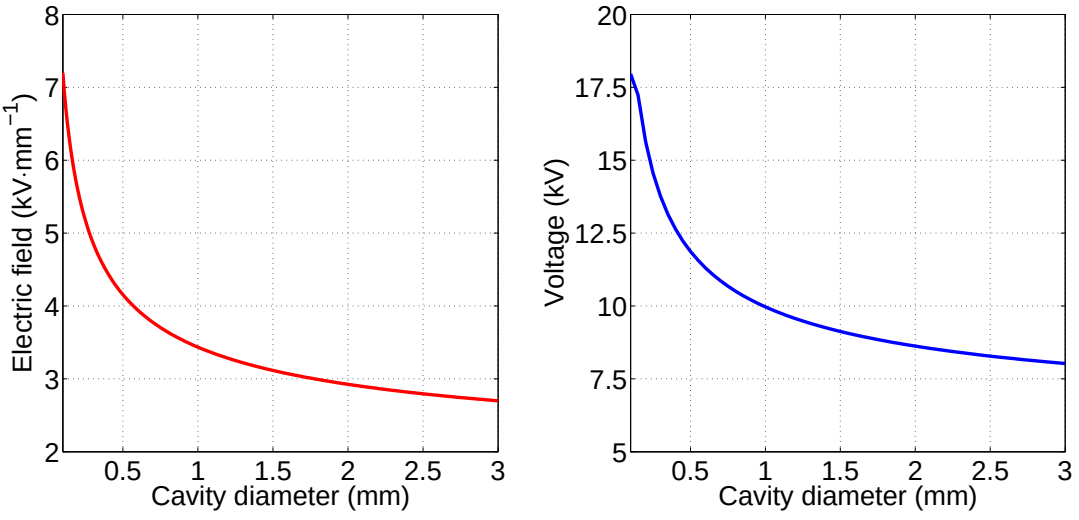

(a) E_{inc} (b) U_{incapp}

FIGURE 8.3: Simulation of E_{inc} and U_{incapp} as a function of spherical cavity diameter.

8.1.4 Simulation of PD charge magnitude

From the FEA simulation of maximum PD real charge, q_{max} and apparent charge magnitude, q'_{max} as a function of spherical cavity size, both q_{max} and q'_{max} increase with increasing spherical cavity, as shown in Figure 8.4 [122]. The PD real charge is the charge that has accumulated along the cavity wall due to PD events while the apparent charge is the charge induced on the electrode as a result of a PD event. From this curve, it has been found that the simulation data in Table 8.1 agrees with the measurement results. If the curve of q'_{max} and q_{max} in Figure 8.4 are extrapolated until the cavity diameter equals to 3 mm, which is the thickness of the material, the apparent charge magnitude will be nearly equal to the real charge magnitude. This is due to when the cavity diameter is larger, the discharge source becomes nearer to the electrode. Thus, the apparent charge magnitude detected on the electrode is nearly equal to the charge magnitude that has accumulated in the cavity.

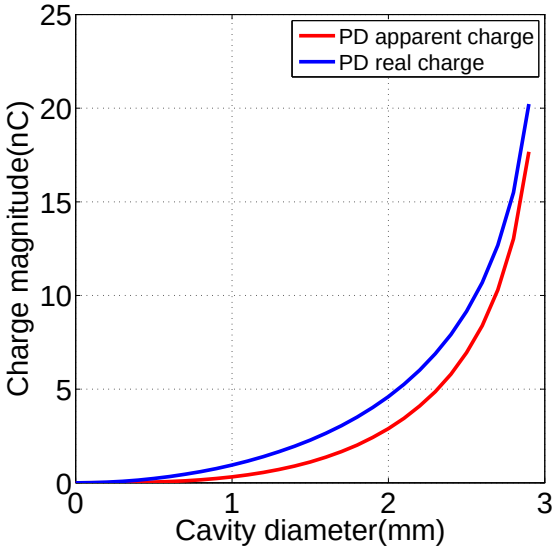

FIGURE 8.4: Simulation of maximum PD real and apparent charge magnitude as a function of spherical cavity diameter (50 Hz, 18 kV).

8.1.5 Simulation for 10 applied voltage cycles

Figure 8.5 and Figure 8.6 show simulation of electric fields, inception field, E_{inc}, PD real charge magnitude and temperature in the cavity, T_{cav} against time for two different spherical cavity diameters over the first 10 cycles. From these figures, assuming the temperature decays exponentially, the average temperature decay time constant, τ_{Tdecay} for the larger cavity is 5.5 ms while the smaller cavity is 1.1 ms. For a smaller cavity size, τ_{Tdecay} is lower because heat can dissipate faster through the surrounding material, resulting in faster temperature decay in the cavity. Referring to Figure 8.6(b), due to higher τ_{Tdecay} and many larger PD charge magnitudes, the temperature in the larger

cavity does not recover to the initial temperature, T_0 between consecutive discharges. Thus, the following PD always occurs at a higher field in the cavity than the initial inception field. However, the temperature in the smaller cavity recovers to T_0 between some consecutive discharges (Figure 8.5(b)). Thus, the temperature change in the cavity has more effect on the occurrence of PD event in a larger cavity.

From the simulation, the average temperature increase per PD event for the larger and smaller cavities are 3K and 1K per PD. Since more PDs with larger charge magnitude occur in the larger cavity, the average temperature rise is also higher. This also corresponds to the higher maximum temperature increase in the larger cavity (11K) than the smaller cavity (6.5K) due to a PD event. The average real charge magnitude of 975 pC causes 1K temperature rise in the larger cavity but for the smaller cavity, only 305 pC charge magnitude increases the cavity temperature by 1K. This means that the temperature rise in the larger cavity is slower than the smaller due to its larger volume.

8.1.6 Simulation of temperature change in the cavity for different cavity sizes

Figure 8.7 shows the simulation of temperature decay time constant, τ_{Tdecay}, as a function of spherical cavity diameter within a dielectric material of thickness 3 mm at 50 Hz, 18 kV applied voltage. Using FEA model, the value for τ_{Tdecay} is calculated by assuming the temperature decays exponentially from 295K to 293K. It seems that the temperature decays slower in a larger cavity size and τ_{Tdecay} increases almost exponentially as a function of spherical cavity diameter.

The simulation of temperature in the middle of various spherical cavity diameters decaying after a PD event is shown in Figure 8.8. It can be seen that for larger spherical cavity diameters, the initial delay of the temperature in the cavity to start decaying is greater. This is due to slower heat dissipation to the surrounding material in larger cavity volumes. This is another factor why the temperature change due to a PD in a larger cavity has a bigger impact on the next PD event.

In order to observe any improvement in the simulation results with the inclusion of temperature change in the cavity due to PD events (S2) in the model, the results is compared with the simulation when the temperature change in the cavity is neglected (S1). A lower least mean square error (MSE) of PD phase and charge magnitude distributions between the measurement and simulation results indicates that the simulation results are better. From Table 8.4, the least MSE of PD phase and charge magnitude distributions between the measurement and simulation results for S2 are slightly lower than S1. Thus, this indicates that the simulation results are better when the temperature change in the cavity due to PD events is considered in the model compared to the model that does not include the temperature change in the cavity.

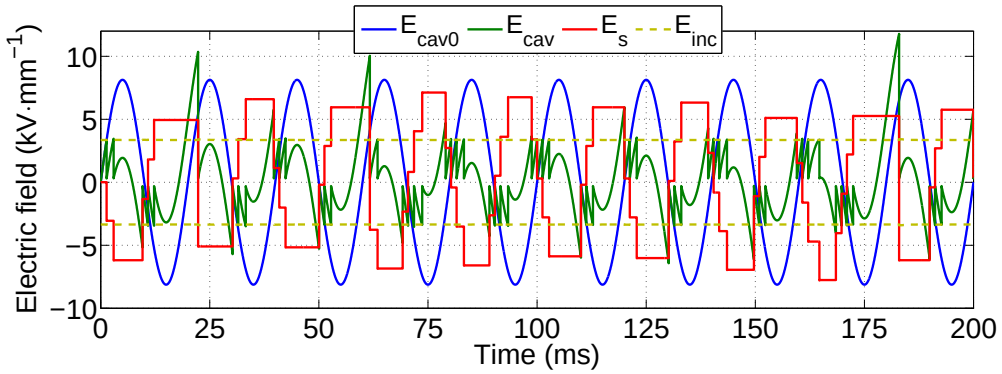

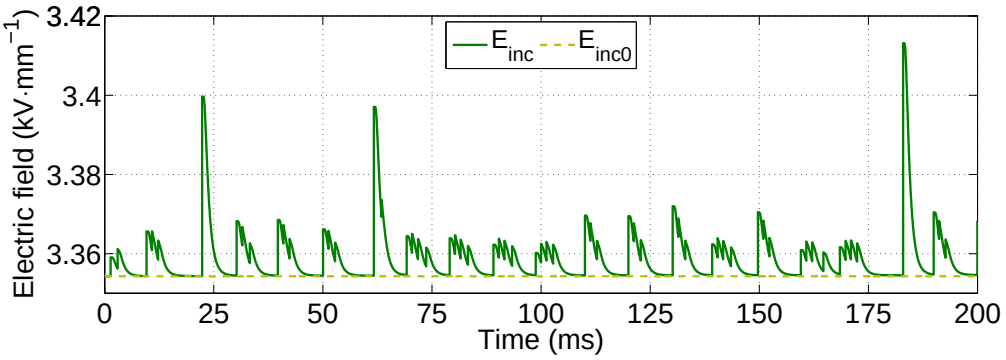

(a) Electric fields and inception field

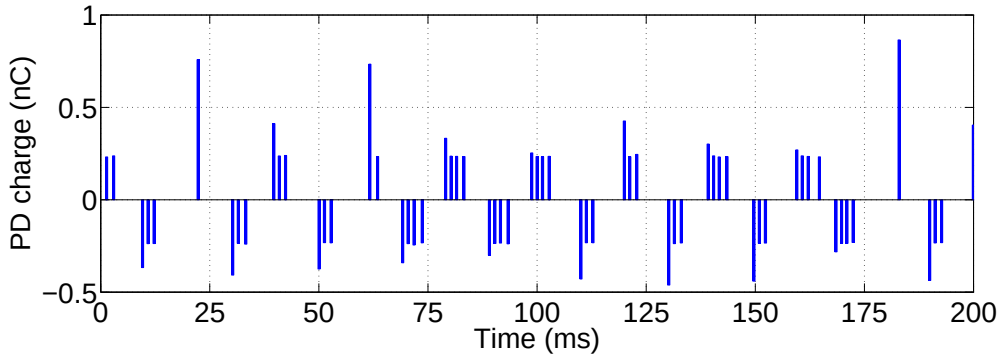

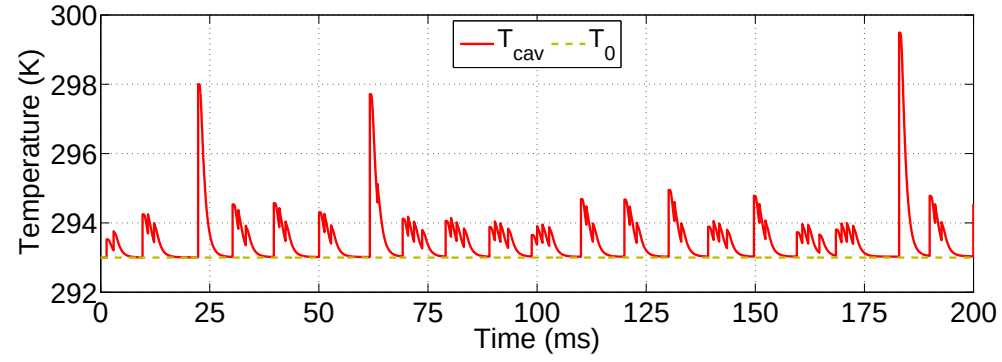

(b) PD real charge magnitude and temperature

FIGURE 8.5: Simulation of electric fields, inception field, PD real charge magnitude and temperature in the cavity, T_{cav} against time for 1.1 mm cavity diameter (50 Hz, 18 kV).

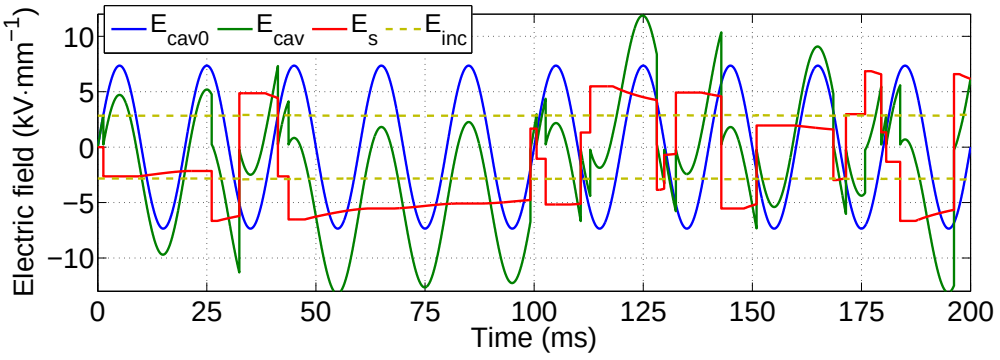

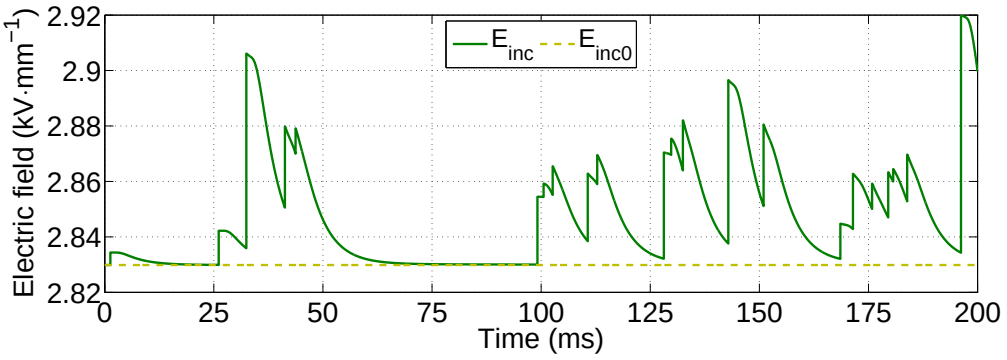

(a) Electric fields and inception field

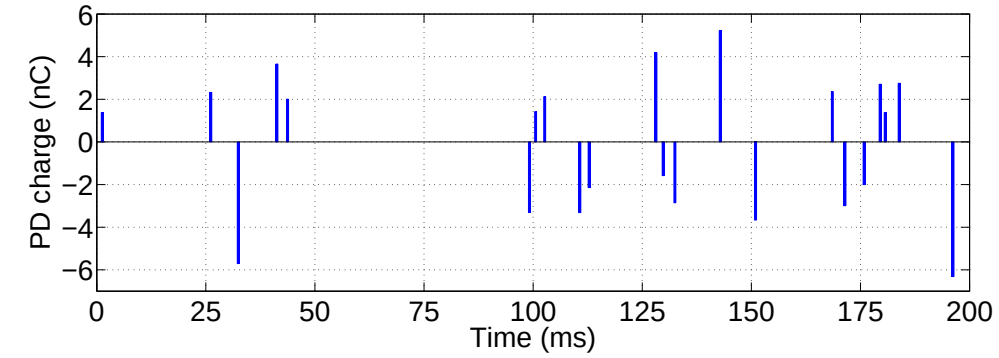

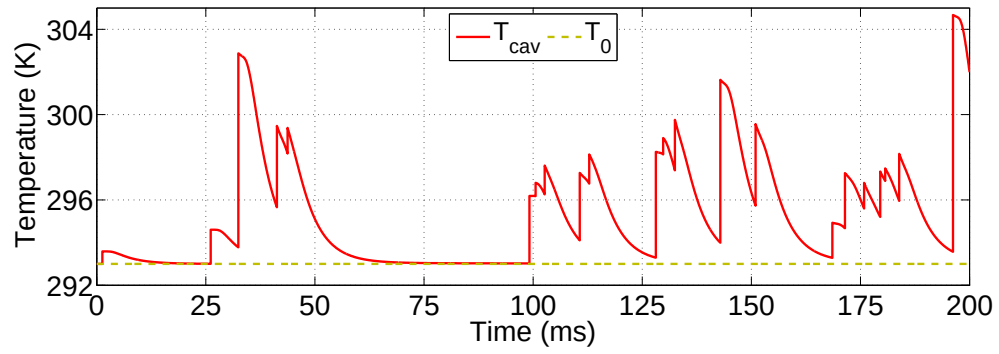

(b) PD charge magnitude and temperature

FIGURE 8.6: Simulation of electric fields, inception field, PD charge magnitude and temperature in the cavity, T_{cav} against time for 2.35 mm cavity diameter (50 Hz, 18 kV).

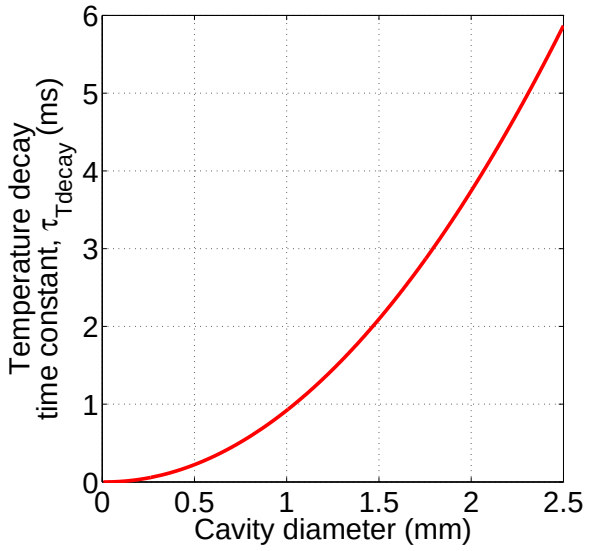

FIGURE 8.7: Simulation of temperature decay time constant as a function of spherical cavity diameter.

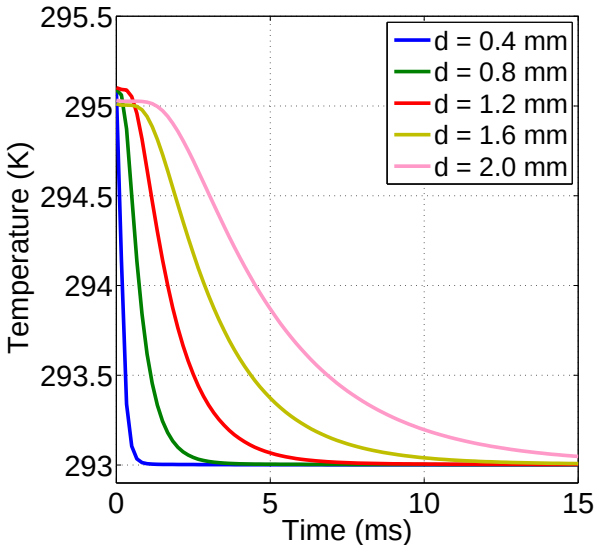

FIGURE 8.8: Simulation of temperature in the cavity after a PD event of different cavity diameters.

Cavity diameter (mm)	**1.1**		**2.35**	
PD distribution	**Phase**	**Charge magnitude ($\times 10^{-18}$)**	**Phase**	**Charge magnitude ($\times 10^{-18}$)**
Least MSE for S1	39.1167	0.1711	8.6111	26.5020
Least MSE for S2	33.6389	0.1661	7.1972	26.3895
Difference between S1 and S2	5.4778	0.0051	1.4139	0.1125
Reduction in S2 from S1 (%)	14.0037	2.9627	16.4195	0.4245

TABLE 8.4: Least MSE of two simulation model for different cavity diameters

8.2 Effect of temperature of the material on PD activity

8.2.1 Comparison of PD patterns

Figure 8.9 shows the ϕ-q-n plots of the measurement and simulation results of PD activity within a spherical cavity of diameter 1.7 mm in a dielectric material of thickness 2.5 mm with a 50 Hz, 20 kV applied voltage as a function of temperature of the material for 250 cycles. The simulation patterns shown here is only for the simulation when the temperature change in the cavity is considered because the simulation patterns by neglecting it are almost similar. At increasing temperature, the 'rabbit-ear' like curves on the charge magnitude-phase axes end at an earlier point on the phase and the end of the curve is sharper while the density of PDs near the minimum charge magnitude increases. At higher temperatures, the electron generation rate is enhanced, resulting in a shorter statistical time lag, resulting in more PDs occuring with lower charge magnitude but less PDs with a higher charge magnitude.

Temperature (°C)	**20**	**35**	**50**	**65**
Measured inception voltage, U_{incapp} (kV)	7.0	7.3	7.6	7.9
Total PDs per cycle	6.5	8.5	10.6	12.4
Total charge per cycle (pC)	3672	5163	5580	6913
Mean charge (pC)	561	610	524	557
Maximum charge magnitude (pC)	2257	1848	1189	1241
Minimum charge magnitude (pC)	400	425	425	438

TABLE 8.5: Measurement results for different temperatures of the material

Temperature (°C)	**20**	**35**	**50**	**65**
Total PDs per cycle	6.5	8.6	10.6	12.3
Total charge per cycle (pC)	4430	4598	4874	5640
Mean charge (pC)	679	532	460	460
Maximum charge magnitude (pC)	2443	1968	1045	931
Minimum charge magnitude (pC)	400	425	425	439

TABLE 8.6: Simulation results for different temperatures of the material when the temperature change in the cavity is neglected

Temperature (°C)	**20**	**35**	**50**	**65**
Total PDs per cycle	6.5	8.6	10.6	12.4
Total charge per cycle (pC)	4341	4543	4878	5717
Mean charge (pC)	663	528	460	462
Maximum charge magnitude (pC)	2375	1838	907	887
Minimum charge magnitude (pC)	400	425	425	438

TABLE 8.7: Simulation results for different temperatures of the material when the temperature change in the cavity is considered

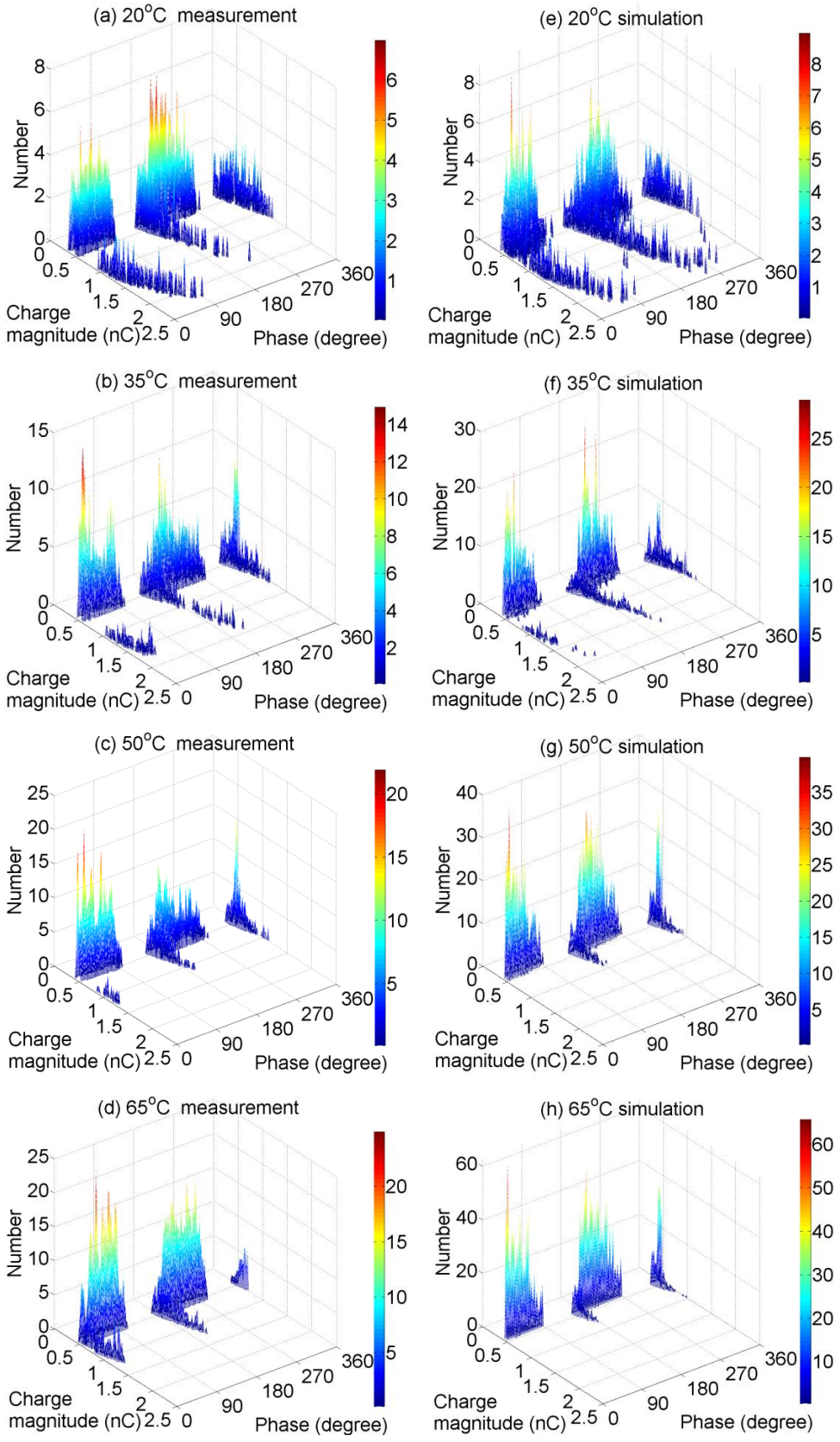

FIGURE 8.9: ϕ-q-n plots of the measurement and simulation results for different material temperatures (Simulation when the temperature change in the cavity is considered).

Table 8.5 to Table 8.7 show the comparison between the measurement and simulation results for different temperatures of the material. From this table, the simulated number of PDs per cycle, the mean, maximum and minimum PD charge magnitudes are within reasonable range of the measurement results for each temperature. However, some simulation and measurement of total charge per cycle are in less agreement with each other. The simulated ϕ-q-n plots are in general agreement compared to the measurement results, except for the temperature 65°C, where there is a higher density of PDs near the minimum charge magnitude in the simulation than seen in the measurement pattern.

8.2.2 Parameter values for the simulation

The definition of parameters used for the simulation is detailed in Table 8.8 and simulation of model parameters as a function of temperature is shown in Figure 8.10. The permittivity of the material, ε_{rmat} obtained from the measurement is used in the simulation. When the temperature increases, the transition of a dielectric from a glassy to a rubber state is enhanced. Thus, the mobility of the polymer structure increases and dipole self-organization is facilitated, resulting in the increase of the material permittivity [50, 101].

In Table 8.8, the measured inception voltage, U_{incapp} increases with the temperature, resulting in higher initial cavity inception field, E_{inc0}. It is known that the inception field depends on the pressure in the cavity. Thus, the initial pressure, p_0 in the cavity may have increased with the temperature. The initial extinction field, E_{ext0} increases with the temperature because a higher cavity pressure may cause a PD to extinguish at a higher field in the cavity [13]. Referring to Figure 8.10(a), E_{inc0} can be expressed in term of material temperature, T (in unit K) using

$$E_{inc0} = 0.01084T + 0.3544 \ [\text{kV·mm}^{-1}] \tag{8.1}$$

The maximum cavity surface conductivity, σ_{smax} from the simulation increases with temperature. This corresponds to a faster movement of free charges on the cavity surface at higher temperatures, resulting in faster charge decay rate [86, 87]. σ_{smax} is not determined using the maximum PD charge magnitude because the measured maximum charge magnitude does not reach the maximum value at 90 and 270 degrees. Thus, σ_{smax} is determined by comparing the curve shape of the 'rabbit-ear' like patterns on the ϕ-q axes of the ϕ-q-n plots between the measurement and simulation because σ_{smax} controls the curve shape of the 'rabbit-ear' like patterns. From the simulation data which is shown in Figure 8.10(b), σ_{smax} can be expressed as a function of temperature using

$$\sigma_{smax} = \alpha \exp(-\beta/T) \ [\text{Sm}^{-1}] \tag{8.2}$$

where α is 0.002504 Sm^{-1} and β is 4372 K.

Parameters related to electron generation rate, which include N_{es0H}, N_{es0L}, N_{ev} and τ_{dec} increase with temperature. They are determined through sensitive analysis method using different combination of N_{es0H}, N_{es0L}, N_{ev} and τ_{dec}, which yields in the lowest mean square error between the measurement and simulation results. The process was started at 20°C to choose the values for N_{es0H}, N_{es0L} and N_{ev} since τ_{dec} has been set as 2 ms at room temperature. However, different combinations of N_{es0H}, N_{es0L}, N_{ev} and τ_{dec} are used for the other temperatures to observe the possibility of changes in those parameters with temperature.

At increasing material temperature, the effective charge decay time constant, τ_{dec} is found to be increased from the simulation [50]. At higher material temperatures, the charge detrapping rate increases due to the thermal detrapping rate constant is higher [124]. Thus, the effective charge decay time constant, τ_{dec} is higher because the amount of charge decay is reduced by higher charge detrapping rate. Higher τ_{dec} causes more PDs per cycle at higher temperature. From Figure Figure 8.10(c), τ_{dec} is estimated as a function of material temperature with

$$\tau_{dec} = 6.52 \times 10^{-6} \exp(0.0427T) \text{ [ms]} \tag{8.3}$$

From sensitivity analysis, it is found that N_{es0H} and N_{es0L} increase with the material temperature. This indicates that the initial electron generation rate from the cavity surface increases with temperature. There may be more charges near the cavity surface detrapped at higher temperatures. Referring to Figure Figure 8.10(d), N_{es0H} and N_{es0L} can be expressed as a function of material temperature, T using

$$\begin{aligned} N_{es0H} &= 0.19T - 54.32 \text{ [ks}^{-1}\text{]} \\ N_{es0L} &= 0.0333T - 8.767 \text{ [ks}^{-1}\text{]} \end{aligned} \tag{8.4}$$

The electron generation due to volume ionization, N_{ev}, is larger at higher temperature. Since higher material temperature increases the pressure in the cavity, higher pressure may generate more initial free electron through volume ionization. From Figure 8.10(e), it is possible to estimate N_{ev} as a function of temperature, T using

$$N_{ev} = 0.006667T - 1.853 \text{ [ks}^{-1}\text{]} \tag{8.5}$$

The temperature decay time constant, τ_{Tdecay} in the cavity depends on the initial temperature of the material since the cavity temperature is influence by the material temperature. Figure 8.11 shows temperature decay time constant, τ_{Tdecay} as a function of

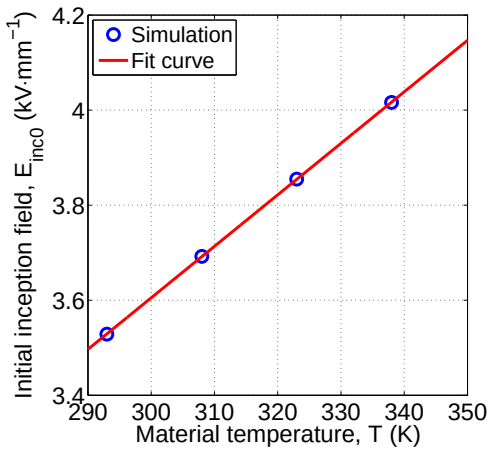

(a) Initial inception field, E_{inc0}

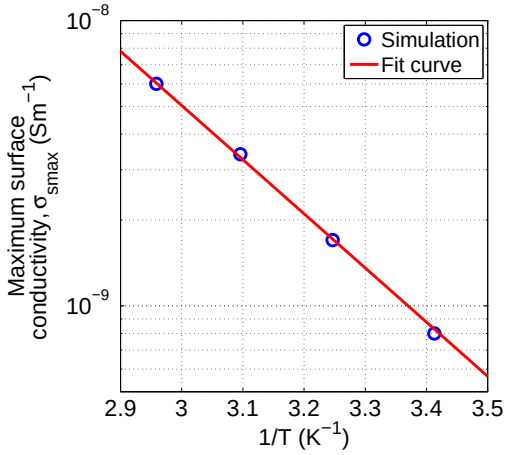

(b) Maximum cavity surface conductivity, σ_{smax}

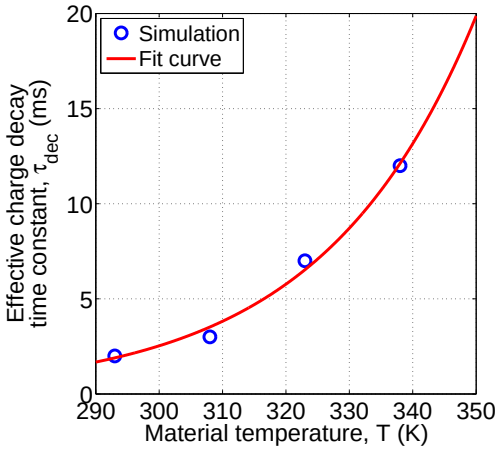

(c) Effective charge decay time constant, τ_{dec}

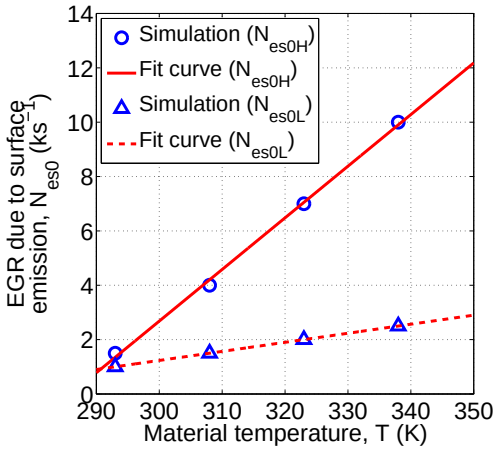

(d) Initial EGR due to surface emission, N_{es0H} and N_{es0L}

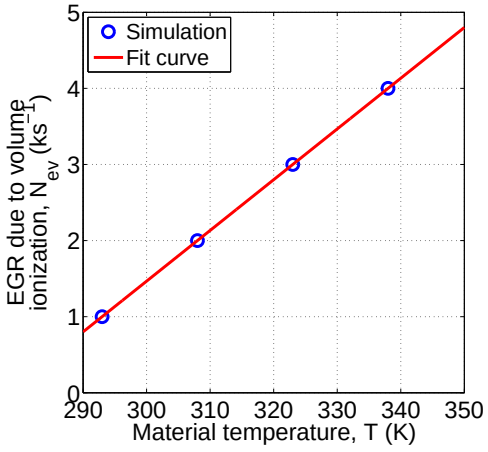

(e) EGR due to volume ionizaiton, N_{ev}

FIGURE 8.10: Simulation of model parameters as a function of temperature.

initial material temperature. Assuming the temperature in the cavity decays exponentially, τ_{Tdecay} is found to decrease at higher initial material temperature. This is due to the faster movement of hot gas towards the cooler surrounding material when the initial

Definition	Symbol	Value	Unit
Cavity diameter	d	1.7	mm
Material thickness	h_{mat}	2.5	mm
Applied voltage	U_{app}	20	kV
Temperature of the material	T_{mat}	20, 35, 50, 65	°C
Permittivity of the material	ε_{rmat}	$4.4_{(20)}$, $4.5_{(35)}$, $4.9_{(50)}$, $6.0_{(65)}$	$1_{(°C)}$
Initial pressure in the cavity	p_0	101	kPa
Initial inception field	E_{inc0}	0.01084T+0.3544	kV·mm^{-1}
Initial extinction field	E_{ext0}	$0.75_{(20)}$, $0.79_{(35)}$, $1.2_{(50)}$, $1.8_{(65)}$	kV·mm$^{-1}{}_{(°C)}$
Effective charge decay time constant	τ_{dec}	6.52×10^{-6} exp $(0.0427T)$	ms
Initial electron generation rate due to surface emission	N_{es0H}	$0.19T-54.32$	ks^{-1}
	N_{es0L}	$0.0333T-8.767$	ks^{-1}
Electron generation rate due to volume ionization	N_{ev}	$0.006667T-1.853$	ks^{-1}
Maximum surface conductivity for charge decay	σ_{smax}	$0.002504\exp(-4372/T)$	Sm^{-1}

*$T = (T_{mat} + 273)$ K

TABLE 8.8: Definition of parameters used in the simulation for different temperature

temperature is higher.

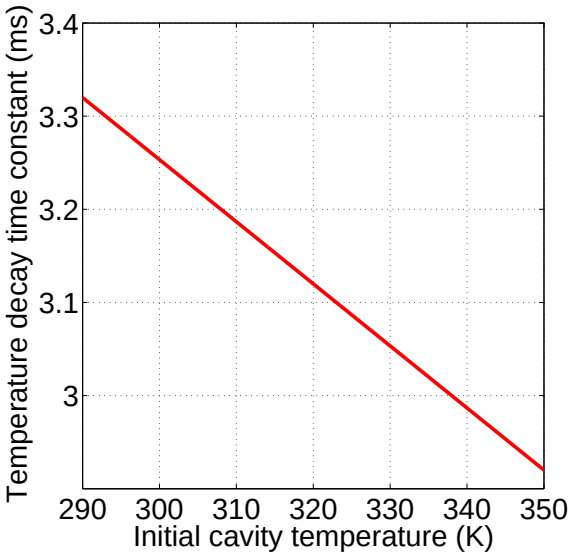

FIGURE 8.11: Simulation of temperature decay time constant as a function of initial temperature of the material.

8.2.3 Simulation for 10 applied voltage cycles

The simulation of electric fields, inception field, PD charge magnitude and temperature in the cavity against time for two different temperatures of the material are shown in

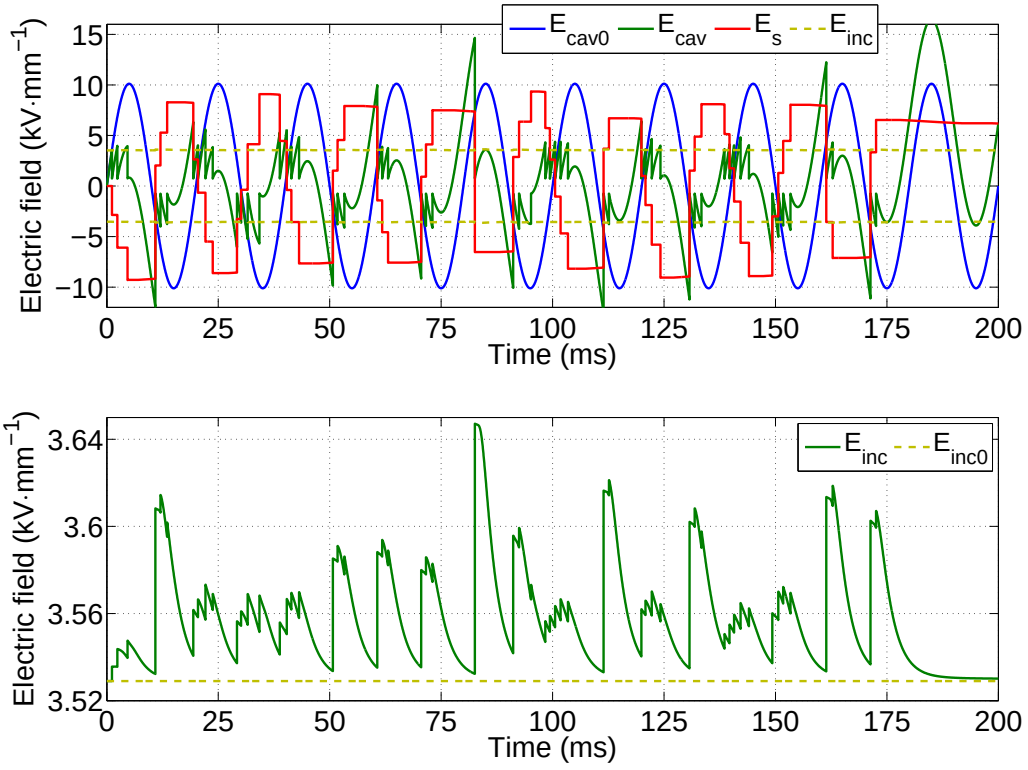

(a) Electric fields and inception field

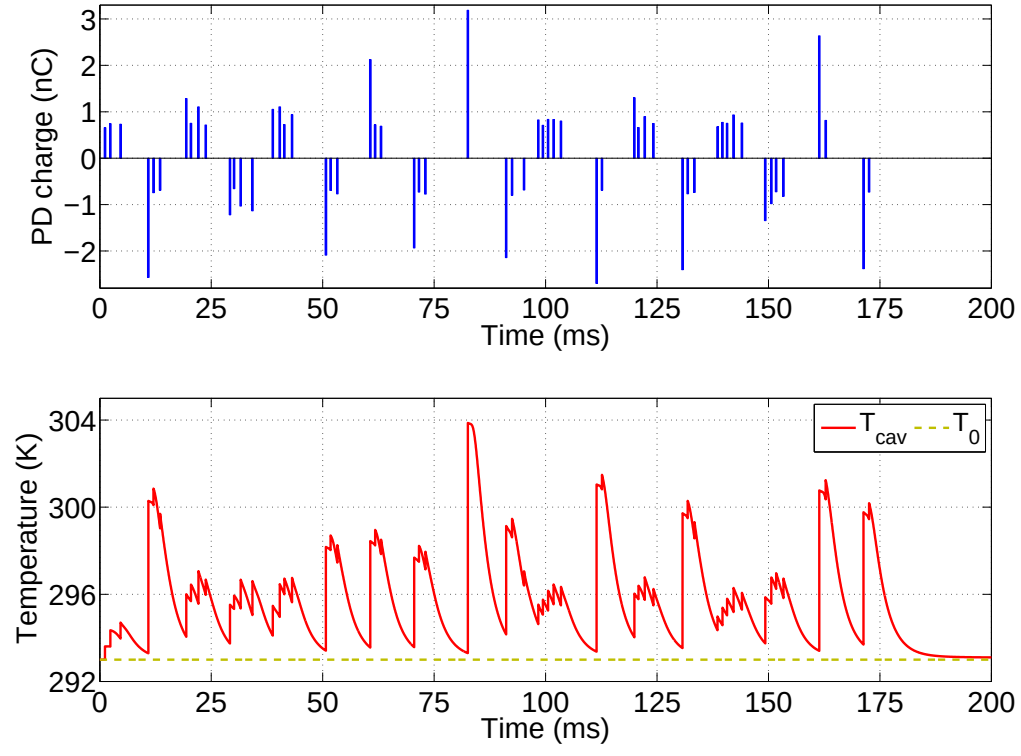

(b) PD charge magnitude and temperature

FIGURE 8.12: Simulation of electric fields, inception field, PD charge magnitude and temperature in the cavity against time for material temperature of 20°C.

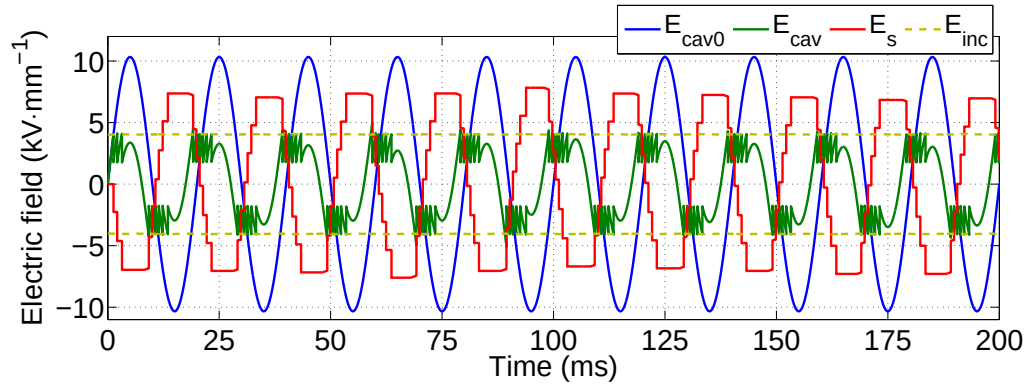

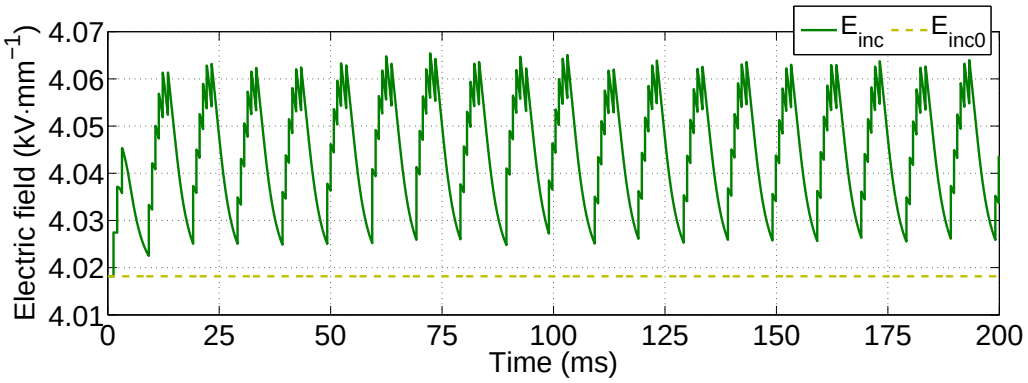

(a) Electric fields and inception field

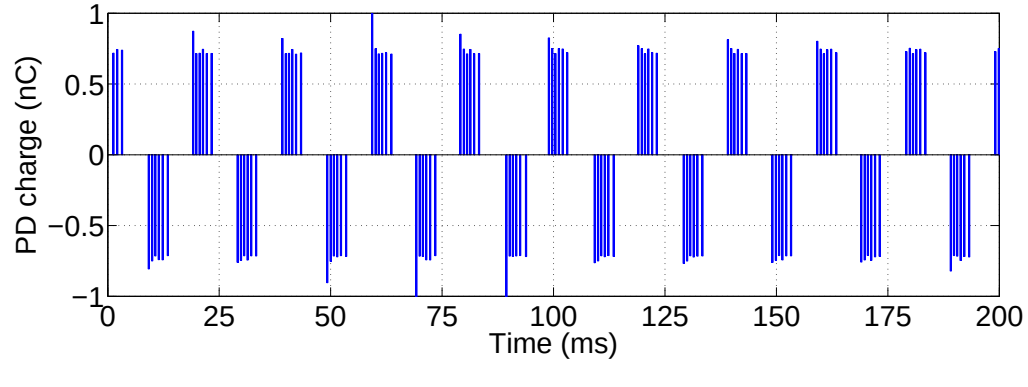

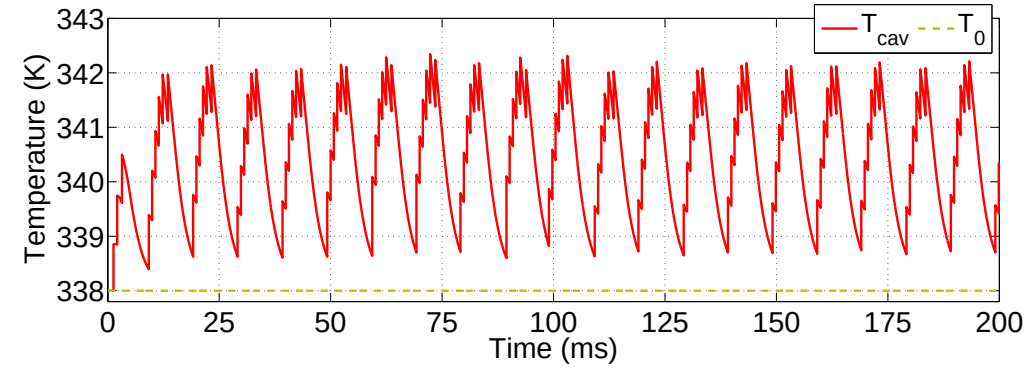

(b) PD charge magnitude and temperature

FIGURE 8.13: Simulation of electric fields, inception field, PD charge magnitude and temperature in the cavity against time for material temperature of 65°C.

Figure 8.12 and Figure 8.13. The applied voltage is 50 Hz, 20 kV ac sinusoidal. Using Figure 8.11, τ_{Tdecay} in the cavity is 3.3 ms when the initial temperature of the material is 20°C while for 65°C, τ_{Tdecay} is 3.0 ms. Although the temperature in the cavity, T_{cav} decays faster at 65°C than 20°C, the temperature does not recover to the initial value, T_0 between consecutive PDs due to higher PD repetition rate, by referring to Figure 8.13(b). However, the average temperature rise per PD at 20°C is larger than at 65°C because there are more PDs with higher charge magnitude at 20°C. A PD with a larger charge magnitude that causes a higher temperature rise in the cavity, increasing the inception field for the next PD. Therefore, the temperature change in the cavity may have more effect on the sequence of PDs at material temperature of 20°C than at higher temperatures.

Table 8.9 and Table 8.10 show the least mean square error (MSE) of PD phase and charge magnitude distributions between measurement and simulation results for the model which neglects (S1) and considers (S2) the temperature change in the cavity after a PD event. The least MSEs are lower for the S2 than S1. Therefore, this again suggests that there is little improvement on the simulation results when the temperature change in the cavity due to PD events is considered.

Temperature, T (°C)	**20**	**35**	**50**	**65**
Least MSE for S1	18.4111	22.3639	45.8972	107.3389
Least MSE for S2	15.2333	21.5694	43.975	95.1028
Difference between S1 and S2	3.1778	0.7945	1.9222	12.2361
Reduction in S2 from S1 (%)	17.2602	3.5526	4.1881	11.3995

TABLE 8.9: Least MSE for PD phase distribution between measurement and simulation results for different material temperatures

Temperature, T (°C)	**20**	**35**	**50**	**65**
Least MSE for S1 ($\times 10^{-18}$)	4.3912	3.7623	5.4534	13.7300
Least MSE for S2 ($\times 10^{-18}$)	3.7467	3.4710	5.3316	12.2975
Difference between S1 and S2 ($\times 10^{-18}$)	0.6445	0.2913	0.1219	1.4325
Reduction in S2 from S1 (%)	14.6761	7.7414	2.2344	10.4334

TABLE 8.10: Least MSE for PD charge magnitude distribution between measurement and simulation results for different material temperatures

8.3 Measurement of PD cycle to cycle behaviour

Figure 8.14 and Figure 8.15 show measurement of charge magnitude of PD event against time for the first 60 applied voltage cycles within a spherical cavity of diameter 1.4 mm in a dielectric material of thickness 2 mm for a 50 Hz 14 and 20 kV ac sinusoidal applied voltage. From these plots, it can be seen that after a PD with higher charge magnitude occurs, there is a PD with lower charge magnitude. Those higher PD charge magnitude

appears after a polarity change of the applied voltage from that of the previous PD while PDs with lower charge magnitude occur when there is no polarity change. In some voltage cycles, no PDs occur especially at the lower 14 kV applied voltage. There are less cycles without PD at all for the 20 kV applied voltage because the higher electron generation rate greatly increases the likelihood of PDs occuring in the cavity.

The sequence of PD activity can also be studied by using plots of applied voltage of PD occurrence against time, examples of which are shown in Figure 8.16 and Figure 8.17. From these plots, PDs seem to occur almost randomly in each voltage cycle and there is no systematic shift of the phase of PD occurrences. Although some systematic phase shift of PD events can be observed in certain voltage cycles, the systematic phase shift

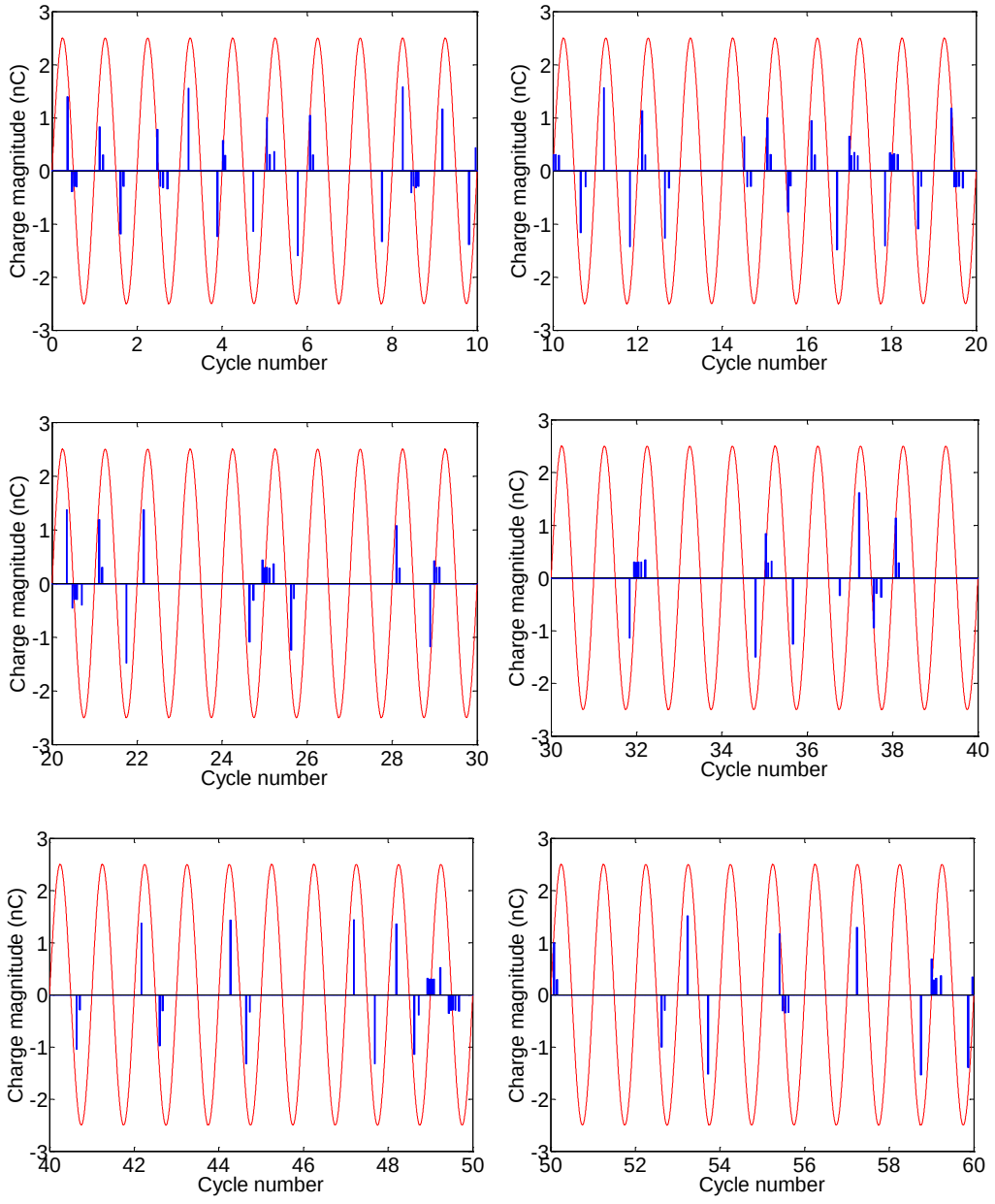

FIGURE 8.14: Measurement of PD charge magnitude against time (50 Hz, 14 kV).

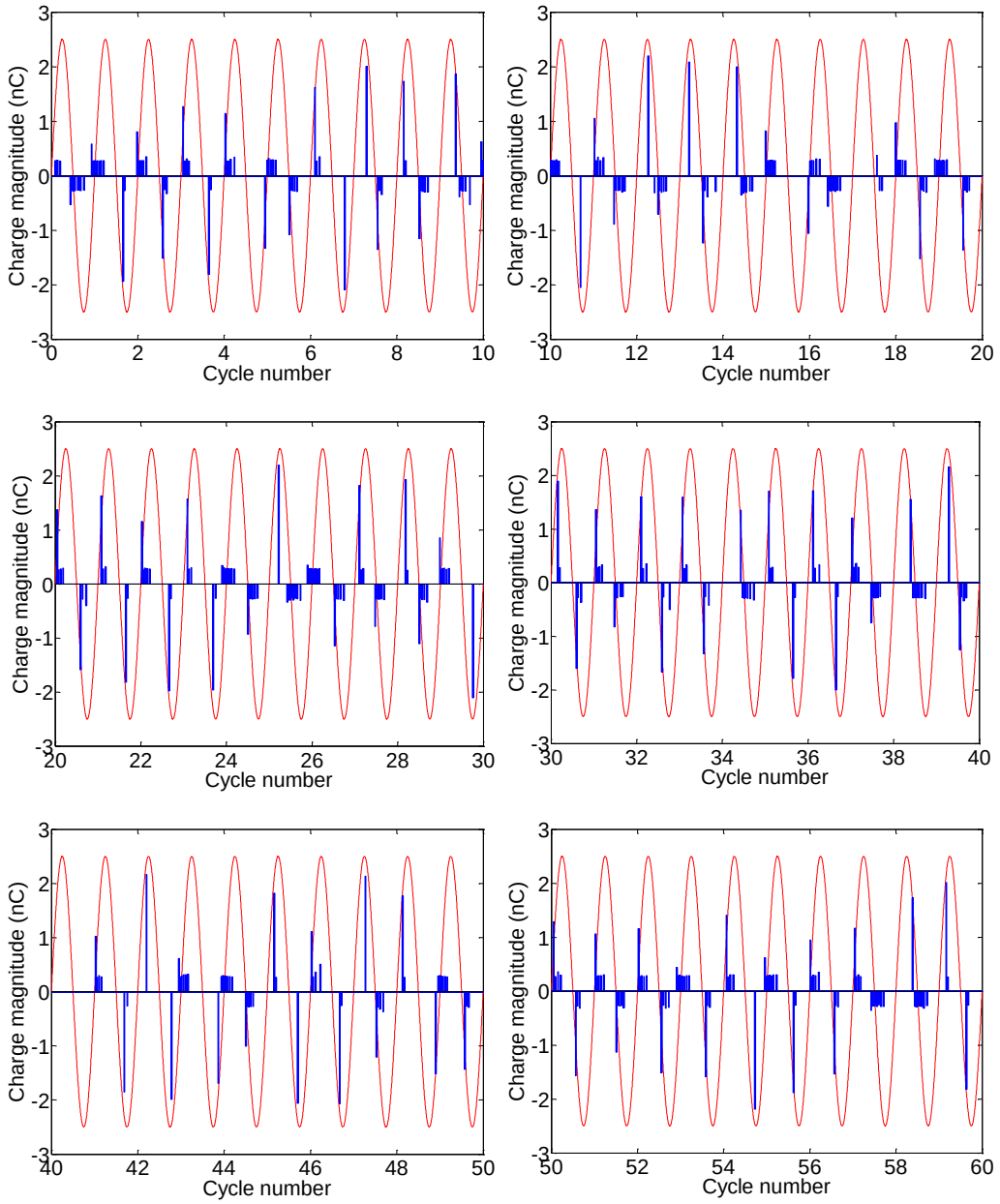

FIGURE 8.15: Measurement of PD charge magnitude against time (50 Hz, 20 kV).

patterns are not continuous. This may be due to variation in initial electron generation rate, inception field level, time delay of getting a free initial electron available or cavity surface properties, such as cavity surface conductivity, detrapping work function and charge trapping in the material, which result in a non-systematic phase shift of PD occurrences.

Referring to the measurement results of PD in a cavity, when no PD occurs at all in certain voltage cycles this may be due to several reasons:

1. The total electron generation rate is too low for PD initiation which may be due to significant surface charge decay over certain voltage cycles. The decay mechanisms

could be charge trapping into deeper traps, the increase in surface conductivity which causes surface charge to decay along the cavity wall, charge recombination and charge neutralization on the cavity surface.

2. There could be no neutral gas molecules available in the cavity to be ionized by initial free electrons to develop an electron avalanche in the cavity. This may happen after a certain number of PD events, where the decrement rate of gas molecule is faster than gas molecule diffusion from outside of the cavity.

3. The electron generation rate due to volume ionization is too low, which may be due to low energy of particles or waves in radiation ionization within in the cavity.

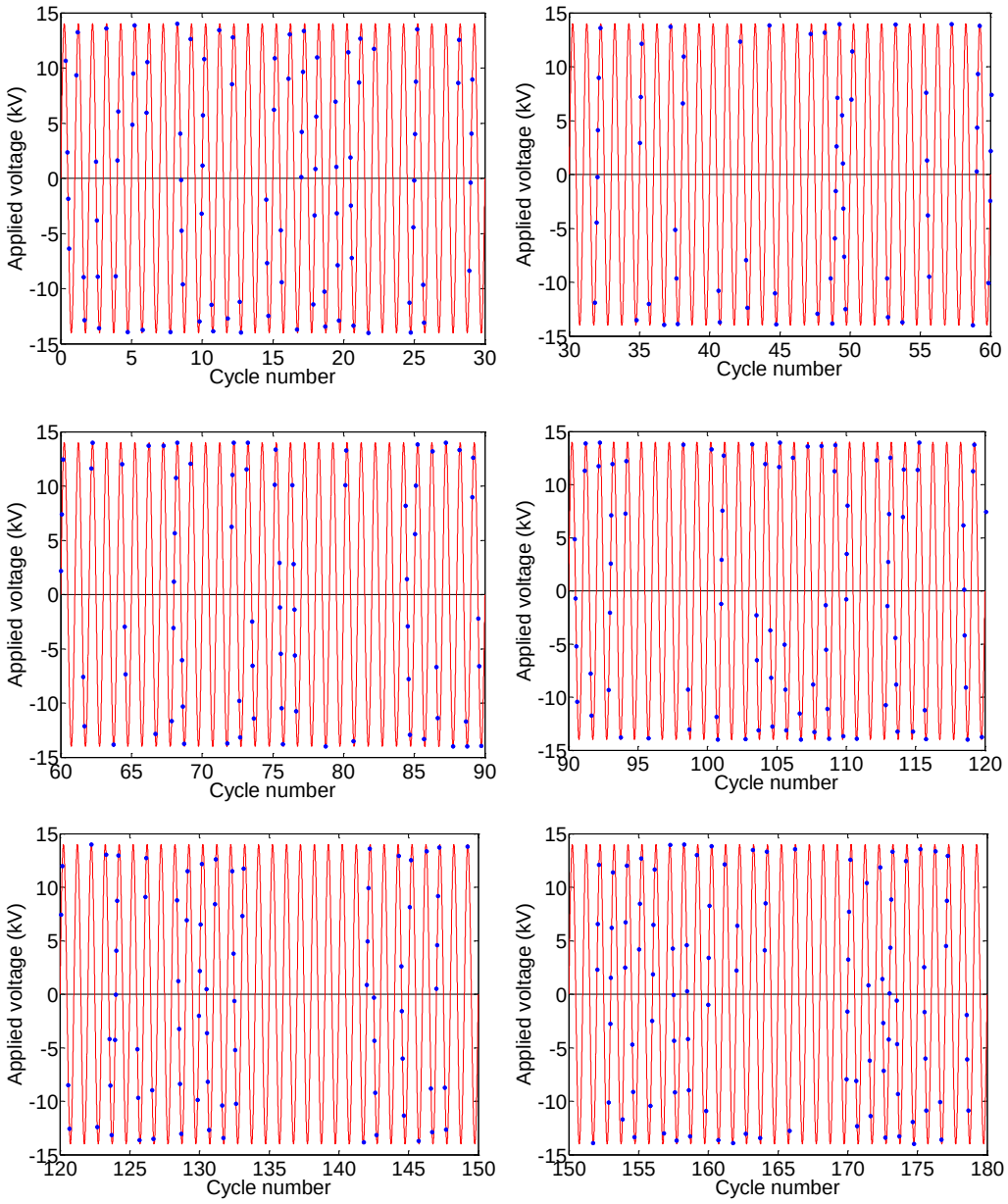

FIGURE 8.16: Measurement of applied voltage of PD event against time (50 Hz, 14 kV).

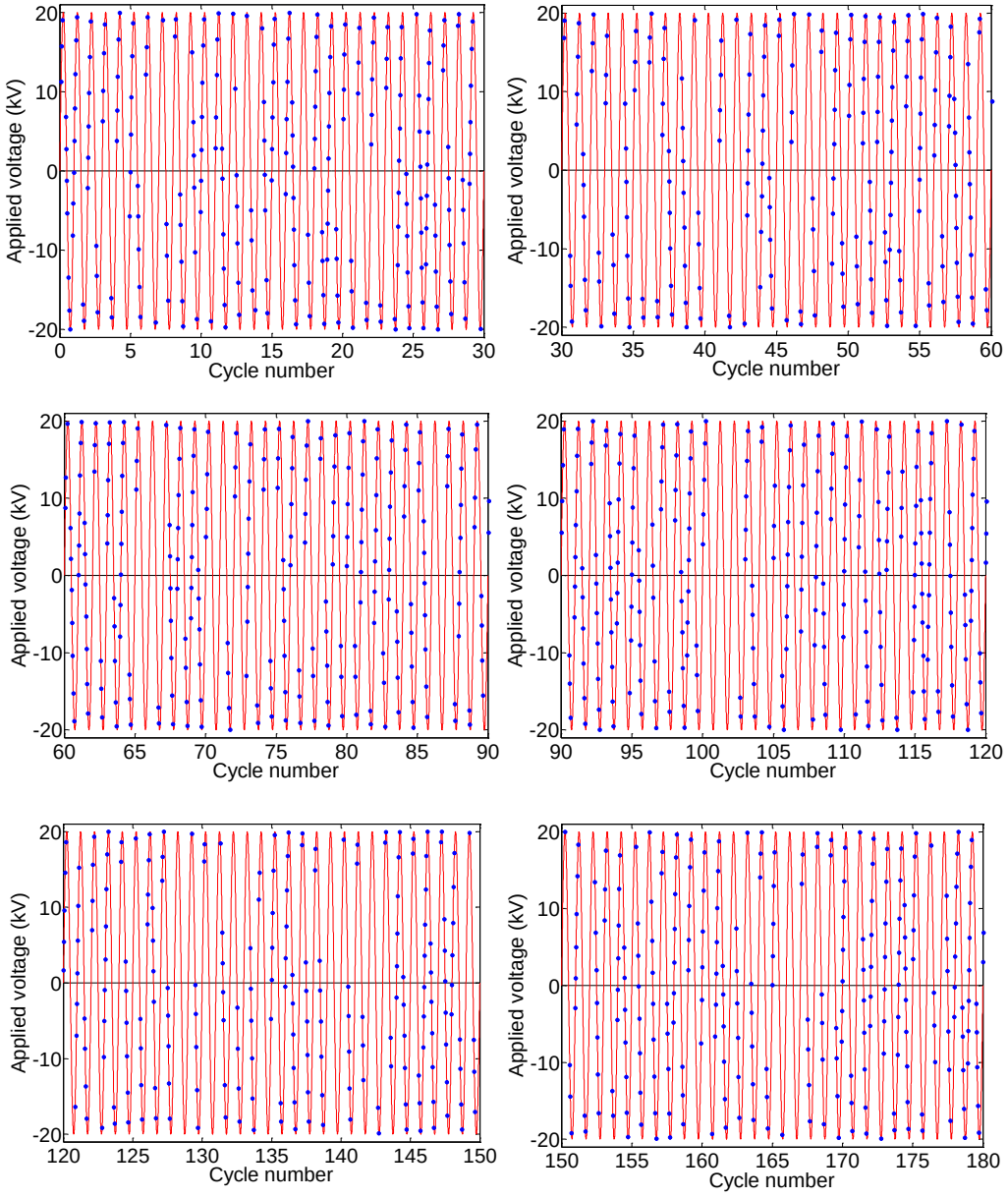

FIGURE 8.17: Measurement of applied voltage of PD events against time (50 Hz, 20 kV).

4. The rise of pressure in the cavity increases the inception field level until it could not be exceeded by the field in the cavity for a PD to occur. This may be due to the formation of gas decompositions after a PD which causes the pressure to increase temporarily before it starts to decrease towards an ambient value.

8.4 Simulation of PD cycle to cycle behaviour

The sequence of PD events against time for 50 Hz, 14 and 20 kV from the simulation is shown in Figure 8.18 to Figure 8.21. In general, the simulation of PD charge magnitude

and applied voltage of PD events against time agrees with the measurement results in Figure 8.14 to Figure 8.17. The matching patterns between the measurement and simulation of PD charge magnitude against time and how they are achieved through simulation are detailed as follows.

A PD with lower charge magnitude occurs immediately after a PD with larger charge magnitude has occurred. From the simulation, the electron generation rate after a larger PD charge magnitude occurrence is high. Thus, the next PD occurs immediately after the inception field is exceeded due to the shorter statistical time lag, resulting in a PD with smaller charge magnitude. Since there is no polarity change of the field in the cavity after a larger PD charge magnitude occurrence when the next PD is likely to

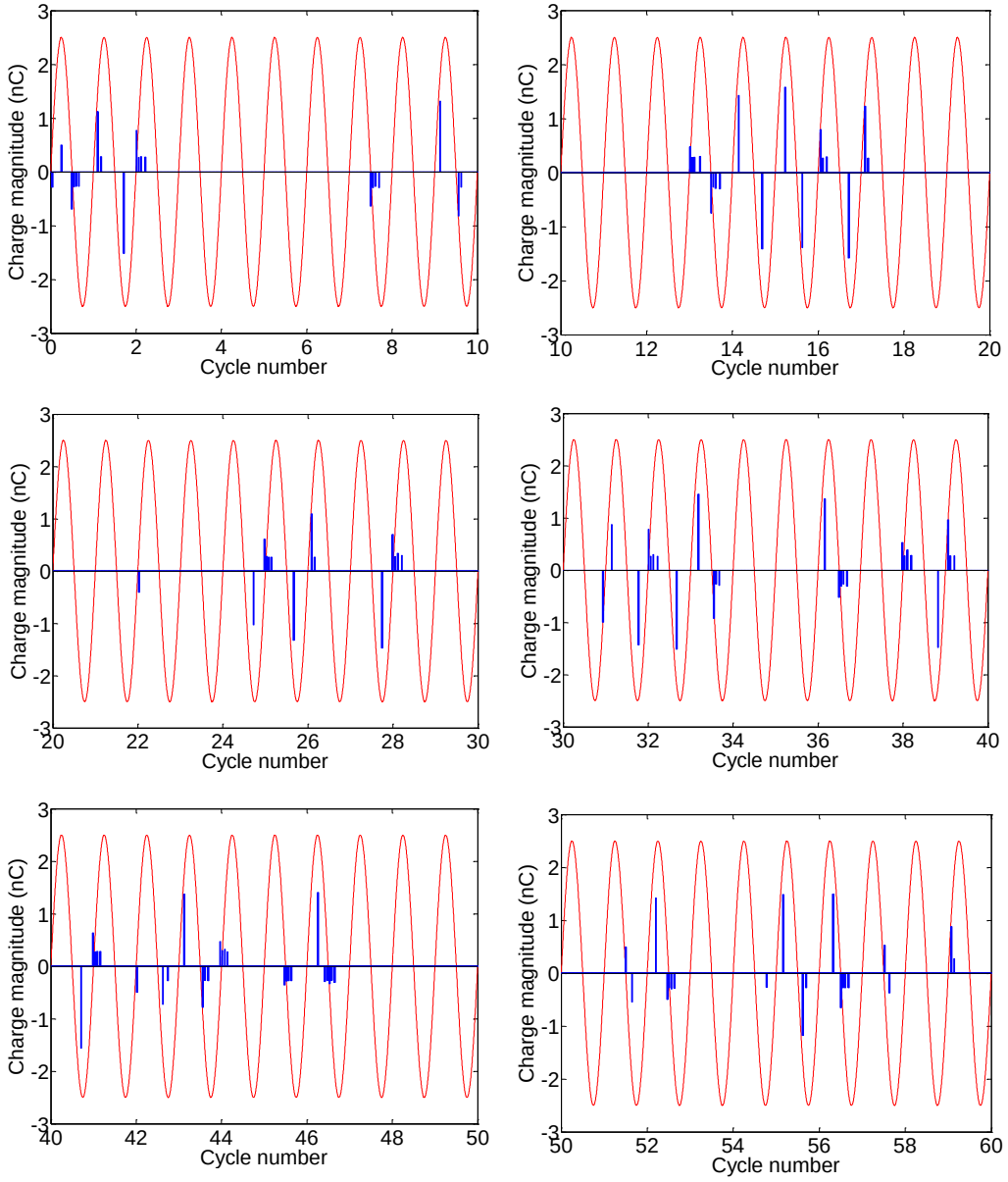

FIGURE 8.18: Simulation of PD charge magnitude against time (50 Hz, 14 kV).

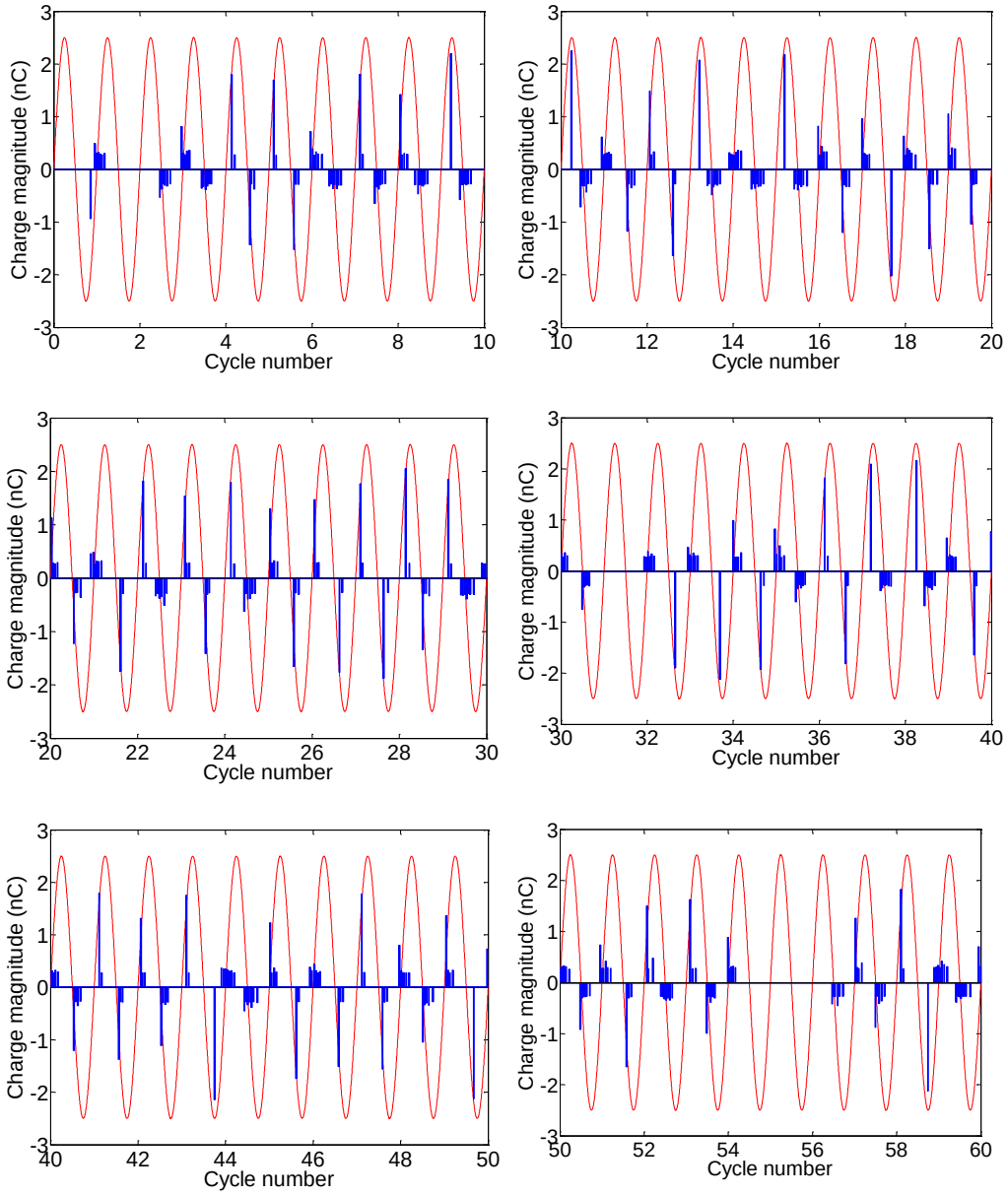

FIGURE 8.19: Simulation of PD charge magnitude against time (50 Hz, 20 kV).

occur, the time interval between consecutive discharges is smaller [125]. Hence, there is less charge decay after a previous PD when the next PD is likely to occur. This yields a higher electron generation rate for the next PD event. As there is no polarity change of the field in the cavity between consecutive discharges, electrons are detrapped from a positively charged cavity surface. Thus, the electron generation rate is higher and this condition is simulated by using a higher value of initial electron generation rate due to surface charge, N_{es0H}.

A PD with higher charge magnitude occurs after the polarity change of the applied voltage occurs, which can be seen in Figure 8.16 and Figure 8.17. In the simulation, a larger PD charge magnitude is obtained after the polarity change of the field in the

cavity between consecutive discharges. When this happens, the field in the cavity is enhanced by the field due to surface charge that has accumulated on the cavity surface from the previous PD. Thus, a PD can occur at higher levels of the field in the cavity. When a PD occurs, the field drop across the cavity is larger, thus resulting in a larger PD charge magnitude.

The statistical time lag between consecutive discharges after a polarity change of the field in the cavity is longer. Since electrons are detrapped from the negative charge cavity surface, the electron generation rate is lower for the next PD occurrence. This condition is simulated by using a lower value of initial electron generation rate due to surface

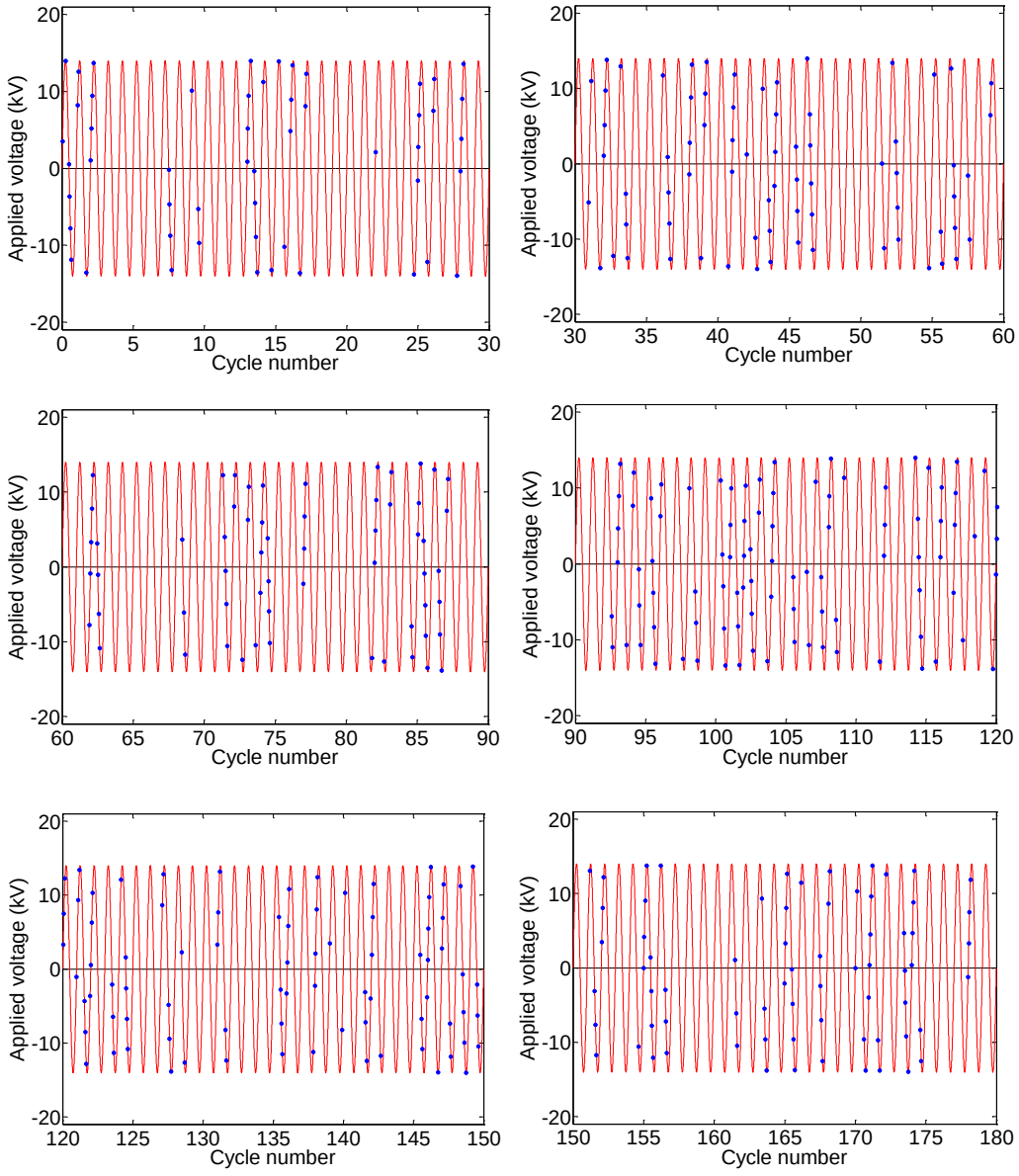

FIGURE 8.20: Simulation of applied voltage of PD events against time over 180 cycles (50 Hz, 14 kV).

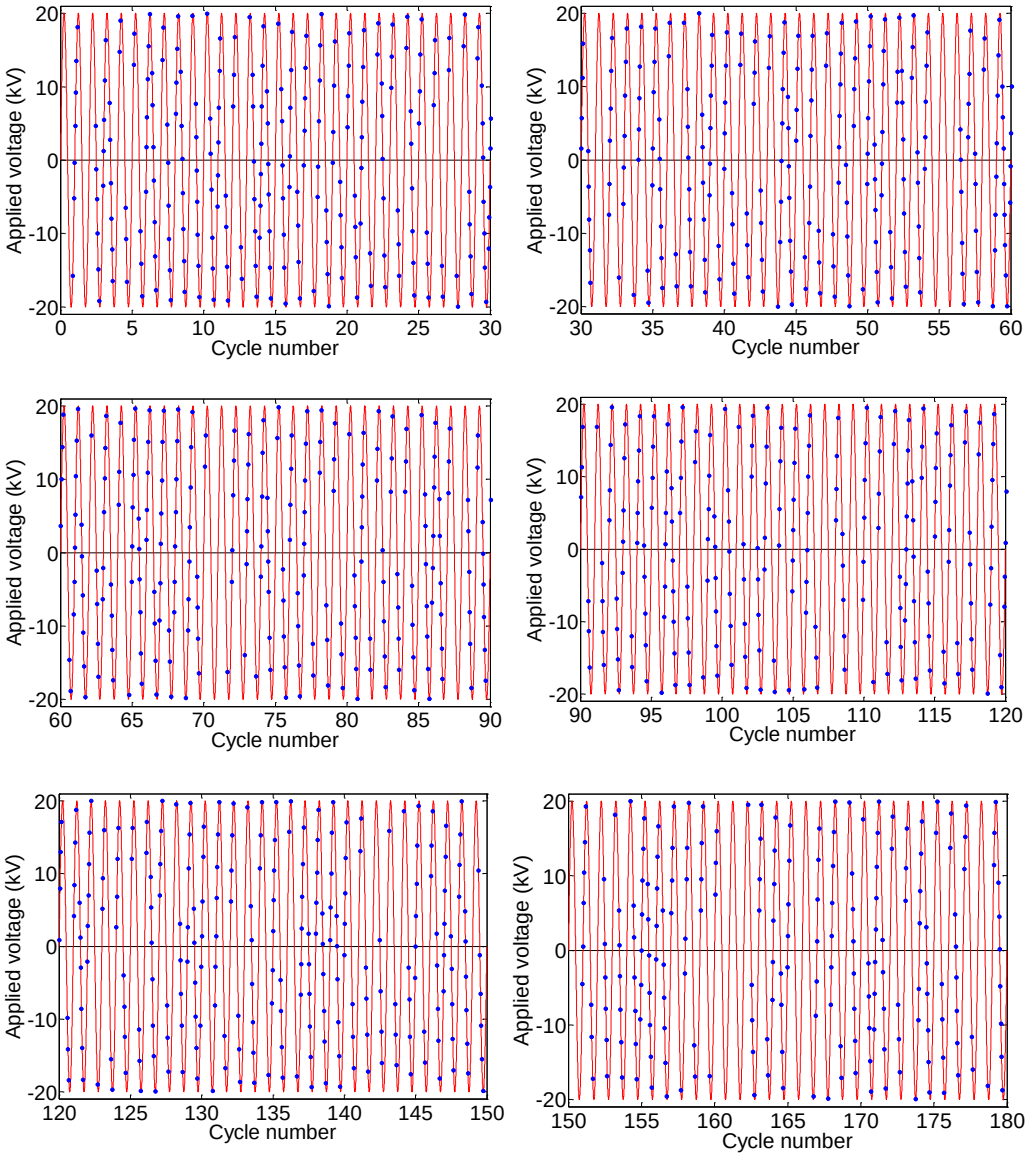

FIGURE 8.21: Simulation of applied voltage of PD event against time over 180 cycles (50 Hz, 20 kV).

charge, N_{es0L} [120]. The surface charge decay effect is also more significant between consecutive discharges because the time interval between two adjacent PDs is longer. Thus, more charges from a previous PD, which act as source of initial free electrons for the next PD, will have decayed through charge trapping when the next PD is likely to occur, reducing the overall electron generation rate. The charge decay rate in the model is controlled by the effective charge decay rate, τ_{dec}. There is the same polarity of the field in the cavity and the field due to surface charge, so the charge also decays through conduction along the cavity wall, causing charge recombination, resulting in a lower electron generation rate. This charge decay rate is controlled by the cavity surface conductivity.

There are variations in PD charge magnitude that occur subsequently after a PD with higher charge magnitude has occurred. It may be due to variation in the inception field level after a PD event. After a PD with higher charge magnitude occurs, heat energy released due to electron ionizations during the PD causes the temperature in the cavity to increase. This results in an increment of the pressure in the cavity, assuming that the cavity volume does not change and the gas in the cavity is an ideal gas. Thus, the inception field increases, resulting in PDs that occur at a field level compared to the field level of the previous PD occurrence.

There are certain voltage cycles where no PD occurs at all in the measurement and simulation. From the simulation, this has been achieved through a combination of probability of PD occurrence equation and a very low electron generation rate, which is due to significant effect of surface charge decay between consecutive discharges. More cycles with no PD at all are observed at 14 kV than at a 20 kV applied voltage in the simulation.

From the studies of cycle to cycle behaviour of PD events, the sequence of PDs can be observed whether it has a random or systematic behaviour of PD phase shift between consecutive discharges or not [40]. The effect of charge accumulation on the cavity surface after each discharge can be clearly observed, which modifies the field in the cavity and controls the sequence of the following PD occurrence [42].

8.5 Summary

From comparison of measurement and simulation results, they are in good agreement. Thus, PD behaviour for different cavity sizes and temperatures of the material can be summarized. The number of PDs per cycle is higher for the smaller cavity than the larger cavity. From the simulation, it has been found that the electron generation rate due to surface emission is higher for the smaller cavity, probably due to higher trapped charge density after a PD occurs. However, the electron generation rate due to volume ionization for the smaller cavity is lower due to its smaller volume. Surface charge decay through conduction along the cavity wall is more significant for the larger cavity than the smaller cavity due to higher density of free charge accummulation on the cavity surface after a PD occurs. The effect of temperature change in the cavity after a PD occurs on the sequence of PD events is higher for the larger cavity. It is due to the temperature decay time constant is higher and there are many PDs occur with large charge magnitude, resulting in a higher average temperature increase in the larger cavity than the smaller cavity.

At increasing temperature of the material, the number of PDs per cycle is higher because of an enhanced electron generation rate due to surface emission and volume ionization.

The initial cavity inception field increases with material temperature because the pressure in the cavity is higher. The permittivity of the material is larger at higher material temperature due to the transition of the material from glassy to rubbery state enhancing dipole orientation. The effective charge decay time constant increases with material temperature because charge detrapping rate is higher. Charge movement along the cavity wall through surface conduction is faster at higher material temperatures, where the cavity surface conductivity increases with material temperature. The temperature decay time constant decreases with initial temperature of the material since heat dissipates faster at higher temperature. The effect of temperature change in the cavity on the sequence of PD events is found to be larger for lower material temperature because there are many PDs that occur with larger charge magnitude, resulting in a higher temperature rise and temperature decay time constant is increased at lower temperature.

Through comparison between measurement and simulation of cycle to cycle behaviour of PD events, important physical mechanisms related to the sequence of PD activity can be identified. These include variation in electron generation rate, surface charge decay rate and temperature change in the cavity between consecutive discharge events. The initial free electron generation is mainly due to surface emission and volume ionization. The possible surface charge decay mechanisms influencing PD behaviour are charge trapping into the deeper traps in the material and charge conduction along the cavity wall, which results in charge recombination. Reasonable agreement between simulation and measurement results has suggested that PD activity in a cavity can be effectively modelled using a probability of PD occurrence with consideration of some physical mechanisms and critical parameters controlling the PD events. Critical parameters identified in affecting the sequence of PDs are the electron generation rate, effective charge decay time constant, cavity surface conductivity, inception field, extinction field and temperature decay time constant in the cavity.

Chapter 9

Discussion, Conclusions and Further Work

9.1 Discussion

Table 9.1 shows a summary of PD measurement data for different applied stresses and cavity conditions. It is obvious that PD activity is strongly dependent on the amplitudes and frequencies of the applied voltage, spherical cavity size and temperature of the material. The critical parameters that have been introduced in the model and physical mechanisms related to PD activity that have been identified through comparison of measurement and simulation results are detailed in Table 9.2 and Table 9.3.

From Table 9.2, some critical parameters related to PD activity are not 'real' physical parameters. Instead, they represent physical mechanisms related to PD and they are determined through comparison between measurement and simulation results. For example, parameters such as N_{es0} and N_{ev} represent the electron generation rate due to surface emission and volume ionization, which controls the total electron generation rate. The maximum cavity surface conductivity, σ_{smax} represents the surface charge decay rate through conduction along the cavity wall. Without using 'real' physical parameters, the critical parameters introduced in the model, represent certain physical mechanisms and provide an insight of how PD behaviour changes for different applied stresses and cavity conditions, as shown in Table 9.3.

From the PD modelling using finite element analysis method (FEA), several advantages have been obtained. These includes:

1. The electric field and temperature distributions in the cavity can be determined from the model geometry, which gives an insight of pre-discharge event.

2. Non-uniform electric field and temperature distributions in the cavity can be calculated.

3. The PD real and apparent charge magnitudes can be calculated numerically from the model through time integration of current during a PD event instead of using an analytical approach.

4. The discharge process can be modelled dynamically by increasing the conductivity in the cavity.

5. The surface charge decay through conduction along the cavity wall can be modelled dynamically using a field and temperature-dependent cavity surface conductivity.

6. The precision of the electric field and temperature distributions can be increased by using a smaller time step and more mesh elements in the model geometry.

7. PD activity can also be modelled in a three-dimensional geometry to increase the flexibility of the model.

However, the disadvantages of using FEA for PD modelling is that the simulation time is greatly increased when more mesh elements and smaller time steps are used compared to an analytical approach.

From the model in this work, surface charge decay through conduction along the cavity wall has been successfully modelled using a field-dependent cavity surface conductivity, which depends on the free charge movement along the cavity wall through surface conduction. The movement of these charges depends on the magnitude and polarity of the field in the cavity and the field due to the surface charge. The surface conductivity is set higher when the polarity of the field in the cavity is the same as the polarity of the field due to surface charge. Surface charge decay through conduction eventually reduces the maximum PD charge magnitude and the number of PDs per cycle.

PD data	**Higher applied voltage**	**Higher applied frequency**	**Larger cavity size**	**Higher material temperature**
Number of PDs per cycle	Higher	Higher	Lower	Higher
Total charge magnitude per cycle	Higher	Higher	Higher	Higher
Mean charge magnitude	Lower	Lower	Higher	No change
Maximum charge magnitude	Higher	No change	Higher	Lower
Minimum charge magnitude	No change	No change	Higher	Higher
Measured inception voltage	No change	No change	Higher	Higher

Table 9.1: Summary of PD data from the measurement

Critical parameter	Higher applied voltage	Higher applied frequency	Larger cavity size	Higher material temperature
Initial electron generation rate due to surface emission, N_{es0}	No change	No change	Lower	Higher
Electron generation rate due to volume ionization, N_{ev}	Higher	Higher	Higher	Higher
Effective charge decay time constant, τ_{dec}	No change	No change	No change	Higher
Cavity inception field, E_{inc0}	No change	No change	Higher	Higher
Cavity extinction field, E_{ext0}	No change	Higher	Higher	Higher
Maximum cavity surface conductivity, σ_{smax}	Higher	Higher	Higher	Higher
Temperature decay time constant, τ_{Tdecay}	No change	No change	Higher	Lower

TABLE 9.2: Summary of critical parameters related to PD activity from the model

Physical mechanism	Higher applied voltage	Higher applied frequency	Larger cavity size	Higher material temperature
Effect of charge decay through surface conduction on PD events	Higher	No effect	Higher	Higher
Effect of charge decay through charge trapping on PD events	No effect	Lower	No effect	Lower
Total electron generation rate	Higher	Higher	Lower	Higher
Effect of temperature change in the cavity on PD	Higher	Higher	Higher	Lower

TABLE 9.3: Summary of critical parameters related to PD activity from the model

The effect of temperature change in the cavity due to PD activity has been studied using the FEA method. Temperature change in the cavity after a PD influences the inception field level due to cavity pressure change. It was observed that the effect of temperature change in the cavity on PD activity is influenced by the amplitudes and frequencies of the applied field, spherical cavity sizes and ambient temperature of the material. Though many assumptions have been made to simplify the model, consideration of temperature change in the cavity due to PD events in the model shows an improvement in the simulation results compared to when temperature change in the cavity due to PD

events is neglected in the model.

Sensitivity analysis has been performed to choose parameter values in the simulation related to electron generation rate through optimization method. The values were chosen based on the combination that yields in the lowest mean square error between simulation and measurement results. Using this method, the simulation results will be close to the measurement results but the model can also represent the change of electron generation rate for different applied stresses and cavity sizes.

Although the simulation and measurement results seem to have general agreement, the simulated ϕ-q-n plots have slight disagreement with measured patterns. The mismatch may be due to either the measurements or the PD model. There may be unavoidable inaccuracies associated with the apparent charge measurement, errors in the measurement of the cavity size or inaccurate measured dielectric permittivity. The mismatch of the simulation may come from less accurate choices of parameter values in the model, inadequate equations to describe PD model or less suitable equations for electron generation rate, probability of PD occurrence and cavity surface conductivity. Further improvements for the model can be suggested.

Different equations to describe electron generation rate due to surface emission and volume ionization and different probability can be used in the model. A probability equation containing Weibull parameters of the discharge magnitude distributions may be considered since it provides more flexibility in controlling the probability functions of PD occurrences.

Various cavity surface conductivity equations when modelling surface charge decay through conduction along the cavity wall can be explored. It is especially for the improvement of the 'rabbit-ear' like patterns of the ϕ-q-n plots in the simulation because the curve is determined by the surface conductivity which controls the charge decay rate through surface conduction.

The temporal change of temperature and pressure in the cavity after a PD event can be modelled with different ways using FEA method. Temperature distribution can be simulated based on electron avalanche process that is occuring during the discharge process.

The model could be further improved by considering surface charge distribution along the cavity wall. Charge propagation along the cavity surface during discharge event and charge movement along the cavity wall after a PD event can be modelled. Discharge events can be modelled by increasing the cavity surface charge density until the field in the cavity drops less than the extinction field.

9.2 Conclusion

A two-dimensional model describing a spherical cavity within a homogenous dielectric material has been developed using Finite Element Analysis (FEA) software in parallel with MATLAB code. The FEA solves for the electric field and temperature distributions in the model. The model developed has been used to dynamically simulate PD activity for different amplitudes and frequencies of the applied voltage, spherical cavity sizes and temperatures of the material. The comparison between simulation and measurement results shows that certain parameters in the model are dependent on the cavity conditions and applied stresses. Thus critical parameters affecting PD activity have been identified through the model, these include the effective charge decay time constant, cavity surface conductivity, initial electron generation rate, inception field, extinction field and temperature decay time constant in the cavity.

When the applied voltage amplitude is higher, the electron generation rate due to surface emission and volume ionization increases. This yields in higher number of PDs and total charge magnitude per cycle due to shorter statistical time lag, which result in more PDs occuring immediately after the inception field is exceeded. However, it is found that surface charge decay rate through conduction along the cavity wall increases with the applied voltage due to higher surface conductivity. At increasing applied voltage as well, the temperature change in the cavity has a more obvious effect on the sequence of the next PD event because of higher number of PDs per cycle.

The effect of surface charge decay between consecutive discharges is less significant at higher frequencies. Thus, the electron generation rate is larger, reducing statistical time lag, resulting in more discharges per cycle. The surface conductivity is larger at higher applied frequency because charge movement along the cavity wall is faster. The temperature change in the cavity obviously affects the sequence of PD at higher applied frequency because the time interval between consecutive PDs is shorter, causing less reduction in temperature when the next PD is likely to occur.

For a larger spherical cavity size, the electron generation rate is found to be lower. Since there is more free charge accumulation on the cavity surface, surface charge decay rate through conduction along the cavity wall is greater. The temperature change in a larger cavity has more effect on the next PD event due to higher temperature decay time constant.

At higher temperatures of the material, the number of PDs per cycle is higher because the electron generation rate is enhanced and the effective charge decay time constant increases. The inception field increases with temperature because the initial pressure in the cavity is greater. The charge movement along the cavity wall is faster at higher temperatures due to larger surface conductivity.

The cycle to cycle behaviour of PD has been studied through the PD charge magnitude

and applied voltage of PD events against time. It has been found that the sequence of PD activity does not have a systematic phase shift of PD event. From the comparison between simulation and measurement results, the sequence of PD events has been effectively modelled using a probability of PD occurrence with consideration of some physical mechanisms related to PD activity. These includes variation in electron generation rate through surface emission and volume ionization, temperature and pressure change in the cavity and charge decay through charge trapping and conduction along the cavity wall.

9.3 Further Work

Experiments of PD activity within a cavity in silicone rubber can be performed to study degradation in the material and possible electrical tree growth due to repetition of PD events in the cavity. A Finite Element Analysis model representing material degradation due to PD within a cavity in silicone rubber can be developed to increase an understanding of insulation breakdown due to PD in void cavities. Simulation results can be validated through comparison with measurement results.

Simulation models can be developed and measurements of PD behaviour can be performed for a material consisting of two voids located closely to each other, a void of different locations within a dielectric material, voids in actual high voltage cables or voids of various shapes, particularly ellipsoidal cavities. It is interesting to see how parameters in the model changes with different conditions of both the cavity and material.

Analysis of the gas decomposition within a void cavity in a dielectric material after a PD occurs could also be performed to obtain a relationship of temperature and pressure change with a PD event and chemical modifications and physical deterioration of the cavity surface due to PD. A PD model which considers the gas decompositions in the cavity after a PD can be developed to study any critical parameters affecting PD behaviour.

Appendix A

List of Publications

Refereed academic journal:

1. Illias, H. A., Chen, G. and Lewin, P. L. Modeling of partial discharge activity in spherical cavities within a dielectric material. In: IEEE Electrical Insulation Magazine, vol. 27(1), p. 38-45, 2011.
2. Illias, H. A., Chen, G. and Lewin, P. L. Partial Discharge Behaviour of a Spherical Cavity within a Solid Dielectric Material as a Function of Applied Voltage and Frequency. In: IEEE Transactions on Dielectrics and Electrical Insulation, vol. 18(2), p. 432-443, 2011.
3. Illias, H. A., Chen, G. and Lewin, P. L. The influence of spherical cavity surface charge distribution on the sequence of partial discharge events. In: Journal of Physics D: Applied Physics, 2011 (Accepted).
4. Illias, H. A., Chen, G. and Lewin, P. L. Partial Discharge within a Spherical Cavity in a Dielectric Material as a Function of Cavity Size and Material Temperature. In: IET Science, Measurement and Technology, 2011 (Submitted).

Refereed international conference:

1. Illias, H. A., Chen, G. and Lewin, P. L. Modelling of Partial Discharges from a Spherical Cavity within a Dielectric Material under Variable Frequency Electric Fields. In: IEEE Conference on Electrical Insulation and Dielectric Phenomena, 26-29 October 2008, Quebec City, Quebec, Canada. p 447-450.
2. Illias, H. A., Chen, G. and Lewin, P. L. Partial Discharge Modelling in a Spherical Cavity within a Dielectric Insulation Material as a Function of Frequency. In: IEEE Electrical Insulation Conference, 31 May-3 June 2009, Montreal, Canada. p 55-59.

3. Illias, H. A., Chen, G. and Lewin, P. L. Modelling of Partial Discharge Activity in Different Spherical Cavity Sizes and Locations within a Dielectric Insulation Material. In: IEEE International Conference on Properties and Applications of Dielectric Materials, 19-23 July 2009, Harbin, China. p 485-488.

4. Illias, H., Chen, G. and Lewin, P. L. Modelling of Surface Charge Decay in a Spherical Cavity within a Solid Dielectric Material using Finite Element Analysis. In: 16th International Symposium on High Voltage Engineering, 24-28 August 2009, Cape Town, South Africa. p 1246-1251.

5. Illias, H., Chen, G. and Lewin, P. L. Partial Discharge Measurements for Spherical Cavities within Solid Dielectric Materials under Different Stress and Cavity Conditions. In: IEEE Conference on Electrical Insulation and Dielectric Phenomena, 18-21 October 2009, Virginia Beach, Virginia, p 388-391.

6. Illias, H. A., Chen, G. and Lewin, P. L. Comparison of Partial Discharge Measurement and Simulation Results for Spherical Cavities within Solid Dielectric Materials as a Function of Frequency using Finite Element Analysis Method. In: IEEE International Symposium on Electrical Insulation, 6-9 June 2010, San Diego, California, USA. p 1-5.

7. Illias, H. A., Chen, G. and Lewin, P. L. Modelling of Cycle to Cycle Behaviour for Partial Discharge Events within a Spherical Cavity in a Solid Dielectric Material by Using Finite Element Analysis. In: IEEE International Conference on Solid Dielectrics, 4-9 July 2010, Potsdam, Germany. p 561-564.

8. Illias, H. A., Chen, G. and Lewin, P. L. Measurement and Modelling of Partial Discharge Behaviour in a Spherical Cavity within a Solid Dielectric Material as a Function of Cavity Diameter. In: IEEE International Conference on Solid Dielectrics, 4-9 July 2010, Potsdam, Germany. p 573-576.

9. Illias, H. A., Chen, G. and Lewin, P. L. Measurement and Modelling of Partial Discharge Behaviour in a Spherical Cavity within a Solid Dielectric Material as a Function of Applied Voltage Amplitude." In: IEEE International Conference on High Voltage Engineering, 11-14 October 2010, New Orleans, USA. p 441-444.

10. Illias, H. A., Chen, G. and Lewin, P. L. Modelling of Temporal Pressure and Temperature Change due to Partial Discharge Activity within a Spherical Cavity in a Solid Dielectric Material using Finite Element Analysis Method. In: IEEE International Conference on High Voltage Engineering, 11-14 October 2010, New Orleans, USA. p 501-504.

11. Illias, H. A., Chen, G. and Lewin, P. L. Measurement and Modelling of Partial Discharge Behaviour in a Spherical Cavity within a Solid Dielectric Material as a Function of Temperature. In: IEEE Conference on Electrical Insulation and

Dielectric Phenomena, 17-20 October 2010, West Lafayette, Indiana, USA. p 430-433.

Appendix B

MATLAB programming code

B.1 Main code

```
%%%%%%%%%%%%
% Main code %
%%%%%%%%%%%%

clear; % Erase all previous data
clc; % Clear command window



for ssss = 1:1:30 % Close figures from previous run
    delete(gcf)
end



% Define constants
d = 1000; % Cavity diameter in um
h = 1000; % Cavity height in um
cav_location = 0e-6; % Cavity location in the material
mat_thick = 1; % Material thickness in mm
mat_diameter = 10; % Material diameter in mm
Scav0 = 0; % Cavity conductivity during no PD
Tmat=293; % Initial temperature in the cavity
P0 = 101000; % Initial pressure in the cavity
Sample=1; % Test sample number
kmat = 0.19; % Material thermal conductivity
Cmat = 1000; % Material specific heat capacity
rhmat = 1250; % Material mass density
Qcav = 0; % Cavity heat source density
Qmat = 0; % Material heat source density
Tamb = 293; % Ambient temperature
Pcav = P0; % Set cavity pressure pressure to P0
Tcav = Tmat; % Set initial cavity temperature to Tmat
```

```
T1 = Tcav; % Set previous cavity temperature to Tcav
Ccav = 1033 -0.2799 *Tcav + 0.0001096 *Pcav + 0.0007429 *Tcav^ 2 -5.003e-007 *Tcav*Pcav +
1.891e-012 *Pcav^ 2 + -4.19e-007 *Tcav^ 3 + 6.184e-010 *Tcav^ 2*Pcav + -4.881e-015 *Tcav*Pcav^ 2
+ -7.753e-020 *Pcav^ 3; % Cavity specific heat capacity
rhcav = 3.562 -0.03445*Tcav + 3.464e-005*Pcav + 0.0001094*Tcav^ 2 -1.13e-007*Tcav*Pcav + 3.494e-013
*Pcav^ 2 -1.142e-007*Tcav^ 3 + 1.211e-010*Tcav^ 2*Pcav-
9.868e-016*Tcav*Pcav^ 2; % Cavity density
kcav = (57.88+9.43*Tcav+0.1049e-3*Pcav-0.002915*Tcav^ 2-1.726e-7*Tcav*Pcav+3.115e-10*Pcav^ 2)*1e-5;
% Cavity thermal conductivity
ChargeReal = 0; % Initial PD real charge
ChargeApparent = 0; % Initial PD apparent charge
Total_q_real = 0; % Initial total PD real charge
cn = 1; % Reset initial counter for field plot
PDc = 0; % Reset initial PD counter
tPD = 0; % Reset initial time elapsed since last PD event
PlotE = 1; % Setting for electric field plot
% Variable pre-allocation to speed up simulation
Questiondlg{15} = zeros(1);
CorrectPhasePD = zeros(1);
q_app = zeros(1);
q_real = zeros(1);
EincCN = zeros(1);
% Pre-indicator
Set_PD = 0; % Set to no PD initially
Respond = 0; % Initial respond value
DuringPD = 0; % Initial setting for application change during PD
AfterPD = 0; % Initial setting for application change after PD
PDoccurred = 0; % Initial indication after PD
FirstTimeSsmax=1;
sequence=1;


while (mat_thick<=h/1000) || (mat_diameter<=d/1000)
      prompt = { 'Enter cavity width, d (um):', 'Enter cavity height, h (um):',
      'Enter material thickness (mm):', 'Enter material diameter (mm):'};
      ansd = inputdlg(prompt, 'PD Analysis',1,{ '1400', '1400', '2', '10'});
      d = str2double(ansd{1}); % Assign cavity diameter
      h = str2double(ansd{2}); % Assign cavity height
      mat_thick = str2double(ansd{3}); % Assign material thickness
      mat_diameter = str2double(ansd{4}); % Assign material diameter
end


volume=4/3*pi*(d*1e-6/2)^ 3; % Volume of the cavity
cav_height=h*1e-6; % Height of the cavity in m
cav_radius = d/2*1e-6; % Calculate cavity radius
cav_radheight=cav_height/2; % Calculate half of cavity height
extract_loc=cav_radheight+cav_location; % Coordinate to extract value
extract_loc_tolE=cav_radheight+cav_location-0.005e-3;
area_middle=pi*cav_radius^ 2; % Area in the middle of the cavity
```

```
while Respond==0
      Respond = 1;
      clc; % Clear command window
      Questiondlg{1} = 'Applied frequency (Hz):';
      Questiondlg{2} = 'Applied voltage amplitude, Uapp (V):';
      Questiondlg{3} = 'Number of cycles to simulate (integer only):';
      Questiondlg{4} = 'Relative permittivity of the material, Ermat:';
      Questiondlg{5} = 'Relative permittivity of the cavity, Ercav:';
      Questiondlg{6} = 'Material conductivity, Smat (S/m):';
      Questiondlg{7} = 'nitial cavity surface conductivity, Ss0 (S/m):';
      Questiondlg{8} = 'Maximum cavity conductivtiy, Scavmax (S/m):';
      Questiondlg{9} = 'Maximum surface conductivity, Ssmax (S/m):';
      Questiondlg{10} = 'Initial EGR due to surface emission, Nes0H (1/s):';
      Questiondlg{11} = 'Initial EGR due to surface emission, Nes0L (1/s):';
      Questiondlg{12} = 'EGR due to volume ionization, Nev (1/s):';
      Questiondlg{13} = 'Effective charge decay time constant, tdec (s):';
      Questiondlg{14} = 'Extinction field, Eext (V/m):';
      Questiondlg{15} = 'Stress-dependent coefficient for Ssmax, alpha (m/V):';
      Defaultdlg = {'50','14000','1','4.4','1','1e-13','1e-13', '5e-3','5e-9','5500','700',
      '100','2e-3','1e6','10e-6'}; % Default values
      Answerdlg = inputdlg(Questiondlg,'PD Analysis',1,Defaultdlg); % Input dialog box
      freq = str2double(Answerdlg{1}); % Update applied frequency
      MaxVolt = str2double(Answerdlg{2}); % Update applied voltage magnitude
      Cycle = round(str2double(Answerdlg{3})); % Update number of cycle
      Ermat = str2double(Answerdlg{4}); % Update Ermat
      Ercav = str2double(Answerdlg{5}); % Update Ercav
      Smat = str2double(Answerdlg{6}); % Update Smat
      Ss0 = str2double(Answerdlg{7}); % Update Ss
      Scavmax = str2double(Answerdlg{8}); % Update Smax
      Ssmax = str2double(Answerdlg{9}); % Update Ssmax
      Nes0H = str2double(Answerdlg{10}); % Update Nes0H
      Nes0L = str2double(Answerdlg{11}); % Update Nes0L
      Nev = str2double(Answerdlg{12}); % Update Nev
      tdec = str2double(Answerdlg{13}); % Update tdec
      Eext = str2double(Answerdlg{14}); % Update Eext
      alpha = str2double(Answerdlg{15}); % Update alpha
      if freq <= 0 || Cycle <= 0 % Error dialog for zero frequency and cycle
         uiwait(errordlg('Frequency or cycle must be more than zero!',
         'PD Analysis','modal'));
         Respond = 0;
      elseif (abs(MaxVolt/(mat_thick*1e-3)) <= abs(Eext)) % Error dialog for invalid Eext
         uiwait(errordlg('Applied field is less than Eext!', 'PD Analysis','modal'));
         Respond = 0;
      elseif (Smat<=0)||(Ss0<=0)||(Ssmax<=0) % Error dialog for invalid conductivity
         uiwait(errordlg('Invalid conductivity value!', 'PD Analysis','modal'));
         Respond = 0;
      elseif (Ermat<=0)||(Ercav<=0) % Error for invalid permittivity
         uiwait(errordlg('Invalid relative permittivity value!', 'PD Analysis','modal'));
         Respond = 0;
      end
      if Respond == 1 % If there is no error detected
```

```
    if d/h == 1
           K=3; % K factor for spherical cavity
    elseif d/h > 1 % K factor for flat ellipsoidal cavity
           u = sqrt(power(d/h,2)-1);
           K = power(u,3)/((1+power(u,2))*(u-atan(u)));
    elseif d/h < 1 % K factor for narrow ellipsoidal cavity
           v = sqrt(1-power(d/h,2));
           K =2*power(v,3)/((1-power(v,2))*(log((1+v)/(1-v))-2*v));
    end
    % Calculate inception field
    if Sample==1; Einc=(0.009417699*Tcav+ 0.6475)*1e6;
    elseif Sample==2; Einc=(0.00805*Tcav+ 0.665450)*1e6;
    elseif Sample==3;Einc = (0.007722*Tcav+0.5673)*1e6;
    elseif Sample==4;Einc = (0.009071*Tcav+0.6965)*1e6;
    elseif Sample==5;Einc = (0.01087*Tcav+0.3441)*1e6;
    end
    Einc0=Einc;
    fprintf('PD SIMULATION WITHIN A CAVITY IN A DIELECTRIC MATERIAL\n');
    fprintf('\nhcav = %4d um\ndcav = %4d um',h,d);
    fprintf('hmat = %6.2f mm\ndmat = %6.2f mm\n',mat_thick,mat_diameter);
    fprintf('Applied frequency, freq = %.2f Hz\n',freq);
    fprintf('Applied voltage amplitude, Uapp = %d V\n',MaxVolt);
    fprintf('Initial iception field, Einc = %d V/m\n',Einc0);
    fprintf('Initial extinction field, Eext = %d V/m\n',Eext);
    fprintf('Number of cycles = %d\n',Cycle);
    fprintf('Material permittivity, Ermat = %.2f\n',Ermat);
    fprintf('Cavity permittivity, Ercav = %.2f\n',Ercav);
    fprintf('Material conductivity, Smat = %.4e S/m\n',Smat);
    fprintf('Cavity conductivity during no PD, Scav0 = %.4e S/m\n',Scav0);
    fprintf('Initial surface conductivity, Ss = %.4e S/m\n',Ss0);
    fprintf('Maximum surface conductivity, Ssmax = %.4e S/m\n',Ssmax);
    fprintf('Stress dependent coefficient Ssmax, alpha = %d m/V\n',alpha);
    fprintf('Effective charge decay time constant, tdec = %.4f s\n',tdec);
    fprintf('Initial EGR due to surface emission, NesOH = %.4f N/s\n',NesOH);
    fprintf('Initial EGR due to surface emission, NesOL = %.4f N/s\n',NesOL);
    fprintf('EGR due to volume ionization, Nev = %.4f N/s\n',Nev);
    fprintf('Material temperature, Tmat = %d K\n',Tmat);
    fprintf('Initial cavity pressure, p0 = %d Pa\n',P0);
    fprintf('Cavity specific heat capacity, Ccav = %.4f J/(kgK)\n',Ccav);
    fprintf('Cavity thermal conductivity, kcav = %.4f W/(mK)\n',kcav);
    fprintf('Cavity density, rhcav = %.4f kg/m^ 3\n\n',rhcav);
    button = questdlg('Are you sure you want to proceed with these parameters?',
    'PD Analysis','Yes','No','No');
    if (strcmp('Yes',button) == 1)
       Respond = 1;
    else
       Respond = 0;
    end
end
if Respond == 1
    button1 = questdlg('Choose the type of datalog display:', 'PD Analysis',
```

```
        'Discharge Datalog','Expanded Datalog','Cancel','Cancel');
        if (strcmp('Discharge Datalog',button1) == 1)
                dtlg = 1;
        elseif (strcmp('Expanded Datalog',button1) == 1)
                dtlg = 2;
        else
                Respond = 0;
        end
    end
    if Respond == 1
        button2 = questdlg('Do you want to save all plots in your folder?',
        'PD Analysis','Yes','No','Cancel','Cancel');
        if (strcmp('Yes',button2) == 1)
                savefig = 1;
        elseif (strcmp('No',button2) == 1)
                savefig = 0;
        else
                Respond = 0;
        end
    end
    if Respond == 1
        button2 = questdlg('Do you want to plot electric field?', 'PD Analysis','Yes',
        'No','Cancel','Cancel');
        if (strcmp('Yes',button2) == 1)
                PlotE = 1;
        elseif (strcmp('No',button2) == 1)
                PlotE = 0;
        else
                Respond = 0;
        end
    end
end


% End of user input
AnsWsp = inputdlg('Enter Workspace Name:','Workspace',1,{''});
AnsSave = char(AnsWsp);
pause(0.05)
Interval = 0.72/(360*freq); % Time step during no PD
DiscInterval = 1e-9; % Time step during PD
StartTime = 0; % Start time
FinishTime = 360/(360*freq)*Cycle-Interval; % End time
Range = StartTime:Interval:FinishTime; % Range of time
fprintf('Time step during no PD = %.4e s (%.2f deg)\n',Interval,Interval*360*freq);
fprintf('Time step during PD = %.4e s (%.5f deg)\n',DiscInterval,DiscInterval*360*freq);
% Assign save filename


if freq <= 0.9
    freq1 = freq * 1000;
    labelHz = 'mHz';
```

```
else
   freq1 = freq;
   labelHz = 'Hz';
end


FigureTitle = ['d' num2str(d) 'um_h' num2str(h) 'um_' num2str(freq1) labelHz '_'
num2str(MaxVolt/1000) 'kV'];
FilenameSave = [AnsSave '_' FigureTitle];
Ers = Ermat; % Assign cavity surface permittivity as Ermat
EincCN(1) = Einc0; % Inception field for field plot
Nextra = 1; % Assign initial value for Nextra
Ss = Ss0; % Assign cavity surface conductivity as Ss0
Scav = Scav0; % Assign cavity conductivity as Scav0
Einc = Einc0; fprintf('\nSimulation starts...\n');
x1 = datestr(now,'mmm dd,yyyy HH:MM:SS');
fprintf('Date Starts :  %s\n\n',x1);
tic % Record simulation start time
% Draw geometries
flclear fem % Initialise model
% COMSOL version
g2=rect2(mat_diameter/2*1e-3,mat_thick*1e-3,'base','corner','pos',[0,-mat_thick/2*1e-3]);
carr={curve2([0,cav_radius,cav_radius], [-cav_radheight,-cav_radheight,0], [1,
0.7071067811865475,1]), curve2([cav_radius,cav_radius,0], [0,cav_radheight,
cav_radheight], [1,0.7071067811865475,1]),
curve2([0,0],[cav_radheight,-cav_radheight],[1,1])};
g3=geomcoerce('solid',carr);
% Analyzed geometry
clear s
s.objs={g2,g3};
fem.draw=struct('s',s);
fem.geom=geomcsg(fem);
carr={curve2([0,cav_radius+0.05e-3,cav_radius+0.05e-3],[-(cav_radheight+0.05e-3),
-(cav_radheight+0.05e-3),0], [1,0.7071067811865475,1]), curve2([cav_radius+0.05e-3,
cav_radius+0.05e-3,0], [0,cav_radheight+0.05e-3,cav_radheight+0.05e-3],[1,
0.7071067811865475,1]), curve2([0,0],[cav_radheight+0.05e-3,
-(cav_radheight+0.05e-3)],[1,1])};
g4=geomcoerce('solid',carr);
clear s
s.objs={g2,g3,g4};
fem.draw=struct('s',s);
fem.geom=geomcsg(fem);
carr={curve2([0,cav_radius],[0,0],[1,1])};
g5=geomcoerce('curve',carr);
g3=move(g3,[0,cav_location]);
g4=move(g4,[0,cav_location]);
g5=move(g5,[0,cav_location]);
clear c s
c.objs={g5};
s.objs={g2,g3,g4};
fem.draw=struct('c',c,'s',s);
```

```
fem.geom=geomcsg(fem);
% Define constants in COMSOL
fem.const = {'MaxVolt',MaxVolt, 'freq',freq, 'Ermat',Ermat, 'Ers',Ers, 'Ercav',Ercav,
'Smat',Smat, 'Pcav',Pcav,'P0',P0, 'T0',Tmat};
% Create mesh
fem.mesh=meshinit(fem,'hauto',5);
fem.mesh=meshrefine(fem,'mcase',0,'boxcoord',[-4E-6 2E-3 -mat_thick/2 mat_thick/2],
'rmethod','regular');
fem.mesh=meshrefine(fem,'mcase',0,'boxcoord',[-4E-6 2E-3 -mat_thick/2 mat_thick/2],
'rmethod','regular');


if dtlg==2
   fprintf('Phase[deg] Ss[S/m] E0[V/m] Ecav[V/m]\n');
else
   fprintf('\n PD Phase q_apparent[pC] q_real[pC]\n');
end


% Main program loop
Time = StartTime;
CorrectTime = Time+Interval;
% Detailed domain (emqvw) settings
clear appl
appl.mode.class = 'QuasiStatics';
appl.mode.type = 'axi';
appl.name = 'emqvw';
appl.module = 'ACDC';
appl.sshape = 2;
appl.assignsuffix = '_emqvw';
clear prop
prop.elemdefault='Lag2';
prop.analysis='transsmallcurr';
appl.prop = prop;
clear bnd
bnd.eltype = {'ax','V0','cont','V','nJ0'};
bnd.magtype = {'A0','A0','cont','A0','A0'};
bnd.V0 = {0,0,0,'MaxVolt*sin(2*pi*freq*t)',0};
bnd.ind = [1,2,1,1,1,3,1,1,4,5,3,3,3,3];
appl.bnd = bnd;
clear equ
equ.sigma = {'Smat',Ss,Scav0};
equ.epsilonr = {'Ermat','Ers','Ercav'};
equ.shape = 1;
equ.ind = [1,2,3,3];
appl.equ = equ;
appl.var = {'nu',freq};
fem.appl{1} = appl;
% Detailed domain (emqvw2) settings
clear appl
appl.mode.class = 'HeatTransfer';
```

```
appl.mode.type = 'axi';
appl.sshape = 2;
appl.border = 'on';
appl.assignsuffix = '_ht';
clear prop
clear weakconstr
weakconstr.value = 'off';
weakconstr.dim = {'lm3'};
prop.weakconstr = weakconstr;
appl.prop = prop;
clear bnd
bnd.type = {'q0','cont','ax'};
bnd.ind = [3,1,3,3,3,2,3,3,1,1,2,2,2,2];
appl.bnd = bnd;
clear equ
equ.C = {Cmat,Ccav};
equ.init = Tmat;
equ.k = {kmat,kcav};
equ.Q = {0,0};
equ.rho = {rhmat,rhcav};
equ.ind = [1,1,2,2];
appl.equ = equ;
fem.appl{2} = appl;
fem.sdim = {'r','z'};
fem.frame = {'ref'};
fem.border = 1;
fem.outform = 'general';
clear units;
units.basesystem = 'SI';
fem.units = units;
fem=multiphysics(fem); % Send fem struct to be analysed by COMSOL
fem.xmesh=meshextend(fem); % Send mesh settings to COMSOL for mesh creation
% Solve model
fem.sol=femtime(fem, ...
'solcomp','V','T', ...  % Solve for both V
'outcomp','V','T','Vt','Tt', ...  % Include Voltage derivatives
'tlist',(0:Interval/2:Interval), ...  % Time steps to solve
'atol','0.01', ...  % Absolute tolerance value
'rtol',0.001, ...  % Relative tolerance value
'tout','tlist', ...
'tsteps','strict'); % Use strict time stepping to solve voltage
fem0 = fem; % Save current model
% Extract cavity field
Ecav = -postinterp(fem,'Ez_emqvw',[0;cav_location],'phase',0,'solnum','end');
MaxfcE0 = Ecav/(sin(2*pi*freq*CorrectTime));
fcE0 = MaxfcE0*sin(2*pi*freq*CorrectTime);



if dtlg == 2
   Ecav1 = MaxVolt*sin(2*pi*freq*CorrectTime); % Calculate applied voltage amplitude
   fprintf('%10.2f %.4e%14.4e%14.4e %14.6f\n',CorrectTime*360*freq,Ss,fcE0,Ecav,Tmat);
```

```
end


if PlotE == 10 % Recording the voltage value
   cn = cn+1;
   CorrectPhaseCN(cn,1) = CorrectTime;
   EcavCN(cn,1) = Ecav;
   fcEOCN(cn,1) = fcE0;
   EincCN(cn,1) = Einc;
   Temp(cn,1) = Tmat;
end


Time = Time+Interval;


while Time <= FinishTime+Interval
      CorrectTime = Time+Interval; % Correct the time
      if PDc >= 1
         if AfterPD==1 || Schange==1;
            clear appl
            appl.mode.class = 'HeatTransfer';
            appl.mode.type = 'axi';
            appl.sshape = 2;
            appl.border = 'on';
            appl.assignsuffix = '_ht';
            clear prop
            clear weakconstr
            weakconstr.value = 'off';
            weakconstr.dim = {'lm3'};
            prop.weakconstr = weakconstr;
            appl.prop = prop;
            clear bnd
            bnd.type = {'q0','cont','ax'};
            bnd.ind = [3,1,3,3,3,2,3,3,1,1,2,2,2,2];
            appl.bnd = bnd;
            clear equ
            equ.init = Tmat;
            equ.rho = {rhmat,rhcav};
            equ.ind = [1,1,2,2];
            AfterPD=0;
            Schange=0;
         end
         equ.C = {Cmat,'1033 -0.2799 *T + 0.0001096 *P0/T0*T + 0.0007429 *T^ 2
         -5.003e-007 *T*P0/T0*T + 1.891e-012 *(P0/T0*T)^ 2 + -4.19e-007 *T^ 3 +
         6.184e-010 *T^ 2*P0/T0*T + -4.881e-015 *T*(P0/T0*T)^ 2 +
         -7.753e-020 *(P0/T0*T)^ 3'};
         equ.k = {kmat,'(57.88+9.43*T+0.1049e-3*P0/T0*T-0.002915*T^ 2
         -1.726e-7*T*P0/T0*T+3.115e-10*(P0/T0*T)^ 2)*1e-5'};
         equ.rho = {rhmat,'3.562 -0.03445*T + 3.464e-005*P0/T0*T + 0.0001094*T^ 2
```

```
-1.13e-007*T*P0/T0*T + 3.494e-013*(P0/T0*T)^2 -1.142e-007*T^3 +
1.211e-010*T^2*P0/T0*T-9.868e-016*T*(P0/T0*T)^2'};
appl.equ = equ;
fem.appl2 = appl;
% After first PD has occurred
if (Ecav/Es) > 0 && ((Es/EstrapPD>0 && (abs(Es) >= abs(EstrapPD)))
|| (Es/EstrapPD<0 && abs(Es-EstrapPD)>0) ) % Surface charge decay
   Tsurf = postinterp(fem,'T',[0;extract_loc],'phase',0,'solnum','end');
   Esurf = -postinterp(fem,'Ez_emqvw',[0;extract_loc_tolE],'phase',0,'solnum','end');
   Ss = Ss0*exp(abs(Esurf)*alpha+Tsurf/Tamb);
   if Ss >= Ssmax
      Ss = Ssmax; % Limit the surface conductivity
      if FirstTimeSsmax == 0
         clear appl
         appl.mode.class = 'QuasiStatics';
         appl.mode.type = 'axi';
         appl.name = 'emqvw';
         appl.module = 'ACDC';
         appl.sshape = 2;
         appl.assignsuffix = '_emqvw';
         clear prop
         prop.elemdefault='Lag2';
         prop.analysis='transsmallcurr';
         appl.prop = prop;
         clear bnd
         bnd.eltype = {'ax','V0','cont','V','nJ0'};
         bnd.magtype = {'A0','A0','cont','A0','A0'};
         bnd.V0 = {0,0,0,'MaxVolt*sin(2*pi*freq*t)',0};
         bnd.ind = [1,2,1,1,1,3,1,1,4,5,3,3,3,3];
         appl.bnd = bnd;
         clear equ
         equ.sigma = {'Smat',Ss,Scav0};
         equ.epsilonr = {'Ermat','Ers','Ercav'};
         equ.shape = 1;
         equ.ind = [1,2,3,3];
         appl.equ = equ;
         appl.var = {'nu',freq};
         fem.appl{1} = appl;
         FirstTimeSsmax = 1;
         Schange=1;
      end
   end
   if Ss  = Ssmax
      clear appl
      appl.mode.class = 'QuasiStatics';
      appl.mode.type = 'axi';
      appl.name = 'emqvw';
      appl.module = 'ACDC';
      appl.sshape = 2;
      appl.assignsuffix = '_emqvw';
      clear prop
```

```
    prop.elemdefault='Lag2';
    prop.analysis='transsmallcurr';
    appl.prop = prop;
    clear bnd
    bnd.eltype = {'ax','V0','cont','V','nJ0'};
    bnd.magtype = {'A0','A0','cont','A0','A0'};
    bnd.V0 = {0,0,0,'MaxVolt*sin(2*pi*freq*t)',0};
    bnd.ind = [1,2,1,1,1,3,1,1,4,5,3,3,3,3];
    appl.bnd = bnd;
    clear equ
    equ.sigma = {'Smat',Ss,Scav0};
    equ.epsilonr = {'Ermat','Ers','Ercav'};
    equ.shape = 1;
    equ.ind = [1,2,3,3];
    appl.equ = equ;
    appl.var = {'nu',freq};
    fem.appl{1} = appl;
    FirstTimeSsmax = 0;
    Schange=1;
end
else
if Ss  = Ss0
    Ss = Ss0; % Reset to initial surface conductivity
    clear appl
    appl.mode.class = 'QuasiStatics';
    appl.mode.type = 'axi';
    appl.name = 'emqvw';
    appl.module = 'ACDC';
    appl.sshape = 2;
    appl.assignsuffix = '_emqvw';
    clear prop
    prop.elemdefault='Lag2';
    prop.analysis='transsmallcurr';
    appl.prop = prop;
    clear bnd
    bnd.eltype = {'ax','V0','cont','V','nJ0'};
    bnd.magtype = {'A0','A0','cont','A0','A0'};
    bnd.V0 = {0,0,0,'MaxVolt*sin(2*pi*freq*t)',0};
    bnd.ind = [1,2,1,1,1,3,1,1,4,5,3,3,3,3];
    appl.bnd = bnd;
    clear equ
    equ.sigma = {'Smat',Ss,Scav0};
    equ.epsilonr = {'Ermat','Ers','Ercav'};
    equ.shape = 1;
    equ.ind = [1,2,3,3];
    appl.equ = equ;
    appl.var = {'nu',freq};
    fem.appl{1} = appl;
    Schange=1;
    FirstTimeSsmax=0;
end
```

```
    end
    fem=multiphysics(fem); % Send fem struct to be analysed by COMSOL
    fem.xmesh=meshextend(fem); % Send mesh settings to COMSOL for mesh creation
    tPD = tPD+Interval; % Increase time elapsed since last PD event
    Pcav = Pcav*Tcav/T1; % Calculate new pressure
    T1 = Tcav; % Assign current temperature value as previous value
    % Calculate inception field
    if Sample==1; Einc=(0.009417699*Tcav+ 0.6475)*1e6;
    elseif Sample==2; Einc=(0.00805*Tcav+ 0.665450)*1e6;
    elseif Sample==3;Einc = (0.007722*Tcav+0.5673)*1e6;
    elseif Sample==4;Einc = (0.009071*Tcav+0.6965)*1e6;
    elseif Sample==5;Einc = (0.01087*Tcav+0.3441)*1e6;
    end
    if q_app(PDc,1)/Ecav<0
       Nes0 = Nes0L; % Assign to high Nes0
    else
       Nes0 = Nes0H; % Assign to low Nes0
    end
end
fem.sol = Process_Ecav_Tcav(fem,fem0.sol,Time,Interval); % Solve field and temperature
fem0 = fem; % Save current model
Ecav = -postinterp(fem,'Ez_emqvw',[0;cav_location],'phase',0,'solnum','end');
Tcav= postinterp(fem,'T',[0;cav_location],'phase',0,'solnum','end');
fcE0 = MaxfcE0*sin(2*pi*freq*CorrectTime);
if (PDc >= 1) && (Ecav/Es) > 0
   Es = Ecav-fcE0; % Calculate field due to surface charge
end
if dtlg == 2
   fprintf('%10.2f %.4e%14.4e%14.4e %14.6f\n',CorrectTime*360*freq,
   Ss,fcE0,Ecav,Tcav);
end
if (PlotE == 1) && (Time <= 10/freq) % Recording for plot
   cn = cn+1;
   CorrectPhaseCN(cn,1) = CorrectTime;
   EcavCN(cn,1) = Ecav;
   fcE0CN(cn,1) = fcE0;
   EincCN(cn,1) = Einc;
   Temp(cn,1) = Tcav;
end
if abs(Ecav) >= Einc % Check cavity field > Inception field
   if PDc>0
      Nes = Nes0*Nextra*exp(-tPD/tdec);
   else
      Nes=0;
   end
   % Check any PD occurs
   Set_PD = Check_anyPDE(Nes,Nev,Ecav,Einc0,Interval,Tmat,Tamb);
   % PD occurrence
   if Set_PD > 0
   % Increase PD event counter
      PDc = PDc+1;
```

```
Time = Time+ Interval; % Correct the time
Nextra = abs(Ecav)/Einc0; % Calculate Nextra
CorrectPhasePD(PDc,1) = CorrectTime; % Record PD phase
Eext1=Eext*Pcav/P0; % Calculate new extinction field
Scav = Scavmax;
% Check cavity field < Extinction field
while abs(Ecav) >= Eext1
      CorrectTime = CorrectTime+DiscInterval; % Correcting the time
      if DuringPD==0;
         clear appl
         appl.mode.class = 'QuasiStatics';
         appl.mode.type = 'axi';
         appl.name = 'emqvw';
         appl.module = 'ACDC';
         appl.sshape = 2;
         appl.assignsuffix = '_emqvw';
         clear prop
         prop.elemdefault='Lag2';
         prop.analysis='transsmallcurr';
         appl.prop = prop;
         clear bnd
         bnd.eltype = {'ax','V0','cont','V','nJ0'};
         bnd.magtype = {'A0','A0','cont','A0','A0'};
         bnd.V0 = {0,0,0,'MaxVolt*sin(2*pi*freq*t)',0};
         bnd.ind = [1,2,1,1,1,3,1,1,4,5,3,3,3,3];
         appl.bnd = bnd;
         clear equ
         equ.sigma = {'Smat',Ss,Scav};
         equ.epsilonr = {'Ermat','Ers','Ercav'};
         equ.shape = 1;
         equ.ind = [1,2,3,3];
         appl.equ = equ;
         appl.var = {'nu',freq};
         fem.appl{1} = appl;
         clear appl
         appl.mode.class = 'HeatTransfer';
         appl.mode.type = 'axi';
         appl.sshape = 2;
         appl.border = 'on';
         appl.assignsuffix = '_ht';
         clear prop
         clear weakconstr
         weakconstr.value = 'off';
         weakconstr.dim = {'lm3'};
         prop.weakconstr = weakconstr;
         appl.prop = prop;
         clear bnd
         bnd.type = {'q0','cont','ax'};
         bnd.ind = [3,1,3,3,3,2,3,3,1,1,2,2,2,2];
         appl.bnd = bnd;
         clear equ
```

```
            equ.init = Tmat;
            equ.ind = [1,1,2,2];
            DuringPD=1;
        end
        equ.C = {Cmat,'1033 -0.2799 *T + 0.0001096 *P0/T0*T + 0.0007429 *T^ 2
        -5.003e-007 *T*P0/T0*T + 1.891e-012 *(P0/T0*T)^ 2-4.19e-007 *T^ 3
        + 6.184e-010 *T^ 2*P0/T0*T-4.881e-015 *T*(P0/T0*T)^ 2
        -7.753e-020 *(P0/T0*T)^ 3'};
        equ.k = {kmat,'(57.88+9.43*T+0.1049e-3*P0/T0*T-0.002915*T^ 2
        -1.726e-7*T*P0/T0*T+3.115e-10*(P0/T0*T)^ 2)*1e-5'};
        equ.Q = {Qmat,Qcav};
        equ.rho={rhmat,'3.562 -0.03445*T+3.464e-005*P0/T0*T+
        0.0001094*T^ 2 -1.13e-007*T*P0/T0*T + 3.494e-013*(P0/T0*T)^ 2
        -1.142e-007*T^ 3 + 1.211e-010*T^ 2*P0/T0*T-
        9.868e-016*T*(P0/T0*T)^ 2'};
        appl.equ = equ;
        fem.appl{2} = appl;
        fem=multiphysics(fem); % Send fem struct to be analysed
        fem.xmesh=meshextend(fem); % Send mesh settings for mesh creation
        fem.sol = Process_Ecav_Tcav(fem,fem0.sol,Time,DiscInterval);
        fem0=fem; % Save current model
        Tcav= postinterp(fem,'T',[0;cav_location],'phase',0,'solnum','end');
        % Integrate current density with time to obtain current
        I1=-postint(fem,'2*pi*r*(Jz_emqvw)','unit','A','dl',6,'edim',1,
        'solnum','end');
        I2=-postint(fem,'2*pi*r*(Jz_emqvw)','unit','A','dl',2,'edim',1,
        'solnum','end');
        ChargeApparent = ChargeApparent+I2*DiscInterval; % Apparent charge
        ChargeReal = ChargeReal+I1*DiscInterval; % Real charge
        Ecav = -postinterp(fem,'Ez_emqvw',[0;cav_location],'phase',0,
        'solnum','end');
        Qcav = abs(Ecav*I1/area_middle);
        Time = CorrectTime; % Equivalent time value
        Pcav = Pcav*Tcav/T1; % Calculate new pressure
        T1 = Tcav; % Assign current temperature as previous temperature
        if dtlg == 2
            fcE0=MaxfcE0*sin(2*pi*freq*(CorrectTime));
            fprintf('%10.2f %17.9f %15.4e %15.4e %12.4f %.4e %.4e\n',
            CorrectTime*360*freq,CorrectTime,fcE0,Ecav,Tcav,I1,Qcav);
        end
    end
    % End of PD event
    AfterPD = 1;
    DuringPD = 0;
    q_app(PDc,1) = ChargeApparent;
    q_real(PDc,1) = ChargeReal;
    if dtlg == 1
        fprintf('%5d%12.2f%15.4f%14.4f\n', PDc,CorrectTime*360*freq,
        ChargeApparent*1e12,ChargeReal*1e12);
    end
    if PDc <= 2 % Plot figures for first 2 PDs
```

```
        Plot_PD(fem,Time,PDc,savefig,FilenameSave)
    end
    % Save PD workspace
    save([FilenameSave '_PDdata.mat'],'CorrectPhasePD','q_app','q_real');
    Scav = Scav0; % Reset cavity conductivity
    tPD = 0; % Reset time elapsed since previous PD event
    PDoccurred = 1; % Indication after PD
    Set_PD = 0; % Reset PD event
    Total_q_real=Total_q_real+ChargeReal; % Calculate total PD Real charge
    Qcav = 0; % Reset heat source density to zero
    % Extract free surface charge after PD
    Qsurfzupdown=postint(fem,'2*pi*r*(Dz_emqvw_up -Dz_emqvw_down)',
    'unit','C','dl',12,'edim',1,'solnum','end');
    fcE0=MaxfcE0*sin(2*pi*freq*(CorrectTime));
    Es = Ecav-fcE0; % Calculate voltage due to surface charge
% Calculate inception field
    if Sample==1; Einc=(0.009417699*Tcav+ 0.6475)*1e6;
    elseif Sample==2; Einc=(0.00805*Tcav+ 0.665450)*1e6;
    elseif Sample==3;Einc = (0.007722*Tcav+0.5673)*1e6;
    elseif Sample==4;Einc = (0.009071*Tcav+0.6965)*1e6;
    elseif Sample==5;Einc = (0.01087*Tcav+0.3441)*1e6;
    end
    if (PlotE == 1) && (Time <= 10/freq)
        cn = cn+1;
        CorrectPhaseCN(cn,1) = CorrectTime;
        EcavCN(cn,1) = Ecav;
        fcE0CN(cn,1) = fcE0;
        EincCN(cn,1) = Einc;
        Temp(cn,1)=Tcav;
    end
    % Calculate minimum surface charge voltage
    EsfreePD = (Qsurfzupdown/Total_q_real*Es);
    EstrapPD = Es - EsfreePD;
    ChargeReal = 0; % Reset PD Real charge
    ChargeApparent = 0; % Reset PD apparent charge
    equ.C = {Cmat,'1033 -0.2799 *T + 0.0001096 *P0/T0*T + 0.0007429 *T^ 2
    -5.003e-007 *T*P0/T0*T + 1.891e-012 *(P0/T0*T)^ 2 + -4.19e-007 *T^ 3
    + 6.184e-010 *T^ 2*P0/T0*T + -4.881e-015 *T*(P0/T0*T)^ 2
    -7.753e-020 *(P0/T0*T)^ 3'};
    equ.k = {kmat,'(57.88+9.43*T+0.1049e-3*P0/T0*T-0.002915*T^ 2
    -1.726e-7*T*P0/T0*T+3.115e-10*(P0/T0*T)^ 2)*1e-5'};
    equ.Q = {Qmat,Qcav};
    equ.rho = {rhmat,'3.562 -0.03445*T + 3.464e-005*P0/T0*T + 0.0001094*T^ 2
    -1.13e-007*T*P0/T0*T + 3.494e-013*(P0/T0*T)^ 2
    -1.142e-007*T^ 3 + 1.211e-010*T^ 2*P0/T0*T
    -9.868e-016*T*(P0/T0*T)^ 2'};
    appl.equ = equ;
    fem.appl{2} = appl;
    clear appl
    appl.mode.class = 'QuasiStatics';
    appl.mode.type = 'axi';
```

```
            appl.name = 'emqvw';
            appl.module = 'ACDC';
            appl.sshape = 2;
            appl.assignsuffix = '_emqvw';
            clear prop
            prop.elemdefault='Lag2';
            prop.analysis='transsmallcurr';
            appl.prop = prop;
            clear bnd
            bnd.eltype = {'ax','V0','cont','V','nJ0'};
            bnd.magtype = {'A0','A0','cont','A0','A0'};
            bnd.V0 = {0,0,0,'MaxVolt*sin(2*pi*freq*t)',0};
            bnd.ind = [1,2,1,1,1,3,1,1,4,5,3,3,3,3];
            appl.bnd = bnd;
            clear equ
            equ.sigma = {'Smat',Ss,Scav0};
            equ.epsilonr = {'Ermat','Ers','Ercav'};
            equ.shape = 1;
            equ.ind = [1,2,3,3];
            appl.equ = equ;
            appl.var = {'nu',freq};
            fem.appl{1} = appl;
            fem=multiphysics(fem);
            fem.xmesh=meshextend(fem);
         end
      end
      % End of PD loop
      if PDoccurred == 0
         Time = Time+Interval; % Increase time step if no PD occur
      end
      PDoccurred = 0; % Reset indication after PD
end


% End of main loop


x2 = datestr(now,'mmm dd,yyyy HH:MM:SS'); % Record simulation ends time
fprintf('\nDate Starts :  %s',x1);
fprintf('\nDate Ends :  %s\n',x2);
sim_time=toc; % Calculate total simulation time
cpumin = sim_time/60;
fprintf('\nCPU Time :  %.2f seconds or %.2f mins (%.2f mins per cycle)\n', sim_time,
cpumin,cpumin/Cycle);
fprintf(' %.2f hours\n',cpumin/60);
fprintf('\nSimulation ends\n');


if PDc > 0 % Plotting p-q-n, various graphs and PD data
   q_app = q_app*1e12;
   q_real = q_real*1e12;
```

```
    CorrectPhasePD = CorrectPhasePD*360*freq;
    CorrectPhaseCC=CorrectPhaseCN*1e3;
    Qmaxpn=2500;
end


save([FilenameSave '_PDdata.mat']) % Save workspace results
```

B.2 'Process' function

```
%%%%%%%%%%%%%%%%%%%%%%
% 'Process' function %
%%%%%%%%%%%%%%%%%%%%%%

function sol = Process_Ecav_Temp(fem,fem0,Time,Interval)

% Mapping current solution to extended mesh
init = asseminit(fem,'init',fem0,'t',Time);
% Evaluating u using previous solution


u = asseminit(fem,'init',fem0,'t',Time);
sol = femtime(fem, ...
      'init',init, ...
      'u',u, ...
      'solcomp',{'V','T'}, ...% Solve for V and T
      'outcomp',{'V','T','Vt','Tt'}, ...% Include derivatives
      'tlist',(Time:Interval/2:Time+Interval), ...% Time to solve
      'atol',{'0.01'}, ...% Absolute tolerance
      'rtol',0.001, ...% Relative tolerance
      'tout','tlist', ...
      'tsteps','strict'); % Strict time steps
```

B.3 'Check_anyPD' function

```
%%%%%%%%%%%%%%%%%%%%%%%%%
% 'Check_anyPD' function %
%%%%%%%%%%%%%%%%%%%%%%%%%

function Set_PD = Check_anyPDE(Nes,Nev,Ecav,Einc0,Interval,Tmat,Tamb)

Net = Nes*exp((abs(Ecav)/Einc0)*Tmat/Tamb)+Nev; % Calculate electron generation rate
Prob = Net*Interval; % Calculate probability of a PD occurrence
Random = rand; % Generate random number R


if Prob > Random % Compare P and R
   Set_PD = 1; % If P>R, PD occurs
```

```
else
   Set_PD = 0; % If P<R, no PD occurs
end
```

B.4 'Plotting_phi-q-n' code

```
%%%%%%%%%%%%%%%%%%%%%%%%%
% 'Plotting_phi-q-n' code %
%%%%%%%%%%%%%%%%%%%%%%%%%

divided = 1000;
chargedisp = '(nC)';
width = 200;
height = 200;
Qmaxall = Qmaxpn/divided;

% Pre-allocation for PD phase and charge magnitude
phasePDPD2 = zeros(1,1);
Charge1PD2 = zeros(1,1);
CasPhasePD2 = zeros(width,width);

% Counting PD events at specific phase with charge magnitude


for PDm = 1:maxPDc
    phi2 = round(PhasePDR(PDm,1)/360*width);
    if phi2 > width || phi2 == 0; phi2 = width; end
    cas2 = round((abs(Charge1R(PDm,1))/divided+Qmaxall)/Qmaxall*height/2);
    if cas2 == 0; cas2 = cas2+1; end
    CasPhasePD2(cas2,phi2) = CasPhasePD2(cas2,phi2)+1;
end


% Plotting phi-q-n graph
scrsz = get(0,'ScreenSize');
fig27 = figure('Position',[scrsz(3)/20 scrsz(4)/19 scrsz(4)*32/30.2
scrsz(3)*20.7/29.8],'NumberTitle','on','Color',[1 1 1]);
[XX,YY] = meshgrid(1:1:width);
axes1 = axes('Parent',fig27,'FontSize',36,'FontName','Arial');
contour3('Parent',axes1,XX/width*360,(YY-height/2)/(height/2)*-Qmaxpn/divided,
CasPhasePD2,200)
colormap(jet);
shading interp
colorbar('location','eastoutside','FontSize',36,'FontName','Arial')
xlabel('Phase (degree)','FontSize',36,'FontName','Arial')
ylabel(['Charge ',sprintf('\n'),'magnitude ' chargedisp],'FontSize',36,'FontName','Arial',
'HorizontalAlignment','left');
zlabel('Number','FontSize',36,'FontName','Arial')
grid on
axis on
set(gca,'XTick',[0 90 180 270 360])
xlim([0 360])
```

```
ylim([-Qmaxpn/divided 0])
% Labelling for charge magnitude axis


if Qmaxpn == 2500
   set(gca,'YTick',-2.5:0.5:0)
   set(gca,'YTickLabel',{'2.5','2','1.5','1','0.5','0'})
elseif Qmaxpn == 5000
   set(gca,'YTick',-5:0)
   set(gca,'YTickLabel',{'5','4','3','2','1','0'})
elseif Qmaxpn == 500
   set(gca,'YTick',-0.5:0.1:0)
   set(gca,'YTickLabel',{'0.5','0.4','0.3','0.2','0.1','0'})
end
```

B.5 'Plotting_various_graphs' code

```
%%%%%%%%%%%%%%%%%%%%%%%%%%%%%%%%
% 'Plotting_various_graphs' code %
%%%%%%%%%%%%%%%%%%%%%%%%%%%%%%%%

for ttt=1:30; delete(gcf); end % Delete all current figures

cpos = 0; % Positive PD counter
cneg = 0; % Negative PD counter
maxPDc = PDc; % Total PD event
Interv = 1;

% Pre-allocations to speed up simulation
phaseP = zeros(1,1);
phaseN = zeros(1,1);
plotchargepos = zeros(1,1);
plotchargeneg = zeros(1,1);
HqnP = zeros(1,1);
HqnN = zeros(1,1);
TotChargePhaseP = zeros(ceil(360/Interv),1);
TotChargePhaseN = zeros(ceil(360/Interv),1);
countphaseP = zeros(ceil(360/Interv),1);
countphaseN = zeros(ceil(360/Interv),1);
ChargePhaseP = zeros(1,ceil(360/Interv));
ChargePhaseN = zeros(1,ceil(360/Interv));
PDdatabase = zeros(Cycle,1);

PhasePDR = (mod(CorrectPhasePD,360)); % Convert phase into 360 degree system
UPDUPDR=round(MaxVolt*sin(pi*PhasePDR/180)); % Calculate voltage of PD event


for PDc=1:1:maxPDc
    PDc % for observation purpose
    if round(PhasePDR(PDc,1))<=0
       PhasePDR(PDc,1)=PhasePDR(PDc,1)+360;
    end
```

```
    phiphi=round(PhasePDR(PDc,1)/Interv);
    if q_app(PDc,1)>=0
       cpos=cpos+1; % Number of positive PDs
       plotchargepos(cpos,1)=q_app(PDc,1); % Positive PD charge
       phaseP(cpos,1)=phiphi; % Positive PD phase
       ChargePhaseP(cpos,phiphi)=q_app(PDc,1);
       TotChargePhaseP(phiphi,1)=TotChargePhaseP(phiphi,1)+q_app(PDc,1);
       countphaseP(phiphi,1)=countphaseP(phiphi,1)+1;
       if phaseP(cpos,1)>=270
          phaseP(cpos,1)=phiphi-360;
       end
       else
       cneg=cneg+1; % Number of negative PDs
       plotchargeneg(cneg,1)=q_app(PDc,1); % Negative PD charge
       phaseN(cneg,1)=phiphi; % Negative PD phase
       ChargePhaseN(cneg,phiphi)=q_app(PDc,1);
       TotChargePhaseN(phiphi,1)=TotChargePhaseN(phiphi,1)+q_app(PDc,1);
       countphaseN(phiphi,1)=countphaseN(phiphi,1)+1;
       if phaseN(cneg,1)<=90;
          phaseN(cneg,1)=phiphi+360;
       end
    end
end



if Qmaxpn >= 1000
   divided = 1000;
   chargedisp = '(nC)';
else
   divided= 1;
   chargedisp = '(pC)';
end


for PDc=1:1:maxPDc
    PDcycle=ceil(round(CorrectPhasePD(PDc,1))/360);
    PDdatabase(PDcycle,1) = PDdatabase(PDcycle,1)+1; % Count PDs at each cycle
end


% For voltage and time difference between 2 PDs plots
UPDUPDR_A=UPDUPDR(2:maxPDc-1);
UPDUPDR_B=UPDUPDR(1:maxPDc-2);
UPDUPDR_C=UPDUPDR(3:maxPDc);
delUPD=UPDUPDR_A-UPDUPDR_B;
delUPDafter=UPDUPDR_C-UPDUPDR_A;
CorrectPhasePD_A=CorrectPhasePD(2:maxPDc-1);
CorrectPhasePD_B=CorrectPhasePD(1:maxPDc-2);
CorrectPhasePD_C=CorrectPhasePD(3:maxPDc);
delTime=(CorrectPhasePD_A-CorrectPhasePD_B)/(360*freq)*1000;
delTimeafter=(CorrectPhasePD_C-CorrectPhasePD_A)/(360*freq)*1000;
```

```
% Calculate PD data
allchargepos=sum(plotchargepos);
allchargeneg=sum(plotchargeneg);
avechargepos=allchargepos/Cycle;
avechargeneg=allchargeneg/Cycle;
allcharge=allchargepos+abs(allchargeneg);
avecharge=allcharge/Cycle;
avephasepos=cpos/Cycle;
avephaseneg=cneg/Cycle;
PDave=(cpos+cneg)/Cycle;
meanCharge=avecharge/PDave;

if (cpos =0); meanChargepos=allchargepos/cpos;
else          meanChargepos=0;
end
if (cneg =0); meanChargeneg=allchargeneg/cneg;
else          meanChargeneg=0;
end

fprintf('\nPD at each cycle :  ');

for PDcycle = 1:1:Cycle
    fprintf('%d ',PDdatabase(PDcycle,1));
end

fprintf('\n\nTotal Pos PD/Cycle = %7.4f\nTotal Neg PD/Cycle = %7.4f', avephasepos,
avephaseneg);
fprintf('\nTotal PD/Cycle = %7.4f\n',PDave);
fprintf('\nMean Pos Charge (pC) = %11.4f',meanChargepos);
fprintf('\nMean Neg Charge (pC) = %11.4f\nMean Tot Charge (pC) = %11.4f\n', meanChargeneg,
meanCharge);
fprintf('\nTotal Pos Charge/Cycle (pC) = %11.4f\nTotal Neg Charge/Cycle (pC) = %11.4f',
avechargepos,avechargeneg);
fprintf('\nTotal Charge/Cycle (pC) = %11.4f\n\n',avecharge);

% Determine minimum and maximum charge amplitude
Qminposall = min(plotchargepos);
Qminnegall = min(abs(plotchargeneg));
Qmaxposall = max(plotchargepos);
Qmaxnegall = max(abs(plotchargeneg));

if Qmaxposall > Qmaxnegall; Qmaxall=Qmaxposall;
else                        Qmaxall=Qmaxnegall;
end

if (Qminnegall==0);               Qminall=Qminposall;
elseif (Qminposall==0);           Qminall=Qminnegall;
elseif (Qminposall < Qminnegall); Qminall=Qminposall;
elseif (Qminposall >= Qminnegall);Qminall=Qminnegall;
end
```

```
fprintf('Qmax ave (pC) = %12.4f\n',(Qmaxposall+Qmaxnegall)/2);
fprintf('Qmax pos (pC) = %12.4f\n',Qmaxposall);
fprintf('Qmax neg (pC) = %12.4f\n',-Qmaxnegall);
fprintf('Qmin ave (pC) = %12.4f\n',(Qminposall+Qminnegall)/2);
fprintf('Qmin pos (pC) = %12.4f\n',Qminposall);
fprintf('Qmin neg (pC) = %12.4f\n\n',-Qminnegall);
fprintf('\n');

% Field plot


if PlotE == 1
   fig13 = figure('Name',['Electric field for ' FigureTitle] ,'NumberTitle','on');
   EincOCN=zeros(1,1);
   for cnnc=1:max(cn); EincOCN(cnnc,1)=EincO; end
   Temp(1)=Tmat;
   subplot(2,1,1,'FontSize',24,'FontName','Arial');
   plot1=plot(CorrectPhaseCC,fcEOCN/1e6,CorrectPhaseCC,EcavCN/1e6,
   CorrectPhaseCC,(EcavCN-fcEOCN)/1e6,CorrectPhaseCC,EincCN/1e6,
   CorrectPhaseCC,-EincCN/1e6);
   set(plot1(1),'LineWidth',2)
   set(plot1(2),'LineWidth',2)
   set(plot1(3),'LineWidth',2,'Color','red')
   set(plot1(4),'LineWidth',2,'LineStyle','--','Color',[0.749 0.749 0])
   set(plot1(5),'LineWidth',2,'LineStyle','--','Color',[0.749 0.749 0])
   grid on
   xlabel('Time (ms)')
   xlim([0 40])
   ylabel('Electric field (kV\cdotmm^ {-1})')
   legend=legend('f_cE_0','E_cav','E_s','E_inc');
   set(legend,'Orientation','horizontal','FontSize',22);
   subplot(2,1,2,'FontSize',24,'FontName','Arial');
   plot2=plot(CorrectPhaseCC,EincCN/1e6,CorrectPhaseCC,EincOCN/1e6);
   set(plot2(1),'LineWidth',2)
   set(plot2(2),'LineWidth',2,'LineStyle','--','Color',[0.749 0.749 0])
   grid on
   xlabel('Time (ms)')
   xlim([0 40])
   ylabel('Electric field (kV\cdotmm^ {-1})')
   legend=legend('E_inc','E_inc0');
   set(legend,'Orientation','horizontal','FontSize',22);
   fig14 = figure('Name',['PD charge magnitude and cavity temperature for ' FigureTitle] ,
   'NumberTitle','on');
   for tt=1:cn
       for bbb=1:size(CorrectPhasePD,1)
           if round(CorrectPhaseCN(tt,1)*360*freq)==round(CorrectPhasePD(bbb,1))
              subplot(2,1,1,'FontSize',24,'FontName','Arial');
              bar(CorrectPhasePD/360/freq*1e3,q_app/1e3,'FaceColor',[0 0 1],
              'EdgeColor',[0 0 1], 'BarWidth',0.4)
              xlabel('Time(ms)')
              ylabel('PD charge(nC)')
              xlim([0 40])
```

```
            grid on
            box on
        end
    end
end
TambCN=zeros(1);
for fff=1:size(CorrectPhaseCC,1); TambCN(fff,1)=Tamb; end
subplot(2,1,2,'FontSize',24,'FontName','Arial');
plot1=plot(CorrectPhaseCC,Temp,CorrectPhaseCC,TambCN);
set(plot1(1),'LineWidth',2,'Color','red')
set(plot1(2),'LineWidth',2,'LineStyle','--','Color',[0.749 0.749 0])
legend=legend('T_cav','T_0');
set(legend,'Orientation','horizontal','FontSize',24);
xlabel('Time(ms)')
ylabel(''emperature (K)')
xlim([0 40])
grid on
box on
end

legendname=['d=' num2str(d) 'um, h=' num2str(h) 'um, Freq=' num2str(freq) 'Hz, Uapp='
num2str(MaxVolt/1000) 'kV'];

% Plot phase of PD occurrences distribution
fig15 = figure('Name',['PD phase distribution for ' FigureTitle],'NumberTitle','on');
axes1 = axes('Parent',fig15,'FontSize',24,'FontName','Arial');
ddd = 0:Interv:360;
hist('Parent',axes1,PhasePDR,ddd)
hh = findobj(gca,'Type','patch');
set(hh,'LineWidth',3,'FaceColor',[0 0 1],'EdgeColor',[0 0 1])
legend1 =legend(axes1,'show',legendname,1);
set(legend1,'FontSize',18,'FontName','Arial');
xlabel('Phase (degree)','FontSize',24,'FontName','Arial')
ylabel('Number of PD occurrences','FontSize',24,'FontName','Arial')
grid on
axis on
set(gca,'XTick',0:45:360)
xlim([0 360])


% Plot phase of PD occurrence distribution
phasecnt=(countphaseP+countphaseN)/Cycle;
smoothnpc=smooth(phasecnt);
fig16 =figure('Name',['PD phase distribution for ' FigureTitle],'NumberTitle','on');
axes1 = axes('Parent',fig16,'FontSize',24,'FontName','Arial');
pppp = 1:1:360;
plot(pppp,smoothnpc,'Parent',axes1,'LineWidth',3)
hh = findobj(gca,'Type','patch');
set(hh, 'LineWidth',3,'FaceColor',[0 0 1],'EdgeColor',[0 0 1])
legend1 =legend(axes1,'show',legendname,1);
set(legend1,'FontSize',18,'FontName','Arial');
xlabel('Phase (degree)','FontSize',24,'FontName','Arial')
```

```
ylabel('Normalized number of PDs per cycle','FontSize',24,'FontName','Arial')
grid on
axis on
xlim([0 360])
set(gca,'XTick',0:90:360)


% Plot PD charge magnitude distribution
fig17 = figure('Name',['PD charge magnitude distribution for ' FigureTitle] ,'NumberTitle','on');
axes1 = axes('Parent',fig17,'FontSize',24,'FontName','Arial');
pppp = -Qmaxall:1/divided:Qmaxall;
hist('Parent',axes1,q_app/divided,pppp)
hh = findobj(gca,'Type','patch');
set(hh,'LineWidth',3,'FaceColor',[0 0 1],'EdgeColor',[0 0 1])
legend1 =legend(axes1,'show',legendname,1);
set(legend1,'FontSize',18,'FontName','Arial');
xlabel(['Charge magnitude ' chargedisp],'FontSize',24,'FontName','Arial')
ylabel('Number of PD occurrencess','FontSize',24,'FontName','Arial')
grid on
axis on
xlim([-Qmaxall Qmaxall])


% Plot voltage of PD occurrence distribution
fig18 = figure('Name',['Voltage of PD plot for ' FigureTitle] ,'NumberTitle','on');
axes1 = axes('Parent',fig18,'FontSize',24,'FontName','Arial');
uuuu = -MaxVolt/10:1:MaxVolt/10;
hist('Parent',axes1,UPDUPDR/10,uuuu)
hh = findobj(gca,'Type','patch');
set(hh,'LineWidth',3,'FaceColor',[0 0 1],'EdgeColor',[0 0 1])
legend1 =legend(axes1,'show',legendname,1);
set(legend1,'FontSize',18,'FontName','Arial');
xlabel('Voltage (kV)','FontSize',24,'FontName','Arial')
ylabel('Number of PD occurrencess','FontSize',24,'FontName','Arial')
grid on
axis on
xlim([-MaxVolt/10 MaxVolt/10])


fig19 = figure('Name',['Plots of H_n(\phi), H_{qs}(\phi), H_{qn}(\phi), H_{qm}(\phi) for '
FigureTitle] ,'NumberTitle','on');
% Hn distribution
phasecnts=smooth(phasecnt);
subplot1=subplot(2,2,1,'Parent',fig19,'FontSize',18,'FontName','Arial');
phasePD=1:1:ceil(360/Interv);
plot(phasePD*Interv,phasecnts,'LineWidth',3)
legend1 =legend(subplot1,'show',legendname,1);
set(legend1,'FontSize',12,'FontName','Arial');
xlabel('Phase (degree)','FontSize',18,'FontName','Arial')
ylabel('Number of PDs per cycle','FontSize',18,'FontName','Arial')
grid on
axis on
```

```
title('(a) H_n(\phi) distribution','FontSize',18,'FontName','Arial')
set(gca,'XTick',0:45:360)
xlim([0 360])


% Hqs distribution
TotChargePhasePs=smooth(TotChargePhaseP/Cycle);
TotChargePhaseNs=smooth(TotChargePhaseN/Cycle);
subplot2=subplot(2,2,2,'Parent',fig19,'FontSize',18,'FontName','Arial');
phasePD=1:1:ceil(360/Interv);
plot(phasePD*Interv,TotChargePhasePs,phasePD*Interv,TotChargePhaseNs,'r',
'LineWidth',3)
legend1 =legend(subplot2,'show',legendname,1);
set(legend1,'FontSize',12,'FontName','Arial');
xlabel('Phase (degree)','FontSize',18,'FontName','Arial')
ylabel(\ phi'(b) Total charge per cycle (pC)','FontSize',18,'FontName','Arial')
grid on
axis on
title('(b) H_{qs}(\phi) distribution','FontSize',18,'FontName','Arial')
set(gca,'XTick',0:45:360)
xlim([0 360])



for phasePD=1:1:ceil(360/Interv)
    if (countphaseP(phasePD,1) =0)
       HqnP(phasePD,1)= TotChargePhaseP(phasePD,1)/countphaseP(phasePD,1);
    else
       HqnP(phasePD,1)= 0;
    end
    if (countphaseN(phasePD,1) =0)
       HqnN(phasePD,1)= TotChargePhaseN(phasePD,1)/countphaseN(phasePD,1);
    else
       HqnN(phasePD,1)= 0;
    end
end



% Hqn distribution
HqnPs=smooth(HqnP/divided);
HqnNs=smooth(HqnN/divided);
subplot3=subplot(2,2,3,'Parent',fig19,'FontSize',18,'FontName','Arial');
phasePD=1:1:ceil(360/Interv);
plot(phasePD*Interv,HqnPs,phasePD*Interv,HqnNs,'-r','LineWidth',3)
legend1 =legend(subplot3,'show',legendname,1);
set(legend1,'FontSize',12,'FontName','Arial');
xlabel('Phase (degree)','FontSize',18,'FontName','Arial')
ylabel(['Mean charge magnitude ' chargedisp],'FontSize',18,'FontName','Arial')
grid on
axis on
title('(c) H_{qn}(\phi) distribution','FontSize',18,'FontName','Arial')
set(gca,'XTick',0:45:360)
```

```
xlim([0 360])
ylim([-Qmaxpn/divided Qmaxpn/divided])


% Hqm distribution
maxp = max(abs(ChargePhaseP));
maxn = -max(abs(ChargePhaseN));
maxps=smooth(maxp/divided);
maxns=smooth(maxn/divided);
subplot4=subplot(2,2,4,'Parent',fig19,'FontSize',18,'FontName','Arial');
phasePD=1:1:ceil(360/Interv);
plot(phasePD*Interv,maxps,phasePD*Interv,maxns,'-r','LineWidth',3)
legend1 =legend(subplot4,'show',legendname,1);
set(legend1,'FontSize',12,'FontName','Arial');
xlabel('Phase (degree)','FontSize',18,'FontName','Arial')
ylabel(['Maximum discharge magnitude ' chargedisp],'FontSize',18,'FontName','Arial')
grid on
axis on
title('(d) H_{qm}(\phi) distribution','FontSize',18,'FontName','Arial')
xlim([0 360])
ylim([-Qmaxpn/divided Qmaxpn/divided])
set(gca,'XTick',0:45:360)



if PDc>2 && sequence == 1
   % Plot voltage difference of PD occurrence distribution
   fig20=figure('Name',['PD voltage difference plot for ' FigureTitle] ,'NumberTitle','on');
   axes1 = axes('Parent',fig20,'FontSize',24,'FontName','Arial');
   pppp = -2*MaxVolt/10:1:2*MaxVolt/10;
   hist('Parent',axes1,Delta UPD/10,pppp)
   hh = findobj(gca,'Type','patch');
   set(hh,'LineWidth',3,'FaceColor',[0 0 1],'EdgeColor',[0 0 1])
   legend1 =legend(axes1,'show',legendname,1);
   set(legend1,'FontSize',18,'FontName','Arial');
   xlabel('Voltage difference (kV)','FontSize',24,'FontName','Arial')
   ylabel('Number of PD occurrences','FontSize',24,'FontName','Arial')
   grid on
   axis on
   xlim([-2*MaxVolt/10 2*MaxVolt/10])
   % Plot time difference of PD occurrence distribution
   fig21 = figure('Name',['PD time difference plot for ' FigureTitle] ,'NumberTitle','on');
   axes1 = axes('Parent',fig21,'FontSize',24,'FontName','Arial');
   pppp = 0:1/(10*freq):max(Delta time);
   hist('Parent',axes1,Delta time,pppp)
   hh = findobj(gca,'Type','patch');
   set(hh,'LineWidth',3,'FaceColor',[0 0 1],'EdgeColor',[0 0 1])
   legend1 =legend(axes1,'show',legendname,1);
   set(legend1,'FontSize',18,'FontName','Arial');
   xlabel('Time difference (ms)','FontSize',24,'FontName','Arial')
   ylabel('Number of occurrence','FontSize',24,'FontName','Arial')
   grid on
```

```
    axis on
    xlim([0 max(Delta time)])
    % Plot DeltaU(n) - DeltaU(n-1) distribution
    fig22 = figure('Name',['Delta U(n) - Delta U(n-1) plot for ' FigureTitle] ,
    'NumberTitle','on');
    axes1 = axes('Parent',fig22,'FontSize',24,'FontName','Arial');
    scatter(Delta UPD/1000,Delta UPDafter/1000,'.','Parent',axes1)
    xlabel('\Delta U_{n-1}=U_n-U_{n-1} (kV)','FontSize',24,'FontName','Arial')
    ylabel('\Delta U_n=U_{n+1}-U_n (kV)','FontSize',24,'FontName','Arial')
    grid on
    axis on
    % Plot Deltat(n) - Deltat(n-1) distribution
    fig23 = figure('Name',['Delta t(n) - Delta t(n-1) plot for ' FigureTitle] ,
    'NumberTitle','on');
    axes1 = axes('Parent',fig23,'FontSize',24,'FontName','Arial');
    scatter(Delta time,Delta timeafter,'.','Parent',axes1)
    xlabel('\Delta t_{n-1}=t_n-t_{n-1} (ms)','FontSize',24,'FontName','Arial')
    ylabel(''\Delta t_n=t_{n+1}-t_n (ms)','FontSize',24,'FontName','Arial')
    grid on
    axis on
    % Plot voltage difference of PD occurrence pattern
    fig24 = figure('Name',['Voltage difference of PD pattern for ' FigureTitle] ,
    'NumberTitle','on');
    axes1 = axes('Parent',fig24,'FontSize',24,'FontName','Arial');
    mmm=1:1:maxPDc-2;
    plot(mmm,Delta UPD/1000,'Parent',axes1,'LineWidth',3)
    legend1 =legend(axes1,'show',legendname,1);
    set(legend1,'FontSize',18,'FontName','Arial');
    xlabel('PD sequence','FontSize',24,'FontName','Arial')
    ylabel('Voltage difference (kV)','FontSize',24,'FontName','Arial')
    grid on
    axis on
    xlim([0 maxPDc-2])
    % Plot time difference of PD occurrence pattern
    fig25 = figure('Name',['Time difference of PD pattern ' FigureTitle] ,
    'NumberTitle','on');
    axes1 = axes('Parent',fig25,'FontSize',24,'FontName','Arial');
    mmm=1:1:maxPDc-2;
    plot(mmm,Delta time,'Parent',axes1,'LineWidth',3)
    legend1 =legend(axes1,'show',legendname,1);
    set(legend1,'FontSize',18,'FontName','Arial');
    xlabel('PD sequence','FontSize',24,'FontName','Arial')
    ylabel('Time difference (ms)','FontSize',24,'FontName','Arial')
    grid on
    axis on
    xlim([0 maxPDc-1])
end


% Plot 2D PRPD histogram
width=200;
```

```
height=200;
Qmaxall=Qmaxpn/divided;
phasePDPD=(PhasePDR/Interv/360*width);
Charge1PD=(-q_app/Qmaxpn*height/2+height/2);
Charge1PD(maxPDc+1,1)=0;
Charge1PD(maxPDc+2,1)=width;
phasePDPD(maxPDc+1,1)=0;
phasePDPD(maxPDc+2,1)=width;
ChargePhasePD=[phasePDPD,Charge1PD];


fig26 = figure('Name',['PRPD histogram for ' FigureTitle],'NumberTitle','on', 'Colormap',
[1 1 1;0 0 0.5608;0 0 0.634;0 0 0.7072;0 0 0.7804;0 0 0.8536; 0 0 0.9268;0 0 1;0 0.0625 1;0
0.125 1;0 0.1875 1;0 0.25 1;0 0.3125 1;0 0.375 1; 0 0.4375 1;0 0.5 1;0 0.5625 1;0 0.625 1;0
0.6875 1;0 0.75 1;0 0.8125 1;0 0.875 1; 0 0.9375 1;0 1 1;0.0625 1 0.9375;0.125 1 0.875;0.1875
1 0.8125;0.25 1 0.75; 0.3125 1 0.6875;0.375 1 0.625;0.4375 1 0.5625;0.5 1 0.5;0.5625 1 0.4375;
0.625 1 0.375;0.6875 1 0.3125;0.75 1 0.25;0.8125 1 0.1875;0.875 1 0.125; 0.9375 1 0.0625;1
1 0;1 0.9375 0;1 0.875 0;1 0.8125 0;1 0.75 0;1 0.6875 0; 1 0.625 0;1 0.5625 0;1 0.5 0;1 0.4375
0;1 0.375 0;1 0.3125 0;1 0.25 0;1 0.1875 0; 1 0.125 0;1 0.0625 0;1 0 0;0.9375 0 0;0.875 0
0;0.8125 0 0;0.75 0 0;0.6875 0 0; 0.625 0 0;0.5625 0 0;0.5 0 0]);
axes1 = axes('Parent',fig26,'FontSize',24,'FontName','Arial','Layer','top');
hold all
grid on
axis on
box on
n = hist3('Parent',axes1,ChargePhasePD,[width width]);
n1 = n';
n1(width+1,width+1) = 0;
xb = linspace(0,width,width+1);
yb = linspace(0,width,width+1);
hhh = pcolor(xb/width*360,(yb-height/2)/(height/2)*-Qmaxall,n1);
shading interp
set(hhh, 'zdata', ones(size(n1)) * -max(max(n)))
fff=0:1:360;
Vapp=Qmaxall*sin(fff/180*pi);
plot(fff,Vapp,'Color','black','LineWidth',3)
colorbar('location','eastoutside','FontSize',24,'FontName','Arial')
title(['f ' num2str(freq) ' Hz, ' num2str(MaxVolt/1000) ' kV']), 'FontSize',24,
'FontName','Arial');
xlabel('Phase (degree)','FontSize',24,'FontName','Arial')
ylabel(['Charge magnitude ' chargedisp],'FontSize',24,'FontName','Arial')
set(gca,'XTick',[0 90 180 270 360])
xlim([0 360])
ylim([(-Qmaxall) (Qmaxall)])
hold off



% Saving the figures
if savefig ==1
   if PlotVolt == 1
      saveas(fig13,[FilenameSave '_FieldPlot'],'fig')
```

```
    end
    if TempVolt == 1
        saveas(fig14,[FilenameSave '_TemperaturePlot'],'fig')
    end
    saveas(fig15,[FilenameSave '_Phase'],'fig')
    saveas(fig16,[FilenameSave '_PhaseNorm'],'fig')
    saveas(fig17,[FilenameSave '_q-n'],'fig')
    saveas(fig18,[FilenameSave '_UPD'],'fig')
    saveas(fig19,[FilenameSave '_HnHqsHqnHqm'],'fig')
    saveas(fig26,[FilenameSave '_PRPD'],'fig')
    if PDc>2
        saveas(fig20,[FilenameSave '_DeltaUPD'],'fig')
        saveas(fig21,[FilenameSave '_Deltatime'],'fig')
        saveas(fig22,[FilenameSave '_DeltaUPD_sequence'],'fig')
        saveas(fig23,[FilenameSave '_Deltatime_sequence'],'fig')
        saveas(fig24,[FilenameSave '_DeltaUPD_pattern'],'fig')
        saveas(fig25,[FilenameSave '_Deltatime_pattern'],'fig')
    end
end


'% Save workspace
save([FilenameSave '_PDdata.mat'])
```

Appendix C

Derivation of heat transfer by conduction equation

The derivation of heat transfer by conduction equation is started with a relationship between heat energy, ΔQ and specific heat capacity, C where

$$\Delta Q = mC\Delta T \tag{C.1}$$

where m is the mass of an object and ΔT is the temperature change. The heat energy absorbed by the object per unit time is given by

$$\frac{dQ}{dt} = mC\frac{\partial T}{\partial t} \tag{C.2}$$

If the mass, m is written in term of density, ρ and volume with $dxdydz$ expressions by referring to Figure C.1, Equation C.2 can also be written as

$$\frac{dQ}{dt} = \rho dxdydzC\frac{\partial T}{\partial t} \tag{C.3}$$

The total heat flow into the object is equal to summation of heat flow from x, y and z-direction into surface area of $dydz$, $dxdz$ and $dxdy$ respectively and heat generated in the object, where

$$\frac{dQ}{dt} = \vec{q_x}\, dydz + \vec{q_y}\, dxdz + \vec{q_z}\, dxdy + hdxdydz \tag{C.4}$$

where $\vec{q_x}$, $\vec{q_y}$and $\vec{q_z}$ are heat flux in x, y and z-direction and h is the heat source density

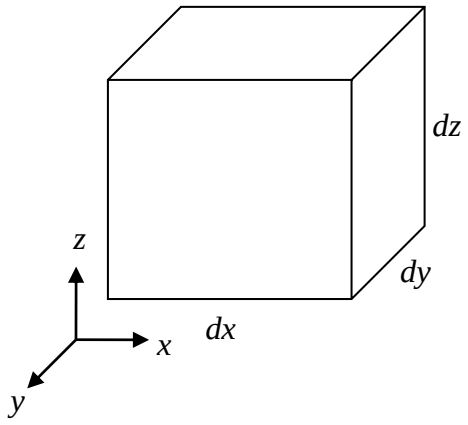

FIGURE C.1: A cube used to derived heat transfer by conduction equation.

in the object. When heat flux is considered from x to $x+dx$, y to $y+dy$ and z to $z+dz$, $\vec{q_x}$, $\vec{q_y}$ and $\vec{q_z}$ are defined as

$$\vec{q_x} = -k\left(\frac{\partial T}{\partial x}(x,t) - \frac{\partial T}{\partial x}(x+dx,t)\right) \tag{C.5a}$$

$$\vec{q_y} = -k\left(\frac{\partial T}{\partial y}(y,t) - \frac{\partial T}{\partial y}(y+dy,t)\right) \tag{C.5b}$$

$$\vec{q_z} = -k\left(\frac{\partial T}{\partial z}(z,t) - \frac{\partial T}{\partial z}(z+dz,t)\right) \tag{C.5c}$$

where k is the thermal conductivity of the object. Inserting Equation C.5a, Equation C.5b and Equation C.5c into Equation C.4,

$$\begin{aligned}\frac{dQ}{dt} = &-k\left[\left(\frac{\partial T}{\partial x}(x,t) - \frac{\partial T}{\partial x}(x+dx,t)\right)dydz + \left(\frac{\partial T}{\partial y}(y,t) - \frac{\partial T}{\partial y}(y+dy,t)\right)dxdz\right.\\ &\left. + \left(\frac{\partial T}{\partial z}(z,t) - \frac{\partial T}{\partial z}(z+dz,t)\right)dxdy\right] + hdxdydz\end{aligned} \tag{C.6}$$

Equating Equation C.3 and Equation C.6, and dividing both sides by $dxdydz$,

$$\begin{aligned}\rho C\frac{\partial T}{\partial t} = &k\left[\frac{\frac{\partial T}{\partial x}(x+dx,t) - \frac{\partial T}{\partial x}(x,t)}{dx} + \frac{\frac{\partial T}{\partial y}(y+dy,t) - \frac{\partial T}{\partial y}(y,t)}{dy}\right.\\ &\left. + \frac{\frac{\partial T}{\partial z}(z+dz,t) - \frac{\partial T}{\partial z}(z,t)}{dz}\right] + h\end{aligned} \tag{C.7}$$

If $dx \rightarrow 0$, $dy \rightarrow 0$ and $dz \rightarrow 0$, Equation C.7 becomes

$$\rho C \frac{\partial T}{\partial t} = k \left[\frac{\partial^2 T}{\partial x^2} + \frac{\partial^2 T}{\partial y^2} + \frac{\partial^2 T}{\partial z^2} \right] + h \tag{C.8}$$

Rearranging the equation and equating $\frac{\partial^2 T}{\partial x^2} + \frac{\partial^2 T}{\partial y^2} + \frac{\partial^2 T}{\partial z^2} = \nabla^2 T = \nabla \bullet \nabla T$, Equation C.8 can be rewritten as

$$\rho C \frac{\partial T}{\partial t} - \nabla \bullet (k \nabla T) = h \tag{C.9}$$

where Equation C.9 is used by FEA software to solve temperature problems in the model.

Appendix D

Derivation of inception field equation

The inception field equation is derived based on the ionization and attachment coefficient of the gas. The gas ionization is controlled by the effective ionization coefficient, $\bar{\alpha}$ which is defined as

$$\bar{\alpha} = \alpha - \eta \tag{D.1}$$

where α and η are ionization and attachment coefficients of the gas. $\bar{\alpha}$ depends on the gas pressure p and the electric field E which is approximated by a power law

$$\bar{\alpha} = \begin{cases} C[(E/p) - (E/p)_{cr}]^{\beta} p & E > E_{cr} \\ 0 & E < E_{cr} \end{cases} \tag{D.2}$$

where C, $(E/p)_{cr}$ and β are gas characterization parameters and E_{cr} is the critical field. $(E/p)_{cr}$ is the pressure reduced critical field when α=η. The constant β and C characterize the increment of $\bar{\alpha}$ with E when critical field E_{cr} is exceeded, which is defined as

$$E_{cr} = (E/p)_{cr} p \tag{D.3}$$

The requirement for streamer inception is the critical avalanche criterion, which can be written as

$$\int_0^{x_{cr}} \bar{\alpha}[E(x)]dx \geq K_{cr} \tag{D.4}$$

where $E(x)$ is field distribution along the streamer path, x_{cr} is the ionization distance and K_{cr} is the logarithm of a critical number of electrons that has to accumulate in the avalanche head to allow the avalanche self-propagating by its own space charge field. Equation (c4) is integrated over the distance x_{cr} within which $\bar{\alpha}$ exceeds 0, i.e. $E(x)$ exceeds E_{cr}.

The electric field $E(x)$ is proportional to the applied field E_0 in the absence of surface charge,

$$E(x) = E_0 e_0(x/d) \tag{D.5}$$

where d is the defect gap and $e_0(x/d)$ is field distribution function which depends on the defect geometry and is a dimensionless number. The starting point of the avalanche is $(x/d) = 0$ and the limit of integration range x_{cr} is determined by

$$E_{cr} = E(x_{cr}) = E_0 e_0(x_{cr}/d) = E_0 e_0(x/d)_{cr} \tag{D.6}$$

Solving for $(x/d)_{cr}$ yields in

$$(x/d)_{cr} = e_0^{-1}(E_0/E_{cr}) \tag{D.7}$$

Replacing Equation D.1, Equation D.3 and Equation D.6 into Equation D.4 and x_{cr} with $(x/d)_{cr}$ yield in

$$\int_0^{(x/d)_{cr}} \left\{ \left[\left(\frac{E_0}{E_{cr}} \right) e_0(x/d) - 1 \right] \right\}^{\beta} d(x/d) \geq \frac{K_{cr}}{Cpd(E/p)_{cr}^{\beta}} \tag{D.8}$$

Solving Equation D.8 for E_0/E_{cr} resulting in the streamer inception criteria, which is denoted by F,

$$(E_0/E_{cr})^{str} = \left(\frac{K_{cr}^{1/\beta}}{(Cpd)^{1/\beta}(E/p)_{cr}} + 1 \right) e_0^{-1}(x/d) = F \tag{D.9}$$

Introducing,

$$B = \frac{(K_{cr}/C)^{1/\beta}}{(E/p)_{cr}} \quad and \quad \eta = 1/\beta \tag{D.10}$$

The simplified form of F is obtained as

$$F = \frac{1 + B/(pd)^{\eta}}{f} \tag{D.11}$$

where f is the field enhancement factor which depends on the relative permittivity of the dielectric material, ε_r and the defect dimensions defined as

$$f = \frac{K\varepsilon_r}{1 + (K-1)\varepsilon_r} \tag{D.12}$$

where K depends on the ratio between the defect length that is parallel and perpendicular to applied field. For spherical cavities, K=3. From Equation D.9 and Equation D.11 the applied electric field ${E_0}^{str}$ to reach the streamer inception is

$$E_0^{str} = E_{cr}F = \frac{(E/p)_{cr}p}{f}\left[1 + \frac{B}{(pd)^{\eta}}\right] \tag{D.13}$$

Therefore, the inception field in the cavity, E_{inc} is calculated by

$$E_{inc} = fE_0^{str} = (E/p)_{cr}p\left[1 + \frac{B}{(pd)^{\eta}}\right] \tag{D.14}$$

For non-attaching gases, the ionization parameters for gas are constant. For air, they have been defined as $(E/p)_{cr} = 24.2$ VPa^{-1}m^{-1}, $B = 8.6$ and $\eta = 0.5$. Replacing these values and $d = 2r$ into Equation D.14 where r is the radius of a spherical cavity,

$$E_{inc} = 24.2p\left[1 + \frac{8.6}{\sqrt{2pr}}\right] \tag{D.15}$$

References

[1] T. Tanaka, "Internal partial discharge and material degradation," *IEEE Transactions on Electrical Insulation*, vol. EI-21, no. 6, pp. 899–905, 1986.

[2] D. A. Seanor, *Electrical Properties of Polymers*. Academic Press, Inc., 1982, ch. Chapter 1, pp. 1–10.

[3] T. Okamoto, T. Kato, Y. Yokomizu, Y. Suzuoki, and T. Tanaka, "PD characteristics as a stochastic process and its integral equation under sinusoidal voltage," *IEEE Transactions on Dielectrics and Electrical Insulation*, vol. 8, no. 1, pp. 82–90, 2001.

[4] N. Hozumi, H. Nagae, Y. Muramoto, M. Nagao, and X. HengKyun, "Time-lag measurement of void discharges and numerical simulation for clarification of the factor for partial discharge pattern," *Proceedings of International Symposium on Electrical Insulating Materials*, pp. 29–32, 2001.

[5] M. Hikita, K. Yamada, A. Nakamura, T. Mizutani, A. Oohasi, and M. Ieda, "Measurements of partial discharges by computer and analysis of partial discharge distribution by the monte carlo method," *IEEE Transactions on Electrical Insulation*, vol. 25, no. 3, pp. 453–468, 1990.

[6] H. Suzuki, K. Aihara, and T. Okamoto, "Complex behaviour of a simple partial-discharge model," *EPL (Europhysics Letters)*, vol. 66, no. 1, p. 28, 2004.

[7] A. Pedersen, G. C. Crichton, and I. W. McAllister, "The functional relation between partial discharges and induced charge," *IEEE Transactions on Dielectrics and Electrical Insulation*, vol. 2, no. 4, pp. 535–543, 1995.

[8] M. G. Danikas, I. W. McAllister, G. C. Crichton, and A. Pedersen, "Discussion: partial discharges in ellipsoidal and spheroidal voids," *IEEE Transactions on Electrical Insulation*, vol. 26, no. 3, pp. 537–539, 1991.

[9] A. Pedersen, G. C. Crichton, and I. W. McAllister, "The theory and measurement of partial discharge transients," *IEEE Transactions on Electrical Insulation*, vol. 26, no. 3, pp. 487–497, 1991.

[10] A. Pedersen, "On the electrodynamics of partial discharges in voids in solid dielectrics," pp. 107–116, 1989.

[11] G. C. Crichton, P. W. Karlsson, and A. Pedersen, "Partial discharges in ellipsoidal and spheroidal voids," *IEEE Transactions on Electrical Insulation*, vol. 24, no. 2, pp. 335–342, 1989.

[12] A. Pedersen, G. C. Crichton, and I. W. McAllister, "PD-related stresses in the bulk dielectric for ellipsoidal voids," pp. 79–84, 1994.

[13] L. Niemeyer, "A generalized approach to partial discharge modeling," *IEEE Transactions on Dielectrics and Electrical Insulation*, vol. 2, no. 4, pp. 510–528, 1995.

[14] F. Gutfleisch and L. Niemeyer, "Measurement and simulation of PD in epoxy voids," *IEEE Transactions on Dielectrics and Electrical Insulation*, vol. 2, no. 5, pp. 729–743, 1995.

[15] C. Forssen and H. Edin, "Partial discharges in a cavity at variable applied frequency part 2: Measurements and modeling," *IEEE Transactions on Dielectrics and Electrical Insulation*, vol. 15, no. 6, pp. 1610–1616, 2008.

[16] C. Forssen, "Modelling of cavity partial discharges at variable applied frequency," PhD Thesis, Royal Institute of Technology (KTH), Stockholm, Sweden, 2008.

[17] C. Forssen and H. Edin, "Modeling partial discharges in a cavity at different applied frequencies," *Conference on Electrical Insulation and Dielectric Phenomena*, pp. 132–135, 2007.

[18] C. Forssen and H. Edin, "Field model of partial discharges at variable frequency of the applied voltage," *Nordic Insulation Symposium - Nord-IS 05*, pp. 121–124, 2005.

[19] C. Forssen and H. Edin, "Modeling of a discharging cavity in a dielectric material exposed to high electric fields," *FEMLAB Conference*, 2005.

[20] P. Rainer and B. Farhad, "Pulse sequence analysis - a diagnostic tool based on the physics behind partial discharges," *Journal of Physics D: Applied Physics*, vol. 35, no. 1, pp. 25–32, 2002.

[21] H. Edin, "Partial discharges studied with variable frequency of the applied voltage," PhD Thesis, Royal Institute of Technology (KTH), Stockholm, Sweden, 2001.

[22] C. Forssen, "Partial discharges in cylindrical cavities at variable frequency of the applied voltage," Licentiate Thesis, Royal Institute of Technology (KTH), Stockholm, Sweden, 2005.

[23] T. Okamoto and T. Tanaka, "Novel partial discharge measurement computer-aided measurement systems," *IEEE Transactions on Electrical Insulation*, vol. 21, no. 6, pp. 1015–1019, 1986.

[24] C. S. Kim, T. Kondo, and T. Mizutani, "Change in PD pattern with aging," *IEEE Transactions on Dielectrics and Electrical Insulation*, vol. 11, no. 1, pp. 13–18, 2004.

[25] R. Bodega, P. H. F. Morshuis, M. Lazzaroni, and F. J. Wester, "PD recurrence in cavities at different energizing methods," *IEEE Transactions on Instrumentation and Measurement*, vol. 53, no. 2, pp. 251–258, 2004.

[26] F. J. Wester, E. Guilski, and J. J. Smit, "Detection of partial discharges at different ac voltage stresses in power cables," *IEEE Electrical Insulation Magazine*, vol. 23, no. 4, pp. 28–43, 2007.

[27] D. Pepper and W. Kalkner, "PD-pattern of defects in xlpe cable insulation at different test voltage shapes," *Eleventh International Symposium on High Voltage Engineering*, vol. 5, pp. 313–316, 1999.

[28] K. Rethmeier, P. Mohaupt, V. Bergmann, W. Kalkner, and G. Voigt, "Fundamentals of partial discharge in the context of field cable testing," *International Conference on Electricity Distribution*, 2007.

[29] M. Muhr and R. Woschitz, "Partial discharge diagnostic," *Proceedings of the 6th International Conference on Properties and Applications of Dielectric Materials*, vol. 1, pp. 223–226, 2000.

[30] E. Kuffel, W. Zaengl, and J. Kuffel, *High Voltage Engineering: Fundamentals*, 2nd ed. Newnes: Butterworth-Heinemann, 2000.

[31] S. A. Boggs, "Partial discharge. iii. cavity-induced PD in solid dielectrics," *IEEE Electrical Insulation Magazine*, vol. 6, no. 6, pp. 11–16, 19–20, 1990.

[32] S. Boggs and J. Densley, "Fundamentals of partial discharge in the context of field cable testing," *IEEE Electrical Insulation Magazine*, vol. 16, no. 5, pp. 13–18, 2000.

[33] P. H. F. Morshuis and F. H. Kreuger, "Transition from streamer to townsend mechanisms in dielectric voids," *Journal of Physics D: Applied Physics*, vol. 23, no. 12, pp. 1562–1568, 1990.

[34] G. C. Montanari, "On line partial discharge diagnosis of power cables," *IEEE Electrical Insulation Conference*, pp. 210–215, 2009.

[35] S. J. Dodd, J. V. Champion, A. S. Vaughan, S. J. Sutton, and S. G. Swingler, "The influence of morphology on electrical treeing in polyethylene blends," *IEEE*

Proceedings of Science Measurement and Technology, vol. 150, no. 2, pp. 58–64, 2003.

[36] P. H. F. Morshuis, "Degradation of solid dielectrics due to internal partial discharge: some thoughts on progress made and where to go now," *IEEE Transactions on Dielectrics and Electrical Insulation*, vol. 12, no. 5, pp. 905–913, 2005.

[37] S. A. Boggs, "Partial discharge: overview and signal generation," *IEEE Electrical Insulation Magazine*, vol. 6, no. 4, pp. 33–39, 1990.

[38] T. Seghir, D. Mahi, T. Lebey, and D. Malec, "Analysis of the electric field and the potential distribution in cavities inside solid insulating electrical materials," *Proceedings of the COMSOL User Conference*, 2006.

[39] N. Ahmed and N. Srinivas, "PD types and their detection possibilities by PD test methods," pp. 307–310, 2001.

[40] M. Hoof and R. Patsch, "A physical model, describing the nature of partial discharge pulse sequences," *International Conference on Properties and Applications of Dielectric Materials*, vol. 1, pp. 283–286, 1997.

[41] R. Bartnikas and J. P. Novak, "On the character of different forms of partial discharge and their related terminologies," *IEEE Transactions on Electrical Insulation*, vol. 28, no. 6, pp. 956–968, 1993.

[42] D. Benzerouk, J. Menzel, and R. Patsch, "The role of accumulated charges in partial discharge processes," pp. 552–555, 2007.

[43] C. Forssen and H. Edin, "Influence of cavity size and cavity location on partial discharge frequency dependence," *Conference on Electrical Insulation and Dielectric Phenomena*, pp. 438–441, 2004.

[44] H. Edin and C. Forssen, "Variable frequency partial discharge analysis of in-service aged machine insulation," *Proceedings Nordic Insulation Symposium*, pp. 29–35, 2003.

[45] U. Garfert, H. Edin, and C. Forssen, "Modelling of partial discharge spectra measured with variable applied frequency," *Proceedings Conference on Properties and Applications of Dielectric Materials*, pp. 839–842, 2003.

[46] E. Gulski and F. H. Kreuger, "Computer-aided recognition of discharge sources," *IEEE Transactions on Electrical Insulation*, vol. 27, no. 1, pp. 82–92, 1992.

[47] Z. Achillides, G. Georghiou, and E. Kyriakides, "Partial discharges and associated transients: the induced charge concept versus capacitive modeling," *IEEE Transactions on Dielectrics and Electrical Insulation*, vol. 15, no. 6, pp. 1507–1516, 2008.

[48] A. Alsheikhly, H. Guzman, and H. G. Kranz, "A new diagnostic tool through computer simulation calculation using expanded partial discharge equivalent circuit," pp. 176–180, 1992.

[49] I. W. McAllister, "Partial discharges in spheroidal voids. void orientation," *IEEE Transactions on Dielectrics and Electrical Insulation*, vol. 4, no. 4, pp. 456–461, 1997.

[50] R. Schifani, R. Candela, and P. Romano, "On PD mechanisms at high temperature in voids included in an epoxy resin," *IEEE Transactions on Dielectrics and Electrical Insulation*, vol. 8, no. 4, pp. 589–597, 2001.

[51] G. Chen and F. Baharudin, "Partial discharge modelling based on a cylindrical model in solid dielectrics," *International Conference on Condition Monitoring and Diagnosis*, 2008.

[52] F. Baharudin, "Modeling partial discharges in a solid dielectric material's cavity using comsol and matlab software," MEng Thesis, University of Southampton, UK, 2007.

[53] R. J. Van Brunt, "Stochastic properties of partial-discharge phenomena," *IEEE Transactions on Electrical Insulation*, vol. 26, no. 5, pp. 902–948, 1991.

[54] P. Molinie, "Measuring and modeling transient insulator response to charging: the contribution of surface potential studies," *IEEE Transactions on Dielectrics and Electrical Insulation*, vol. 12, pp. 939–950, 2005.

[55] A. Cavallini, F. Ciani, G. Mazzanti, and G. C. Montanari, "First electron availability and partial discharge generation in insulation cavities: effect of light irradiation," *IEEE Transactions on Dielectrics and Electrical Insulation*, vol. 12, no. 2, pp. 387–394, 2005.

[56] R. Bodega, A. Cavallini, P. H. F. Morshuis, and F. J. Wester, "The effect of voltage frequency on partial discharge activity," *Conference on Electrical Insulation and Dielectric Phenomena*, pp. 685–689, 2002.

[57] W. Hauschild, A. Cavallini, and G. C. Montanari, "Effect of supply voltage frequency on testing of insulation system," *IEEE Transactions on Dielectrics and Electrical Insulation*, vol. 13, no. 5, pp. 1189–1191, 2006.

[58] E. Lindell, T. Bengtsson, J. Blennow, and S. M. Gubanski, "Measurement of partial discharges at rapidly changing voltages," *IEEE Transactions on Dielectrics and Electrical Insulation*, vol. 15, no. 3, pp. 823–831, 2008.

[59] B. Florkowska, M. Florkowski, J. Furgal, and P. Zydron, "Influence of different voltage waveforms on PD formation in hv insulation systems," *Electrical Insulation Conference*, pp. 51–54, 2009.

[60] N. Zainuddin, M. Yoshinabu, H. Naohiro, and N. Masayuki, "Effect of humidity on time lag of partial discharge in insulation-gap-insulation system," *International Conference on Properties and applications of Dielectric Materials*, pp. 199–203, 2006.

[61] R. Soltani, r. David, and L. Lamarre, "The impact of humidity on partial discharge activity of large rotating machines," *IEEE International Symposium on Electrical Insulation*, 2010.

[62] B. Florkowska, M. Florkowski, J. Roehrich, and P. Zydron, "Partial discharge mechanism in non-homogenous electric field at higher pressure," pp. 326–330, 2008.

[63] I. W. McAllister, "Decay of charge deposited on the wall of gaseous void," *IEEE Transactions on Electrical Insulation*, vol. 27, pp. 1202–1207, 1992.

[64] W. Kai, T. Okamoto, and Y. Suzuoki, "Effects of discharge area and surface conductivity on partial discharge behavior in voids under square voltages," *IEEE Transactions on Dielectrics and Electrical Insulation*, vol. 14, no. 2, pp. 461–470, 2007.

[65] D. M. Taylor and T. P. T. Williams, "Decay of surface charge in the presence of a time-dependent bulk conductivity," *J. Phys. C: Solid State Phys.*, vol. 11, pp. 111–117, 1978.

[66] C. Hudon, R. Bartnikas, and M. R. Wertheimer, "Surface conductivity of epoxy specimens subjected to partial discharges," pp. 153–155, 1990.

[67] K. Temmen, "Evaluation of surface changes in flat cavities due to ageing by means of phase-angle resolved partial discharge measurement," *Journal Physics. D: Applied Physics*, vol. 33, pp. 603–608, 2000.

[68] A. Cavallini, R. Ciani, M. Conti, P. F. H. Morshuis, and G. C. Montanari, "Modeling memory phenomena for partial discharge processes in insulation cavities," *Conference on Electrical Insulation and Dielectric Phenomena*, pp. 723–727, 2003.

[69] K. Tsuruta and H. Ebara, "A model of gas temperature decay after arc extinction of small air gaps," pp. 377–380 vol.1, 1991.

[70] K. Tsuruta and H. Ebara, "Modeling of gas temperature decay after arc discharge in small air gaps," *IEEE Transactions on Electrical Insulation*, vol. 27, no. 3, pp. 451–456, 1992.

[71] P. Das and S. Chakravorti, "Studies on partial discharge simulation based on a stochastic model considering the variation of discharge area and temperature of the void surface," *International Journal for Computational Methods in Engineering Science and Mechanics*, vol. 10, no. 5, pp. 393 – 405, 2009.

[72] H. A. Illias, G. Chen, and P. L. Lewin, "Partial discharge behavior within a spherical cavity in a solid dielectric material as a function of frequency and amplitude of the applied voltage," *IEEE Transactions on Dielectric and Electrical Insulation*, vol. 18, no. 2, pp. 432–443, 2011.

[73] I. W. McAllister, "Surface current density k: an introduction," *IEEE Transactions on Electrical Insulation*, vol. 26, no. 3, pp. 416–417, 1991.

[74] H. A. Illias, G. Chen, and P. Lewin, "Modelling of partial discharge activity in spherical cavities within a dielectric material," *IEEE Electrical Insulation Magazine*, vol. 27, no. 1, pp. 38–45, 2011.

[75] Y. V. Serdyuk and S. M. Gubanski, "Computer modeling of interaction of gas discharge plasma with solid dielectric barriers," *IEEE Transactions on Dielectrics and Electrical Insulation*, vol. 12, no. 4, pp. 725–735, 2005.

[76] A. Bojovschi, W. S. T. Rowe, and K. L. Wong, "Dynamics of partial discharge in dielectrics: a computational approach," *International Symposium on High Voltage Engineering*, 2009.

[77] A. A. Ganjovi, N. Gupta, and G. R. G. Raju, "A kinetic model of a PD pulse within voids of sub-millimeter dimensions," *IEEE Transactions on Dielectrics and Electrical Insulation*, vol. 16, no. 6, pp. 1743–1754, 2009.

[78] S. Matsumura and S. Chen, "Effect of plasma resistance on electron temperature measurement by means of an electrostatic probe," *Journal of Applied Physics*, vol. 43, no. 8, pp. 3357–3361, 1972.

[79] B. M. Smirnov, "Modeling of gas discharge plasma," *Physics-Uspekhi*, vol. 52, no. 6, p. 559, 2009.

[80] J. Hilsenrath, *Tables of thermal properties of gases.* U.S. Govt. Print. Off, 1955.

[81] A. A. Vasserman, *Thermophysical properties of air and air components.* Academy of Sciences of the USSR, 1971.

[82] G. Kaye, *Tables of physical and chemical constants*, 16th ed. Harlow : Longman, 1995.

[83] H. A. Illias, G. Chen, and P. L. Lewin, "Modeling of partial discharges from a spherical cavity within a dielectric material under variable frequency electric fields," *Conference on Electrical Insulation and Dielectric Phenomena*, pp. 447–450, 2008.

[84] J. Kindersberger and C. Lederle, "Surface charge decay on insulators in air and sulfurhexafluoride part i: Simulation," *IEEE Transactions on Dielectrics and Electrical Insulation*, vol. 15, no. 4, pp. 941–948, 2008.

[85] A. K. Jonscher and E. F. Owede, "Time and frequency-resolved surface currents on insulators," *IEEE Transactions on Electrical Insulation*, vol. 25, no. 6, pp. 1077–1084, 1990.

[86] B. M. Weedy, D. Chu, and A. E. Davies, "Electric stresses in an hvdc cable through joint," *IEEE Transactions on Power Apparatus and Systems*, vol. PAS-103, no. 2, pp. 383–388, 1984.

[87] B. M. Weedy, "Dc conductivity of voltalit epoxy spacers in sf6," *IEE Proceedings A Physical Science, Measurement and Instrumentation*, vol. 132, no. 7, pp. 450–454, 1985.

[88] E. Occhini and G. Maschio, "Electrical characteristics of oil-impregnated paper as insulation for hv dc cables," *IEEE Transactions on Power Apparatus and Systems*, vol. PAS-86, no. 3, pp. 312–326, 1967.

[89] K. Nakanishi, A. Yoshioka, Y. Arahata, and Y. Shibuya, "Surface charging on epoxy spacer at dc stress in compressed sf6 gas," *IEEE Transactions on Power Apparatus and Systems*, vol. PAS-102, no. 12, pp. 3919–3927, 1983.

[90] G. C. Montanari, A. Cavallini, L. Testa, S. Serra, and L. A. Dissado, "Model of ageing inception and growth from microvoids in polyethylene-based materials under ac voltage," *Conference on Electrical Insulation and Dielectric Phenomena*, pp. 29–32, 2008.

[91] P. Morshuis, A. Cavallini, G. C. Montanari, F. Puletti, and A. Contin, "The behavior of physical and stochastic parameters from partial discharges in spherical voids," *Proceedings of the 6th International Conference on Properties and Applications of Dielectric Materials*, vol. 1, pp. 304–309, 2000.

[92] H. A. Illias, G. Chen, and P. L. Lewin, "Partial discharge modelling in a spherical cavity within a dielectric insulation material as a function of frequency," *IEEE Electrical Insulation Conference*, pp. 55–59, 2009.

[93] J. Brandrup, *Polymer Handbook*, 2nd ed. New York: A Wiley Interscience publication, 1975.

[94] A. M. James, *Macmillan's chemical and physical data.* London: Macmillan, 1992.

[95] P. F. Bruins, *Epoxy Resin Technology.* New York: Interscience Publishers, 1968.

[96] D. R. Lide, *CRC handbook of chemistry and physics : a ready-reference book of chemical and physical data*, 88th ed. Boca Raton, Fla.: CRC Press, 2008.

[97] A. S. Vaughan, Y. Zhao, L. L. Barr, S. J. Sutton, and S. G. Swingler, "On additives, morphological evolution and dielectric breakdown in low density polyethylene," *European Polymer Journal*, vol. 39, no. 2, pp. 355 – 365, 2003.

[98] U. Braunsberger, "Investigations of the dielectric strength of epoxy resin," *European Electromagnetic Launch Society 18th Topical Meeting*, 2007.

[99] H. E. L. Bharat, *Transformers*. McGraw-Hill Professional Engineering, 2005.

[100] S. A. Boggs, "Partial discharge. ii. detection sensitivity," *IEEE Electrical Insulation Magazine*, vol. 6, no. 5, pp. 35–42, 1990.

[101] V. Scaronvor, ccaron, k, J. Krlov, V. Rybka, J. Plescaronek, Jarmila, erven, and V. Hnatowicz, "Temperature dependence of the permittivity of polymer composites," *Journal of Polymer Science Part B: Polymer Physics*, vol. 39, no. 8, pp. 831–834, 2001, 10.1002/polb.1057.

[102] D. Guo, A. Nesbitt, D. M. Hepburn, C. Zhou, B. G. Stewart, X. Zhou, and F. Baumann, "Time varying characteristics of p-q-n patterns from natural voids in resin," pp. 1–5, 2005.

[103] D. Guo, D. M. Hepburn, A. Nesbitt, and C. Zhou, "Change in pattern of void-type PD with ageing," pp. 109–112, 2008.

[104] C. Forssen and H. Edin, "Partial discharges in a cavity at variable applied frequency part 1: Measurements," *IEEE Transactions on Dielectrics and Electrical Insulation*, vol. 15, no. 6, pp. 1601–1609, 2008.

[105] R. Miller and I. A. Black, "Partial discharge measurements over the frequency range 0.1 hz to 50 hz," *IEEE Transactions on Electrical Insulation*, vol. EI-12, no. 3, pp. 224–233, 1977.

[106] N. Ahmed and N. Srinivas, "On-line versus off-line partial discharge testing in power cables," *IEEE/PES Transmission and Distribution Conference and Exposition*, vol. 2, pp. 865–870, 2001.

[107] M. Budde and M. Kurrat, "Partial discharge diagnostics of micro cavities in epoxy insulating materials and their modelling," *IEEE International Symposium on Electrical Insulation*, pp. 369–372, 2008.

[108] H. P. Burgener and K. Frohlich, "Probability of partial discharge inception in small voids," pp. 298–302, 2001.

[109] H. P. Burgener, T. H. Teich, and K. Frohlich, "Simulations of partial discharges of small microcracks parallel to the electrical field in polymeric materials," *Conference on Electrical Insulation and Dielectric Phenomena*, pp. 146–150, 2002.

[110] T. Do, O. Lesaint, and J. L. Auge, "Streamers and partial discharge mechanisms in silicone gel under impulse and ac voltages," *IEEE Transactions on Dielectrics and Electrical Insulation*, vol. 15, no. 6, pp. 1526–1534, 2008.

[111] T. M. Do, J. L. Auge, and O. Lesaint, "A study of parameters influencing streamer inception in silicone gel," *IEEE Transactions on Dielectrics and Electrical Insulation*, vol. 16, no. 3, pp. 893–899, 2009.

[112] N. P. Kolev and N. M. Chalashkanov, "Modelling of partial discharge inception and extinction voltages using adaptive neuro-fuzzy inference system (anfis)," pp. 605–608, 2007.

[113] M. Di Lorenzo del Casale and R. Schifani, "Investigation of temperature effect on an epoxy resin: Aging due to partial discharges," pp. 509–512, 2001.

[114] M. D. L. del Casale, "On multistress aging of epoxy resins: PD and temperature," *IEEE Transactions on Dielectrics and Electrical Insulation*, vol. 8, no. 2, pp. 299–303, 2001.

[115] S. Boggs and J. Densley, "New studies on PD measurements on mv cable systems at 50hz and sinusoidal 0.1hz (vlf) test voltage," *IEEE Electrical Insulation Magazine*, 2000.

[116] R. Candela, R. Schifani, and P. Romano, "Optimisation of a numerical model for analysis of partial discharge phenomena in a flat cavity," pp. 689–692, 2001.

[117] B. Florkowska, J. Roehrich, P. Zydron, and M. Florkowski, "Partial discharge characteristics of enameled wire of electric machine winding under exploitation stresses," *International Conference on Solid Dielectrics*, 2010.

[118] D. E. A. Mansour, K. Nishizawa, H. Kojima, N. Hayakawa, F. Endo, and H. Okubo, "Charge accumulation effects on time transition of partial discharge activity at gis spacer defects," *IEEE Transactions on Dielectrics and Electrical Insulation*, vol. 17, no. 1, pp. 247–255, 2010.

[119] N. Hayakawa, D. E. A. Mansour, F. Endo, H. Kojima, and H. Okubo, "Surface charge accumulation and partial discharge activity for small gaps of electrode/epoxy interface in sf6 gas," *IEEE Transactions on Dielectrics and Electrical Insulation*, vol. 16, no. 4, pp. 1150–1157, 2009.

[120] H. A. Illias, G. Chen, and P. L. Lewin, "Modelling of surface charge decay in a spherical cavity within a solid dielectric material using finite element analysis," *International Symposium on High Voltage Engineering*, pp. 1–6, 2009.

[121] C. Forssen and H. Edin, "Measured partial discharge inception voltage for a cavity at different applied frequencies," *Proc. Nordic Insulation Symposium*, pp. 59–62, 2007.

[122] H. A. Illias, G. Chen, and P. L. Lewin, "Modelling of partial discharge activity in different spherical cavity sizes and locations within a dielectric insulation

material," *International Conference on Properties and Applications of Dielectric Materials*, pp. 485–488, 2009.

[123] M. Budde, V. Ermel, and M. Kurrat, "Partial discharge diagnostics of micro cavities and its modelling," *International Symposium on High Voltage Engineering*, 2009.

[124] G. Chen and Z. Xu, "Charge trapping and detrapping in polymeric materials," *Journal of Applied Physics*, vol. 106, no. 12, pp. 123 707–123 707–5, 2009.

[125] H. A. Illias, G. Chen, and P. L. Lewin, "Modelling of cycle to cycle behaviour for partial discharge events within a spherical cavity in a solid dielectric material by using finite element analysis." *IEEE International Conference on Solid Dielectrics*, pp. 561–564, 2010.